Natural Ventilation in Buildings: Modeling, Control and Optimization

by

Karine Ip Kiun Chong

B.S., Mechanical Engineering
Brown University, 2012

Submitted to the Department of Mechanical Engineering
in partial fulfillment of the requirements for the degree of

Masters of Science in Mechanical Engineering

at the

MASSACHUSETTS INSTITUTE OF TECHNOLOGY

September 2014

Signature redacted

Author .....
Department of Mechanical Engineering
August 8, 2014

Signature redacted

Certified by .....
Leon Glicksman
Professor
Thesis Supervisor

Signature redacted

Accepted by .....
David Hardt
Chairman, Department Committee on Graduate Theses

Natural Ventilation in Buildings: Modeling, Control and Optimization

by

Karine Ip Kiun Chong

Submitted to the Department of Mechanical Engineering
on August 8, 2014, in partial fulfillment of the
requirements for the degree of
Masters of Science in Mechanical Engineering

Abstract

Natural ventilation in buildings has the potential to reduce the energy consumption usually associated with mechanical cooling while maintaining thermal comfort and air quality. It is important to know how building parameters, in particular its thermal mass properties and heat loads incurred, affect a building's transient thermal response to incoming outdoor air. A proper ventilation schedule is also needed to make optimal use of the free direct or night cooling.

To investigate these factors, a first principles heat transfer energy model is developed to numerically simulate in MATLAB the air temperature profile of a single-zone cross-ventilated room. The physics behind natural ventilation at building level is also investigated using multi-zone modeling, as done in CoolVent, an existing MIT airflow modeling tool. In the process, the simulation capabilities of MIT Design Advisor, an existing building energy simulation tool, are expanded upon from shoe-box to interconnected multi-zone modeling.

Optimal natural ventilation scheduling, with a view to maximizing thermal comfort, is then studied using two optimization techniques: dynamic programming and global search optimization, using the simple room energy model as the simulation engine. In the process, an algorithm framework is developed to optimize the ventilation scheduling on a rolling day-horizon basis based on input weather data and occupancy schedule. The use of rule-based control, as opposed to the aforementioned model-optimized control, is also explored due to its ease of implementation in building automation software. The former form of control is found to maintain comparable thermal comfort when seperate rules for specific scenarios, such as night-overcooling or day-overheating, are gathered together to constrain the room air temperature. It is however critical to identify and calculate proper set-points for these rules.

Thesis Supervisor: Leon Glicksman
Title: Professor

Acknowledgments

First, I would like to express my sincere gratitude to Professor Glicksman for allowing me to conduct this research project under his guidance. I am grateful for his advice, encouragement and dedication to the academic enrichment of his students.

I would also like to thank the MIT Energy Initiative and United Technologies, my first-year energy fellowship sponsor, for providing me the stepping stone to pursue research in the energy field and get in. I am grateful to the Department of Energy's Energy Efficient Buildings Hub for the financial support and the opportunity to be involved in the large-scale project of making building energy modeling and simulation more accessible

I extend my thanks to the faculties, staff and students of the Building Technology Program who have made these two years a gratifying experience, in particular to Kathleen Ross who as the departmental administrator makes us feel at home. Thanks to my lab mates, Alonso, Suhrid, David and John for being a desk away for support and advice. Special thanks to the early contributors of CoolVent and Design Advisor, your work and code comments have made it possible to keep contributing to the improvement of these tools.

Thanks to my family and friends, Kavish, Martin, Pablo, Gabby, Fer, Cindy, Yael. Near or far, your love and moral support keep me going.

Dedicated with love to Papi, Mami and Gege.

Table of Contents

List of Figures

List of Tables

Chapter 1

Introduction

1.1 Thesis motivation

In developed countries, building energy consumption amounts to 40% of the total final energy consumption and more than half of this amount is consumed in Heating, Ventilation and Air Conditioning (HVAC) systems[1]. In the U.S, 41% of primary energy was consumed by the buildings sector as shown in figure 1-1, and this constitutes 20 quads of delivered (site) energy annually[2]. Out of this, 10% is used for space cooling and 3% for ventilation, as shown in figure 1-2.

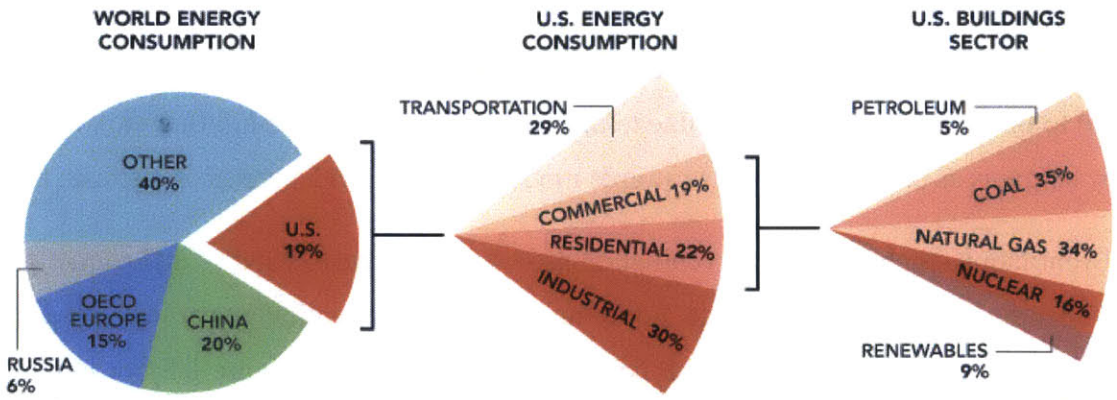

Figure 1-1: World and U.S energy consumption and its breakdown by sectors [2]

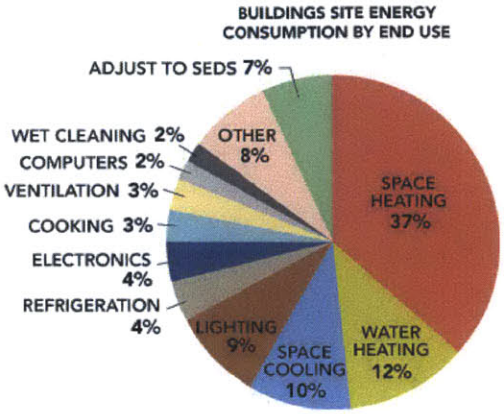

Figure 1-2: Building energy consumption breakdown by end use [2]

Several studies have shown that natural ventilation has the potential to significantly reduce the energy costs, both first and operating costs, associated with mechanical ventilation of buildings, while maintaining ventilation rates that are consistent with acceptable indoor air quality and comfort [3]. In fact, it has been suggested that naturally ventilated buildings have lower sick building syndrome, which potentially increases occupant productivity, amongst others advantages [4]. As natural ventilation is being touted by the "green buildings" community as a means of reducing energy costs and improving indoor air quality within commercial buildings, there has been an increase in the past decades in naturally-ventilated commercial buildings worldwide, even in moderate and cold climates such as Central Europe. This has been partially attributed to increase in internal loads (due to more electrical equipment, lighting etc), as well as higher solar gains as architecture tends towards modern building with extensive glazing [5].

Natural ventilation can be defined as ventilation provided by thermal, wind or diffusion effects through openings in the building façade. Equipment required for ventilative cooling in residential or commercial buildings is available. This could be through windows (figure 1-3), or louvre and damper arrangements (figure 1-4). Hybrid variations of these systems are also available, whereby mechanical devices are added to enhance the performance and control, in the form of volume control dampers or exhaust fans for example. Natural ventilation is usually used in mixed-mode buildings, whereby natural ventilation, mechanical ventilation, as well as mechanical air conditioning are used to provide space cooling. Savings from mixed-mode cooling, as opposed to solely standard air conditioning, could be expected to range from 5% to

30% [6]. These variations are due to locations, climate variability, and building design, in particular its amount of thermal mass.

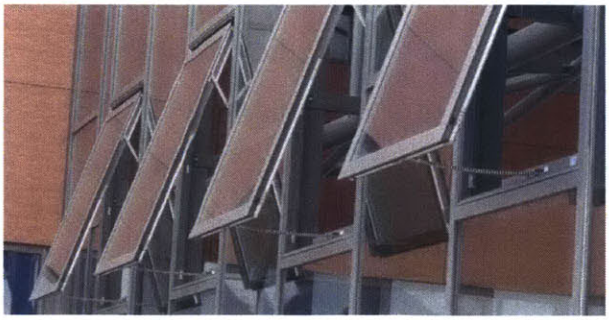

Figure 1-3: Automated windows with hydraulic actuation [7]

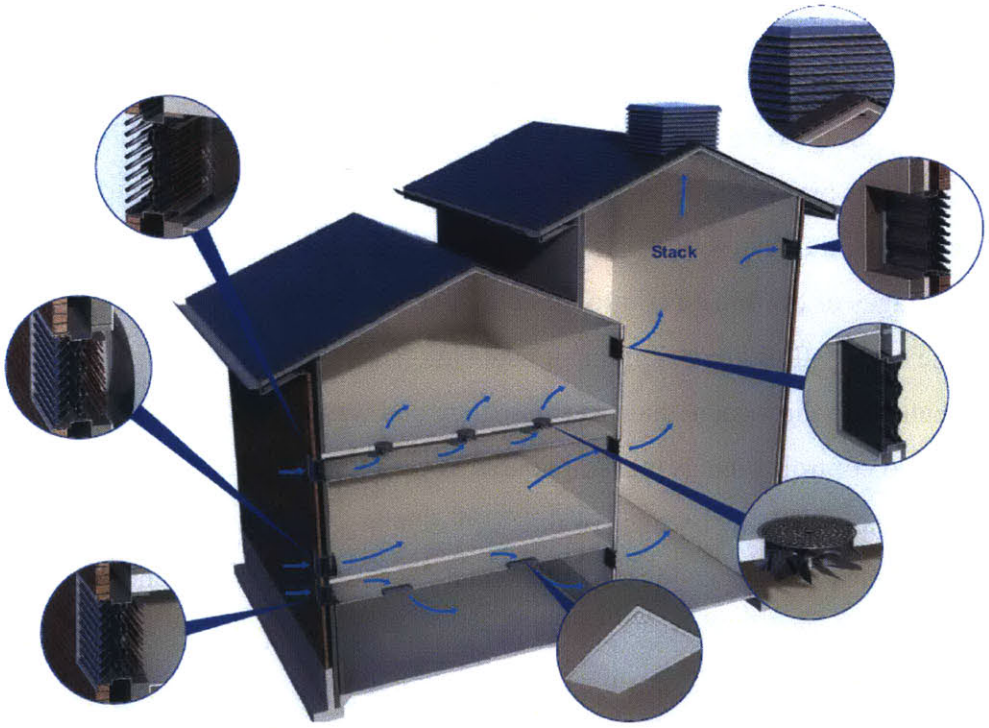

Figure 1-4: Typical natural ventilation systems, including louvre intake and damper arrangement, floor and ceiling grilles, ceiling laminar flow diffusers, floor outlet swirl diffusers, transfer grilles, exhaust wall outlets, penthouse exhaust turret (going clockwise from top left bubble) [8]

However, the question of when to use natural ventilation remains without any definite answers. Day ventilation and/or night ventilation can be used to maintain thermal comfort, depending on climatic conditions and building parameters. Often times, high outdoor temperatures can make thermal comfort worse. Givoni suggested the use of simple rule of thumb of using night-time

cooling mainly for arid regions, where comfortable indoor conditions cannot be met by day ventilation, and which have day-time temperature range of 30-36°C , and night-time temperatures below 20°C [9]. In general, night-cooling is used in climates with high maximum day temperatures (which means high cooling demand) and low minimum night temperatures (which means high cooling potential). In some cases, night-time ventilation is the only option when day-time conditions are prohibitive: for instance, traffic noise, air pollution, high wind speed or high-security occupancy limits the opening of windows or dampers.

The most prevalent form of building controls for natural ventilation in industry is rule-based, for which the set-points are derived from general rule of thumbs and fine-tuning for a specific building. When it is ideally best to use natural ventilation is a complex optimization problem. The optimization can be done with respect to maximizing thermal comfort, minimizing energy consumption, or even minimizing peak electricity demand. Numerous studies are being done on optimization of building controls in these fields in the academic sphere, notably using Model Predictive Control. A proper optimization is three-pronged: it entails a proper definition of (i) the building as an energy model, (ii) the optimization problem itself and (iii) the control systems [10]. The advantages of optimized control are clear: since it essentially requires the active modeling of the energy flows in buildings, it takes into consideration the building parameters, as well as disturbances to the system such as occupancy and weather variations. On the other hand, detailed optimized control, such as that implemented by a Model Predictive Control, is not used extensively in industry till now because of the need of a knowledgeable authoritative entity in charge of these three aspects, in addition to the need for a robust building energy model.

1.2 Thesis outline

This thesis seeks to explore the three-pronged approach to optimization of building controls with respect to natural ventilation with the goal of maintaining thermal comfort. To do so, it is essential to identify and focus on the building and climate parameters which affect natural ventilation. Note that these parameters can be either fixed or variable. For example, fixed parameters are the building properties such as thermal mass and volume; variable parameters are the current active parameters such as solar heat gains, daily mean temperature, daily temperature swings and occupational variations (plug loads, lighting usage) etc.

The aim of this research is to have a holistic approach to addressing the problem of optimized control of natural ventilation. It is three-pronged: (i) building a simple energy model based on the examination of the building physics, both analytically and numerically with relevant parameter variations; (ii) formulating the optimization problem; (iii) using the optimization algorithm on the building energy model to obtain the optimal window schedule, and comparing the optimal results to rule-based control results.

In Chapter 2, a preliminary study of the underlying physics of first a simple room, then a multi-zone network representation of a building is carried out. Such a study allows us to define the parameters which have a first-order effect on the thermal behavior of a building. To do so, a dimensional analysis of the energy balance is carried out. Numerical simulations to predict the room air temperature given variations in those identified parameters are then carried out.

In Chapter 3, a study of physics of the multi-zone network representation of a building is expanded upon, using two existing stand-alone simulation tools: CoolVent and Design Advisor. CoolVent is a simulation tool for coupled thermal-airflow with natural ventilation, whereas Design Advisor is a building energy simulation with mechanical ventilation capabilities. An integration of those two tools is carried out to allow enhanced natural ventilation capabilities while taking advantage of its already-integrated packages for calculating precise heat gains (through wall, window, solar radiation, roof heat gain).

Chapter 4 looks more closely at natural ventilation strategies covered in literature. It also looks at the impact of cyclical ventilation, as opposed to continuous ventilation, in modulating the resulting room temperature, by using the simple numerical energy model set up in chapter 2.

Chapter 5 does a preliminary overview of building controls as covered in industry and in the academic sphere, in particular, the use of Model Predictive Control as a framework for optimized control. In its section, it looks at two different optimization techniques, namely global optimization and dynamic programming, and the algorithm framework needed to wrap around the room energy model.

Chapter 5 looks at the optimization results for different case studies with variation in climate and building parameters. The optimization results are then compared to derived rule-based controls in terms of thermal comfort performances.

Chapter 2

Thermal modeling

2.1 General building energy modeling

Ventilation aims to keep the climate within a building at a wanted level of thermal comfort and air quality. While indoor air quality procedures are used to maintain specific target contaminant concentrations or levels of acceptability of indoor air quality and dictate a minimum ventilation rate based on the occupancy category [11], this thesis will not be concerned with the constraint of ventilation limit. On the other hand, thermal comfort level imposes important lower and upper temperature limits for to the thermal modeling of buildings. ASHRAE standard 55 defines the thermal comfort criteria to encompass the temperature (air, radiant and surface), humidity, air speed [12]. That of air temperature is to be considered in this thesis.

A building, or to a simpler level even a room, undergoes many modes of heat transfer. Energy exchanges take place through conduction, convection and radiation and mass transfer, through the building envelope, between the outdoor and indoor environment, and between the surfaces inside a room. There are solar radiations absorbed by the window pane, wall and even the roof. Arons [13] and Urban [14] covered in details the derivations for net solar radiation reaching inside the room through different building façades, including double-skin and different window types with or without blinds. Ray [15] extended similar energy modeling to different roof-tops including green, bitumen and cool roofs. These were implemented as separate modules in Design Advisor as will be covered in the next chapter.

Apart from solar gain, internal gains contribute to the heat load in a building. Internal gain is comprised of heat released by equipment (plug load), people (sensible and latent heat), or light

fixtures. Hence this type of internal gain can be called an occupational heat gain, and follows the building's occupancy schedule.

Thermal mass is an important consideration in building energy modeling, because its high heat capacity enables it to store heat during the day and release it at night, thus dampening the temperature of the room air. External thermal mass includes walls or roofs which are directly exposed to both the ambient and indoor air. Internal thermal mass such as furniture and concrete slabs are not directly exposed to the ambient air but only to the indoor environment. Zhou et al presented a study where the effect of external thermal mass was investigated analytically [16]. The external thermal adds complexity to the thermal modeling because the interface with the exterior presents added radiation, which changes with solar radiation intensity changes throughout the day. Moreover, the external thermal mass, i.e. the wall, often consists of insulating materials such as gypsum and fiberglass. These materials have low conductivity and hence do not contribute much to the thermal mass effect, as heat cannot penetrate deeply and be conducted back to the air effectively. Thermal mass, henceforth, will refer to the internal concrete mass.

A building with natural ventilation can be considered as an open system, due to air flow in and out. The change in internal energy of the inside air is the sum of the heat transferred into the system and the heat generated within it. This energy balance combines the effect of all the modes of heat transfers through the different interfaces. It is assumed that the temperature is uniform within the identified control volume for the open system. The general equation representing the energy balance for a zone in a building is:

$$mc\frac{dT_i(t)}{dt} = \sum_{\substack{interface \\ j}} UA(t)\left(T_j(t) - T_i(t)\right) + \sum_{\substack{connected \\ zone\ j}} \dot{m}_{ji}(t)c_p\left(T_j(t) - T_i(t)\right) + q_i(t)A \quad (2.1)$$

The first term on the right-hand side is the conduction heat transfer from outside to inside through walls, window panes and other interfaces. The second term represents the convection heat transfer for when a window is open or air is brought in from outside. The last term is the generated internal heat gain.

All of this is used to predict the indoor air temperature variation with time. This prediction can serve to calculate the heating and cooling loads throughout the year, when the inside air temperature does not meet thermal comfort standard and the system needs to be mechanically cooled or heated.

2.2 Single-zone level energy modeling

For simplification, the single-room level represents a one-zone building with connection with the outside, i.e. with the inside at uniform temperature and uni-directional air-flow from outside to inside and back out, without back-flow of air as air can be assumed to be exhausted to a zone at same temperature as the outside temperature. The control volume is a single zone and is assumed to have thermal mass, internal heat gain. The energy balance for the system is the following:

$$mc\frac{dT(t)}{dt} = \left(\sum UA(t) + \dot{m}(t)c_p\right)\left(T_{out}(t) - T(t)\right) + hA\left(T_{thermal\ mass}(t) - T(t)\right) + q_i(t)A \quad (2.2)$$

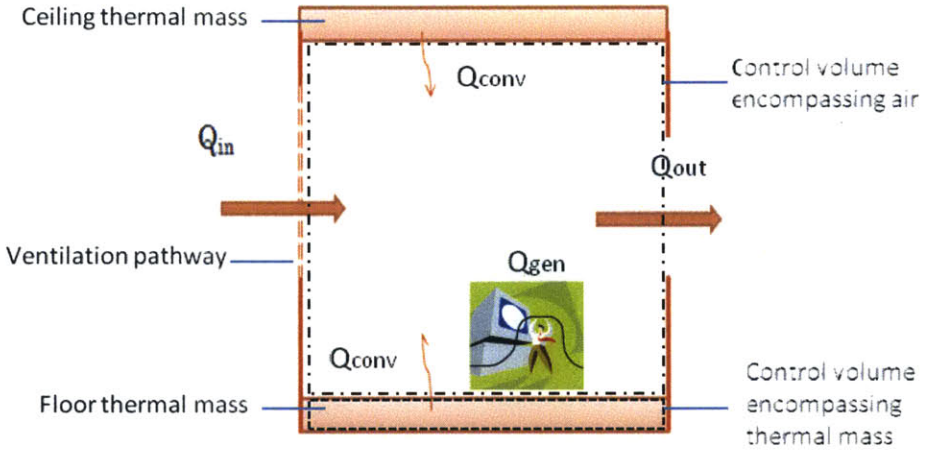

Figure 2-1: Energy flows in a one-zone building model

At the most detailed level, all these terms could be a function of time, making any general analytical solution difficult to obtain. To zoom in on the effect of ventilation and thermal mass on the inner thermal environment, it is necessary to make several simplifications:

(i) the room can be assumed to be well insulated enough that the U-value for the envelope is small enough;

(ii) The heat load q(t) can be assumed to be constant or to follow the occupancy schedule and take only 2 values.

(iii) The airflow rate $\dot{m}$ can be assumed to be constant. While in reality, the airflow rate is determined by the drop in pressure across an orifice (window), it is often augmented mechanically to a suitable level by exhaust fans. Hence, it can be attributed a nominal value of 5 roomful/h for air change rate.

(iv) $T_{out}(t)$ can be approximated to a sinusoidal with period of a day, with the minimum temperature occurring at 12am, such that:

$$T_{out}(t) = T_{mean} + \Delta T sin\left(\frac{2\pi t}{24*3600} - \frac{\pi}{2}\right) \quad (2.3)$$

(v) The solar heat gain is not considered here. Hence, the thermal mass does not have any form of absorbed solar radiation and internal radiation is no considered.

The fourth assumption is made so that weather temperature inconsistencies do not mar the analysis. T_{mean} is the mean monthly outside temperature, while ΔT is the amplitude of the diurnal temperature swing, which can range from 2°C only in Hong-Kong to 14°C in California to 23°C in Loma, Montana [17] . A good average will be 5°C for most cities.

Hence a simplified version of equation 2 is:

$$mc\frac{dT(t)}{dt} = \dot{m}c_p\left(T_{out}(t) - T(t)\right) + hA\left(T_{thermal\,mass}(t) - T(t)\right) + q_iA \quad (2.4)$$

This partial differential equation for air temperature represents a first- order system, which is coupled to a first-order system for the thermal mass as follows:

$$(mc)_{thermal\,mass}\frac{dT_{thermal\,mass}}{dt} = hA\left(T(t) - T_{thermal\,mass}(t)\right) \quad (2.5)$$

The crux of this thesis is how the temperature variation of the concrete affects the temperature of the air spatially and temporally for a given set of building and weather parameters. This is investigated by first looking at the solution and dimensional parameters of the equation.

2.3 Dimensional Analysis

Before solving the above differential equations, it is important to identify the dimensionless parameters, especially for heat transfer problems governed by differential equations that are difficult to solve analytically. This will allow a concise form of the solution to be formulated, be it for experimental or numerical data. The behavior of the system can thus be given by a single curve, whereby the different variables in the dimensionless parameters do not all have to be varied to obtain the same system response. Instead, the global variation in the dimensionless parameters is what matters.

According to the Buckingham pi theorem [18], the following dimensionless groups can be formed from the variables of our problem:

Temperature wise: $\frac{T_{Tmass}\dot{m}c_p}{qA}$, $\frac{T_{out}\dot{m}c_p}{qA}$, $\frac{T_{in}\dot{m}c_p}{qA}$,

Time wise: $\frac{t\,\dot{m}c_p}{mc_{Tmass}}, \frac{t\,\dot{m}c_p}{m_{air}c_v}, \frac{hAt}{m_{air}c_v}, \frac{\dot{m}c_p}{hA}$

Energy wise: $\frac{c_p}{c_v}$

The Buckingham Pi theorem gives us a good indication of the dimensionless parameters involved in the dimensional analysis of equations 2.3 and 2.4, which is needed for a generalization of our problem in terms of dimensionless parameters. To capture the convective heat transfer and internal gain, $\tilde{T} = \frac{T\dot{m}c_p}{qA}$ is used as a temperature scaling parameter. As the thermal mass logically dictates the time constant of the heat transfer phenomenon, $\tilde{t} = \frac{t\dot{m}c_p}{mc_{Tmass}}$ is used as a time scaling parameter. Equations 2.3 and 2.4 can be re-written as:

$$\frac{(mc)_{air}}{(mc)_{Tmass}}\frac{d\tilde{T}(\tilde{t})}{d\tilde{t}} + \tilde{T}(\tilde{t}) - \tilde{T}_{out}(\tilde{t}) + \frac{hA}{\dot{m}c_p}\left(\tilde{T}(\tilde{t}) - \tilde{T}_{T\,mass}(\tilde{t})\right) = 1 \qquad (2.6)$$

Because $(mc)_{Tmass} \gg (mc)_{air}$, the first term can be neglected, thus:

$$\left(\tilde{T} - \tilde{T}_{out}\right) + \frac{hA}{\dot{m}c_p}\left(\tilde{T} - \tilde{T}_{Tmass}\right) = 1 \qquad (2.7)$$

$$\frac{d\tilde{T}_{Tmass}}{d\tilde{t}} = \frac{(\tilde{T}_{out} - \tilde{T}_{Tmass})}{1+\frac{\dot{m}c_p}{hA}} + \frac{1}{1+\frac{\dot{m}c_p}{hA}} \tag{2.8}$$

From this dimensional analysis, the following dimensionless parameter pops out, $\lambda = \frac{\dot{m}c_p}{hA}$. It represents the coupling between the two energy balances and measures the relative strength of convective heat transfer at the thermal mass surface.

It is interesting to note that the Buckingham Pi theorem gives three time constants for our phenomenon: $\tau_1 = \frac{(mc)_{thermal\ mass}}{\dot{m}c_p}$; $\tau_2 = \frac{(mc)_{thermal\ mass}}{hA}$; $\tau_3 = \frac{m_{air}c_v}{\dot{m}c_p}$. As shown in table 2-1, the time constant due to air is negligible because of its low thermal heat capacity, while those due to the thermal mass and ventilation are not.

Air properties: ρ_{air}=1.2 kg/m^3; ACH=5 roomful/h; c_p1008 J/kgK; c_v= 720 J/kgK; height$_{room}$=3.5m **Thermal mass properties:** $\rho_{concrete}$=2500kg/m^3; $c_{concrete}$=880J/kgK; thickness$_{concrete}$=5"; $h_{convective}$=8 W/m^{2}K	
τ_1(h)	13.2
τ_2(h)	9.7
τ_3(h)	0.1

Table 2-1: Time constants for a simplified model of a ventilated room with thermal mass

Yam investigated deeply the nonlinear coupling between thermal mass and natural ventilation in buildings, without the cycling associated with night-ventilation, i.e. windows are assumed to be always open [19]. Similar dimensionless parameters to those derived by our dimensional analysis were mentioned. Four general cases of such interactions were identified: (1) the thermal mass in thermal equilibrium with the room air and fixed ventilation rate, (2) the thermal mass not in thermal equilibrium with the room air and fixed ventilation rate, (3) thermal mass in equilibrium and buoyancy-driven ventilation, (4) thermal mass not in equilibrium and buoyancy-driven ventilation. Analysis of the first two cases is done below.

2.4 Thermal mass in thermal equilibrium with the room air

With the thermal mass as a lumped mass is at the same temperature as the inside air, the convective term from the thermal mass surface disappears. Assuming that the heat capacity of the thermal mass is much more than that of the room air, the energy balance is simplified to:

$$(mc)_{thermal\ mass}\frac{dT}{dt} = \dot{m}c_p(T_{out}(t) - T(t)) + qA \tag{2.9}$$

For this first order differential equation with a sinusoidal forcing element, an analytical solution can readily be obtained by integration by parts. It should be noted that the thermal mass has impact on the amplitude of the fluctuations and the time-lag, but not on the mean indoor temperature value. The solution is given by:

$$T(t) = T_{out\ mean} + \frac{qA}{\dot{m}c_p} + \frac{\Delta T_{out}}{\sqrt{1+\omega^2\tau^2}}(\sin(\omega t - \beta)) + constant * e^{-\frac{\Delta t}{\tau}} \tag{2.10}$$

Where τ is the thermal mass time constant, i.e. $\tau = \frac{(mc)_{thermal\ mass}}{\dot{m}c_p}$.

The short-term solution is represented by exponential term which is the natural response, given an initial value condition. The long-term sinusoidal behavior is the forced response to sinusoidal outside temperature of forcing frequency ω corresponding to one waveform per day, given by:

$T_{out}(t) = T_{mean} + \Delta T_{out}(\sin(\omega t))$. It can be seen that the mean long-term temperature is determined by the mean outside temperature T_{mean} and the temperature increase due to the internal heat gain, $T_E = \frac{qA}{\dot{m}c_p}$. There is also a phase shift β which represents the phase lag due to the thermal mass, as shown in figure 2-2. In fact, the phase shift is a function of the thermal mass time constant: $\beta = \tan^{-1}(\omega\,\tau)$. More importantly, the effect of the thermal mass in dampening the fluctuation of the air inside the room can be observed through the coefficient of the sine term, $\frac{\Delta T_{out}}{\sqrt{1+\omega^2\tau^2}}$. With larger thermal mass, a larger dampening occurs. The long-term steady-state solutions for a range of ventilation rates and outside temperature amplitudes were investigated and resulting temperatures are plotted below for the range of variable parameters given in table 2-2 below.

Parameters	Values
c, specific heat of thermal mass (J/kgK)	1-50
τ, thermal mass time constant (h)	0.02-24
ΔT_{out} (C)	1-10

Table 2-2: Parameters used in the simulation for thermal mass in equilibrium

For illustration, figure 2-2 shows the effect of different thermal masses on the damping factor and phase shift. With a larger thermal mass, the higher thermal time constant τ causes more damping (ΔT_{air} = 2.0°C compared to ΔT_{air} = 4.9°C) and a greater phase shift in the resulting room air temperature (β = 5.0 h compared to β = 3.4 h).

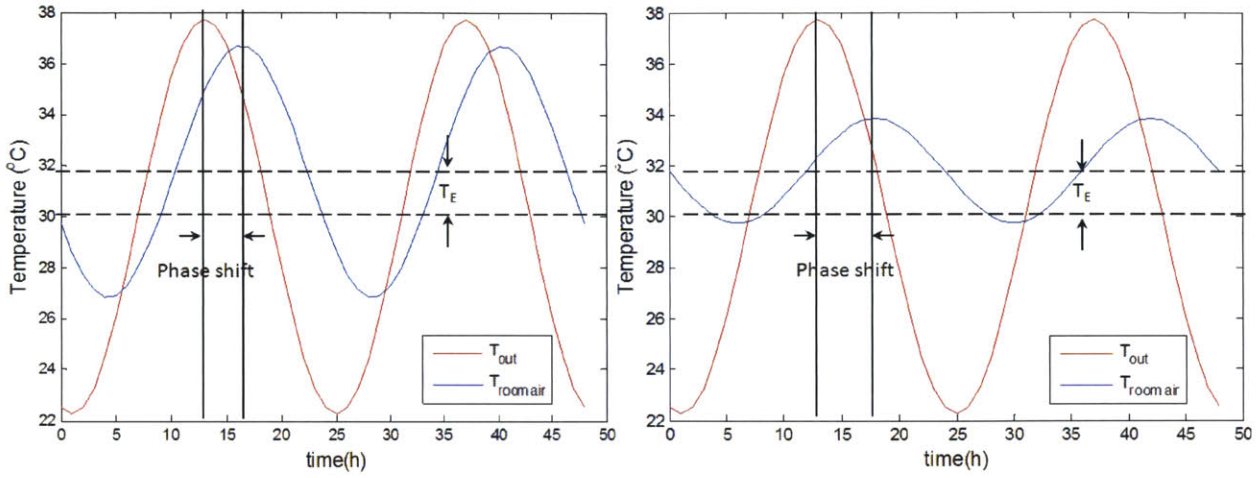

Figure 2-2: Temperature profiles for room air temperature in equilibrium with (a) normal thermal mass (c=880J/kgK, τ = 4.6 h), (b) high thermal mass (c=3x880J/kgK, τ =14 h)

As seen by dimensional analysis, different combinations of the variables within the common dimensionless parameter can give rise to the same system response. Consequently, the long-term response, in terms of the normalized resulting room temperature amplitude and phase shift, can be better analysed in terms of the variation in time constant due to the thermal mass. Figure 2-3 shows the collapse of the indoor temperature behavior for variation in time constant (thermal mass properties or ventilation rate). Note that the amplitude of indoor air temperature fluctuation has been normalized by the amplitude of outdoor temperature fluctuation. For this simulation, the internal heat gain was kept constant at 15W/m^2, which does not affect the indoor temperature fluctuation in itself, but causes a vertical temperature shift of $T_E = \frac{qA}{\dot{m}c_p}$. Figure 2-4 shows the phase shift expected of the response to a sinusoidal input signal.

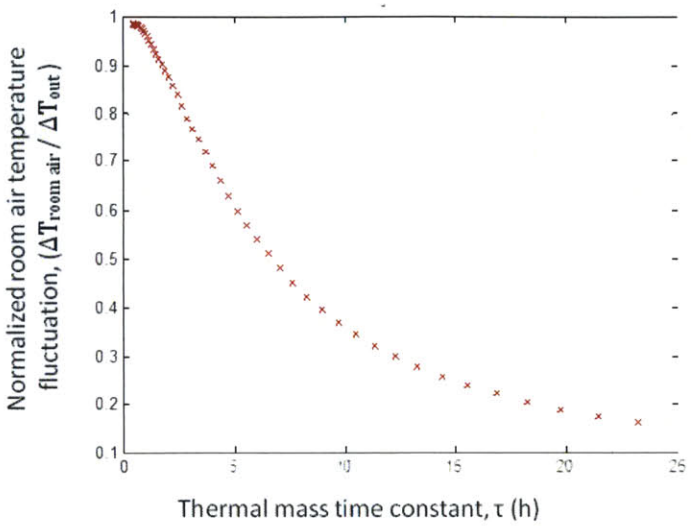

Figure 2-3: Normalized room temperature fluctuation with variation in time constant τ for room air temperature in equilibrium with thermal mass

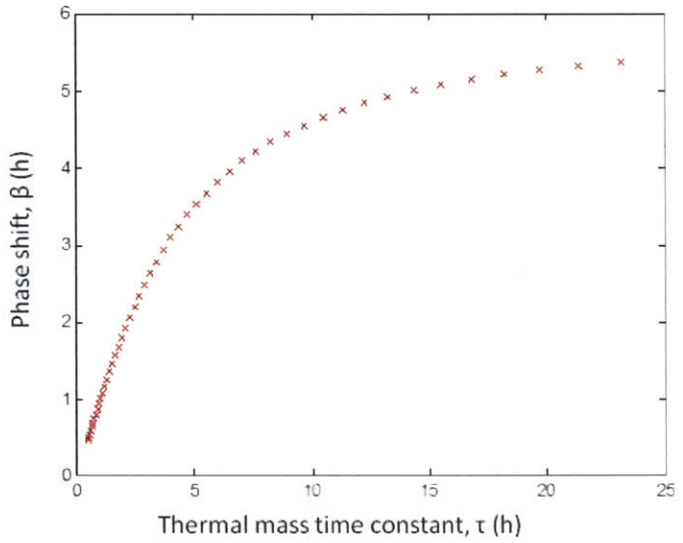

Figure 2-4: Phase shift of room temperature with variation in time constant τ for room air temperature in equilibrium with thermal mass

2.5 Thermal mass not in thermal equilibrium with the room air

When the thermal mass is not in thermal equilibrium with the room air, there is convection which follows Newton's law of cooling. As a result, the energy balance is given by equation 2.4. This is energy balance of the room air is coupled to that of the thermal mass through the convection heat transfer in equation 2.5.

$$mc\frac{dT(t)}{dt} = \dot{m}c_p\big(T_{out}(t) - T(t)\big) + hA\big(T_{thermal\,mass}(t) - T(t)\big) + q_i \quad \text{A} \tag{2.4}$$

$$(mc)_{thermal\,mass}\frac{dT_{thermal\,mass}}{dt} = hA\big(T(t) - T_{thermal\,mass}(t)\big) \tag{2.5}$$

While the room air can be assumed to be at a single uniform temperature due to other forms of heat transfer than thermal conduction, can the same be done for the thermal mass?

Air has a thermal diffusivity $\propto_{air}$ = 2e-5 m^2/s , whereas concrete has a thermal diffusivity of $\propto_{concrete}$= 2e-7 m^2/s. Moreover, air can allow for natural and forced convection as a means of heat transfer throughout its body, unlike a solid thermal mass and assuming no single-sided ventilation which will allow for thermal air stratification. Over the time-scale of 1 minute, the penetration depth($\sim\sqrt{\alpha t}$) is of 3mm, while over a time-scale of 1 hour, the penetration depth is of 2cm. Hence, one can assume gradation in temperature in the concrete and a well-mixed assumption for the air temperature.

In the case of our single-zone model, the question is whether the thermal mass can be idealized as a single lumped layer, and by how much the room air thermal response differs if the thermal mass needs to be discretized spatially into how many layers.

For the case when the thermal mass is one lumped model, it is possible to obtain an analytical solution by solving equations 2.4 and 2.5. From equation 2.4, it can be assumed that the first term is negligible as the air has a negligible internal energy compared to the internal heat gain and convected heat gain. Thus,

$$0 = \dot{m}c_p(T_{out}(t) - T(t)) + hA(T_{thermal\,mass}(t) - T(t)) + q_iA \tag{2.11}$$

Rearranging equation 2.11 gives:

$$T_{thermal}(t) = \left(1 + \frac{\dot{m}c_p}{hA}\right)T(t) - \frac{\dot{m}c_p}{hA}T_{out}(t) - \frac{q}{hA} \tag{2.12}$$

Substituting equation 2.12 into equation 2.11, the following differential equation for the room air temperature is obtained for a sinusoidal outside temperature:

$$\tau\frac{dT(t)}{dt} + \frac{\lambda}{1+\lambda}T(t) = \frac{\lambda}{1+\lambda}\,(T_{mean} + T_E) + \frac{\dot{\lambda}}{1+\lambda}\Delta T_{out}(\sin(\omega t) + \frac{\omega\tau}{\lambda}\cos(\omega t)) \tag{2.13}$$

Where $\tau = \frac{(mc)_{thermal\ mass}}{\dot{m}c_p}$ and $\lambda = \frac{hA}{\dot{m}c_p}$.

The analytical solution for this first-order differential equation can be obtained by superposing the homogenous solution and the particular solutions. The overall solution obtained is as below, similar to that obtained by Yam [19]:

$$T(t) = T_{mean} + T_E + \Delta T_{out}\sqrt{\frac{\lambda^2+\omega^2\tau^2}{\lambda^2+\omega^2\tau^2(1+\lambda)^2}}\sin(\omega t - \beta) + constant * e^{-\lambda/(1+\lambda)\omega\tau} \quad (2.14)$$

Where $\beta = \tan^{-1}(\frac{\lambda^2\omega\tau}{\lambda^2+\omega^2\tau^2(1+\lambda)})$

The exponential term represents the homogenous solution while the independent and trigonometric terms represent the particular solutions, which can be obtained using the method of undetermined coefficients [20] to solve for the step forcing term and the trigonometric forcing term. The corresponding explicit equation for the thermal mass temperature is obtained by substituting the above in equation 2.12:

$$T_{thermal}(t) = \left(1 + \frac{\dot{m}c_p}{hA}\right)\left(T_{mean} + T_E + \Delta T_{out}\sqrt{\frac{\lambda^2+\omega^2\tau^2}{\lambda^2+\omega^2\tau^2(1+\lambda)^2}}\sin(\omega t - \beta) + constant * e^{-\frac{\lambda}{(1+\lambda)\omega\tau}}\right) - \frac{\dot{m}c_p}{hA}(T_{mean} + \Delta T_{out}\sin(\omega t)) \quad - \frac{qA}{hA} \quad (2.15)$$

From the explicit solutions for the air and thermal mass temperatures, it can be seen that once the transient dies out, the air temperature has a maximum and minimum as below:

$$T_{\max_{air}} = T_{mean} + T_E + \Delta T_{out}\sqrt{\frac{\lambda^2+\omega^2\tau^2}{\lambda^2+\omega^2\tau^2(1+\lambda)^2}} \quad (2.16)$$

$$T_{\min_{air}} = T_{mean} + T_E - \Delta T_{out}\sqrt{\frac{\lambda^2+\omega^2\tau^2}{\lambda^2+\omega^2\tau^2(1+\lambda)^2}}. \quad (2.17)$$

Comparatively, the thermal mass temperature has a maximum and minimum as below:

$$T_{\max_{t\,mass}} = \left(1 + \frac{\dot{m}c_p}{hA}\right)\left(T_{mean} + T_E + \Delta T_{out}\sqrt{\frac{\lambda^2+\omega^2\tau^2}{\lambda^2+\omega^2\tau^2(1+\lambda)^2}}\right) + \frac{\dot{m}c_p}{hA}(T_{mean} + \Delta T_{out}) - \frac{qA}{hA} \quad (2.18)$$

$$T_{\min_{t\,mass}} = \left(1 + \frac{\dot{m}c_p}{hA}\right)\left(T_{mean} + T_E - \Delta T_{out}\sqrt{\frac{\lambda^2+\omega^2\tau^2}{\lambda^2+\omega^2\tau^2(1+\lambda)^2}}\right) + \frac{\dot{m}c_p}{hA}(T_{mean} - \Delta T_{out}) - \frac{q}{hA} \quad (2.19)$$

These limits can be used to define the domain of the state space of the temperatures during the optimization part.

As can be seen the dimensionless parameters identified by the dimensional analysis, namely $\tau = \frac{mc}{\dot{m}c_p}$ and $\lambda = \frac{hA}{\dot{m}c_p}$, appears here too. A generalization of the thermal behavior, in terms of the increase indoor air temperature fluctuation and its phase shift with respect to the outdoor air temperature, of a continuously ventilated room can thus be made based on these parameters. Figure 2-5 shows the collapse of the indoor temperature behavior for variation in time constant (thermal mass properties or ventilation rate) and convective heat transfer parameter λ (heat transfer coefficient and ventilation rate). As parameter λ goes to infinity, i.e. h goes to infinity, the thermal mass is perfectly coupled to the air temperature, such that there is thermal equilibrium. This gives the same collapse as in figures 2-3 and 2-4. The values used to generate the plots in figures 2-5 and 2-6 are given in table 2-3. Important observations which can be drawn from figures 2-5 and 2-6: for typical values of λ (0.2 for low h=3W/m^{2}K and high ACH=15 roomful/h to 13 for high h=15 W/m^{2}K and low ACH=1 roomful/h) and a building with thermal mass time constant of 13h, this gives a damping factor of outdoor fluctuation of half, and a low phase-shift of 1 hour or so. For that same range of λ, increasing the time constant, through a higher thermal mass, does not improve the damping. Another interesting observation is that for same range of λ, the phase shift increases then decays to zero with increasing thermal mass or time constant [19].

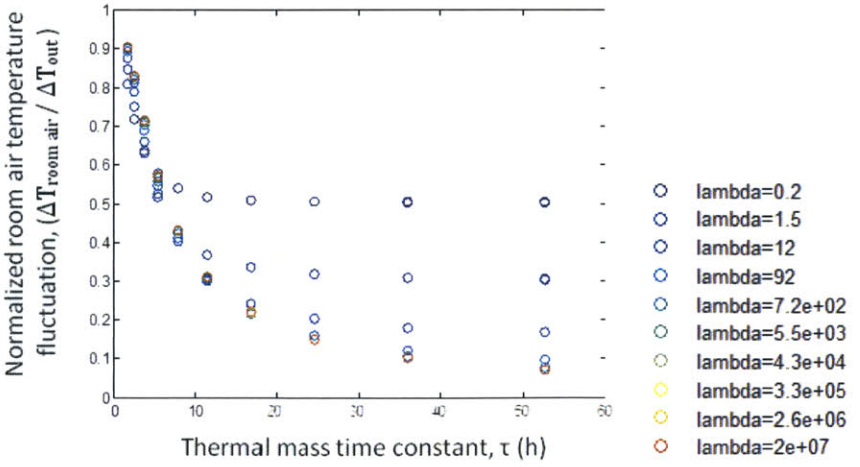

Figure 2-5: Normalized room temperature fluctuation with variation in time constant τ and convective heat transfer number λ

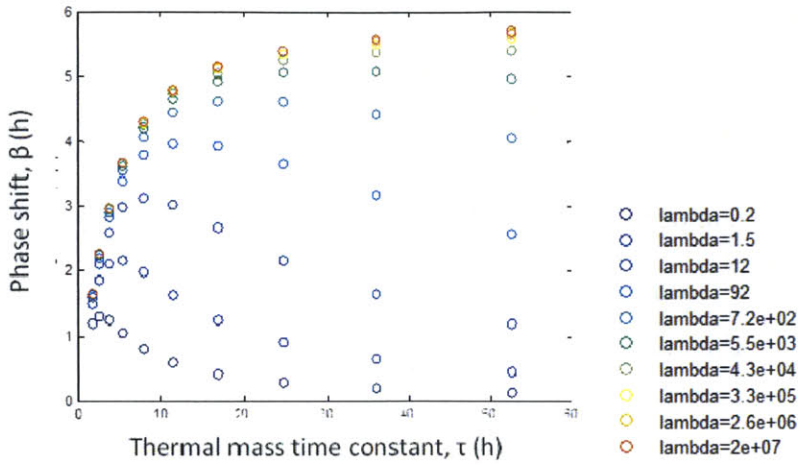

Figure 2-6: Phase shift of indoor air temperature with variation in time constant τ and convective heat transfer number λ

Parameters	Values
c, specific heat of thermal mass (J/kgK)	1-3000
thal, thermal mass time constant (h)	0.02-53
ΔT_{out} (C)	1-10
h, heat coefficient (W/m^2K)	$1\text{-}10^8$

Table 2-3: Parameters used in the simulation for thermal mass not in equilibrium

2.6 Numerical methods and solutions

While analytical solutions are faster to compute, numerical solutions are needed when there are no general closed-form solutions to the differential equations, when the disturbances are not periodic, or when control decisions or calculations occur at small time-steps. Example of these are when then the thermal mass cannot be considered as a lumped capacity or the differential equations are coupled and non-linear, when the outside temperature is not sinusoidal or it is cumbersome to find the coefficient of the Fourier series representing it, or when the heating and cooling loads need to be calculated at small time-steps. The analytical solutions for the lumped capacity case developed previously in the chapter can however be used to validate the numerical methods and determine the discretization level needed for sufficient accuracy. The analytical solution presents a caveat as it has to be solved as an initial value problem to determine the constant term for different initial conditions at each period time-step, which turns out to be more

computationally expensive in MATLAB than time-stepping using finite difference numerical solutions.

The heat energy balance for the room control volume is coupled to the differential equation governing heat diffusion through the thermal mass. Solving these coupled ordinary differential equations can be solved analytically as has been done above. However, solving them for a number of sequential time-steps to get the temperature values throughout hours and days can be tedious as the explicit equations for each variable need to be written out for different initial conditions. Hence a time-advancing scheme can be used to solve these coupled ordinary equations numerically using finite difference method. The Crank-Nicholson scheme is used as it is second order accurate in time: it uses the average temperature over the duration of the time-step and is an average of the forward and backward Euler method. In iteration notation, equation 2.4 becomes:

$$mc\frac{\frac{(T^{t+1}+T^{t})}{2}}{\Delta t} = \dot{m}^{t}c_{p}\left(\frac{T_{out}^{t+1}+T_{out}^{t}}{2} - \frac{(T^{t+1}+T^{t})}{2}\right) + hA(T_{t\,mass}^{t} - \frac{(T^{t+1}+T^{t})}{2}) + q_{i}^{t}A \qquad (2.20)$$

The corresponding equation for the energy balance around the thermal mass is:

$$(mc)_{t\,mass}\frac{\frac{(T_{t\,mass}^{t+1}+T_{t\,mass}^{t})}{2}}{\Delta t} = hA(\frac{(T^{t+1}+T^{t})}{2} - \frac{(T_{t\,mass}^{t+1}+T_{t\,mass}^{t})}{2}) \qquad (2.21)$$

On the other hand, there can be a temperature gradient within the thermal mass. This is the case when the internal resistance to heat transfer is small compared to the external resistance. This ratio is represented by the dimensionless Biot number, $Bi = \frac{hL}{k}$. Unless Bi<<1, the internal resistance is not negligible and there is a temperature gradient. This heat diffusion is represented by a parabolic partial differential equation with equation 4 as one of the boundary conditions:

$$\frac{\partial T_{t\,mass(x,t)}}{\partial t} = \propto \frac{\partial^{2} T_{t\,mass\,(x,t)}}{\partial x^{2}} \qquad (2.22)$$

Where $\propto = \frac{k}{\rho c_{tmass}}$.

With Neumann boundary conditions:

(i) At top slab surface, x=0: $-k\frac{dT_{t\,mass}}{dx}|_{x=0} = hA(T_{air} - T_{t\,mass}|_{x=0})$;

(ii) At bottom slab surface, x=L, slab thickness: $\frac{dT}{dx}|_{x=L} = 0$, since the interface of the concrete to the ground can be assumed adiabatic.

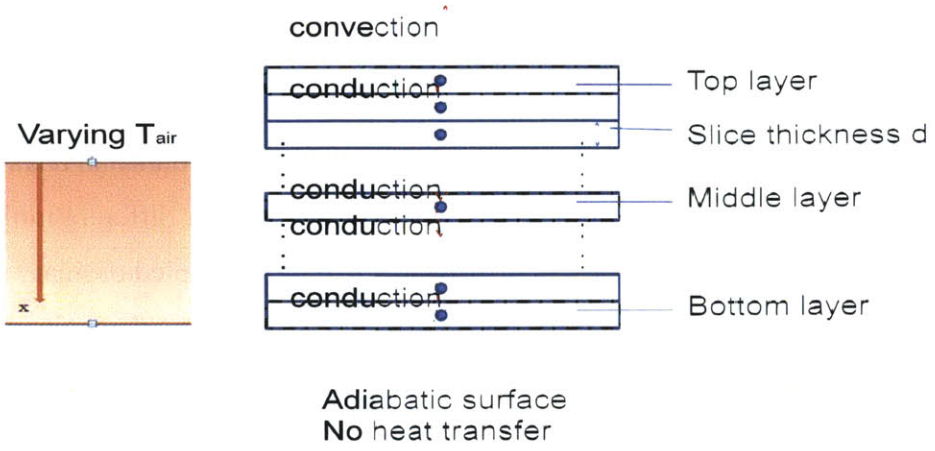

Figure 2-7: Multi-slice representation for thermal mass

An analytical solution to this coupled partial differential equation problem is hard formulate for multiple slices of thermal mass as it will require convolution of the thermal responses of the individual thermal mass slices together. Comparatively, a numerical solution can easily be implemented using finite difference. For the space and time discretization of equation 2.22, the Crank Nicholson method can be used. It is second-order accurate in both space and time. The heat diffusion equation is essentially an energy balance which can be done for each thermal mass slice. The bottom and top slices have slightly different energy balances because of the boundary conditions.

Middle slices:

$$\frac{mc\,(T^{t+1}_{slice\,x} - T^{t}_{slice\,x})}{\Delta t} = \frac{kA}{d}(\bar{T}_{slice\,x+1} - \bar{T}_{slice\,x}) + \frac{kA}{d}(\bar{T}_{slice\,x-1} - \bar{T}_{slice\,x}) \qquad (2.23)$$

Top slice:

$$\frac{mc\,(T^{t+1}_{slice\,x=1} - T^{t}_{slice\,x=1})}{\Delta t} = \frac{kA}{d}(\bar{T}_{slice\,x=2} - \bar{T}_{slice\,x=1}) + hA(\bar{T}_{air} - \bar{T}_{slice\,x=1}) \qquad (2.24)$$

Bottom slice:

$$\frac{mc\,(T^{t+1}_{slice\,x=N} - T^{t}_{slice\,x=N})}{\Delta t} = \frac{kA}{d}(\bar{T}_{slice\,x=N-1} - \bar{T}_{slice\,x=N}) \qquad (2.25)$$

Where $\bar{T} = \frac{T^{t}+T^{t+1}}{2}$.

For N slices, these energy balances result in a system of N linear equation of the form $[A][T^{t+1}] = [C][T^t] + [Q]$, where A and C are tridiagonal NxN matrices, and Q is an Nx1 vector representing non-conduction heat transfer terms. For our case this includes the convection term for the top slice x=1.

For instance, for a thermal mass with 5 slices, the A, C and Q matrices will be as follows:

$$A = \begin{bmatrix} mc + \frac{kA\Delta t}{2d} + \frac{hA\Delta t}{2d} & -\frac{kA\Delta t}{2d} & 0 & 0 & 0 \\ -\frac{kA\Delta t}{2d} & mc + \frac{kA\Delta t}{d} & -\frac{kA\Delta t}{2d} & 0 & 0 \\ -\frac{kA\Delta t}{2d} & -\frac{kA\Delta t}{2d} & mc + \frac{kA\Delta t}{d} & -\frac{kA\Delta t}{2d} & 0 \\ 0 & 0 & -\frac{kA\Delta t}{2d} & mc + \frac{kA\Delta t}{d} & -\frac{kA\Delta t}{2d} \\ 0 & 0 & 0 & -\frac{kA\Delta t}{2d} & mc + \frac{kA\Delta t}{2d} \end{bmatrix}$$

$$C = \begin{bmatrix} mc - \frac{kA\Delta t}{2d} - \frac{hA\Delta t}{2d} & \frac{kA\Delta t}{2d} & 0 & 0 & 0 \\ \frac{kA\Delta t}{2d} & mc - \frac{kA\Delta t}{d} & \frac{kA\Delta t}{2d} & 0 & 0 \\ 0 & \frac{kA\Delta t}{2d} & mc - \frac{kA\Delta t}{d} & \frac{kA\Delta t}{2d} & 0 \\ 0 & 0 & \frac{kA\Delta t}{2d} & mc - \frac{kA\Delta t}{d} & \frac{kA\Delta t}{2d} \\ 0 & 0 & 0 & \frac{kA\Delta t}{2d} & mc - \frac{kA\Delta t}{d} \end{bmatrix}$$

$$Q = \begin{bmatrix} hAT_{air}\Delta t \\ 0 \\ 0 \\ 0 \\ 0 \end{bmatrix}$$

It is necessary to find numerical methods for solving the differential equations, which are stable and accurate. With the Crank-Nicholson scheme which is unconditionally stable and second-order accurate in time and space, relatively big time-step and few slices can be used. However, there is a compromise which needs to be made in terms of convergence to the accurate solution,

as accuracy is lost thus. A time step of 7 minutes was seen to be fast and accurate enough. While the explicit forward Euler is unstable with high Fourier number with time-step of 7 minutes, the Crank-Nicholson scheme is not. Figure 2-8 shows that a space discretization of 10 slices was seen to be accurate enough, using the same way to define accuracy, which occurred for Biot number<1/2.

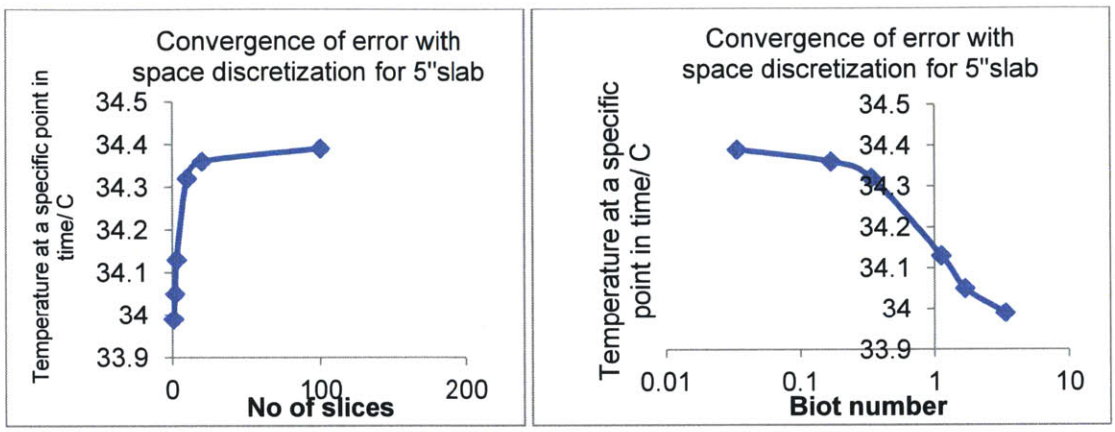

Figure 2-8: Convergence of errors for different levels of thermal mass discretization as a function of (a) number of slices used, (b) the corresponding Biot number

2.7 Heat transfer coefficient

A heat transfer coefficient, h is used to characterize the heat transfer between the thermal mass and the room air. While air itself, being transparent, does not take part in radiative heat transfer, it is assumed that the heat radiated between surfaces in the room eventually end up being convected into the room air. Thus, h represents the combined value for convection and radiation.

$$h = h_{rad} + h_{conv} \tag{2.26}$$

The radiation coefficient can be computed using the linearized Stefan-Boltzmann law:

$$h_{rad} = 4\varepsilon\sigma {T_{avg}}^3 \tag{2.27}$$

Where σ, the Stefan-Boltzmann constant = $5.67\text{x}10^{-8}$ W/m^2K^4,

T_{avg} is the average temperature of the thermal mass surface and other radiating surface in kelvin (K),

ε, the effective emissivity of the these 2, assuming that they are large and parallel to each other, such that [18]

$$\varepsilon = \frac{1}{\frac{1}{\varepsilon_{tmass\,surface}} + \frac{1}{\varepsilon_{other\,surface}} - 1} \tag{2.28}$$

For a concrete surface, ε ~0.8, and assuming a range of T_{avg} of 8-30°C, h_{rad} is of the order of 5W/m^{2}K.

The convective heat transfer coefficient is less easily defined as it depends on the air-flow regime within the building, and whether it is buoyancy-driven or dominated by forced convection. Numerous correlations exist for different surfaces. For our room model, where the thermal mass is assumed to be most significant in the floor and ceiling, those for stably-stratified horizontal surfaces apply (warm air above cool floor) and for buoyant-flow from horizontal surfaces (cool air above a warm floor). According to Beausoleil, a convection correlation can be derived including both as follows using the Hammond correlation [21]:

$$h_{conv,buoyant} = \left(\left\{ \left[1.4 \left(\frac{\Delta T}{D_h} \right)^{\frac{1}{4}} \right]^6 + \left[1.63 \Delta T^{\frac{1}{3}} \right]^6 \right\}^{1/2} + \left\{ \left[\frac{T_s - T_{diffuser}}{\Delta T} \right] [0.159 + 0.0116(ACH)^{0.8}] \right\}^3 \right)^{1/3} \tag{2.29a}$$

$$h_{conv,stratified} = \left(\left\{ 0.6 \left(\frac{\Delta T}{D_h^2} \right)^{\frac{1}{5}} \right\}^3 + \left\{ \left[\frac{T_s - T_{diffuser}}{\Delta T} \right] [0.159 + 0.0116(ACH)^{0.8}] \right\}^3 \right)^{1/3} \tag{2.29b}$$

$$h_{conv} = \left(h_{conv,buoyant}^3 + h_{conv,stratified}^3 \right)^{1/3} \tag{2.29c}$$

Where ΔT is the absolute value of the surface-air temperature difference, D_h (m) is the hydraulic diameter of the horizontal floor or ceiling such that D_h= 4 x Area/Perimeter, T_s is the thermal mass surface temperature, $T_{diffuser}$ is the ventilation air (outdoor) temperature, ACH is the air change rate in roomful/h.

The most influential parameters in equations 2.29a and 2.29b above are ΔT and T_s-$T_{diffuser}$. When the windows are closed, only the first terms of equations 2.29a and 2.29b matter. Their values for a range of ΔT are plotted below. When windows are open and natural ventilation takes place (mechanically aided or not), the second terms need to be considered. Since $\frac{T_s - T_{diffuser}}{\Delta T} =$

$\frac{T_s - T_{out}}{T_s - T_{room\ air}}$ and $T_{room\ air}$ follows T_{out} as seen in section 2.5, $\frac{T_s - T_{diffuser}}{\Delta T}$ is of the order of unity. Consequently, for normal values of ACH less than 10 roomfuls/h, the second terms are negligible compared to the first terms. Hence, as seen in figure 2-9, for a reasonable of $T_{room} - T_{surface}$ values, h_{conv} can be approximated to be 3 W/m^2K.

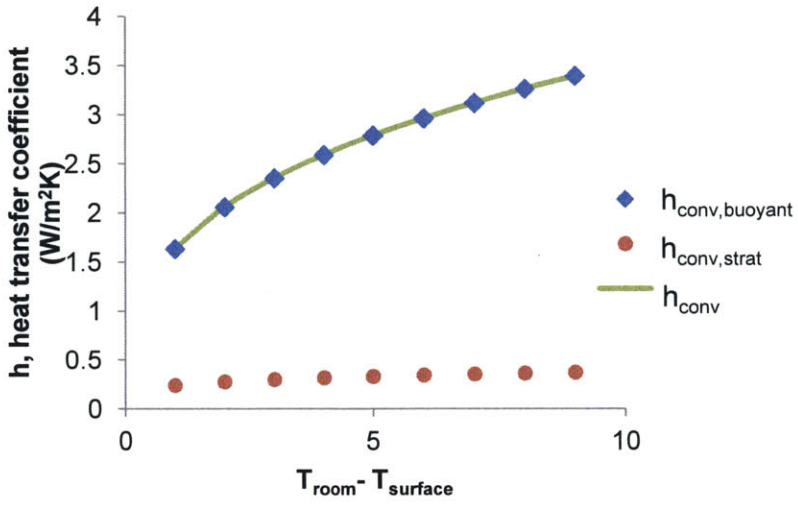

Figure 2-9: Convective heat transfer coefficient and its components for a range of ($T_{room} - T_{surface}$) values

Therefore, h=5+3=8W/m^2K is a reasonable value for the heat transfer coefficient, and that value would henceforth be used in simulations.

2.8 Effective heat transfer coefficient

As seen in the thermal modeling section 2.6, assuming a lumped-capacity model is valid for Biot number << 1. For a concrete slab of thickness of 5", thermal conductivity of 0.4W/mK and heat transfer coefficient of 8 W/m^2K, Bi=3.4. In fact, for a normal range of heat transfer coefficient and thermal conductivity, 10 slices are needed to approximate the conduction through the thermal mass numerically with reasonable accuracy. However, as will be seen in section 5, it is better to use fewer temperature states to reduce the temperature state space which needs to be covered. For this reason, an effective heat transfer coefficient is needed to approximate the internal conduction resistance throughout the thermal mass, such that only its top slice temperature needs to be defined.

An approximation of this internal conduction resistance can be made by considering the temperature disturbance towards the center of the slab in a time constant length of time. It has been shown that a good approximation to within 20% of the current value [22] for the internal resistance is given by

$$R_{internal} = \frac{\frac{L}{2}}{kA} \tag{2.30}$$

This enables us to write the net effect of the convective and conductive resistance using an effective heat transfer coefficient, i.e.

$$h_{eff} = \frac{hk}{k+\frac{hL}{2}} \tag{2.31}$$

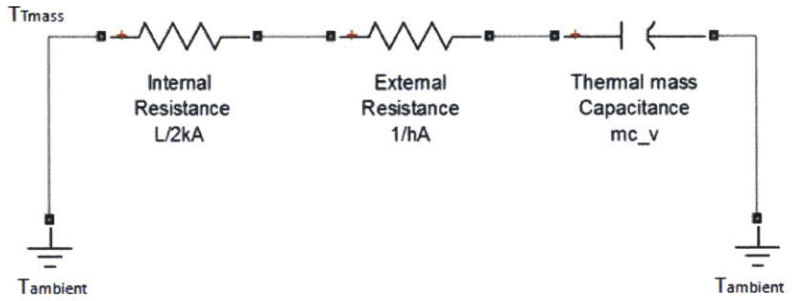

Figure 2-10: Approximate effective thermal circuit with lumped thermal mass

However, this transient thermal modeling has been validated for a constant ambient temperature boundary condition, and not a sinusoidal room temperature dictated by a naturally-ventilated room. Since it is unlikely that the coefficient of half can be used for this case, a resistance-capacitance model is pursued by using the electrical circuit analogy to the situation involving many slices of thermal mass. Note that with the last slice having a one-sided adiabatic boundary condition, the equations representing this circuit are similar to equations 2.20 (without representation for the internal heat gain), and 2.23-2.25. The situation is represented in the figure below for the case when number of slice, N=3.

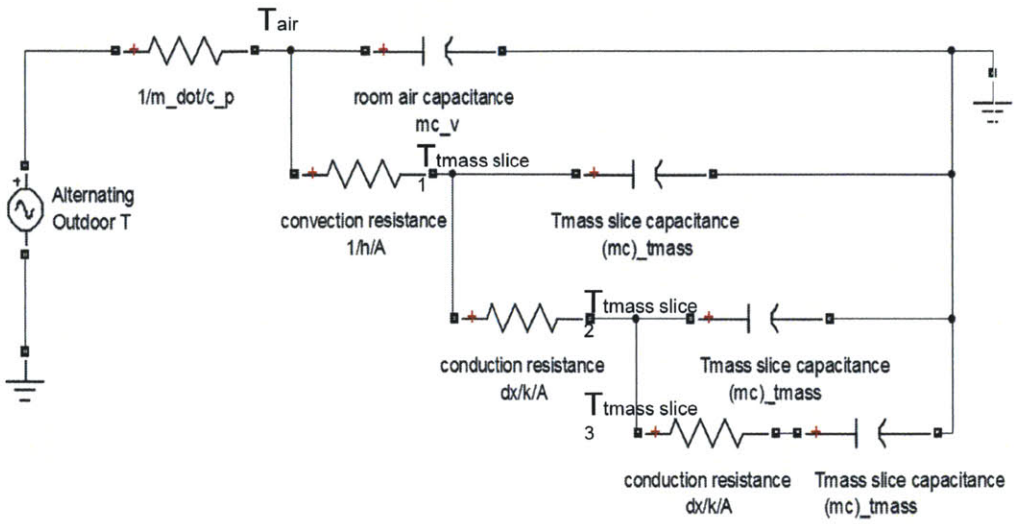

Figure 2-11: Circuit equivalent for a room thermal model with thermal mass divided into 3 slices

An equivalent circuit to above can be used to simplify the parallel sets of capacitors-resistors by considering their impedance. This can be done in the complex plane or the s-plane. A complex plane representation is possible for a steady-state A.C signal, which is the case for a sinusoidal outdoor temperature, for which the angular frequency $w = \frac{2\pi}{3600*24} = 7e-5\ rad/s$. For simplification, one can assume that each thermal mass slice is of similar thickness, each with a capacitance C and resistance R.

In the complex-plane,

$$Capacitor\ impedance, Z_C = 1/jwC \tag{2.32}$$

$$Resistor\ impedance, Z_R = R \tag{2.33}$$

The rules for impedance Z_1 and Z_2 in parallel and series are:

$$Z_{series} = Z_1 + Z_2 \tag{2.34}$$

$$Z_{parallel} = \frac{Z_1 Z_2}{Z_1 + Z_2} \tag{2.35}$$

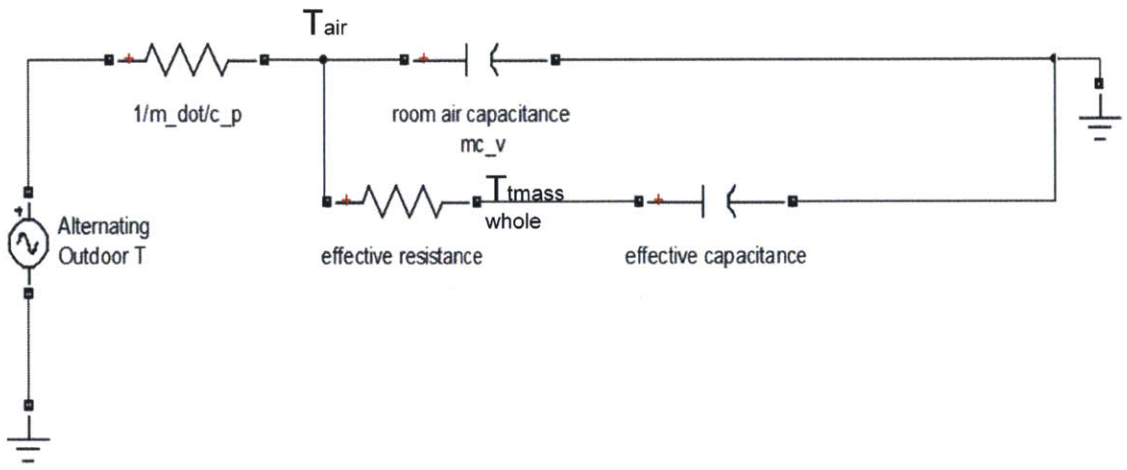

Figure 2-12: Circuit equivalent for thermal model of a room with effective lumped capacity model of thermal mass

An effective impedance representing the simplification of the circuit from figure 2-11 to figure 2-12 was derived using equations 2.34 and 2.35, with the symbolic simplification done in Maple software:

$$Z_{effective} = \frac{(C^2R^2w^2+5)R}{C^4R^4w^4+10C^2R^2w^2+9} - j\left(\frac{C^4R^4w^4+8C^2R^2w^2+3}{wC(C^4R^4w^4+10C^2R^2w^2+9}\right) \tag{2.36}$$

Since the terms containing w are very small, e.g. $C^2R^2w^2 < 1$ for typical values of thermal mass parameters, this can be simplified to an effective impedance, which can be broken down in an effective resistance and capacitance:

$$Z_{effective} = \frac{5R}{9} - j\left(\frac{1}{3wC}\right) \tag{2.37}$$

$$R_{effective} = \frac{5R}{9} \tag{2.38}$$

$$C_{effective} = 3C \tag{2.39}$$

This indicates that for a steady state A.C signal representation of a typical ventilated room, the thermal mass circuit representation can be reduced to an effective resistance with its capacitance unchanged. Compared to equation 2.30 which gives an approximate coefficient of 0.5, this yields a different coefficient of 0.185, as for the thermal mass of thickness L divided into 3 slices, the effective resistance is:

$$R_{effective} = \frac{5R}{9} = \frac{5}{9}\frac{\frac{L}{3}}{kA} = \frac{0.185L}{kA} \tag{2.40}$$

Similar complex-plane simplification was carried out for thermal masses divided into a range of slice numbers. A sample Maple code used for this simplification can be found in appendix A. The resulting equivalent coefficients are shown below in figure 2-13. This shows that dividing the thermal mass into more than 10 slices does not bring much change in the equivalent coefficient. Since a slice number of 10 was found to be sufficient spatial discretization for a reasonable level of accuracy for a range of thermal mass parameters, a coefficient of 0.29 is chosen to represent the effective circuit. Hence, this gives a "penetration depth" of 0.29L, and an effective heat transfer coefficient of 4.0 W/m^{2}K for an original heat transfer coefficient of 8 W/m^{2}K.

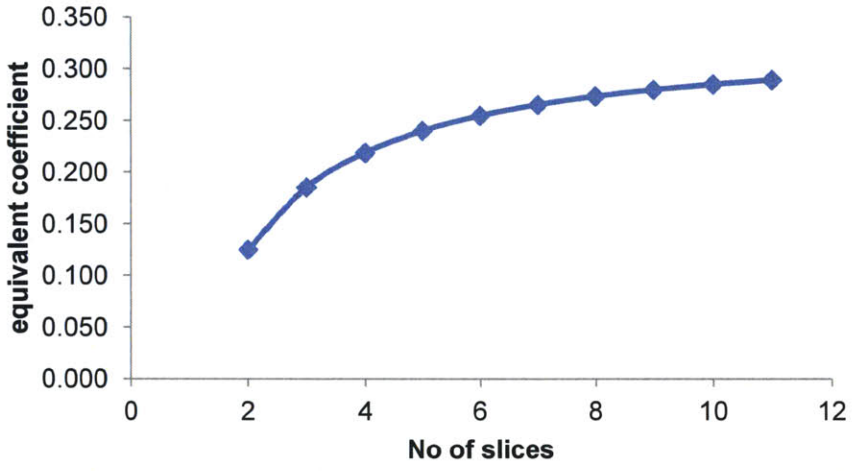

Figure 2-13: Equivalent coefficient for effective lumped capacitance model for thermal mass

For validation, a thermal circuit with 10 slices with the original heat transfer coefficient and another thermal circuit with 1 slice with the effective heat transfer coefficient were simulated and compared using Simulink, and shown. Note that the Simulink scope graph results below show the temperature values as referenced from a mean outdoor temperature of 0.

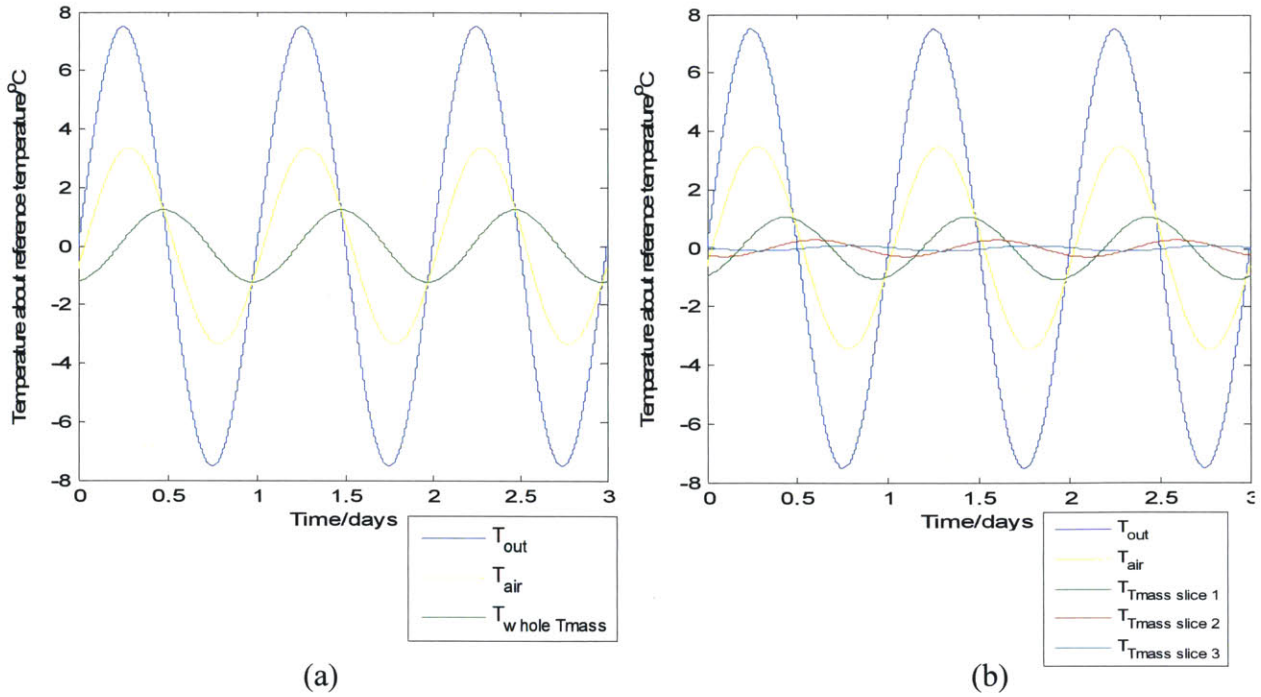

Figure 2-14: Temperature or voltage profiles at identified circuit nodes in (a) figure 2-11 and (b) figure 2-12

Chapter 3

Coupled airflow and thermal mass modeling at building level

3.1 Multi-zone energy modeling

The simplified assumptions of a multi-zone model make it suitable enough for fast computation of the bulk flow in the whole building, yet accurate enough to be able to capture the temperature and airflow differences between different critical zones. Results from multi-zone modeling are sufficient for comfort estimates without the need for CFD simulations, which are more time-consuming [23]. Each zone considers the air as an ideal gas, and as well-mixed with uniform density and temperature. The multi-zone modeling is carried out by solving the coupled airflow-thermal and mass models at incremental time-steps.

The airflow solution with mass balance is first determined by solving for the pressure differences between neighboring zones, which depend on their respective air-flow rates. This is determined by the following non-linear equation (Yuan, 2007):

$$airflow\ rate,\ \dot{m}_{ij} = C * (\Delta P)^{1/2} \tag{3.1}$$

where C, the discharge coefficient, is dependent of the type of opening (rooftop, internal openings, windows) lining the zone,
ΔP is static pressure difference between zone I and j,
Airflow rate $\dot{m}_{ij}$ is between zone I and j.

Each zone's net airflow rate obeys mass conservation law. Thus, the airflow rates through all the zones can be solved iteratively till convergence to the absolute criterion for residuals using the Newton-Raphson method, which can solve non-linear equations [24]. As done in CoolVent, the

convergence rate can be improved by incorporating the bisection method [24]. The pressure difference itself is temperature-dependent as total pressure includes dynamic pressure (due to wind velocity) and static pressure, which is given eventually given by the ideal gas constitutive relation:

$$static\ pressure, P_s(Pa) = \rho_{(T)} gH = \frac{P_{atm}}{RT} \tag{3.2}$$

where g is the gravitational constant ($9.81 m/s^2$),
H is the relative zone elevation (m),
P_{atm} is the atmospheric pressure (Pa),
R is the ideal gas constant (J/kgK),
T is the zone temperature in kelvin (K).

The zone temperatures can be obtained by solving for the coupled energy balances for all zones. Recall the energy balance for each zone i in a multi-zone model can be written thus:

$$mc_v \frac{\partial T_I}{\partial t} = \sum_j \dot{m}_{ji}\, c_p T_j - \sum_i \dot{m}_{ij}\, c_p T_i + S_i \tag{2.1}$$

where $\dot{m}_{ij}$ is mass flow rate from zone j to zone I,
T_j is air temperature of zone j,
T_i is air temperature of zone I,
S_i regroups heat fluxes from interfaces, solar and internal heat gain of zone I.
Note that the heat flux from the thermal mass interface to the zone air is calculated based on an energy balance on it, with conduction through thermal mass system dictated by:

$$\frac{\partial T}{\partial t} = \lambda \nabla^2 T \tag{2.22}$$

where T is the temperature of the space-discretized thermal mass material,
λ is its thermal diffusion coefficient.
The difference with thermal in a single-zone here is that the thermal mass acts as connection between the zones on either side. Hence, if both are present, the boundary condition at each extremity is set as a heat-flux Neumann condition. If not, the extremity connected to the ground or air is set as adiabatic.

Equations 3.1 and 2.1 for all the zones in the building result in linear matrix equations, which are solved for each zone's temperature and mass flow rate. Because of the interdependence of the mass flow rate and temperature, a numerical coupling strategy is needed for the solution. Two strategies exist: "Ping-pong" and "Onion". The "Ping-pong" strategy solves both sets of equations in sequence without iterations within each time-step, whereas the "Onion" strategy is more computationally expensive as it allows iteration. CoolVent implements the "Ping-pong" strategy as small time-steps are inherently needed to capture the nonlinear dynamics effect [25]. Thus the mass flow rates and temperatures are solved in two quick steps, by for instance, Newton-Raphson method and LU decomposition respectively. Convergence through the Newton Raphson method requires a convergence criterion: sum of mass flow rates through all zones, should sum to 0, with a tolerance of 10^{-6}. It is worth noting that In CoolVent, the thermal mass temperatures are solved for using the new values for the air temperatures. Hence, the air temperatures use the heat fluxes calculated from the old thermal mass temperatures. Because the time-step is small, the differences between the new and old temperatures are not so significant as to affect the thermal mass heat fluxes calculated.

3.2 Design Advisor and CoolVent description

Design Advisor is an online simulation user-friendly building design tool, aimed for use at the early design stage at which a high level of details of the building parameters and HVAC system is not available. Design Advisor enables the rapid simulation and analysis of different building designs and their impact on the energy consumption. More details can be obtained on its website (designadvisor.mit.edu) and in the works of past generations of students [14], [15]. The main difference between Design Advisor and CoolVent is in their program architecture: Design Advisor treats each room with different window orientation separately as a shoe-box, while CoolVent divides the building structure into interconnected zones. The goal of each software differs: Design Advisor provides a holistic design-oriented approach to knowing how the building envelope specification impacts energy consumption mainly in a non-naturally ventilated building, while CoolVent seeks to provide details of the airflow rate and temperature distribution throughout a naturally-ventilated building. Moreover, Design Advisor has a more detailed treatment of the heat flux, namely the wall, roof and window fluxes while CoolVent considers adiabatic conditions for the wall and roof, and a hard-coded U-value for the windows.

Additionally, Design Advisor has a daylighting simulation module, which provides daylighting images for the rooms and the ensuing lighting requirement. Because Design Advisor's calculations for these fluxes are done in locked classes of previously-written codes, the network architecture of CoolVent was implemented into the body of Design Advisor program and not the other way round, so as to be able to call upon the daylighting model, wall, window and roof modules. In effect, Design Advisor's HVAC loads module will be taken over by a natural ventilation module, which will provide zonal temperature and airflow predictions.

More details are given below on the aforementioned features of CoolVent and Design Advisor which are to be retained. Then, the architecture of the combined software is explained.

3.2.1 CoolVent

The current energy modeling done in Design Advisor does not currently take into consideration natural ventilation for different categories of building geometry. To cater to that, CoolVent, an existing package dedicated to natural ventilation modeling is being adapted and integrated into Design Advisor.

Building types

A number of different building geometries are considered: 1.Unconnected sides; 2. open-plan cross-ventilated floors; 3. Central atria; 4. Side atria, which are representative of chimneys. The definition of the dimensions of the atrium's opening can be changed to simulate airflow through ducts of different sizes, for instance.

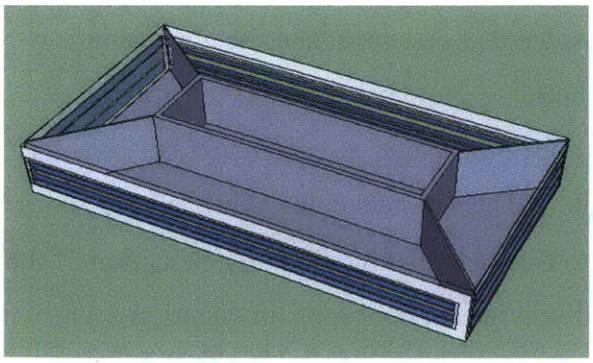

(a)

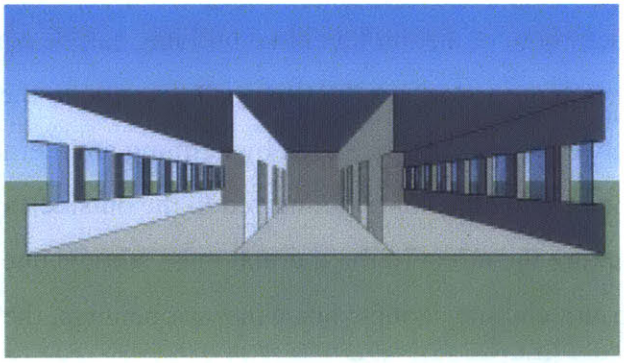

(b)

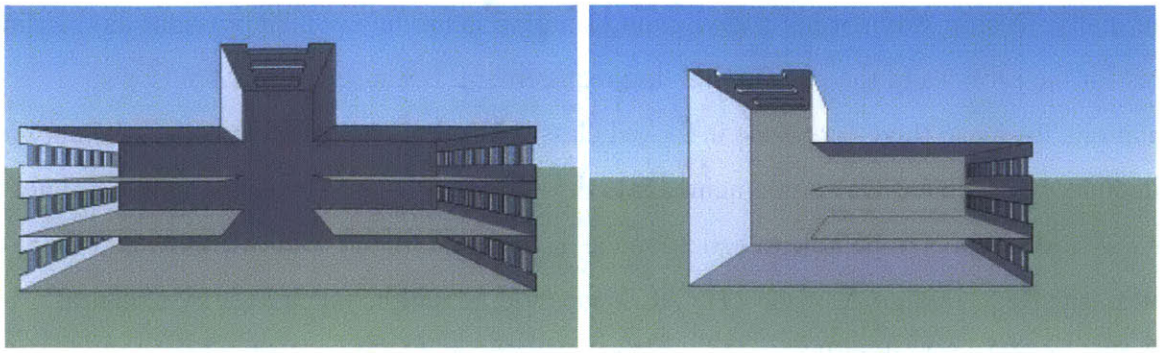

(c) (d)

Figure 3-1: Building types in CoolVent: (a) single-sided, (b) cross-ventilated, (c) atrium and (d) chimney

The building airflow and thermal simulation

This more accurate multi-zone modeling of natural ventilation would simulate wind-driven as well as buoyancy-driven flows, which is an important driving force in buildings with multiple floors and large temperature differences. Since the thermodynamics and the fluid dynamics are strongly coupled in a naturally-ventilated building, the airflow and temperature solutions are strongly coupled as well, and are solved concurrently.

Our modeling also has the option of specifying a mechanical aid to help natural ventilation. The options include user-defined light-duty, medium-duty or heavy-duty fans which are assumed to be situated in the atrium/chimney. Another option is letting CoolVent choose the best fan, which turns on when any zone's temperature overshoots a user-defined temperature set-point.

Each room or atrium level in a building can be considered as one zone, and the zones are interconnected as per the flow-path specific to the building geometry. The inner partitions between rooms are modeled by defining an internal opening discharge coefficient between the zones. Only the zones connected to the outside capture the solar heat gains, while all the zones capture the effect of the thermal mass storage due to floor and ceiling, with the exception of the atrium/chimney zones. For window openings, the discharge coefficient (C in equation 3.1), hence the pressure difference, is determined by the Swami and Chandra model [26] for given weather conditions, wind speed and direction.

The multi-zone modeling is carried out by solving the coupled airflow-thermal and mass models at incremental time-steps of 30s using the quasi-implicit Crank-Nicholson method time-discretization scheme.

Ventilation control options

Because it is detrimental to allow natural air-flow when the outside temperature is not optimal to occupant's thermal comfort, it is essential to control when natural ventilation is allowed. CoolVent has the possibility of including user-defined night-cooling and window operation strategies. Night-cooling is currently defined in the modeling by the closing (morning) and opening times (evening) of the windows at user-defined times. Another strategy would be to control at what temperature threshold (outdoor or zonal) the windows should be closed.

Thermal mass

Because the thermal mass of a building is considerable, it has an important influence on the transient behavior of the system's air-flow and temperature, due to the interaction between the air and the thermal mass. The original CoolVent has the choice of different thermal mass thicknesses and types (concrete, steel, and brick) for the floor and ceiling.

Because the modeling is multi-zonal, it allows thermal connection between floors through the thermal mass slabs in between them and models insulation with the ground for the lowest floor and insulation with the outside at the roof by setting the boundary conditions there as adiabatic in the thermal mass heat/energy balance. Figure 3-2 shows a sample snapshot in time of resulting airflow and temperature distribution in the zones and thermal mass slabs of an atrium-style building. Note that the skewedness of the thermal mass temperature profile results because the floor has an assigned heat transfer coefficient of 8 W/m^2K, while the ceiling's is 3 W/m^2K (Layer 10 is a floor connection while layer 1 is a ceiling connection). The exception arises for the ground (Tmasses 1 and 6) and top (Tmasses 5 and 10) thermal masses which are adiabatic. Hence, an accurate yet fast modeling of air flow requires a multi-zone approach with the thermal mass connections defined between floors.

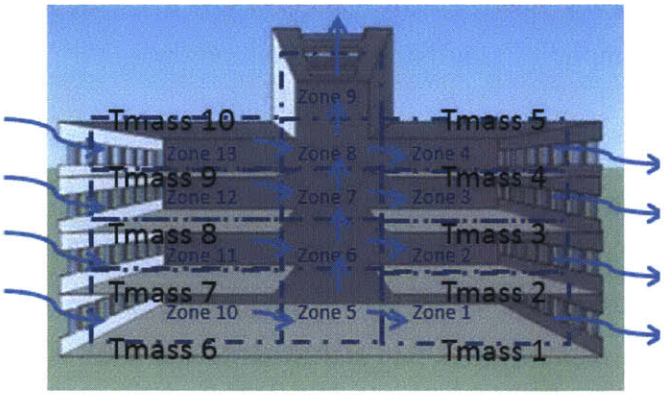

(a) Airflow directions

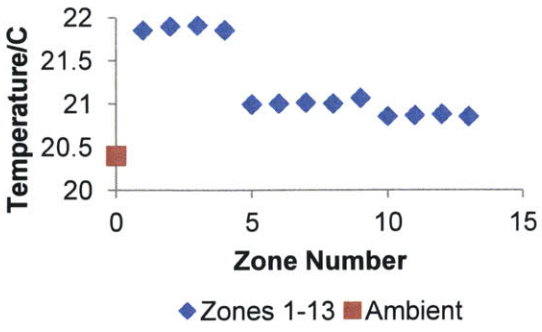

(b) Zonal Temperatures

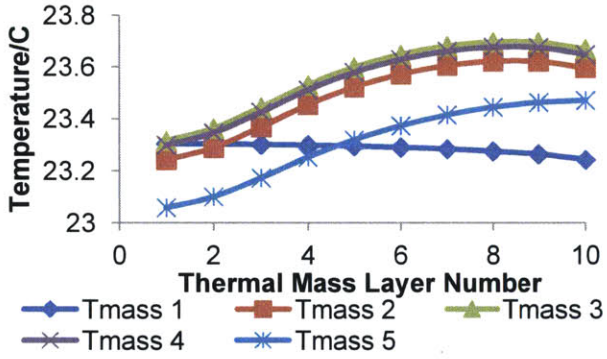

(c) Temperature distributions in right-hand floor slabs

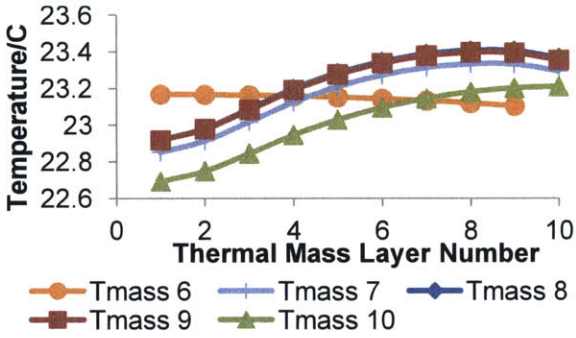

(d) Temperature distributions in left-hand floor slabs

Figure 3-2: Sample temperature distribution in the zones and relevant thermal masses (each consisting of 10 layers, with 1 the lowest) for a 4-floor atrium style building with airflow defined by the arrows in (a)

Improvement to numerical solving for thermal mass

The old CoolVent code solved equation 2.22, by using the explicit exponential solution for the energy balance of each thermal mass slice. A neater approach was implemented to solve for the thermal mass solutions using Thomas algorithm. This is possible because the differential equation 2.22 can be represented by a tri-diagonal banded matrix system, as a slice can only be connected to two other slices, and to one slice at the extremities. In fact, similar tridiagonal matrices to the A and C matrices discussed in section 2.6 are obtained when the space and time discretizations are done using the Crank-Nicholson method likewise. For the multi-zonal

modeling however, the thermal mass has convective heat fluxes from its top and bottom surfaces. Thus, if the thermal mass layer is discretized into 5 slices, the A matrix, C matrix and Q vector are represented by:

$$A = \begin{bmatrix} mc + \frac{kA\Delta t}{2d} + (\frac{hA\Delta t}{2d} \text{ or } 0) & -\frac{kA\Delta t}{2d} & 0 & 0 & 0 \\ -\frac{kA\Delta t}{2d} & mc + \frac{kA\Delta t}{d} & -\frac{kA\Delta t}{2d} & 0 & 0 \\ -\frac{kA\Delta t}{2d} & -\frac{kA\Delta t}{2d} & mc + \frac{kA\Delta t}{d} & -\frac{kA\Delta t}{2d} & 0 \\ 0 & 0 & -\frac{kA\Delta t}{2d} & mc + \frac{kA\Delta t}{d} & -\frac{kA\Delta t}{2d} \\ 0 & 0 & 0 & -\frac{kA\Delta t}{2d} & mc + \frac{kA\Delta t}{2d} + (\frac{hA\Delta t}{2d} \text{ or } 0) \end{bmatrix}$$

$$C = \begin{bmatrix} mc - \frac{kA\Delta t}{2d} - (\frac{hA\Delta t}{2d} \text{ or } 0) & \frac{kA\Delta t}{2d} & 0 & 0 & 0 \\ \frac{kA\Delta t}{2d} & mc - \frac{kA\Delta t}{d} & \frac{kA\Delta t}{2d} & 0 & 0 \\ 0 & \frac{kA\Delta t}{2d} & mc - \frac{kA\Delta t}{d} & \frac{kA\Delta t}{2d} & 0 \\ 0 & 0 & \frac{kA\Delta t}{2d} & mc - \frac{kA\Delta t}{d} & \frac{kA\Delta t}{2d} \\ 0 & 0 & 0 & \frac{kA\Delta t}{2d} & mc - \frac{kA\Delta t}{d} - (\frac{hA\Delta t}{2d} \text{ or } 0) \end{bmatrix}$$

$$Q = \begin{bmatrix} hAT_{zone\ below}\ \Delta t \text{ or } 0 \\ 0 \\ 0 \\ 0 \\ hAT_{zone\ above}\ \Delta t \text{ or } 0 \end{bmatrix} \tag{3.3}$$

Thomas algorithm makes use of the fact that entries of the matrix are zeros, except within the tri-band, to reduce computation time: while the normal methods to solve linear systems of equation is LU decomposition, it is inefficient for tridiagonal systems as pivoting about the zeros is unnecessary [24].

The Crank-Nicholson formulation for solving for the thermal mass solution was validated against the old original method, as shown in figure 3-3. The new zone air temperature solution is seen to

agree to within 0.2 ^{0}C. A comparison of the two aforementioned numerical methods of solving linear systems of equations, i.e. LU decomposition and Thomas Algorithm was done in figure 3.4. It can be observed that the Thomas Algorithm is consistently more efficient. The x-axis represents the number of floors used in the simulation. While increasing floor number represents an increase in number of slabs, it also represents increase in number of zones. As the thermal mass calculations only represent a fraction of the overall simulation, the saving in computational time increases but not significantly so for increasing number of floors.

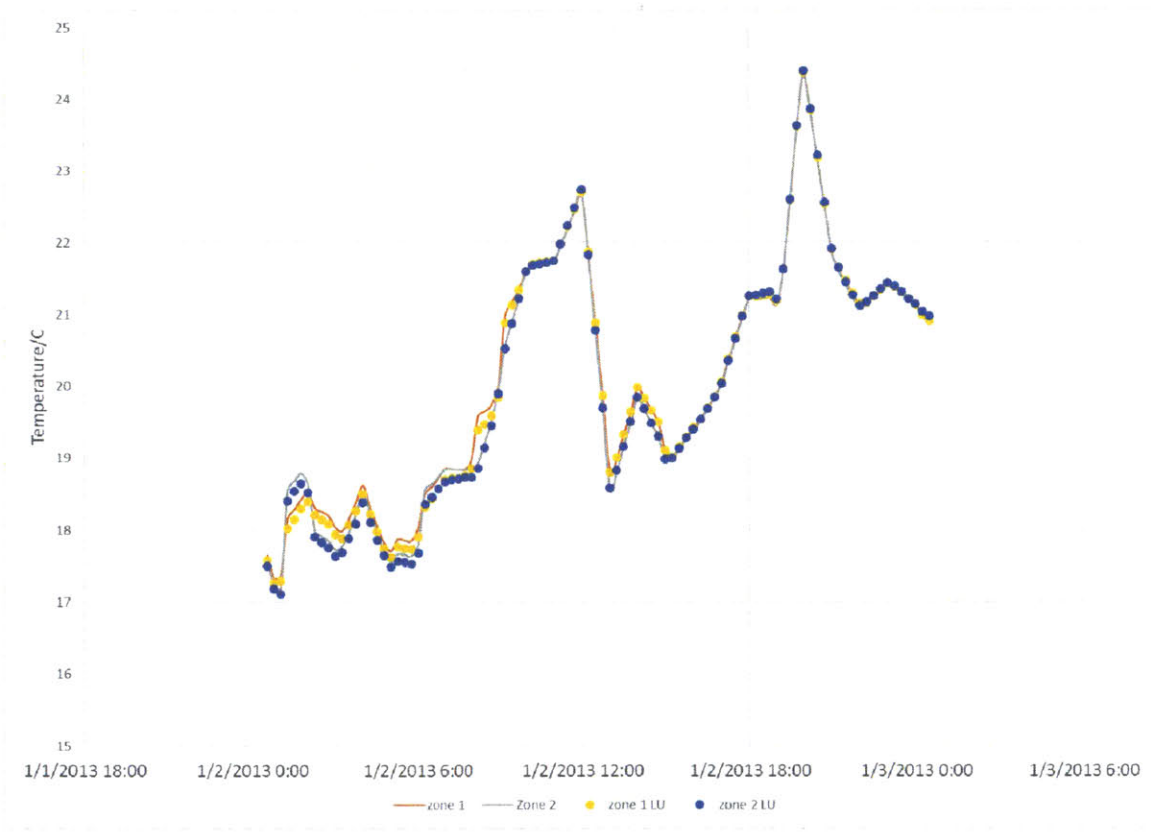

Figure 3-3: Comparison of resulting air temperatures of 2 selected zones within an atrium-style building for a sample day (the dots representing the improved solution with the Crank-Nicholson method, the lines represent the original solution)

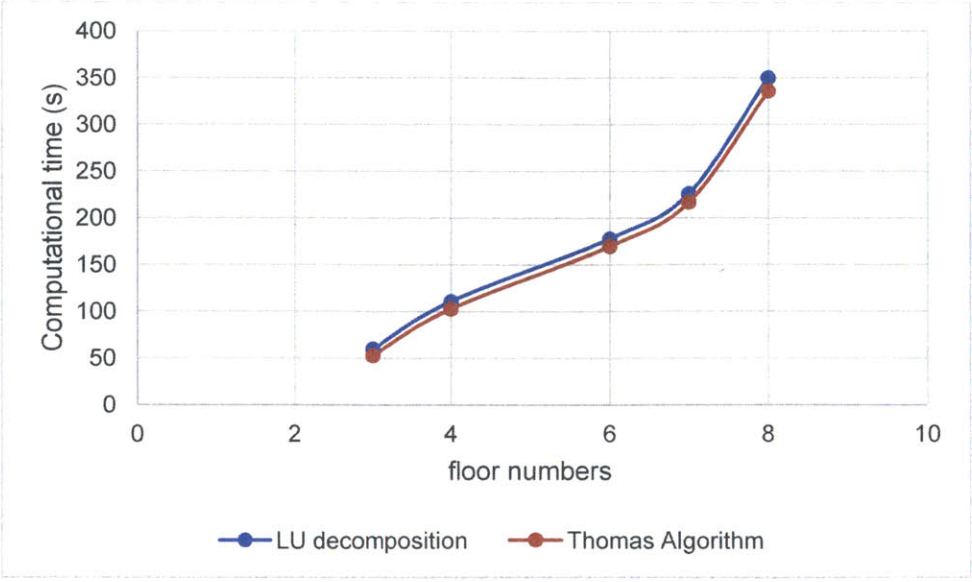

Figure 3-4: Comparison of computational time using 2 numerical methods for solving for thermal mass temperatures (LU decomposition in blue and Thomas Algorithm in red)

3.2.2 Design Advisor

Design Advisor's aim is to use first-order effects and the basic physics of the building components to predict the building energy consumption with mechanical ventilation and heating. The HVAC system kicks in when needed to meet thermal comfort, i.e. when the next-step temperature given by the energy-balance does not meet the thermal comfort standard. It also fixes the air change rate when needed. The relevant physics-based calculations for the overall energy balance and the different modules of the building (floor thermal mass, wall, window, roof) are given below. Note that these calculations are done for each room, which is considered as individual shoe-box models.

Overall Energy Balance

Design Advisor calculates zone temperatures every 60 seconds. The room temperature is given by the energy balance, which incorporates all the heat gains and heat fluxes:

$$T_{next} = \frac{mC_{in}*T_{in}+dt*\left(q_{const}+q_{tm}+q_{window}+q_{wall}+q_{roof}+T_{out}*mC_{out}*\frac{ACR}{3600}\right)}{dt*mC_{out}*\frac{AR}{3600}+mC_{in}} \quad (3.4)$$

where mC is the heat capacity of one roomful of air,

ACR is the air change rate in roomfuls per hour,

dt is the time step size (60 seconds),

q_{const} is the heat gain from internal loads (occupants, equipment, and light)

$q_{thermal\ mass}$, q_{window}, q_{wall}, q_{roof} are the heat fluxes from the thermal mass, the window, the wall, and the roof respectively. The thermal mass heat flux is calculated every 60 seconds, while the remaining fluxes are calculated every 15 minutes.

Window module

The heat flux conducted through the window and convected into the room is calculated by means of a resistor network to model the different heat transfers (radiation and conduction) from one window component to another. Different window types have different overall thermal resistance and can be made up from different options: with single, double or triple glazing; with a user-defined glass coating type; with or without blinds. When no blinds are present, there are radiation and convection heat exchanges between the environment and the outside of the window unit as well as between the room and the inside of the window. If a window with multiple glazing is chosen, radiation and conduction between the glass sheets are calculated, with only the air gap having non-negligible conduction resistance.

$$R_{overall} = \frac{R_{conv,out}R_{rad,out}}{R_{conv,out}+R_{rad,out}} + \sum_{gap=1}^{n} \frac{R_{cond,gap}R_{rad,gap}}{R_{cond,gap}+R_{rad,gap}} + \frac{R_{conv,in}R_{rad,in}}{R_{conv,in}+R_{rad,in}} \quad (3.5)$$

There is a resulting heat flux, due to the difference between the last window node layer's and the room air's temperature and. This heat flux which gets convected into the room is the q_{window} heat flux term in the energy balance.

The solar radiation heat flux which gets through the window is assumed to be 80% absorbed as a heat gain by the thermal mass, and 20% radiated back to the room air.

The presence of blinds adds more details to the heat flux calculation. The blinds in effect as another pane with the transmitted, absorbed and reflected radiation fraction through it computed according to user-defined blind geometry. This fraction is calculated by means of view factors between individual slats and between the blinds and the window or room, which are calculated using the crossed-strings method.

Wall module

Heat flux through the walls of the building is determined via a similar thermal circuit model. In fact, the wall is computationally considered as a single-glazing window with zero solar and infrared transmissivity, and with a user-defined R-value for its insulation level (R_{wall}). Similar to equation 3.5 for windows, heat is transferred to and from the wall on both sides via radiation and convection. The overall resistance is given by:

$$R_{overall} = \frac{R_{conv,out}R_{rad,out}}{R_{c,onv,out}+R_{rad,out}} + R_{wall} + \frac{R_{conv,in}R_{rad,in}}{R_{conv,in}+R_{rad,in}} \quad (3.6)$$

It should be noted that the convective heat transfer coefficient is given by published correlations for convection on building facades and natural convection. The radiative resistance is the linearized form of the radiation equation. More information on the values can be found in the Urban thesis [14].

Roof module

The roof module enables Design Advisor to take into consideration 3 roof technologies which have energy saving potential: bitumen, cool, and green roof. Details about these can be found in the works of a past generation student [15]. In brief, bitumen is an asphalt-based roof, cool roof is one with high solar reflectance and thermal emittance, while green roof is one covered with vegetation. All roof types have the option of roof insulation, with user-defined insulation material and location (top of bottom of roof). The main difference with the green roof is that layers of grass and soil are present on top. In terms of numerical modeling, the cool and bitumen roofs are modeled as concrete slab slices with the top one accepting a net heat gain, due to long-wave radiation and convective heat transfer. The green roof additionally accounts for radiation within the vegetation layer, evaporation from the soil and transpiration of the grass. The material properties used in Design Advisor for these three roof types can be found in the Ray thesis [15].

Daylighting module

Design Advisor has an advanced daylighting module which computes the sunlight illuminance levels throughout rooms with different window orientations, using the net illuminance calculated by the window module. It considers the three-dimensional reflections from building surfaces to generate a workplane illuminance level. More information on this can be obtained from the

works of a previous generation student [27]. The daylighting module allows the calculation of the lighting fixture load requirements needed to meet the illuminance level for a particular user-specified occupancy type and lighting control strategy. The hourly lighting load calculations affect the room energy balance in that the thermal energy generated by the lights is assumed to be equal to the electrical lighting load.

Net solar heat gain calculations

While CoolVent, like Design Advisor, makes use of ASHRAE's method for calculating the solar angle of incidence (θ) onto the building surface [28], Design Advisor's calculation steps for solar heat gain past that stage are more detailed:

(i) Overhang:

Design Advisor also has the option of adding an overhang to the windows. This has the effect of diminishing the direct and diffuse solar radiation reaching the window pane by a geometrical factor.

(ii) Incident solar flux:

CoolVent assumes that the reflected-incident radiation is negligible, and considers only the direct ($E_{direct,\ incident}$) and diffuse ($E_{diffuse,\ incident}$) solar radiations.

$$E_{direct,incident} = E_{direct,normal}\ cos\theta \tag{3.7}$$

$$E_{diffuse,incident} = Y\ E_{diffuse,horizontal} \tag{3.8}$$

where $Y = \max(0.45, 0.55 + 0.437cos\theta + 0.131\cos^2\theta)$

Comparatively, Design Advisor additionally calculates the reflected-incident radiation from the ground to the window surface as follows [14]:

$$E_{reflected,,incident} = E_{direct,normal}\ (C + sin\beta)\rho_g - \frac{1-cos\Sigma}{2} \tag{3.9}$$

where astronomical ratio C=0.118,

Ground reflectivity ρ_g=0.20,

Vertical surface tilt $\Sigma = 90^0$.

(iii) Window transmissivity:

CoolVent assumes an arbitrary value of 0.6 for the window transmissivity. Comparatively, Design Advisor allows a detailed definition of the windows and

computes the net radiation, allowing for the first set of internal internal reflections throughout the different layers. Spectrally-selective material coating defined by the user considers IR radiation, visible light, and solar-thermal radiation separately. In effect a net window bulk-behavior transmissivity value, or transmittance, is calculated for a user-defined window type. For instance, for a clear single-glazed window, the transmittance results to 0.77.

(iv) Blinds:

In Design Advisor, the user has the option of including an interior blind, which can potentially respond to temperature and solar intensity. Blinds up to now affect only the solar radiation and illuminance, and the blocking effect of window blinds on the airflow is not considered. More information can be obtained from Aron's thesis [13].

3.3 Integration of CoolVent into Design Advisor

The main changes involve expanding Design Advisor's engine capability to allow multi-zone modelling in addition the original shoe-box single-room modeling. Multi-zone modeling is made available for the four building types defined in figure 3-1, when pure natural ventilation is chosen in the "Ventilation system" tab. Note that in that case, Design Advisor's HVAC module is not used as the natural ventilation takes over without air-conditioning or heating. The Design Advisor's input variables are augmented to allow the definition of these building geometries. Terrain properties inputs are also added to allow a better definition of the pressure distribution on the building surface according to the Swami and Chandra model [26]. Additional inputs are included to define the internal openings in terms of area and discharge coefficient. Ventilation schedule options such as night-cooling options and temperature thresholds are also added.

Treatment of heat fluxes and gains

The building loads can be divided into the following for each zone, and their computations are carried out by their respective original Design Advisor modules, unless otherwise mentioned:

(i) Temperature-independent loads:

- Lighting heat gain (dependent on solar radiation);
- Occupancy heat gain (with occupancy schedule);

- Equipment heat gain (with occupancy schedule).

(ii) Solar heat gains: The solar radiation which gets through the window and blinds (if present) is calculated by the window module.

(iii) Temperature-dependent loads:

- Latent loads for moisture balance. Note that these are set to zero for naturally-ventilated buildings.
- Sensible loads:
    - Window heat flux: It should be noted that during natural ventilation, when the windows are open, the window heat flux still operates.
    - Wall heat flux
    - Roof heat flux (if roof is present)
    - Thermal mass heat flux: Its calculation is incorporated in CoolVent's multi-zone modeling since the temperature gradient throughout the thermal mass affects the convective heat transfer to the zone's air on either side of the thermal mass, as depicted in figure 3-2. Note that the top ceiling thermal mass is disabled if a roof is defined, as roof heat flux is then used in the energy balance instead.

All the heat gains are assumed to be partially absorbed by the floor thermal mass' top slice, and partially transmitted to the zone air. In fact, 80% of the solar heat gain is taken to be absorbed by the thermal mass, and 20% added to the zone air. In comparison, 50% of the sum of the remaining heat gains (lighting, occupancy, equipment) is taken to be absorbed by the thermal mass, and the remaining 50% added to the zone air. The window heat flux, wall heat flux and roof heat flux (if present) are assumed to be totally convected to the room air, as the internal radiation between the floor thermal mass and the ceiling, wall and window surfaces is assumed to be negligible. Therefore, 50% of non-solar heat gains, 20% of solar gain, the aforementioned window heat flux, and the thermal mass heat flux all goes into the zone air's energy balance. Conversely, 50% of the non-solar heat gains and 80% of the solar heat gains gets absorbed by the thermal mass' surface slice.

It should be noted that the combined Design Advisor-CoolVent software now considers both the ceiling and floor as thermal mass. Hence, half of the zone heat gains destined to thermal mass

goes to the surface slice of the ceiling and the remaining half goes to the surface slice of the floor thermal mass. Additionally now, because thermal mass is critical in naturally-ventilated building, it is important to train the software for a few days such that the thermal mass settles to a reasonable initial temperatures, reasonable based on the weather conditions of the last week of December, before the start of the yearly simulation. Thus, 10 training days are used.

Assumptions

The heat fluxes from the wall, window and roof (if present) are calculated every hour. They are therefore based on the zone temperatures at the start of the hour. It is estimated that the computational time saved on solving the systems of equations representing their resistance networks is more advantageous than getting accurate fluxes for each computational time-step. For the zonification of the building, several assumptions are made for simplification:

(i) the thermal masses of adjacent zones are not considered connected or at the same temperatures, as conduction across a dimension other than the thickness is considered negligible and programming-wise, connection between zones only occur at the mass air flow level.

(ii) The work-plane of the daylight is considered to be that of the extremity zones. Hence, inner zones are assumed not to receive sunlight as they are usually partitioned away.

(iii) While the building geometries considered for natural ventilation are essentially one-dimensional, the wall heat flux considered comes from two façade sides for middle zones and from three façade sides for exterior zones.

Sample results

For illustration, a cross-ventilated building with Boston weather (May 20-23) is simulated using the combined program and the results presented below. The parameters used for this simulation case-study used are listed in table B-1 of appendix B. Figure 3-5 shows the resulting zonal temperature profiles for a cross-ventilated building divided into 3 zones. As seen in section 2.5, the thermal mass dampens the zone air temperature. Note that although the building is constantly naturally ventilated, when the wind speed drops. The air temperature equilibrates to the thermal mass temperature. This behavior can be seen for the small zone temperature increases during the night of May 21.

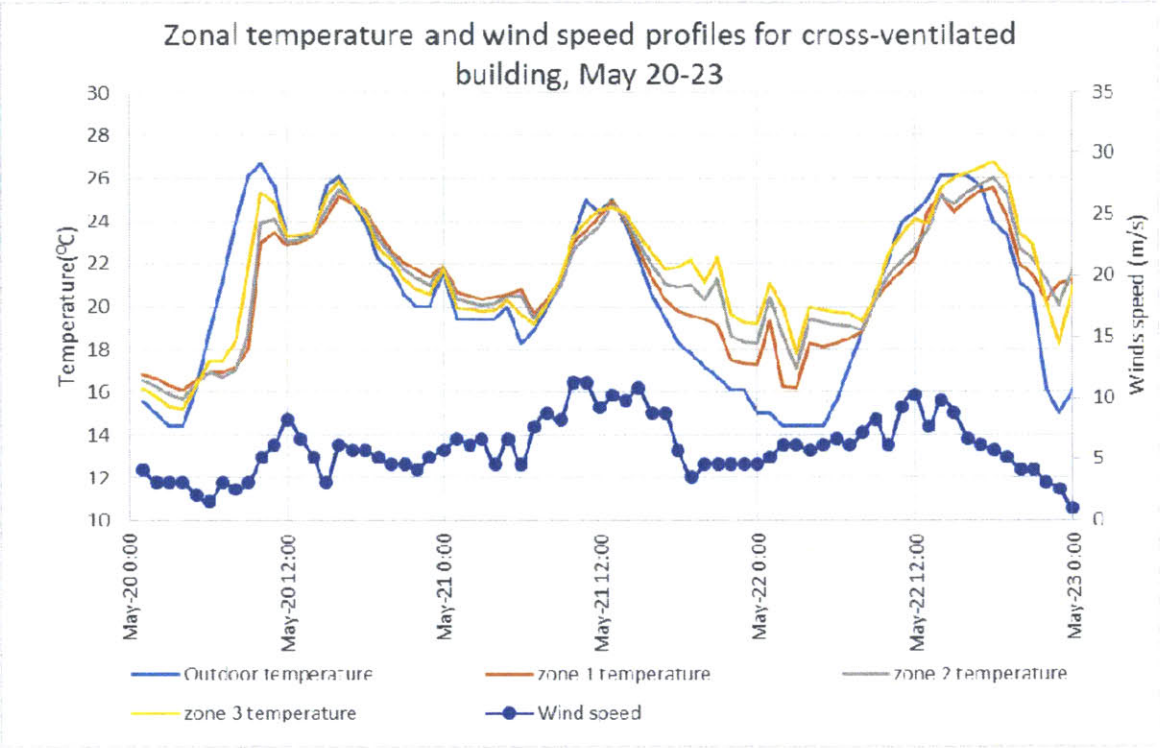

Figure 3-5: Zonal temperature and wind speed profiles for case-study with cross-ventilated building in Boston weather (May 20-23)

The following figures illustrate the effect of having more details in defining the heat gains to each zone, through the aforementioned modules. Figure 3-6 shows the heat gains for the relevant zones, resulting from occupancy heat gain, the net solar radiation transmitted through the window (blue lines), the heat conducted through the window(brown lines), the heat conducted through the wall (pink lines), and the heat generated by the use of lightings (gold lines) during occupancy hours. Note that the zones 1 and 2 are exterior zones, while zone 1 is an interior zone. As a result, the interior zone receives no window heat conduction, a lower wall conduction due to smaller wall area and a higher lighting use since the interior zone is assumed not to receive daylight. Because zones 1 and 2 have opposite window orientations, they have different window heat conduction and net solar radiation transmitted. Because the input lighting control has been set to efficient, the exterior zones do not require lighting during most of the occupancy hours.

Figure 3-7 shows the effect of using blinds with a control scheduled set to respond to solar intensity. During midday when the solar intensity is too high, the blinds are closed. This results in no solar radiation transmitted and an increase in lighting use.

Figures 3-8 to 3-12 show typical thermal mass temperatures for an adiabatic ceiling, a cool roof without insulation, a cool roof with insulation, a green roof without insulation and a green roof with insulation respectively. The effect of the implemented roof modules can thus be observed. Details of the roof properties used can be found in appendix A-1 and more information in Ray's thesis [15]. Figure 3-8 shows the temperature gradient which exists within the thermal mass which has been discretized into 10 slices. As seen in section 2.5, the thermal mass temperature knows a phase shift and damping with respect to the incoming outdoor air temperature. Figure 3-9 shows the temperature gradient through of a cool roof, which includes an outer cover-board. The connection of this outer exposed slice occurs in terms of heat gain due to solar irradiation and conduction to the outside. Therefore, this cover-board (roof slice 1) has a higher temperature than the rest of the roof slices, which are slabs. Figure 3-10 shows that adding roof insulation reduces the heat conducted from the outer roof surface to the inside. Figure 3-11 shows the temperature distribution within the green roof which has no outer cover-board, but a vegetation slice (roof slice 1), 12 soil slices (roof slices 2-13) and 11 slab slices (roof slices 14-24). It shows that even without insulation, the low thermal conductivity of the soil limits the heat conduction from the outside to inner zone air temperature. With added top insulation, the heat transfer to the inner slabs of the green roof is even more hindered, as shown in figure 3-12. As an overview, figure 3-13 compares the effect of using different roof types on the resulting connected zone air temperatures. As expected, an adiabatic roof does not translate to the indoor zone air temperature the effect of a high outdoor temperature during the day and that of a low outdoor temperature at night. A cool roof with no insulation results in the highest day zone air temperatures. Comparatively, a cool or green roof with insulation performs the best, with the lowest day zone air temperatures. A green roof (with 0.15 m of soil) with no insulation performs almost as well without insulation because of the soil already insulates without the need of a roof top insulation between the soil and slab.

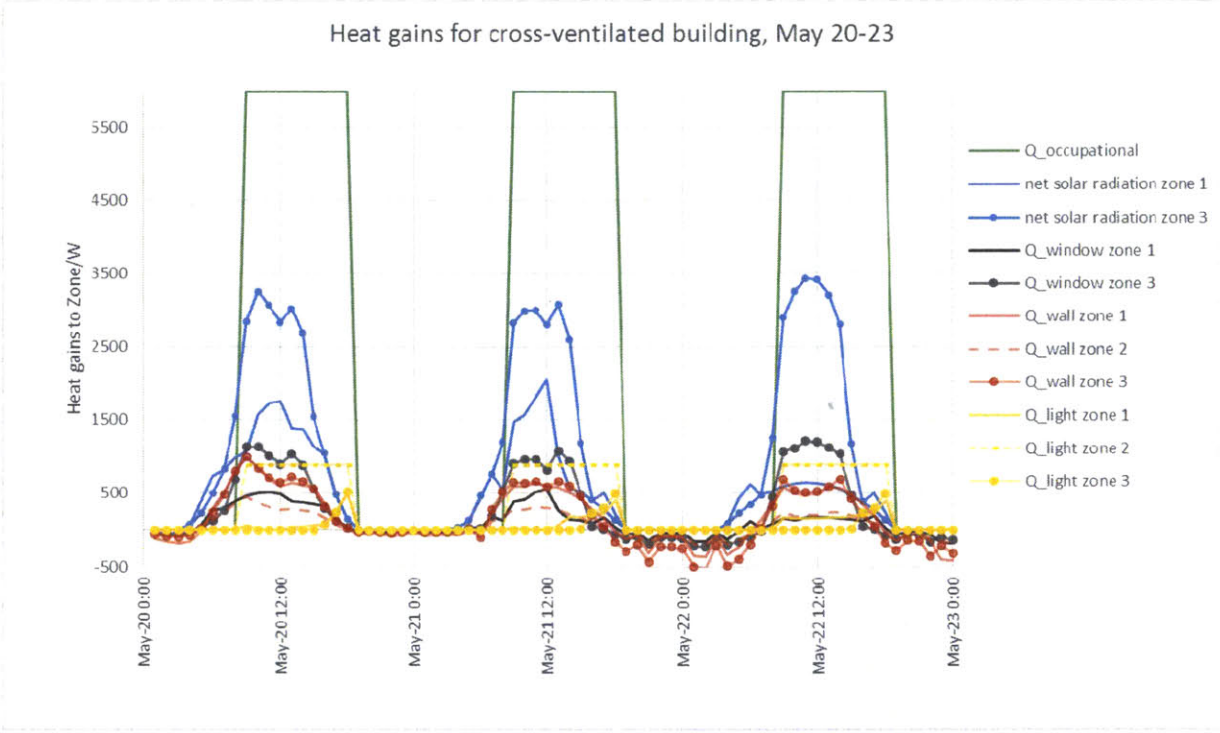

Figure 3-6: Heat gains within the 3 air zones for the case-study with cross-ventilated building without blinds, in Boston weather (May 20-23)

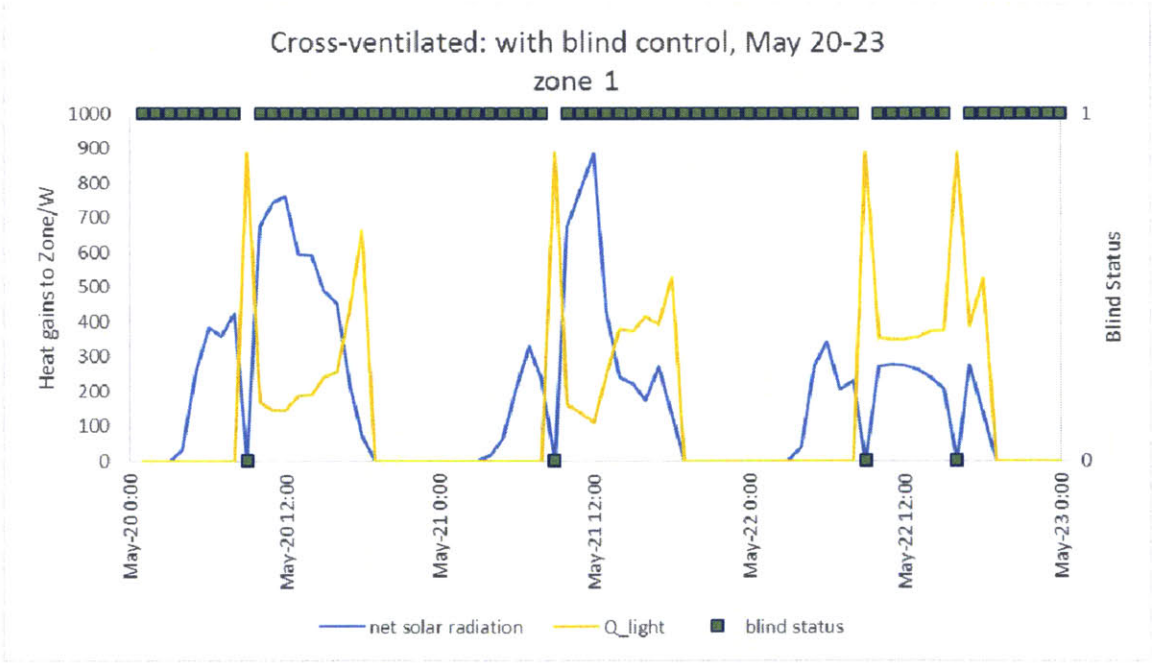

Figure 3-7: How blind schedule affects the net solar radiation and the lighting requirements, for the case-study with cross-ventilated building with blinds, in Boston weather (May 20-23). Blind status of 1 indicates open blinds; 0 indicates closed blinds.

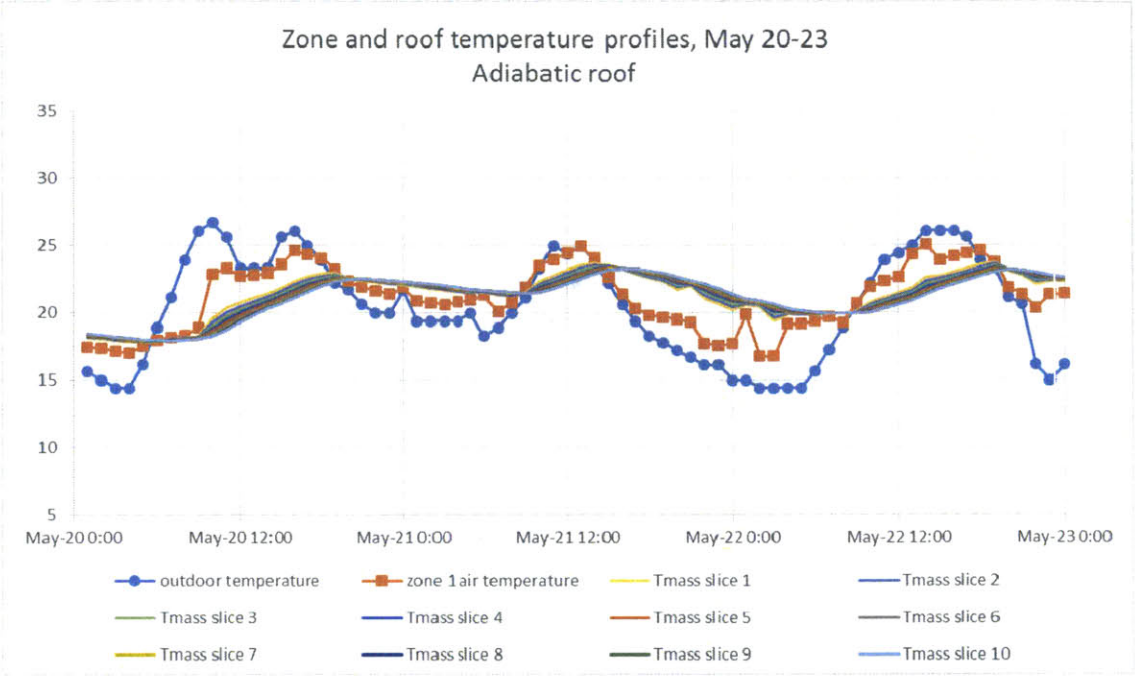

Figure 3-8: Resulting air and roof temperature profiles in one zone for the case-study with adiabatic roof (10 slices, with slice 1 being in contact with zone air)

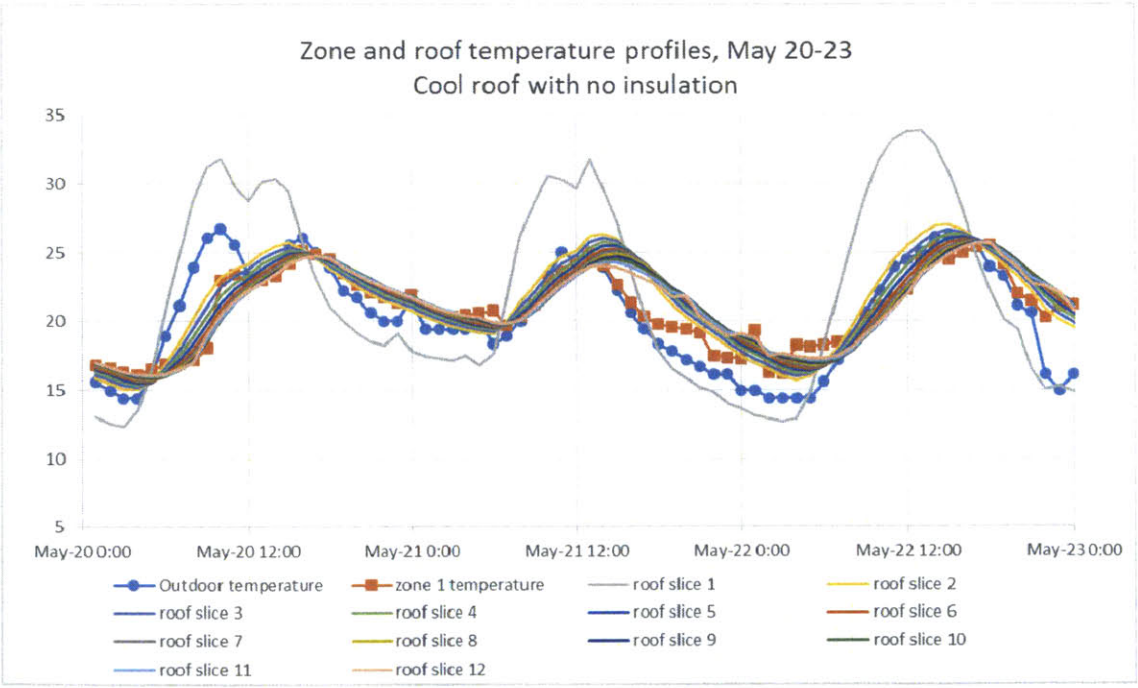

Figure 3-9: Resulting air and roof temperature profiles in one zone for the case-study with cool roof (12 slices). Cool roof has 1 slice for the cover-board (roof slice 1) and the remaining slices (2 to 12) form the slab, with slice 12 being in contact with zone air (roof properties are in table B-1). No roof insulation is used.

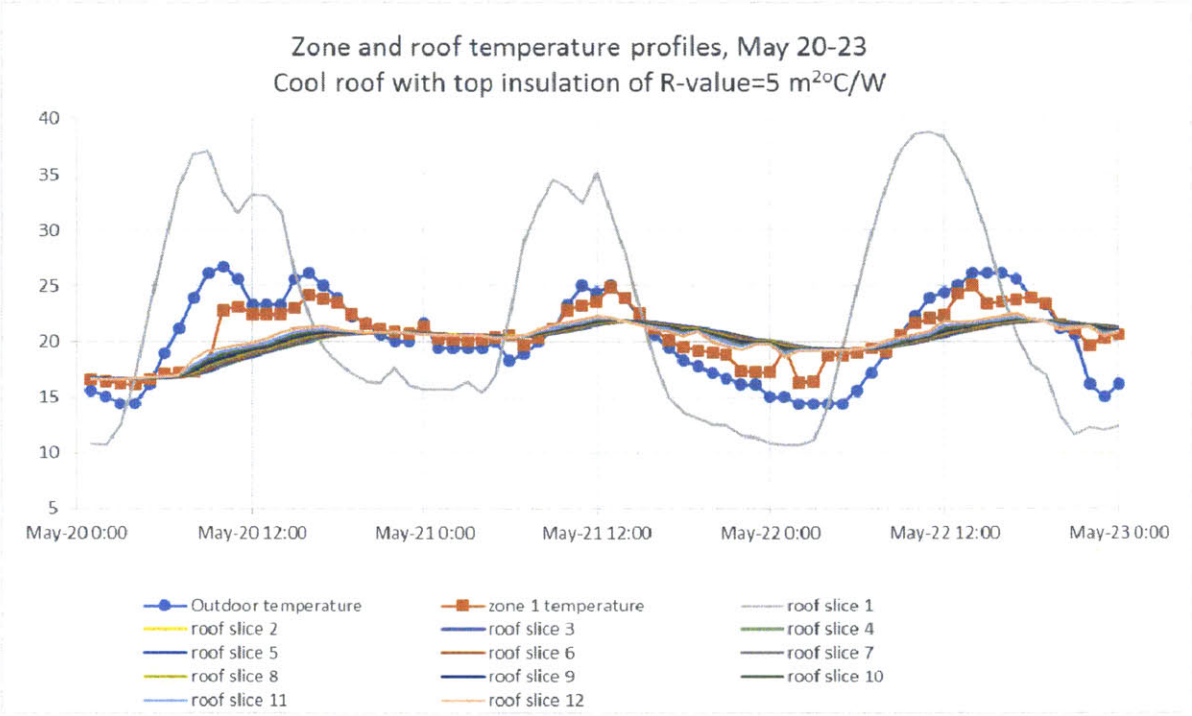

Figure 3-10: Resulting air and roof temperature profiles in one zone for the case-study with cool roof (12 slices). Roof insulation of R-value=5 m^2°C/W used.

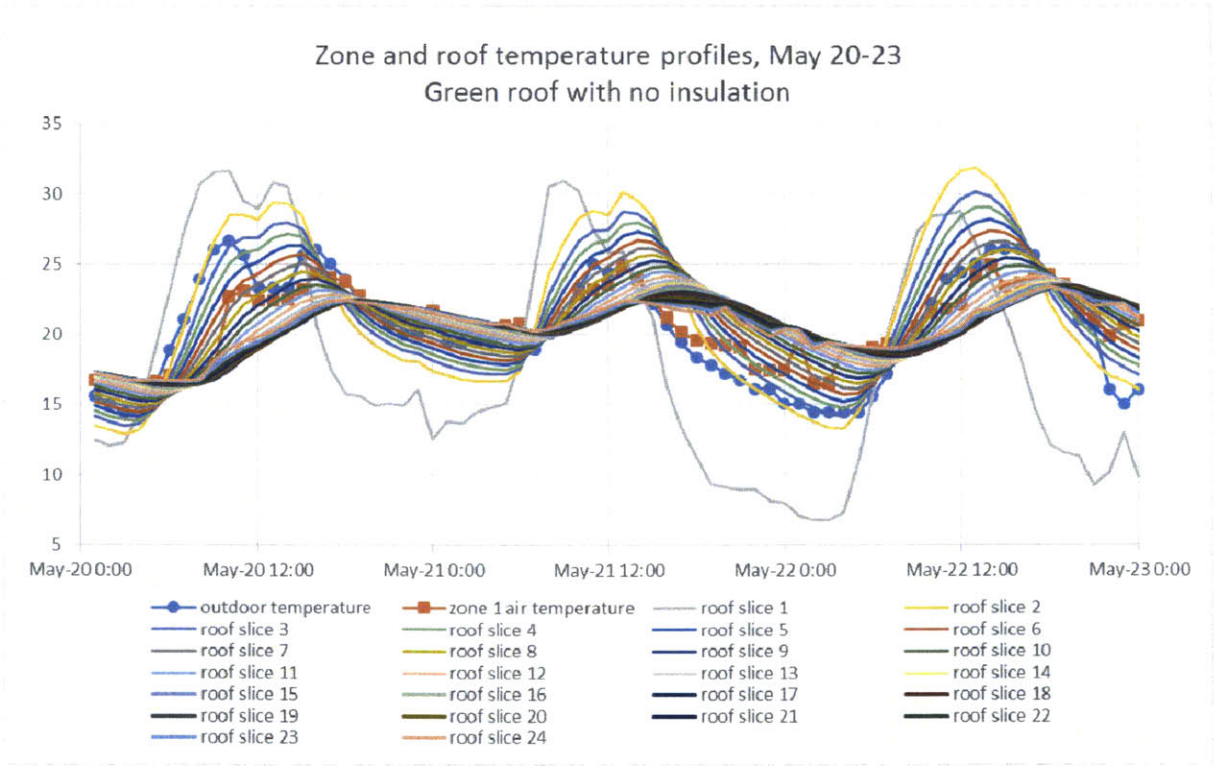

Figure 3-11: Resulting air and roof temperature profiles in one zone for the case-study with green roof (24 slices). Green roof used has 1 slice for the vegetation (roof slice 1), 12 slices for

the soil (roof slices 2-13) and the remaining slices (14 to 24) form the slab, with slice 12 being in contact with zone air (properties are in table B-1). No roof insulation used.

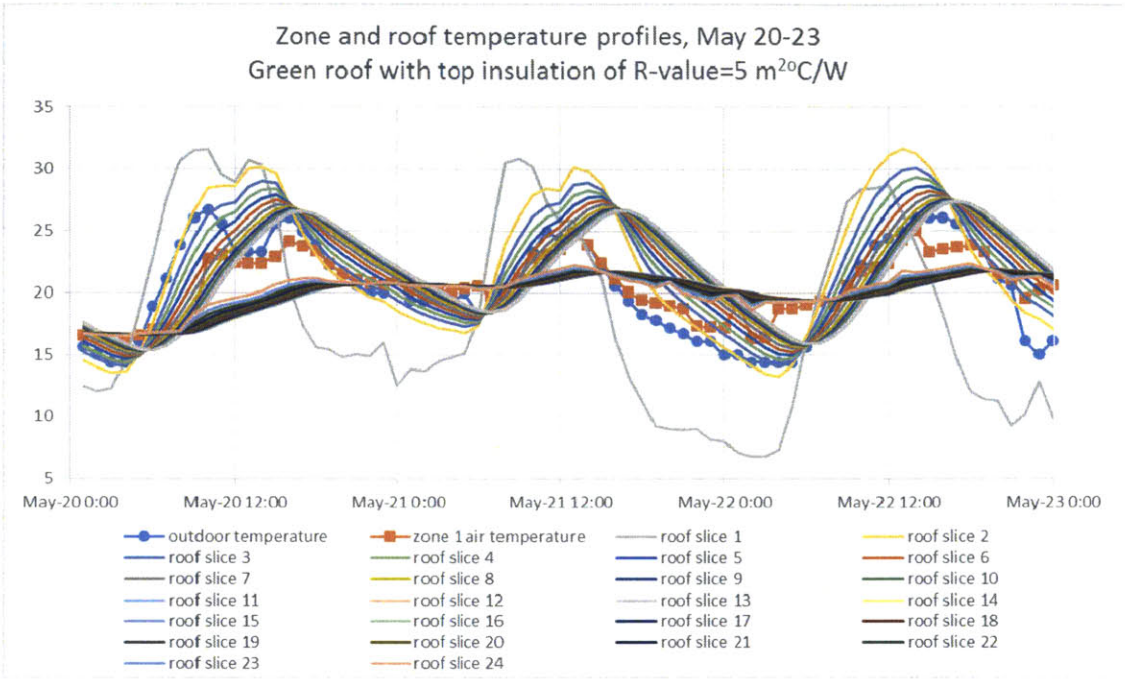

Figure 3-12: Resulting air and roof temperature profiles in one zone for the case-study with green roof (24 slices). Roof insulation of R-value=5 m^2°C/W used.

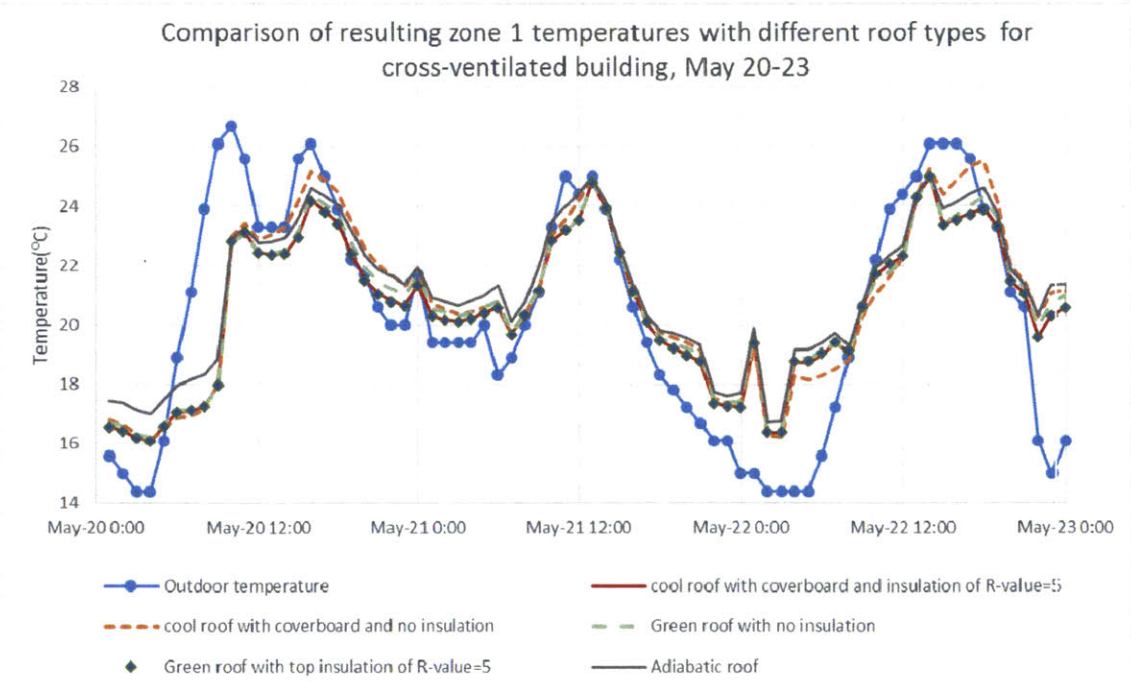

Figure 3-13: Comparison of resulting zone 1 temperatures with different roof types (adiabatic, cool with and without insulation, green with and without insulation)

Combined Design-Advisor CoolVent program structure

In summary, the combined Design Advisor-CoolVent program structure is as depicted in figure 3-14 below, with the bridging with Design Advisor done at the load, heat flux and thermal mass levels. The combined program retains its original capability (in green) of using mechanical ventilation to find the heating, cooling and lighting load of its shoe-box building model in order to meet user-defined thermal comfort and lighting requirement. Figure 3-15 and 3-16 show the data logic progression for the whole simulation and the hourly simulation respectively.

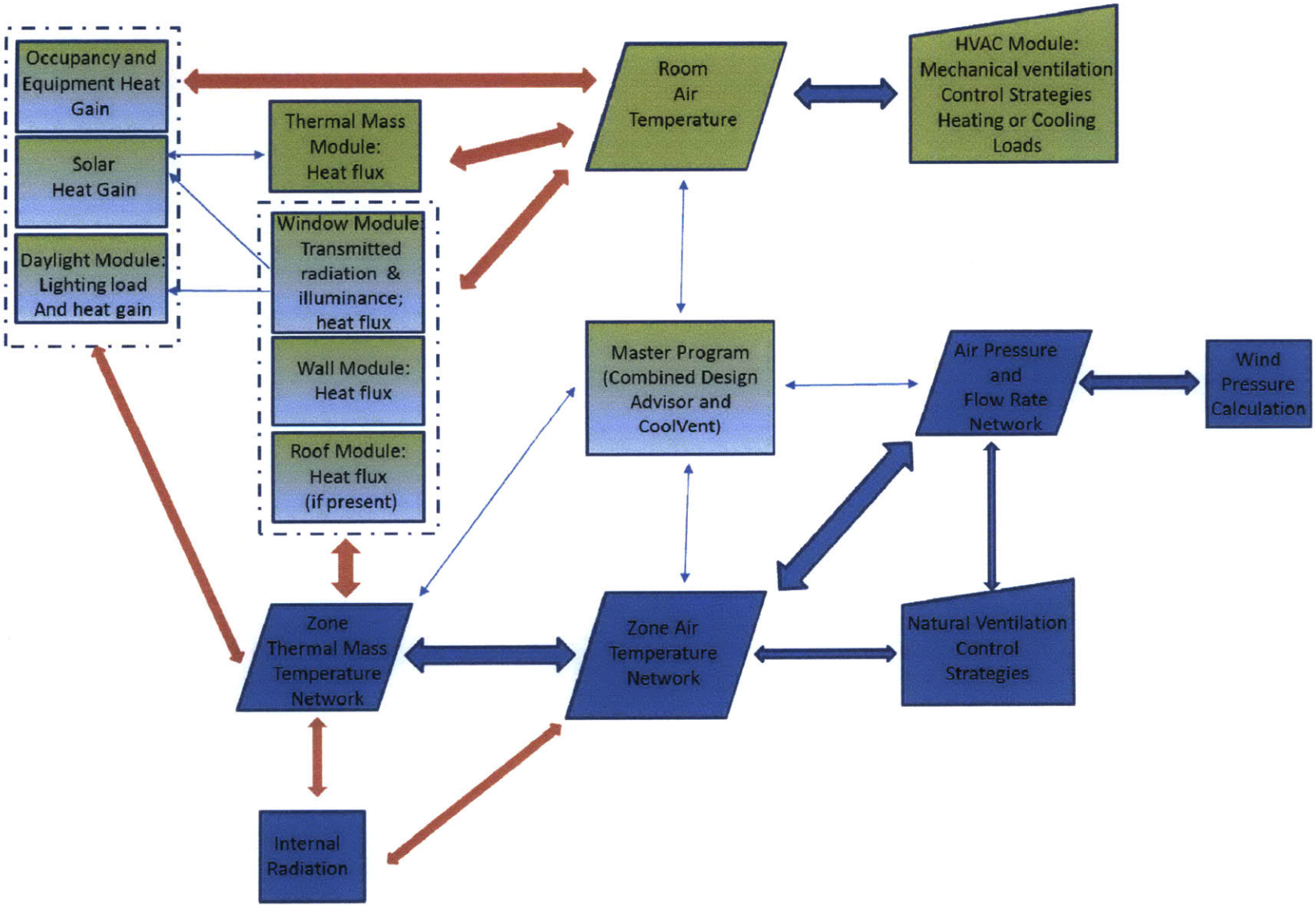

Figure 3-14: Overall combined Design Advisor-CoolVent program structure (blue: original CoolVent, green: original Design Advisor functions)

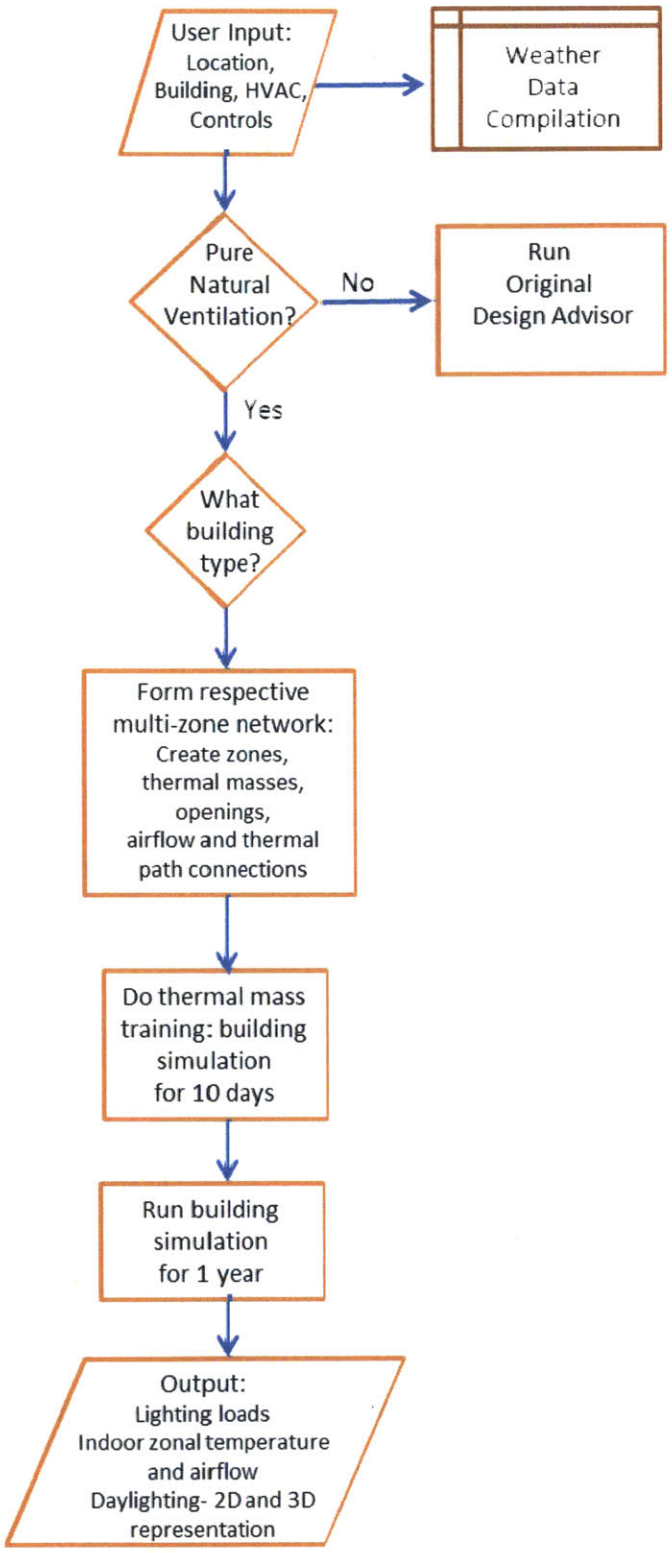

Figure 3-15: Data logic flow for the overall combined Design Advisor- CoolVent simulation

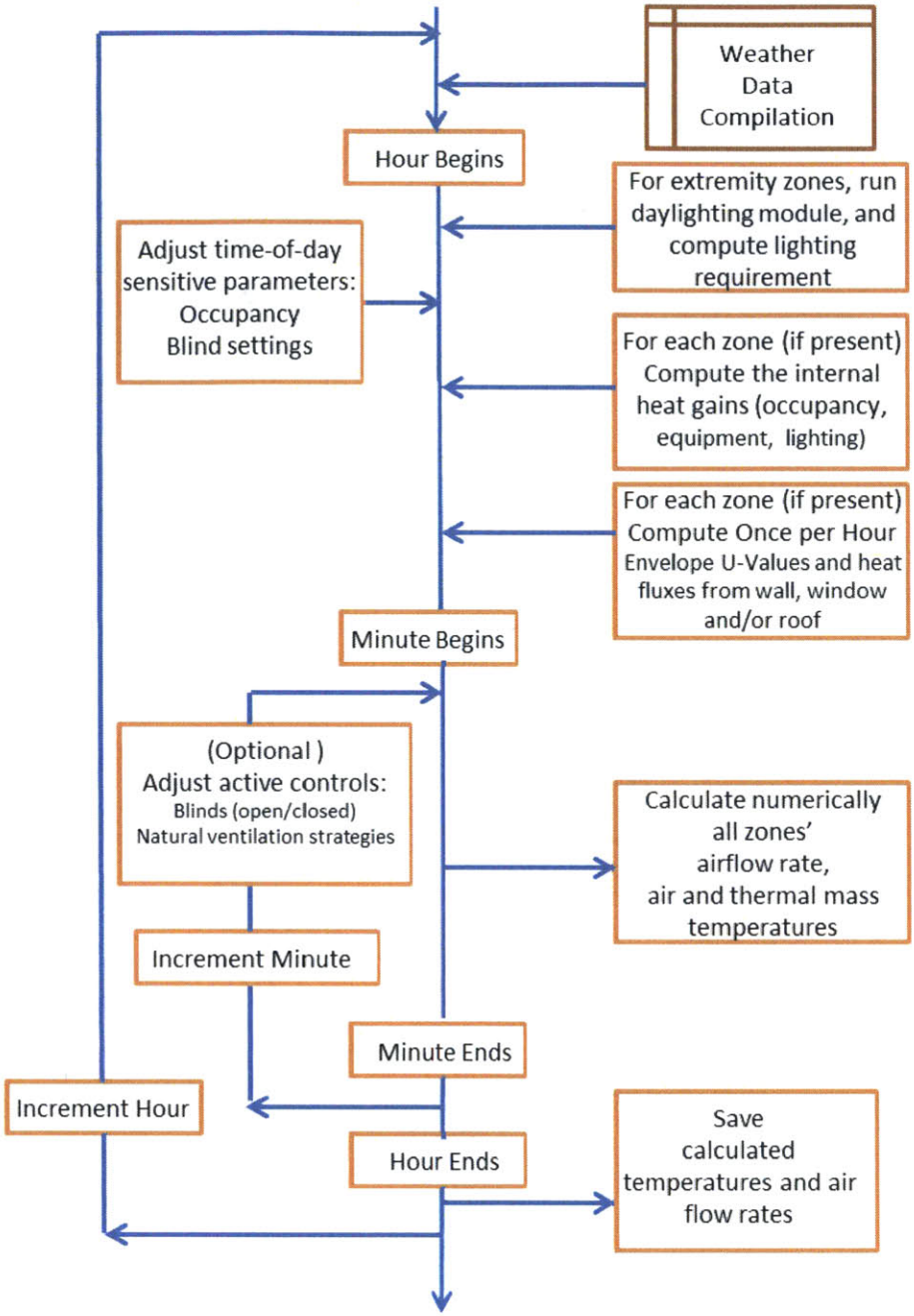

Figure 3-16: Data logic flow for the combined Design Advisor- CoolVent hourly simulation

Chapter 4

Ventilation strategies

4.1 Literature review

Two forms of passive cooling are commonly used in buildings: natural ventilation and earth-to-air heat exchanger. The other form of passive cooling, earth-to-air heat exchanger, consists of pipes buried in the ground through which air is drawn to the surface for ventilation. The exchanger is located at a depth such that the ground temperature is low enough to cool surface air temperature in summer, and hot enough to warm it in winter [9]. Again, this goes back to how a high thermal mass, in this case the earth, dampens and shifts temperature fluctuations as seen in the thermal modeling section. While the earth-to-air exchanger can operate for heating too, Breesch et al. found out natural night ventilation is more efficient than an earth-to-air heat exchanger for cooling [29]. On the other hand, as will be examined in section X, the cooling potential through night-ventilation depends largely on the thermal mass.

Both forms of passive cooling depend on three type of parameters: the climatic parameters (T_{out}-T_{in}, T_{mean}), the building parameters (thermal mass and heat transfer parameters), and control parameters (control strategy, and actual ventilation rate set if mechanically aided) [29], [30].

4.1.1 Direct ventilation versus night-cooling

Night-cooling is the use of natural ventilation during the night because daytime outdoor temperatures exceed the indoor cooling set-point temperature and direct ventilation is no longer useful. By restricting ventilation to nighttime, the building's thermal mass can be cooled with outdoor air and can thus offset daytime internal gains. Night-cooling is mainly suitable for low peak air temperature [31] and large diurnal temperature swings. Givoni suggested a general rule

of thumb of an average of 10-12C as minimum diurnal temperature swing for night-ventilation to be effective [9].

The table below shows the results of Axley et al in determining a location's natural ventilation's potential using hourly WYEC2 weather data for four climate zones. The effectiveness of night-cooling was calculated as the number of days when the night cooling potential q_{cool} offsets the internal gain q_{in}. Axley assumed that the building had infinite thermal mass i.e. the cooling potential is perfectly sustained by the thermal mass:

$$q_{cool} = \frac{1}{time\ open} \int \dot{m}\, c_p \left(T_{i_{csp}} - T_{out(t)}\right) dt \tag{4.1}$$

when $T_{out} < T_{i_{csp}}$ (which is at night-time).

Hence, the potential of night-cooling here is an upper limit.

	Direct Cooling				Night Cooling[1]
	10 W/m^2	20 W/m^2	40 W/m^2	80 W/m^2	
Miami, FL – FLMIAMIT.WY2 data {FLMIAMIT.WY2 data} Hot-Humid-Coastal					
Vent. Rate or Cooling Potential	3.1 ±2.6 ACH	6.0 ±5.3 ACH	11.9 ±10.6 ACH	23.9 ±21.2 ACH	2.9 ±1.9 W/m^2-ACH
% Effective[2]	26.5%	27.3%	27.3%	27.3%	26% (79 days)
Los Angeles, CA – CALOSANW.WY2 data Hot-Arid-Coastal					
Vent. Rate or Cooling Potential	1.5 ±1.0 ACH	3.0 ±2.1 ACH	5.9 ±4.2 ACH	11.8 ±8.4 ACH	5.9 ±2.3 W/m^2-ACH
% Effective[2]	94.9%	97.8%	97.8%	97.8%	93% (27 days)
Kansas City, MO – MOKANCTW.WY2 data Temperate-Continental					
Vent. Rate or Cooling Potential	1.9 ±1.8 ACH	2.6 ±3.1 ACH	4.8 ±6.1 ACH	9.7 ±12.1 ACH	4.5 ±3.2 W/m^2-ACH
% Effective[2]	37.8%	67.4%	73.9%	73.9%	57% (81 days)
Madison, WI – WIMADSNT.WY2 data Cold-Continental					
Vent. Rate or Cooling Potential	1.8 ±1.7 ACH	2.4 ±2.8 ACH	4.1 ±5.2 ACH	8.2 ±10.4 ACH	6.0 ±3.0 W/m^2-ACH
% Effective[2]	39.3%	72.4%	88.7%	88.7%	82% (68 days)

[1] Night cooling for subsequent days when direct cooling is not effective.
[2] For direct cooling % = hours effective ÷ 8760 hours; for night cooling % = days effective ÷ days needed.

Table 4-1: Climate suitability statistics for natural ventilation for four U.S. locations [32]

Some interesting results from that study are worth mentioning here. In hot cities like Miami, where the outside temperature is not apt to be below the indoor cooling set-point temperature

often, natural ventilation cooling is not possible most of the year. On the other hand, direct natural ventilation can be expected to be most feasible and effective in the cooler locations, as in Kansas City, for moderate to high internal gains. This is because at low internal gain and low outdoor temperature, the resulting indoor temperature is less that the heating set point temperature needed to require natural ventilation. While there may or may not be any thermal comfort penalty, there is penalty in terms of air quality. Hence, some form of mechanical ventilation is needed when natural ventilation is not possible.

4.1.2 Night-ventilation studies

Night-cooling is simply the use of natural ventilation during the night because daytime outdoor temperatures exceed the indoor cooling set-point temperature and direct ventilation is no longer useful. By restricting ventilation to nighttime, the building's thermal mass can be cooled with outdoor air and can thus offset daytime internal gains. Night-cooling is mainly suitable for low peak air temperature [31] and large diurnal temperature swings. Night-cooling has been shown to be effective in mild UK weather and is in fact one of the default design options for "green" office buildings [33]. Common evaluation criteria for how effective the night-cooling can be are:
1. Reduced peak day air-temperatures; 2. Reduced average temperature during the morning; 3. Reduced slab day temperatures; 4. Time-lag between outdoor and indoor maximum temperatures.

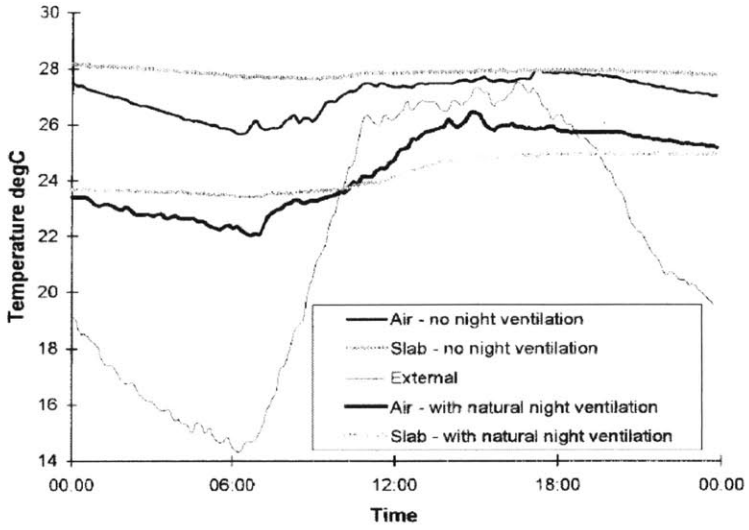

Figure 4-1: Typical monitored effect of natural ventilation on indoor and thermal mass temperature [31]

Similar to Axley [32], Artmann et al investigated climate suitability for natural ventilation, but based off European climate [5]. His metrics for climate suitability are overheating degree hours (ODH) and mean daily climatic cooling potential (CCP). ODH was defined as the number of hours room temperature was above 26°C during working hours for a simple representation of thermal comfort. CCP was defined as the number of hours during non-working hours for which the outdoor temperature was below the room temperature, for a representation of the climate's potential for ventilative cooling [5]:

$$CCP = \frac{1}{N}\sum_{n=1}^{N}\sum_{h=h_i}^{h=h_f} m_{n.h}(T_{b,n,h} - T_{e,,n,h}) \begin{cases} m = 1\ h\ if\ T_b - T_e \geq \Delta T_{crit} \\ m = 0\ \ if\ T_b - T_e < \Delta T_{crit} \end{cases} \quad (4.2)$$

Where T_b= building temperature, T_e= outdoor temperature, h= time of day, h_i=starting hour for night ventilation, h_f= final hour for night ventilation, ΔT_{crit}= critical threshold temperature difference for night ventilation.

Artmann et al. conducted building energy simulations using HELIOS [34] to find the effect of varying identified parameters on the resulting room temperature [35]. The parameters varied during his study were: climate, thermal mass, heat gain, air change rate and heat transfer coefficients. He found out that the climatic conditions and air flow rates during night-ventilation had the largest effects while sensitivity to the heat transfer coefficients occurred for h<4 W/m^{2}K , with the effects measured in terms of overheating degree hours. An interesting observation pertinent to my quest is the effect of thermal mass and internal heat gains as shown in the figure below. For instance, increasing the thermal mass from c/A=193kJ/m^{2}K (light-weight) to c/A=692kJ/m^{2}K(heavy) reduced overheating from 164 to 23Kh/a for a medium heat gain office, while increasing the internal heat gain from 159Wh/m^{2}d (low) to 313 Wh/m^{2}d (high) increased overheating from 33 to 177Kh/a for a medium-weight building. It should also be noted that the overheating effect of increasing heat gain has smaller sensitivity in heavy-weight buildings.

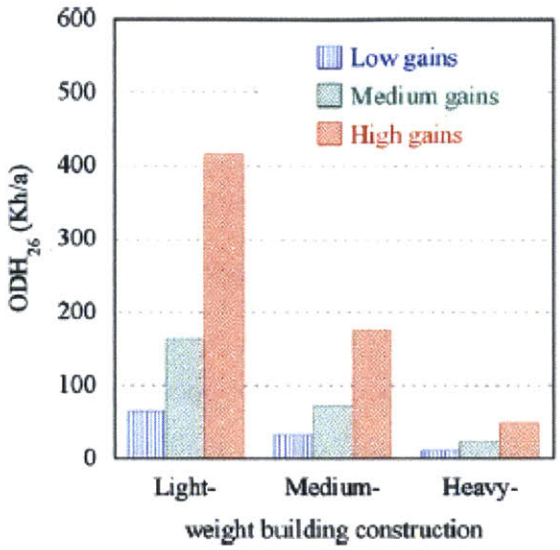

Figure 4-2: Effect of thermal mass and internal heat gains on thermal comfort (ODH>26°C) for a night-ventilated building simulation for Zurich weather with h=7.7W/m^{2}K [35]

However, in the parametric study, Artmann et al. used similar ventilation control parameters despite varying the building parameters as shown in the table below.

Parameters	**Artmann study**
Night-ventilation schedule	7p.m to 7a.m
Night-ventilation ACH used	6 ACH
Set-point constraint Overcooling constraint	$T_{out} < T_{room\ surface}$- 3°C 24-h Mean of T_{out}> unspecified cooling setpoint and $T_{room\text{-}surface}$> 20 °C
Day ventilation	2 ACH
Heat gains	Conduction through exterior and partition walls

Table 4-2: Control parameters for night-ventilation numerical simulation in Artmann's study [35]

Multiple studies on night-ventilation have been conducted experimentally as well to investigate the cooling potential of night-cooling. However, no clear control strategies defined by the building or climate parameters, were determined when instigating the night-cooling. For instance, Blondeau carried out his study on an office building in La Rochelle, France [30]. Three test rooms were unoccupied (hence without internal heat gain) and night-ventilated through two opened windows, allowing for one-sided ventilation. He tested through trial and error during a month period, what the optimal working conditions would be for their night-ventilation strategy. Their night-ventilation control sequence used was:

Control parameters	Blondeau study
Night-ventilation schedule	9p.m to 8a.m
Night-ventilation ACH used	8 ACH
Set-point constraint	$T_{out} < T_{room\ air}$ - 2°C
Overcooling constraint	N/A
Day ventilation	Windows closed

Table 4-3: Control parameters for night-ventilation in Blondeau's experimental study [30]

Breesch carried out an experimental study involving a night-ventilated low-energy office building in Belgium [29]. The building was a 2-floor open-plan occupied office with a flow path similar to that in the chimney-style of CoolVent, i.e. it allows for wind-driven and buoyancy-driven air flow. By day, the ventilation system also involves an earth-to-air heat exchanger which pre-cools the supply air flow. Again there is no hard-and-fast way by which the ventilation control parameters were determined, as "the control parameters were optimized after the first summer", to give the following heuristic parameters:

Control parameters	Breesch study
Night-ventilation schedule	10p.m to 6a.m
Night-ventilation ACH used	Natural air flow rate
Set-point constraint	$T_{out} < T_{room\ air}$ - 2°C If relative humidity<70% If no rainfall If wind speed<10m/s If previous day's $T_{out,max}$>23°C and $T_{room\ air}$>20°C
Overcooling constraint	If $T_{room\ air}$>20°C
Day ventilation	Proportional control: from 5400 to 8000m^3/h for $T_{room\ air}$ from 23 to 26°C

Table 4-4: Control parameters for night-ventilation in Breesch's experimental study [29]

Other rules of thumb exist for setting the ventilation parameters. Zimmerman suggests the following for an efficient night-ventilation: outside temperature should be at least 5K below room temperature for more than 6h at air exchange rates of 5 ACH [36]. In her study of night-ventilated buildings in Germany, Eicker highlighted that different starting times for night-ventilation give rise to different cooling potential: for starting time of 9pm the maximum cooling potential was of 5.5kWh and 4.7kWh for starting time of 6pm [37]. However, no specific control parameters were mentioned. For mechanically-aided night-ventilation, she noted that COP of the fans varied between 5 and 10, which was still more energy-efficient than conventional chillers.

Although numerous studies have covered parametric and experimental studies of parameters affecting night-ventilation potential, only heuristic rules actually govern the ventilation control parameters such as set-point and ACH values, based on prior experimentation.

4.2 Ventilation modeling in buildings

Ventilation involves the closing and opening of windows. This can be done by automatic actuation of the mechanical openings or by using vents. Natural ventilation involves mass-flow rate supported by a buoyancy-driven or wind-driven air flow, and is thus variable. A wind-driven mass-flow rate depends on the wind-speed and discharge coefficient of the opening. A buoyancy-driven mass-flow rate additionally depends on the density or temperature difference between two zones. However, natural ventilation can be mechanically-aided to achieve a wanted air change rate using exhaust fans. Hence, a fixed air change rate of 5 ACH is assumed, as the standard air quality requirement for an office building [12].

4.2.1 Cyclical ventilation with scheduling

Ventilation involves the closing and opening of windows. Although infiltration occurs when windows are closed, the actual resulting ACH is usually very low, ACH=0.35 roomful/h for an office building [12]. For a better analysis of energy simulation with windows closed, the mass transfer term in energy equation 2.3 is neglected by setting $\dot{m} = 0$.

$$mc_v \frac{dT(t)}{dt} = hA\big(T_{thermal\ mass}(t) - T(t)\big) + q_i A \tag{4.3}$$

This equation is coupled to equation 2.5, which assumes a lumped-capacity model for the thermal mass (i.e. thermal mass is at a uniform temperature):

$$(mc)_{thermal\ mass} \frac{dT_{thermal\ mass}}{dt} = hA\big(T(t) - T_{thermal\ mass}(t)\big) \tag{2.5}$$

Compared to the scenario of open windows, $mc_v \frac{dT(t)}{dt}$ is no longer negligible. This can be seen in figure 4-3: there is a crook in the air temperature solution when the window is just closed; then the temperature equilibrates to the steady solution with $mc_v \frac{dT(t)}{dt}$ negligible, which is just a linear increase with time.

Rearranging equation 2.5 and substituting into equation 4.3 gives the following second-order ordinary differential equation:

$$\frac{mc_v}{hA}\frac{d^2T}{dt^2} + \frac{dT}{dt}\left(1 + \frac{mc_v}{(mc)_{T\,mass}}\right) = \frac{qA}{(mc)_{T\,mass}} \tag{4.4}$$

Solving equation 4.4 by the method of undetermined coefficients gives the following solution using $T_{air}=T_{ini}$ and $T_{T\,mass}=T_{tmass\_ini}$ at t=0 for this initial value problem:

$$T_{air}(t) = T_{ini} + \frac{qAt}{mc_v+(mc)_{T\,mass}} + \left(T_{ini} - T_{tmass\,ini} - \frac{\frac{qA\tau_2}{mc_v+(mc)_{T\,mass}}}{\left(1+\frac{\tau_1}{\tau_2}\right)}\right)e^{-\left(\frac{1}{\tau_1}+\frac{1}{\tau_2}\right)t} \tag{4.5}$$

$$T_{T\,mass}(t) = \frac{qA(t-\tau_2)}{mc_v+(mc)_{T\,mass}} + T_{ini} - \left(T_{ini} - T_{tmass\,ini} - \frac{\frac{qA\tau_2}{mc_v+(mc)_{T\,mass}}}{\left(1+\frac{\tau_1}{\tau_2}\right)}\right)\left(1 + \frac{\tau_1}{\tau_2}e^{-\left(\frac{1}{\tau_1}+\frac{1}{\tau_2}\right)t}\right) \tag{4.6}$$

Where $\tau_1 = \frac{mc_v}{hA}$ *and* $\tau_2 = \frac{(mc)_{Tmass}}{hA}$.

For $mc_v \ll (mc)_{Tmass}$, $\frac{\tau_1}{\tau_2}$ is negligible and $\frac{qA\tau_2}{mc_v+(mc)_{Tmass}} = \frac{q}{h}$. $T_{air}(t)$ and $T_{T\,mass}(t)$ can be simplified to:

$$T_{air}(t) = T_{ini} + \frac{qAt}{mc_v+(mc)_{T\,mass}} + \left(T_{ini} - T_{tmass\,ini} - \frac{\frac{qA\tau_2}{mc_v+(mc)_{T\,mass}}}{\left(1+\frac{\tau_1}{\tau_2}\right)}\right)e^{-\left(\frac{1}{\tau_1}+\frac{1}{\tau_2}\right)t} \tag{4.7}$$

$$T_{T\,mass}(t) = T_{tmass\,ini} + \frac{qAt}{(mc)_{T\,mass}} \tag{4.8}$$

For $t>>\tau_1$, the air temperature, like the thermal mass temperature, equilibrates to a linear increase with time for a constant interior heat gain. This is seen in figure 4-3, where the simulation uses the simple single-zone energy model developed in chapter 2, with normal thermal mass parameters (c=880 J/kgK, thickness=5", h=8 W/kgK) and a room volume of 1000m^3 and area of 100m^2.

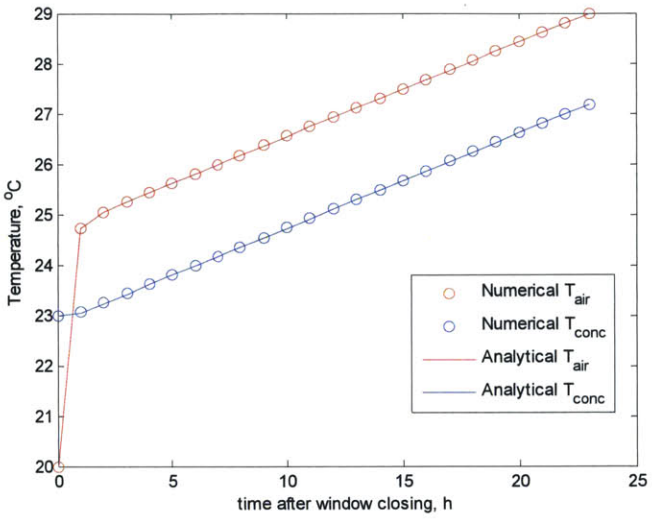

Figure 4-3: Resulting temperature profiles using numerical and analytical solutions with closing at time t=0 h

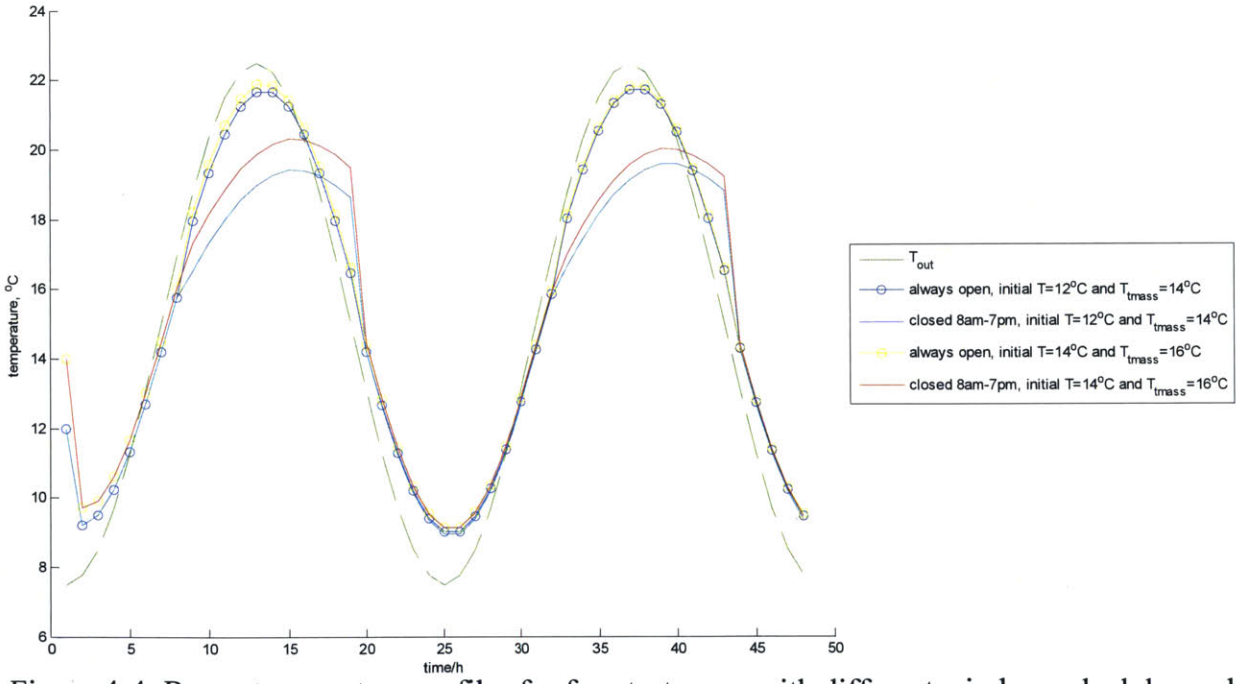

Figure 4-4: Room temperature profiles for four test cases with different window schedules and initial temperatures

The above figure shows the resulting room temperature profiles for four test cases (with the simulation using the same energy model as in figure 4-3 above): 1. always open, with initial air and thermal mass temperatures of 12°C and 14°C respectively; 2. closed from 8am to 7pm, with initial air and thermal mass temperatures of 12°C and 14°C respectively; 3. always open, with initial air and thermal mass temperatures of 14°C and 16°C respectively; 4. closed from 8am to

7pm, with initial air and thermal mass temperatures of 14°C and 16°C respectively. Figure 4-4 shows that different initial thermal mass temperature conditions, as well as different ventilation schedules, result in different temperature profiles. This is because the time constant due to the thermal mass used is of the order of 15 hours and hence it takes time for the system to equilibrate to the steady-state temperature profile. This is more so with the cyclical ventilation schedule than with the constant ventilation schedule.

4.2.2 Effective heat transfer coefficient with cyclical ventilation

In section 2.8, the use of an effective heat transfer coefficient was used to obtain the same thermal response from the thermal mass when it is numerically modeled as one slice at one net temperature, as compared to when it is numerically modeled as many slices with a temperature gradient. However, this simplification of using an effective heat transfer coefficient was derived for the variables being in the complex plane, i.e. for steady-state A.C signal in the circuit analogy, or in continuous natural ventilation with a sinusoidal outdoor temperature in physical terms. This is because second or greater order effects of the capacitance in parallel do not arise but for non-steady signals. To see this, a similar analysis is done in the s-plane.

In the s-plane,

$$Capacitor\ impedance, Z_C = 1/sC \tag{4.9}$$

$$Resistor\ impedance, Z_R = R \tag{4.10}$$

Using the series and parallel rules in equation 2.X, the effective impedance is now:

$$Z_{effective} = \frac{C^2R^2s^2+3CRs+1}{sC(C^2R^2s^2+4CRs+3)} \tag{4.11}$$

Hence, for non-steady state A.C signal, the thermal mass section of the circuit cannot be reduced to an effective resistance and capacitance without some errors as second or more order effects are unaccounted for. The effect of non-steady signals on the error range for this effective representation is investigated numerically using MATLAB by comparing the results with temperature generated using a thermal circuit with 10 slices. Figures 4-5(a)-(f) compare the resulting temperature profiles, always open and with a ventilation schedule, for the following

cases: (i) with no occupational heat gain; (ii) with an occupational heat gain of $15 W/m^2$; (iii) with an occupational heat gain of $30 W/m^2$. Note that for the profiles below, heat gain followed an occupational schedule of 8a.m to 9p.m. For constant ventilation, it can be seen that the effective circuit gives the correct room air temperature profile, while if only 1 slice is used with the original heat transfer coefficient, the room temperature is more damped than in actuality. However, with a ventilation schedule (here set to 8a.m to 9p.m), error slips in. Error is maximum when the window has just been closed, and increases for greater occupational heat gain. This is to be expected: with an unsteady signal, a single capacitance charging or discharging respectively overestimates or underestimates the resulting room temperature than several capacitances in parallel (the thermal mass slices) at different temperatures. Nevertheless, the resulting errors are of less than $1^{\circ}C$, and are consequential mostly for high internal gains and after a change in ventilation. Hence, the effective heat transfer coefficient ($h_{eff} = \frac{hk}{k+0.29hL}$) is adopted as a means to reduce the number of dimensions of the temperature space during the dynamic programming optimization process.

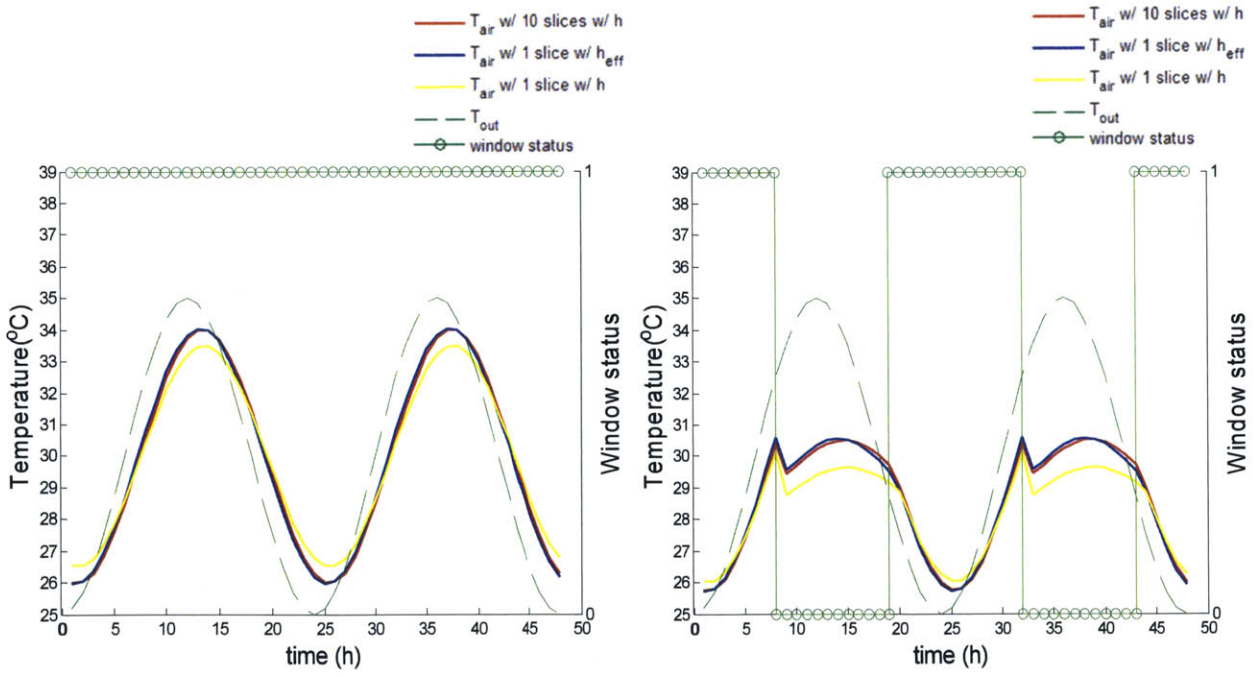

(a) (b)

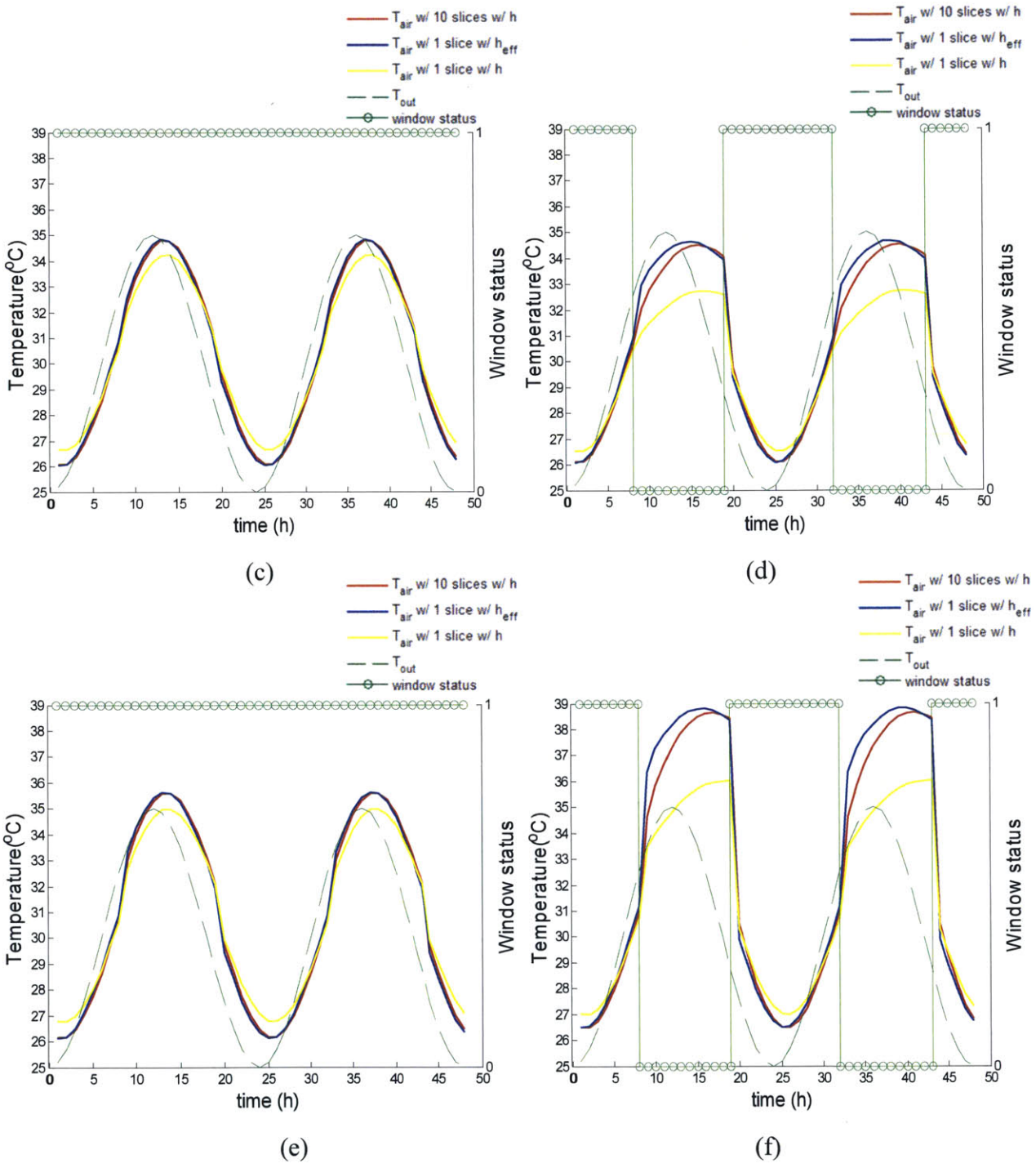

Figure 4-5: Temperature profiles with (a) no heat gain and constant ventilation, (b) no heat gain and ventilation schedule, (c) with heat gain of 15 W/m^2 and constant ventilation, (d) with heat gain of 15 W/m^2 and ventilation schedule, (e) with heat gain of 30 W/m^2 and constant ventilation, (f) with heat gain of 30 W/m^2 and ventilation schedule (with heat gain and ventilation schedule both from 8am to 19pm)

Chapter 5

Optimization

5.1 Building control and optimization in literature

5.1.1 Current building controls

Controls are prevalent in commercially available HVAC systems: they can be pneumatic, electric or electronic and are monitored using energy management systems (EMS) or Building Automation Systems (BAS). Control systems consist of the sensor, controller and controlled device. The control actions can be on-off action, timed on-off action (with delay), floating action, modulating action (example: proportional control). The last three actions are usually used for HVAC systems focused on mechanical heating and cooling. For instance, PID controllers are used to maintain the room temperature at a user-defined set-point for an air-conditioning system. In our case, for natural ventilation, on-off actions are used to control the dampers (figure 1.2) or mechanically-actuated windows according to the rule-based control defined by the BAS. For example, Levermore analyzed the rule-based control at the PowerGen building in Coventry, UK, which was used for night-ventilation [38]. The excerpt is below:

Initiate and maintain cooling by opening all controlled apertures when:

1. *The average room/zone temperature at the end of the day exceeded 23C*
2. *The maximum outside temperature during the day exceeded 21C*
3. *The room/zone temperature exceeded 18C.*

If condition 3 is violated, night cooling is not resumed until room/zone temperature rises above 20C.

The rules above are an example of rule-based controllers used by the BAS. The control inputs can be based on a series of rules of the kind "if *condition* then *action*". The conditions and actions typically involve numerical parameters (usually threshold values of inputs) as control parameters. The shortcoming of rule-based controls is that for good performance of the control system, a good set of rules, as well as the associated parameters is required.

PID controllers and rule-based controllers are the norm in building control systems because of the simplicity of its implementation. However, such simple heuristic strategies usually only consider indoor and outdoor conditions, and do not incorporate an ongoing optimized control. The controls do not actively seek to minimize cost or maximize thermal comfort, by taking into consideration disturbances, such as predicted weather, and the building thermal dynamics (characterized by a physical or data-driven model of the building).

5.1.2 Optimization for ventilation

Optimization is needed for the most effective use of natural ventilation. Extensive research exists on the optimization of ventilation in buildings. However, the majority of it is carried out on optimized controls of dual-mode (mechanical and natural cooling) ventilation in mixed-mode buildings. As hybrid-mode ventilation was in question, the typical objective function to maximize was the electricity savings from the natural cooling. Three types of optimization predominate: 1. Model predictive control strategies, 2. user-behavior based controls, 3. passive optimization. Passive optimization operates at the design level, while user-behavior based controls have been developed more as a tool for building energy and air-flow modeling. Model predictive control strategies, on the other hand, aim to optimize the control of the HVAC systems during its daily operations.

Passive Optimization

Passive optimization involves modifying the building's envelope and thermal properties to affect its thermal response. Wang conducted a study of optimization of the cost-return for mixed -mode ventilation through a parametric run of varying thermal mass [39]. He developed a semi-empirical model which is half building physics based, and half obtained by regression of data to obtained fitting coefficients C_1 and C_2 for a certain climate. The empirical model used was:

$$\frac{E_{saving}}{E_{mechanical}} = \left(C_1 exp\left(-\frac{A}{A_0}\right) + C_2 \right)\left(\frac{\tau}{\tau_0} - \left(C_3\left(\frac{A}{A_0}\right) + C_4\right)\right)\left(1 - exp\left(-\frac{1}{\frac{\tau}{\tau_0} - C_2}\right)\right) \qquad (5.1)$$

Wang defined the time constant as $\tau = \frac{\rho c d}{h}$, similar to $\frac{mc}{hA}$. The C_1 to C_4 coefficients somehow encompass the effect of the building parameters such as area and insulation level, and were found by fitting a simulation study result. It should be noted that in his simulations the natural ventilation had the following heuristic set-points:

Working hours (8am-17pm): 15 °C< T_{out}<22 °C and T_{in}> 19°C

Non-working hours: 10 °C < T_{out}< 22°C

While equation 5.1 is data specific, Wang's results were shown to agree with EnergyPlus simulations, and do give an important indication of the impact of thermal mass on enhancing the use of natural ventilation. The growth rate of savings initially increases with increasing the thermal mass time constant, but eventually tapers off. This can be tied to the simple thermal model analysis in section 2.5: as thermal mass time constant increases the steady state damping factor tapers off. An interesting finding in his results is that increasing thermal mass in Miami weather actually gives rise to a decrease in electricity saving for cooling. This was explained by a larger time constant meaning that the building takes longer to gather the cooling potential overnight [39]. However, it could be argued that the heuristic set-point strategies for natural ventilation used in their study do not take into consideration the thermal mass. Essentially, this highlights the need for a better natural ventilation control strategy by taking into consideration the transient response of the thermal mass.

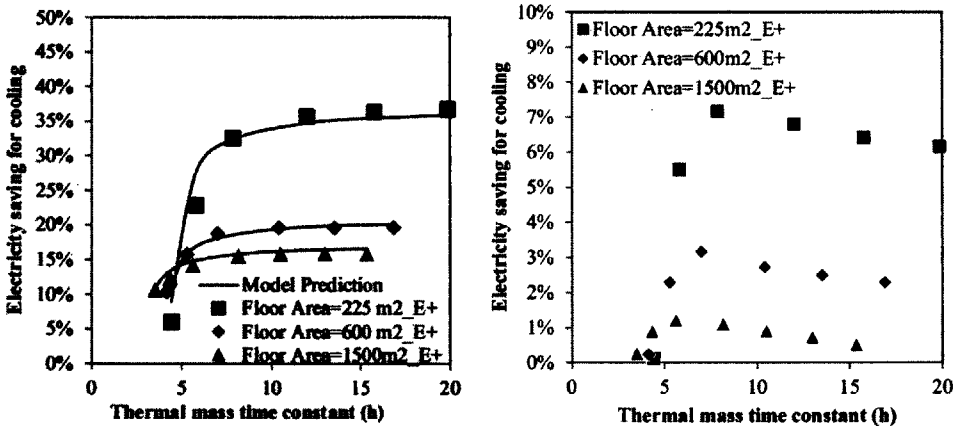

Figure 5-1: Effects of thermal mass, floor area and climate (left: moderate Philadephia, right: warm Miami weather) on electricity savings in simulation of a naturally-ventilated building [39]

User-behavior based Controls

Rijal et al.[40] carried out a field survey on 15 existing buildings in the UK to gauge users' control behavior of windows in buildings. Using logistic regression analysis, they came up with an algorithm, called the Humphrey model, which could be embedded in building simulation software to emulate the effect of building design on users' window-opening behavior, given the actual outdoor and indoor temperatures. This algorithm is a very indirect way of optimizing ventilation to maintain instant thermal comfort based on statistics. However, it assumes that the actions (closing or opening of windows) of the people in the survey are actually the optimal ones, and not the thermal comfort they perceive. Furthermore, knowledge of future disturbance, such as weather forecast, cannot translate through the occupants' immediate action. Hence, occupants cannot be expected to behave in an energy-efficient manner.

5.1.3 Model Predictive Control Strategies

The past decade has seen a growth in research on Model Predictive Control (MPC). MPC is a control methodology that produces strategies for a given time horizon so as to minimize a defined cost function, by making use of the predictions of a building energy model. MPC can be online or offline: offline MPC has a defined horizon over which optimization is carried out; online MPC is real-time optimization whereby the inputs and disturbances to the systems are continuously being fed back to the model, hence considering the real-time results of the optimization and allowing for correction due to model mismatch. Because the control is based on a mathematically or physically-based model of the process in question, it can account for linear or non-linear dynamics, and simple or complex interactions, defined by the model. The shortcoming of MPC is that the model needs to be well-defined. Three kinds of models have been investigated in literature: (i) forward (white-box) models; (ii) inverse (black-box) models; (iii) hybrid (gray-box) models. Forward models are based on physical building parameters with energy and mass balances solved numerically including those seen in Chapters 2 and 3; so they require a lot of input details for proper modeling. Inverse models are data-driven, i.e. they require training based on on-site measurements; based on empirical data only, they might not model physical behavior properly. The gray-box model [41] seeks to reconcile their shortcomings using transfer functions with parameters that are constrained to satisfy simple

energy balance of energy flows in the building; it requires a smaller set of building parameters and yet makes use of training data to better characterize the building.

MPC has been examined related to buildings in several fields: optimal control of active and passive building thermal storage [42]; optimal scheduling of fans in hybrid-mode building, and control modes of mixed-mode buildings using data-driven (gray-box) models [6], [43]; and controls of windows in a mixed-mode office building using forward (black-box) models [44], [45]. A more thorough study of MPC was carried out by a Siemens BT study, with modeling, design and implementation done for 64 room types at four European sites [10], [46]: besides thermal comfort maximization and energy usage minimization, minimization of peak electricity demand was also a consideration.

Spindler and Norford [43], [47] developed flexible and accurate linear thermal models, whose characterizations depend on measurements at several time intervals of indoor air and thermal mass temperatures, loads and outdoor conditions. Spindler concurrently developed a flexible type of regression, called Principal Hessian Direction Regression Tree (PHDRT), to deal with nonlinearities expected for buildings with natural ventilation. While genetic algorithms and simulated annealing were initially used as the optimization techniques, Spindler found them to be inefficient; instead an optimization framework was developed whereby a set of cooling strategies were defined and ranked. The optimization was carried out with respect to maximization of thermal comfort and minimization of fan energy use.

Comparatively, May-Ostendorp's model was physics-based [44], [48]. In fact, the simulation was carried out in EnergyPlus for a standard DOE office building with natural ventilation. Within the MPC framework, optimization of the window opening schedule was done using a Particle Swarm Optimization (PSO) algorithm. Their optimization was carried out with respect to minimization of cooling and heating energy and fan energy consumption while maintaining thermal comfort. A weighted penalty which scales with the number of window state switching was also incorporated. The optimization was shown to be effective compared to a reference case where the non-optimization window schedule was defined by the Humphrey model discussed above: a 54% savings was noted; compared to a base case where only mechanical cooling and heating were available, a 10% savings was noted. The optimization results, for a summer –long

worth of Boulder (CO) weather data, were then generalized for a defined model parameter set, using a statistical technique with generalized linear models derived through multiple logistic regression. They concluded that statistically-generated predictions, used offline in the same baseline building as the MPC study, achieved 70-90% of the energy savings predicted by the MPC [44].

The MPC study carried out by Hu and Karava [45], [49] expanded on a similar MPC framework to May-Ostendorp's by adding and varying parameters in their building model, namely the shading system heuristic controls, thermal mass variation and the presence/absence of an exhaust fan. The building model itself was a multi-zone thermal and airflow model they developed in MATLAB. Like in May-Ostendorp's study, the optimization was carried out by a PSO algorithm. Their optimization results, for five summer days with Montreal weather data, was carried out with respect to minimization of mechanical cooling energy while maintaining thermal comfort. The optimization was shown to be effective compared to a base case where only mechanical cooling was available, a 75% of energy savings was noted. Strikingly, a reference case where the non-optimization window schedule was defined by a simple rule-based heuristic control (notably, minimum and maximum ambient temperature set-points of 15-25 ^{0}C) was seen to perform better in terms of energy savings (83%); however, thermal comfort was not maintained always maintained in that case.

The application of MPC in buildings has garnered a lot of attention in the academic sphere because of its effectiveness in providing substantial energy savings and improved indoor comfort. However, it faces difficulties for its implementation in the supervisory control of actual buildings: In addition to the numerous data (training or physical) needed to put up a suitable model of the building, MPC requires cost and knowledge for data processing and its maintenance. In particular, because the numerical optimization computation required by MPC does not fit in the memory of actual Programmable Logic Controllers (PLC), a separate computational core needs to be attached to the BAS [50]. In its implementation in two test buildings, Cigler et al noted that MPC deployment required many months of monitoring and tuning: one project has been ongoing for four years, with the modeling taking 60% of that time, and the MPC development taking 35%. They also noted that for the lightweight building

investigated, there was no payback: the existing conventional rule-based control worked well enough as the thermal dynamics could not be exploited [50]. In fact, in the Siemens BT study, MPC controls were found to be more beneficial over rule-based controls for buildings with high energy fluxes and during transition seasons, as well as for heavyweight buildings [10], [46].

5.1.4 Optimized rule-based controls

While current research is focused on the afore-mentioned predictive algorithms, some reviews have concluded that there is not much difference between from simple fixed-rules and these predictive controls [51], [52]. Some of the simple fixed-rules for night-ventilation have been addressed in literature (see section 4.1.2). However, most of these rules have set-point and overcooling constraints with temperature thresholds which have been deemed most appropriate after months of experimentation on the demonstration buildings through manual adjustments. Nevertheless, according to Gyalistras, these kinds of rule-based controls are convenient and flexible enough because they are easily implemented in non-standardized Building Automation applications [53]. Therefore, they experimented with optimized predictive and non-predictive rule-based controls to taking into account historical data, or weather forecast, internal gains and occupancy predictions.

Gwerder et al. looked at improving current ruled-based control strategies [53]. Improvements were made by looking at 2 types of rule-based controls: (i) non-predictive, (ii) predictive control algorithms. The non-predictive control algorithm was based on historical data, i.e. measured outside air temperature and calculated heat gains of the last 24 hours for the night-ventilation control, whereas the predictive control algorithm was based on the predicted data for the next 24 hours.). An example of optimized rule-based controls used for the natural night-time ventilation subsystem is given in figure 5.2. The historical or predicted data was used to calculate the natural night-time ventilation limit, an outside air temperature threshold defined to prevent overcooling. It was the value for which the average internal heat gains compensated the heat loss through the façade, with the room temperature assumed to be in the middle of the comfort range. The predictive rule-based controls were found to outperform the non-predictive rule-based controls in terms of non-renewable primary energy usage. However, the controls operated on a different systems, namely blinds, free-cooling, mechanical night-time ventilation operation, natural night-

time ventilation and energy-recovery operation [53]. As such, it is difficult to ascertain for which systems the non-predictive rule-based controls did not fare as well as its predictive counterpart.

(a)

```
If (outside air temperature > natural night-time ventilation limit) &
(unoccupied night-time)
    if (room temp. > natural night-time vent. target room temp. setpoint)
        natural night-time ventilation operating mode = UNLOAD;
    else
        natural night-time ventilation operating mode = LOAD;
    end
else
    natural night-time ventilation operating mode = LOAD;
end
```

(b)

- **Operating mode LOAD**

```
Do not force natural night-time ventilation.
```

- **Operating mode UNLOAD**

```
If (outside air temperature < room temperature)
    // perform natural night-time ventilation
    automated window position = open;
else
    // do no mechanical night-time ventilation
    automated window position = closed;
end
```

Figure 5-2: (a) Example of optimized rule-based controls used for the natural night-time ventilation subsystem in a Siemens BT study [46], with the definition of the two operating modes in (b). Note that the target room temperature set-point was set to 1 K above the lower temperature set-point of the thermal comfort range.

Levermore reported a similar adaptive threshold in the night-ventilation controls of the Ionica building in Cambridge, UK [38]. To prevent overcooling, the controls included a self-learning schedule to limit the night degree cooling hours, based on the day degree-hour heating and the average day room temperature. If that temperature was above a predefined set-point, the night cooling degree hour were increased beyond the day heating degree hour; if it was below, the night cooling degree hours were decreased. However, the thermal performance with this type of control was not reported.

This literature review has shown that building controls, in literature research or actual site use, are not straight-forward to optimize. Two main approaches can be seen: predictive control and rule-based controls. Both approaches will be investigated in chapter 6, using the simple physics-based energy model developed in chapter 2. The predictive control, using dynamic programming as the optimization technique (covered in the next section), will provide the benchmark results against which the rule-based control can be measured in terms of thermal performance.

5.2 Optimization problem formulation

All optimization problems can be formulated as an objective function to maximize or minimize, subject to constraints. Optimization problems can be divided into three main cases: when the problem is linear and the solution space is convex, when the problem is non-linear and the solution space is convex, or when it is non-linear and the solution space is non-convex. Linear programming is usually used for the first case and quadratic or non-linear programming for the second case. Many optimization techniques exist for the third case, for instance: dynamic programming (DP), combinatorial optimization, integer programming, heuristics such as genetic algorithm (GA) or particle swarm optimization (PSO).

Our problem consists of choosing the optimal ventilation schedule (opening and closing times for windows) for a pre-defined time horizon for a given set of climatic and building parameters, with the objective of maximizing thermal comfort for that time period, i.e. wanting the room air within thermal comfort limits for as long as possible during occupation. Our problem is non-linear and non-convex: the objective is not a linear function of the pattern of window closing and opening, and there is not necessarily a global optimal solution as different window schedules can give almost similar thermal comfort level. Therefore, the optimization techniques chosen for our problem are dynamic programming and combinatorial optimization. The heuristic methods mentioned above were not chosen because although faster than dynamic programming or combinatorial optimization, they approximate the solution and converging on a solution is not efficient if the swarms or generations are not defined and generated properly. Moreover, the size of our problem is not so bad in terms of memory or running time as to require any approximation.

The hierarchy of controls for natural ventilation only entails closing and opening windows. In physics term, this means it affects the flow rate of outside air entering the room, hence the convective heat transfer. The controls operate on an hourly basis, as determined optimally every time period by the dynamic programming.

In all natural ventilation simulation results, it is assumed that an air change rate of 5 ACH is met with the window open, with negligible energy cost associated with fan usage to meet this air change rate.

Reward/cost function definition

An optimization problem needs to be defined in terms of a cost or reward function to be minimized or maximized. Our problem aims to maximize thermal comfort. For this reason, it is necessary to define the thermal comfort limits uniformly throughout all simulations. These can be defined by the ASHRAE thermal comfort standards 55. Two standards exist:

1. Predictive Mean Vote (PMV) used for air-conditioned buildings
2. Adaptive model (for buildings without mechanical systems)

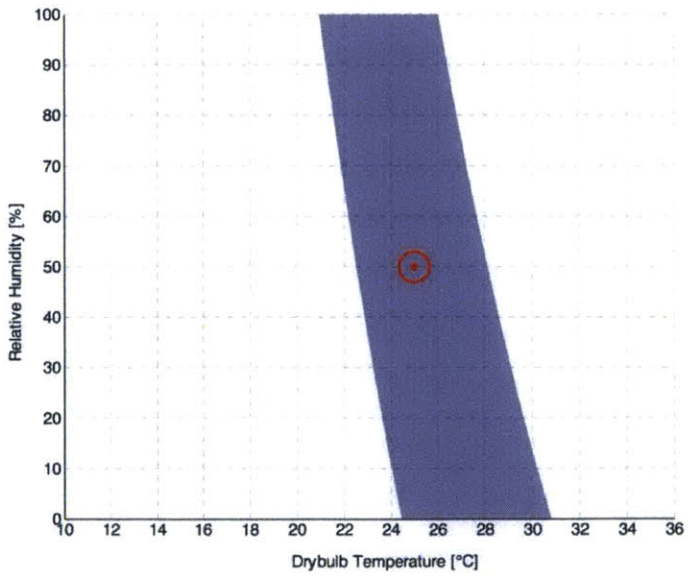

(a)

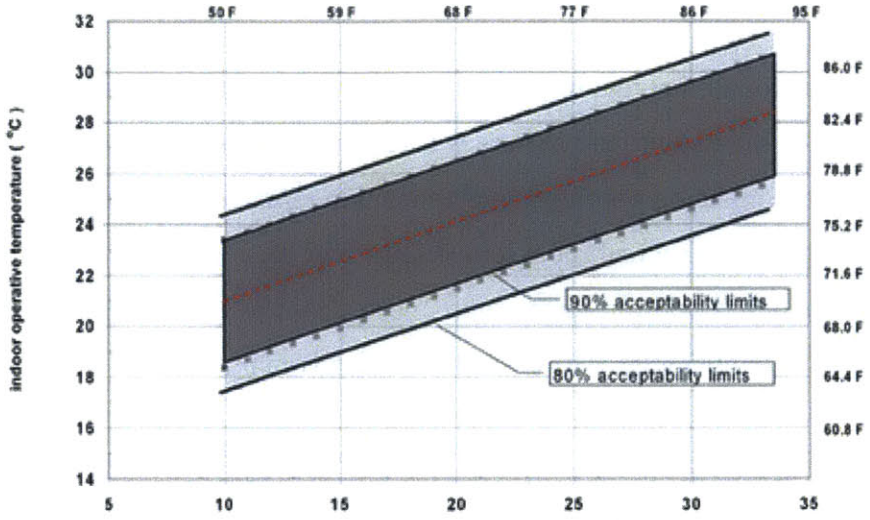

(b)

Figure 5-3: Thermal comfort models: (a) Predictive Mean Vote model, (b) Adaptive model

The adaptive thermal comfort model takes into account people's thermal responses in terms of recent thermal experiences, clothing adaptation, availability of control options and their expectations in naturally conditioned spaces. The model thus relates the acceptable range of indoor temperatures to the outdoor climate, without the need for humidity, air-speed limit and clothing values [12]. Because of its simple derivation, this adaptive model was chosen for determining the thermal comfort range for a particular mean outdoor temperature. The mean monthly outdoor temperature in the figure above is the average of the mean daily minimum and mean daily maximum outdoor (dry-bulb) temperature for the month. Based on the 90% acceptability limit for the adaptive comfort model, the minimum and maximum temperature for thermal comfort can be put as a function of the outside temperature as:

$$T_{\text{min comfort}} = 0.3 * (\text{T}_{\text{out}} - 15) + 20 \ (in\ °C) \tag{5.1}$$

$$T_{\text{max comfort}} = 0.3 * (\text{T}_{\text{out}} - 25) + 28 \ (in\ °C) \tag{5.2}$$

Initially, a reward function was used whereby, if the state of the indoor temperature was within the thermal comfort range at a particular time-step, the reward was incremented by 1, else it given a value of 0. The overall reward for the time period (1h) was then normalized by the total possible reward within that period. The resulting cost function could be defined thus:

$$cost = \frac{\Sigma_{timestep\ t=1\ to\ n}\ X}{n} \tag{5.3}$$

Where X=0 if $T_{\text{min}\,comfort} < {T_{air}}^{t} < T_{\text{max}\,comfort}$, else X=1.

However, it was found that that binary form of reward was not sensitive enough to distinguish and reward when the indoor temperature was closer to the thermal comfort range than when it is not. Now, the optimization problem is formulated in terms of a cost function, which is defined as a difference between the actual room temperature and the closest thermal comfort threshold, i.e. the minimum and max comfort temperature, normalized by the difference between that minimum and max comfort temperature. The cost function is given by:

$$cost = \frac{\sum_{timestep\ t=1\ to\ n} \min(|{T_{air}}^{t} - T_{\min comfort}|*X, |{T_{air}}^{t} - T_{\max comfort}|*X)}{n*(T_{\max comfort} - T_{\min comfort})} \tag{5.4}$$

Where X=0 if $T_{\min comfort} < {T_{air}}^{t} < T_{\max comfort}$, else X=1.

5.2.1 Combinatorial optimization

Combinatorial optimization involves finding the optimal solution from a finite set of possible solutions [54]. As the set of solutions is discrete, the solution search can be exhaustive if the set is not too large.

Combination optimization is ideal for my case where the solution set is restricted to having closing and opening once or twice. Thus it can be used to investigate optimization of night-ventilation, where windows are only closed and opened once. This is computationally feasible as there are fewer than 24^2 possible combinations of closing and opening hours, since the opening hours can be restricted to occur after the closing hour, when there is no risk of overcooling such that windows need to be closed before midnight. Thus, each combination gives a possible window ventilation strategy schedule, and the thermal comfort cost resulting from a whole horizon simulation with each schedule can be calculated. The optimal solution is then found by sorting the resulting cost list and extracting the window ventilation schedule which gives the least cost.

5.2.2 Dynamic programming

Dynamic programming is an optimization technique suitable for non-convex problems involving sequential decision processes, which are inherently Markov Chain processes, i.e. the future/

previous state depends only on the current state. Dynamic programming decomposes big problems into many smaller ones, by defining time periods. Moreover, it can cater for stochastic disturbances to the system by using expectancy based on a corresponding probability distribution. Dynamic programming is chosen as one of the optimization techniques for optimizing the ventilation schedule because energy modeling of buildings inherently involves non-linear behavior over even a single time-period; for instance, buoyancy-driven flows for which the air flow rate depends on the temperature difference between zones. While, for our simple single-zone model, such non-linearity does not arise, the aptitude of dynamic programming can be tested before expanding to more complex energy models. Moreover, the scheduling of ventilation involves making decision after regular time intervals.

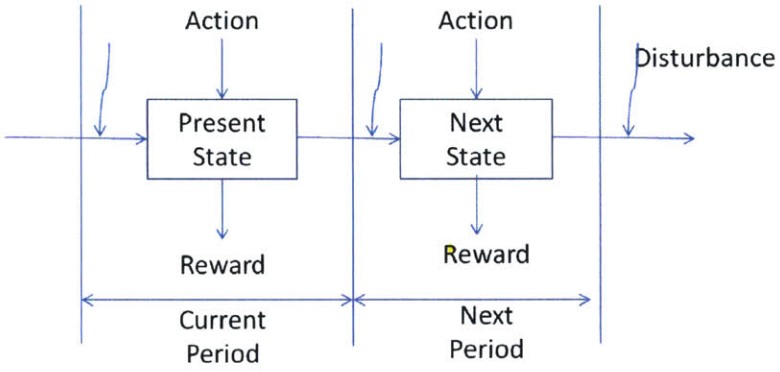

Figure 5-4: Dynamic programming schematic for optimization

Three forms of dynamic programming exist: backward induction, forward induction and approximate dynamic programming. Backward induction is chosen as it gives control in defining the optimal path in the future based on what current state one is in. Backward induction is also more familiar as it is similar in concept to how decision trees are solved by "folding back", i.e. working backward from right to left. Comparatively, forward induction gives control in defining the states one wants to end in, and the optimal path leading to them. In approximate dynamic programming, it is not necessary to visit all states exhaustively. However the value function needs to be iteratively approximated using stochastic gradient algorithms for convergence.

Compared to combinatorial optimization, dynamic programming breaks down the whole horizon into smaller processes, but does not go through all the possible combinations of actions. Instead,

it benefits from the folding back of the decision trees to weed out later actions which are discarded as not optimal. Hence, it is less computationally expensive than combinatorial optimization: the latter would have run a total of 2^{24} possible combinations of opening and closing actions, if these actions were to be made every hour over a 24-hour horizon.
Dynamic programming requires the definition of the following key elements [55]:

(i) Decision period, t

For our problem, the decision period can be defined as a 1 hour time period as that is the interval at which weather data are obtained, and a smaller decision period would be too frequent for the mechanical actuation of the windows.

(ii) State space, S

It is critical to choose the state space properly. It needs to be a variable which requires no history memory, and is a function of the action and disturbance. It could be multi-dimensional if it has more than one variable. The domain the each state space can be subjected to different constraints for each time period. For our problem, our multivariable state space consists of room air temperature and thermal mass temperature. Contrary to discrete problems for which dynamic programming is usually used for in system operations management (as in inventory problems for instance), our states need to be discretized to suitable number of bins (B) to provide enough accuracy.

(iii) Action space, X

The state space has only 1 action variable, i.e. x=window action. The possible window actions which can be made at each decision point: close (set ACH=0) or open (set ACH=maximum). Intermediate actions such has half-closed have been discarded as it has been proved that temperature is not a convex function of the mass flow rate (see section 6.1.1 on the finite-difference rule). Hence, it is always better to maximize or minimize the air flow rate.

(iv) Stochastic element space, W

The stochastic element space represents the variables which have uncertainty. It can also involve stochastic disturbances such as predicted weather forecast or occupational level. However for our simple model, the stochastic element is not necessary as weather files are usually used and for a first-level design occupancy can be approximated.

(v) Reward or cost, $C(x_n, S_n)$

The reward (to be maximized) or cost (to be minimized) is computed at each period, and is a function of the current state. For my case, the cost function is determined by the thermal comfort level as described by equation 5.4.

(vi) Transition function

The transition function defines how to move from one state to another, from one time period to the other based on decision (window-opening) and information (weather). The transition function, which gives the value of the states at the next time epoch, is governed by the following recursion:

$$S_{t+1} = S^{model}(S_t, X_t, W_t) \tag{5.4}$$

For our problem, it cannot be explicitly described in terms of the states and actions. The move from one state of temperature variables to another is determined by the coupled differential energy equations governing the building physics, which are solved numerically as explained in chapter 2.2. For this problem, the transition function S^{model} is determined by my black-box MATLAB function representing the energy simulation engine, using a single thermal mass element. The model evaluates numerically the temperature states S_{t+1} at the next decision time step given the current states S_t, the decision action X_t to close or open window for the hour, and the exogenous weather information W_t.

(vii) Value/contribution function:

$$V_n(S_n) = \max_{x_n} C(x_n, S_n) + \gamma V_{n+1}(S_{n+1}|S_n)\} \tag{5.5}$$

This equation is the finite horizon (of N time periods) dynamic programming version of the Bellman's optimality equation. The contribution or value function calculates the value of being at a particular state S_n, at a particular time period. That value incorporates the current value for the time period, i.e. the cost $C(x_n,S_n)$, as well as the future value of being at the next state s_{n+1} calculated by the transition function. The discount γ can be set to zero, as the value associated with thermal comfort does not need to depreciate with time.

(viii) Objective function

The objective function is given by the following equation:

$$\max_{\pi} \text{ or } \min \sum_{n=0 \text{ to } N} V_n(\text{state } S_n, \text{decision } x_n(S_n|S_{n=0})) \tag{5.6}$$

For our case, the objective function defines the optimum window policy π that maximizes the thermal comfort over a time horizon of N=24 hours, given initial conditions for our states.

The figure below shows a simple schematic of backward induction dynamic programming for our problem. Note that the red arrows are an example of an optimal policy for the actions.

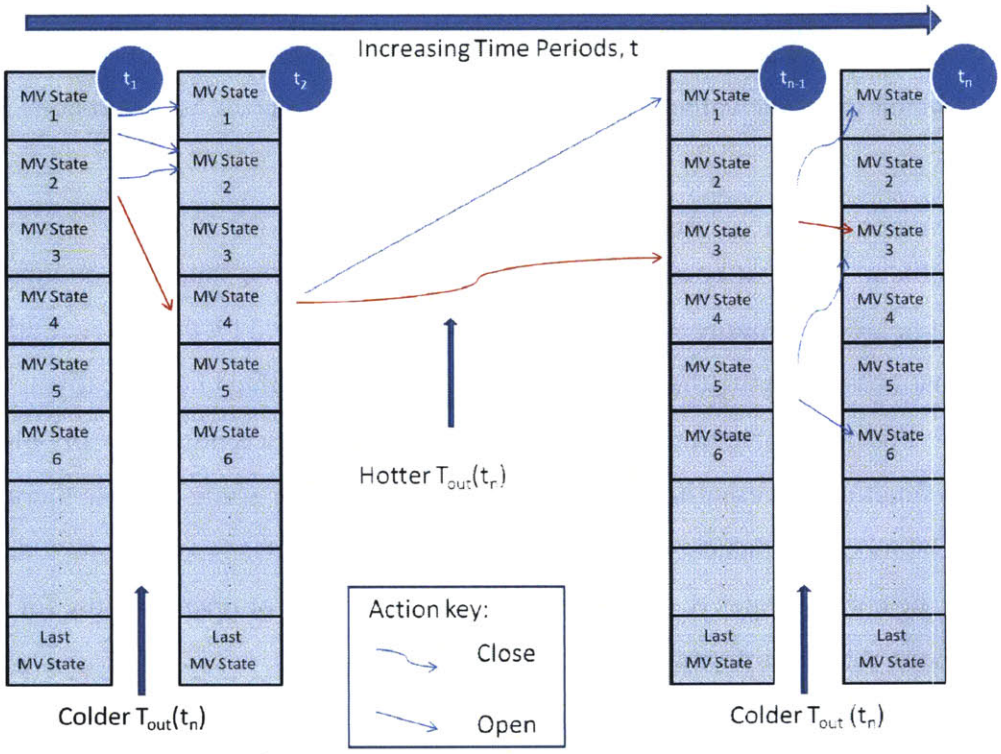

Figure 5-5: Sample dynamic programming schematic for optimizing the closing/opening of windows, where the columns indicates the multivariable state bins for a given time period t_n, and the red arrows represent a sample optimal path of window actions

Figure 5-3 indicates some of the downsides of using dynamic programming. There are three such "curses of dimensionality": state space of I dimensions which can take L possible values, can have L^I possible states; uncertain Information space of J dimensions which can take J possible values, can have M^J random signals; action space of K dimensions which can take N possible values, can have N^K possible values [55]. For my case, stochastic elements are disregarded and action space is one-dimensional with only 2 values. Hence, the dimensionality of my problem depends on the temperature (air and thermal mass) states and their possible values.

Therefore, the constraints need to be imposed on our state space. The constraints are based on the building physics and dictate the range of values adopted for the states. The simplest constraints are that the state values have to be smaller than the maximum outdoor temperature and bigger than the minimum outdoor temperature. The range of values needs to be discretized so as to give enough accuracy in approximating in which bin the periodically computed next value state falls.

The whole point of the dynamic programming is that it captures the effect of future decisions at the current decision time. The dynamic programming optimization algorithm works for whatever disturbance, i.e. occupational schedule, outside temperature, and initial temperature imposed. For instance, for Miami temperature for May 15-17 obtained from TMY3 weather data, the optimal window schedule looking over successive time horizon of 25 hours for 3 days is shown below. Figure 5-6 also shows the resulting optimal values of the state variables (room air temperature, T_{air} and thermal mass temperature T_{Tmass}) in the blue and red line respectively, and the given disturbance T_{out} in green line, and occupancy schedule in the third subplot. The thermal comfort limits, which define the cost function, are also shown.

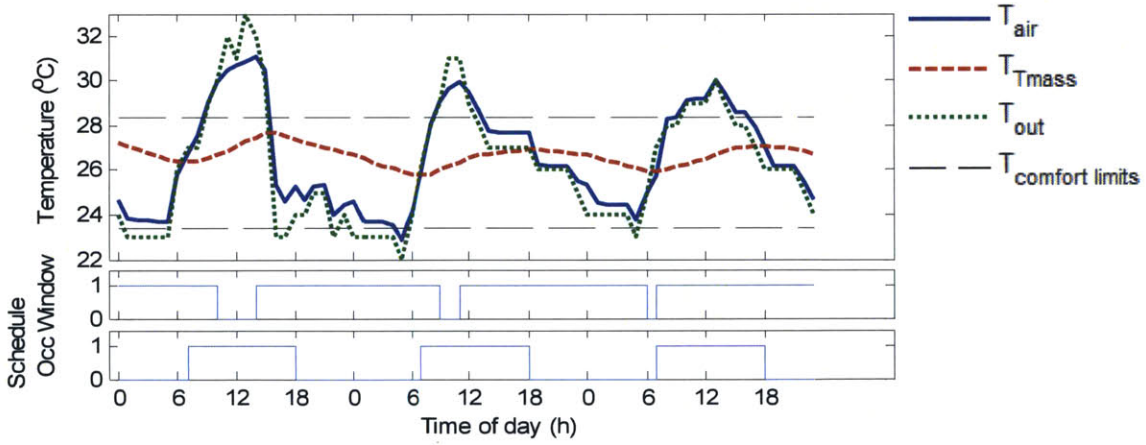

Figure 5-6: Resulting optimal window strategy for Miami weather May 15-17 Energy model parameters used: low heat gain, q=15W/m^2; normal thermal mass heat capacity c=880 J/kgK. Thermal cost for each day=[2.7, 1.0, 1.1]

In the parametric investigations of the effect of different building parameters on the window opening/closing strategy, a simple sinusoidal outside temperature with a period of a day is first used. In doing so, it is easier to validate the models using known analytical solutions and account for the general sinusoidal temperature patterns rather than having temperature weather anomalies distort the DP strategy investigation.

Dynamic programming usually deals with discrete states. Because, the window-actions do not result in a linear mapping in the post-decision state but instead by a function mapping determined by the hour's energy balance, the state space needs to be discretized in a large enough number of bins, such that the dynamic programming can choose the optimal path based on the closest bin to the resulting temperature at the end of the hour. The temperature change within the hour is a function of the building and outside temperature parameters, and can be as low as 0.1 C for high thermal mass. Hence, in that case, a state discretization of the order of a hundred is needed for a state space spanning 10 degrees. As can be noted in the above figures, when a large enough state space is used, the resulting temperature profile is accurate enough such that energy balance is maintained between each decision period.

The dynamic programming optimization method gives us a means of establishing the optimal window strategy with hourly decision pattern, whatever the disturbances. Thus the dynamic programming optimization algorithm can be implemented in a simulation engine in a similar way to how model predictive control is wrapped over a desired time horizon to dictate the optimal strategy over a time period less than the time horizon, given the weather forecast. It is however computationally expensive: as described before the accuracy of the computation depends on the state space, i.e. the larger the state space, the more accurate the temperature profile. While for the above simulations, the only disturbance was the outside deterministic temperature forecast, it can be expanded to include stochastic element, and a wider range of actions.

The nature of the sequential window action problem suggests the use of dynamic programming over a rolling finite horizon. Its downside is that it becomes computationally heavy with a larger energy model, which has more states in terms of zone temperatures for example. However dynamic programming is still more computationally efficient that global optimization if there is no constrained of one opening and closing per day, since the backward inductions help to weed out non-optimal sequential paths of the window actions.

Chapter 6

Case-studies of optimized and rule-based controls

As was seen in section 4.2 on ventilation modeling, it is not clear what the optimal ventilation schedule is, with respect to thermal comfort. This chapter seeks to use the two optimization techniques developed in section 5.2 to identify the optimal ventilation schedule for different case-studies, with variation in the parameters defined in chapter 2. Two categories of case-studies are carried out: (i) simplified sinusoidal outdoor temperature profiles of known mean temperature and amplitude; (ii) sample dry-bulb outdoor temperature profiles from four different cities.

The two optimization techniques allow two types of optimal ventilation schedules to be developed within reasonable computational simulation times: (i) dynamic programming allows multiple onsets of natural ventilation throughout the day; (ii) brute-force global optimization allows only one onset of natural ventilation daily, i.e. this is night-ventilation mode whereby there is only one closing/opening. Optimization runs utilizing brute-force global optimization use an energy model with spatially-discretized thermal mass (10 slices), while optimization runs utilizing dynamic programming use an energy model with thermal mass at a uniform temperature (1-slice) and the effective heat transfer coefficient developed in section 2.8. This is done so as to limit the state domain space through which the optimization algorithm has to search, hence limiting simulation time.

In the process, simple easily-implemented heuristic rules, which do not require real-time energy simulations, are sought. These rules are then tested and its results compared against the optimized ventilation schedules generated using dynamic programming and brute-force global optimization.

The developed heuristic rules are used to form a holistic optimized rule-based control algorithm to cater for a wide range of parameters. The holistic control algorithm is then used to predict the

optimal ventilation schedule for simulations using real weather data for different cities. The results are then compared to those generated by the optimization techniques, in terms of thermal comfort cost.

In effect, the optimization techniques used can be considered to take part in an offline Model Predictive Control framework, whereby the energy model is physics-driven and kept simple to one defined by energy equation 2.4, and whereby the cost minimization is simply that of thermal comfort. The overall framework for this is shown in figure 6-1. The optimal control which results can be used as a benchmark against which the developed optimized rule-based control algorithm can be measured.

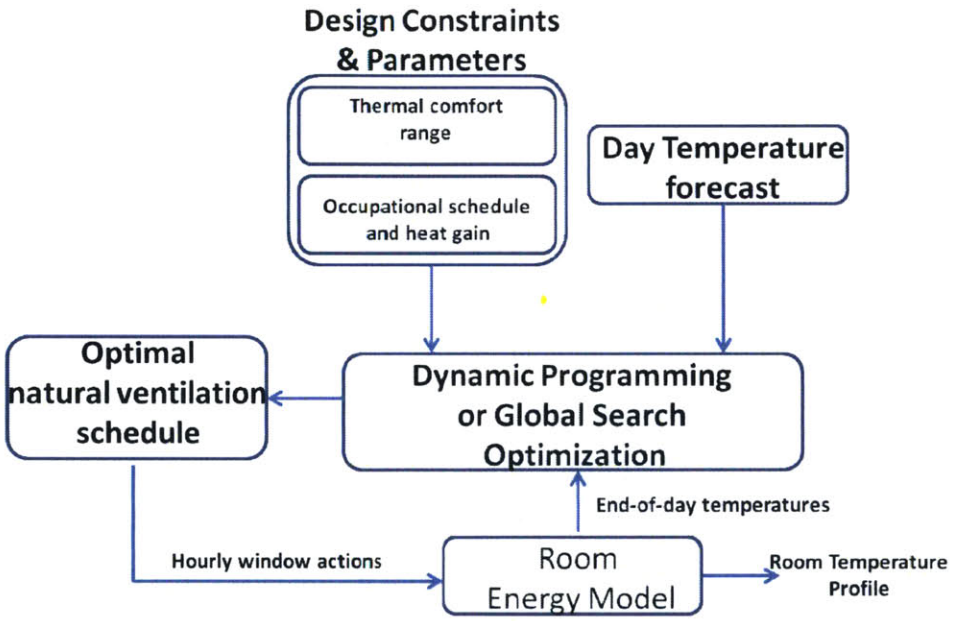

Figure 6-1: Overall algorithm framework for optimizing ventilation control to maintain thermal comfort

6.1 Rule extraction

The ventilation strategies section highlighted the lack of an optimized natural ventilation schedule, which takes into consideration the building, climatic, and ventilation parameters. The window schedules resulting from dynamic programming optimization can reasonably be assumed to be the optimal one over a 24-hour horizon and given a set of constraints. Four types of simple ventilation rules or strategies were investigated:

1. Heuristic rule: when the outside air temperature is greater than inside temperature, close the windows, i.e. put ACH=0;
2. One-hour horizon: at every decision period, run the simulation with windows closed and open and choose the action which gives the lowest resulting room temperature.
3. Finite-difference rule: this rule chooses the action which gives the lowest resulting room temperature. This is an improvement over the one-hour horizon strategy in that the window opening/closing decision can be made based on the current time period's values of temperatures and forecast outdoor temperature instead or running the simulation twice to determine what is the best action. This is done using the equations developed in the next section.
4. Overcooling-prevention strategy: this strategy is needed to makes sure that night-ventilation is not so excessive that the thermal mass is pre-cooled causing the room air temperature at the start of occupation to be below minimum thermal comfort level. As such, this strategy is more involved than the above rules as it requires knowledge of the room's thermal dynamics and thermal history.

6.1.1 Finite-difference rule

The heuristic rule is the simplest logical one. In order to lower the indoor temperature, it is beneficial to open the windows when the outdoor temperature is lower than indoors. However, the benefit of closing the windows if the temperature outside is greater than inside is not as straightforward: if there is a high interior heat gain, it might still be more beneficial to allow natural ventilation such that the convective heat transfer, through air mass transfer, prevents the interior heat gain from accumulating. This is catered for by rule 2 and 3, quantitatively so by rule 3.

The finite-difference rule is an approximation of the room temperature T at the next time step. Several time-marching variations of the energy balance equation can be made.
Written explicitly, the room energy balance from equation 2.4 is first-order accurate in time:

$$T^{t+1} = T^t + \frac{\dot{m}c_p\Delta t}{mc_v}(T^t_{out} - T^t) + \frac{hA\Delta t}{mc_v}(T^t{}_{T\,mass} - T^t) + \frac{qA\Delta t}{mc_{T\,mass}} \quad (6.1)$$

Written implicitly, the energy balance from equation 2.4 is still first-order accurate in time:

$$T^{t+1} = T^t + \left(\frac{1}{mc_{T\,mass} + \dot{m}c_p\Delta t + hA}\right)\{\dot{m}c_p\Delta t(T^t_{out} - T^t) + hA\Delta t({T^t}_{T\,mass} - T^t) + qA\Delta t\} \quad (6.2)$$

However, these formulations do not allow minimization of T^{t+1} with respect to the mass flow rate $\dot{m}$ as $\frac{\partial T^{t+1}}{\partial \dot{m}} \neq f(\dot{m})$.

Written semi-implicitly using the trapezoid rule, also known as the second-order Runge-Kutta numerical method [24], the energy balance from equation 2.4 becomes second-order accurate in time and gives. Using the trapezoidal rule, i.e $T^{t+1} = T^t + \Delta t \frac{\frac{dT^{t+1}}{dt} + \frac{dT^t}{dt}}{2}$:

$$T^{t+1} = -T^t + 2\bar{T}_{out} + T^{t+1}_{out} + \left(\frac{1}{mc_{T\,mass} + \frac{\dot{m}c_p\Delta t}{2} + \frac{hA\Delta t}{2}}\right)\{2\,m_{air}c_v(T^t - \bar{T}_{out}) + hA\Delta t(\bar{T}_{Tmass} - \bar{T}_{out}) + \bar{q}A\Delta t\} \quad (6.3)$$

Where $\bar{T}_{out} = \frac{T^t_{out} + T^{t+1}_{out}}{2}$ and $\bar{q} = \frac{q^{t+1} + q^t}{2}$

This formulation can be used as the basis for the finite difference rule as it allows minimization of T^{t+1} by variation of the mass flow rate $\dot{m}$, hence the window state.

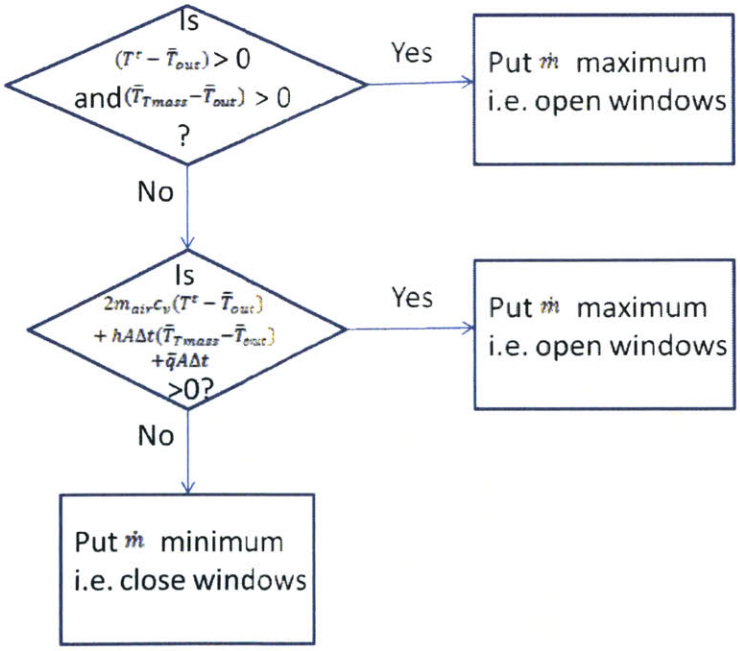

Figure 6-2: Control logic for finite-difference rule

The finite-difference rule enables the decision of whether to start or stop natural ventilation as shown in the control logic in figure 6-2, given knowledge of the current room air and thermal mass temperatures, and of the heat gains. However, the finite-difference rule is not easily implemented using normal Building Automation software, as it requires exact temperature of the thermal mass. As highlighted by in literature, monitoring the thermal mass temperature is difficult and not encouraged as the temperature is very sensitive to position and surface depth [38].

6.1.2 Over-cooling strategies

Overcooling strategies are needed to prevent the thermal mass from being pre-cooled to such an extent at night that the room air temperature at the start of occupation is below minimum thermal comfort level.

Strategy 1: thermal mass temperature estimate threshold

One strategy would be to make use of the thermal mass surface temperature as the room air, having comparatively low heat capacity and having a low time constant of the order of a quarter-hour, rapidly equilibrates towards that temperature when ventilation stops. Hence, night-ventilation is stopped when the thermal mass temperature drops below the minimum thermal comfort limit temperature, $T_{min\ comfort}$. From chapter 2, for continuous ventilation, the thermal mass temperature at time t can be obtained using equation 2.12, as a function of the active variables which can comparatively be more easily measured (T^t, T^t_{out}, q^t, $\dot{m}^{t-1}$):

$$T_{T\,mass}{}^{t} = \left(1 + \frac{\dot{m}^{t-1}c_p}{hA}\right)T^t - \frac{\dot{m}^{t-1}c_p}{hA}T^t_{out} - \frac{q^t}{h} \tag{6.4}$$

Hence, the control logic is as shown in the figure below, and is only sensible because after occupational hours, the outdoor temperature keeps decreasing and allows the thermal mass to cool down further.

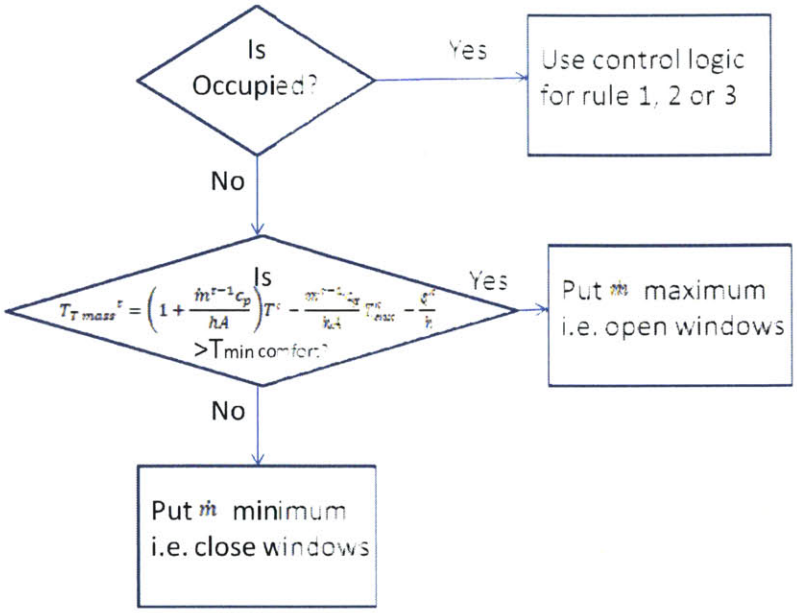

Figure 6-3: Control logic for overcooling strategy 1

Strategy 2: degree-hour self-adjusting algorithm

Like strategy 1, strategy 2 seeks to find the cut-off point for night-ventilation. However, contrary to strategy 1, it does not require building parameter characterization or assume that equation 2.12, i.e. a simple room energy model with only one thermal mass time constant is an accurate enough representation of the energy flows. Instead, it self-adjusts the day ratio of "heating" degree hours to "cooling" degree hours. Unlike Levermore's self-learning algorithm [38] referred to in chapter 5.1, this strategy is not based on the mean day temperature and an obscure set-point, but on the performance of the previous day's ratio, i.e. the resulting room temperature deviation from thermal comfort at start of occupation, $\Delta T_{day\ D} = (T_{air} - T_{min\ comfort})_{h=occupation\ onset\ on\ day.}$ The degree hours are used with respect to a reference temperature. The minimum thermal comfort limit was chosen as that reference temperature. "Heating" degree hours are the sum of hourly resulting room air temperatures departing positively above the reference temperature, with the summation done over 24h starting from occupation onset. "Cooling" degree hours are for those departing negatively. The degree hours are defined thus because the learning curve of the self-learning algorithm is small: any day is likely to have a room air temperature above $T_{min\ comfort}$ due to occupational heat gain -hence allowing calculation of heating degree hours, as well as room air temperature below $T_{min\ comfort}$ due to night cooling -hence allowing calculation of

heating degree hours. A self-learning algorithm makes use of the previous day's performance in order to determine the subsequent day's ratio and hence the stopping point for night-ventilation. An example of the algorithm used is as follow Note that each day count is started at the start of occupation.

For hour=8am on day D to 8am on day D+1
If (hour==8am)
If $\Delta T_{day\ D}$ *equal or close to* 0
Keep the same ratio, i.e. ratio level increment=0;
else if $\Delta T_{day\ D} < 0$
Increase ratio for less cooling degree hours, i.e. ratio level increment=+1;
else
Decrease ratio for more cooling degree hours, i.e. ratio level increment=-1;
end
end
ratio $level_{day\ D}$*=ratio* $level_{day\ D-1}$*+ratio level increment;*
cumulate cooling degree $hours_{day\ D}$ *if any;*
cumulate heating degree $hours_{day\ D}$ *if any;*
maximum cooling degree $hours_{day\ D} = \frac{total\ heating\ degree\ hours_{day\ D}}{ratio\ corresponding\ to\ ratio\ level_{day\ D}}$;
If cumulated cooling degree $hours_{day\ D}$*<maximum cooling degree* $hours_{day\ D}$
stop night-ventilation;
else
continue night-ventilation;
end
end

6.2 Baseline parameters and parametric runs

In all the parametric runs, the following baseline case was used and the thermal mass' specific heat capacity and the room heat gain were individually varied as shown in table 6-1 below.

Baseline Parameters	**Values**
Climatic:	
Type 1: sinusoidal profile with minimum at midnight	
outdoor T_{mean} (°C)	[20, 25]
outdoor T_{amp} (°C)	7.5
Type 2: weather data	TMY3 data for Miami, Madison, Los Angeles and Kansas
Building:	
Room dimensions (m)	10 x 10 x 10

Thermal mass thickness (in) Thermal mass material properties Heat transfer coefficient (W/m^2K) Walls and windows	5" Concrete (ρ=2500kg/m^3, k=0.3W/mK) 8.0 or 4.0 (effective value for 1-slice thermal mass simulation) Adiabatic and without thermal mass
Controls and schedules: Ventilation ACH Occupational schedule	 5 roomful/h 7am-18pm
Varied Parameters	**Range**
Specific heat of thermal mass, c (J/kgK) Time constant with ventilation, $T_{Tmass}=\frac{(mc)_{Tmass}}{\dot{m}c_p}$(h) Phase lag, $\beta = \tan^{-1}[\frac{\lambda^2\omega\tau}{\lambda^2+\omega^2\tau^2(1+\lambda)}]$ (h) Time constant without ventilation, $\tau_2 = \frac{(mc)_{Tmass}}{hA}$ (h)	[220 880 2640] [3.3 13 40] [0.3 0.8 1.3] [2.4 9.7 29.1]
Heat gain when occupied (W/m^2) Heat gain when unoccupied (W/m^2)	[15 30 45] 0

Table 6-1: Parameters used in parametric runs during optimization and rule-extraction simulations

Varied parameters

The heat gain considered here is the "q" term of the room air energy balance of equation 2.4. The range of values used is typical of an office building, where the lighting and normal equipment electrical loads average from 10 to 50W/m^2 [56]. Although a more detailed simulation would include incident solar radiation and heat conduction through non-insulated walls and roof as done in more complete energy-modeling software packages such as Design Advisor (figure 3-6), the occupational heat load is the most significant one. Hence, the occupational heat gain is a step function, which turns on during the occupancy schedule of 7a.m-18p.m. The heat gain is assumed to go directly to the air only. The specific heat capacity is varied to represent variations in a building's thermal mass. Typically, the latter can be characterized as light, medium or heavy weight.

Thermal cost calculations

The occupancy schedule is taken into consideration when calculating thermal comfort cost. Hence, the cost function of the optimization is modified such that room temperatures below minimum thermal comfort have no associated cost when there is no occupancy. During occupancy schedule, the thermal cost is calculated according to equation 5.4.

Steady-state

In section 4.2.1, it was seen through figure 4-4 that different initial conditions give different resulting temperatures for the same ventilation strategy and outdoor temperature day-profiles and other simulation parameters. Hence, it is important to note that for each simulation run, the results were only considered if the temperature profiles have reached "steady-state", i.e. the model was "trained" for a number of days until the difference in thermal mass temperature from one day to the other was less than 0.1°C per slice of thermal mass. The temperature of the thermal mass and not the air was chosen to define the convergence criterion because the thermal mass has a much greater time constant than the air and hence takes longer to reach steady state. In practical terms, this pre-optimization run can be considered as the training of the energy model with the same weather day temperature profile. For the simulation runs with cities' weather data, because the temperature profile varies from day to day, the energy models were "trained" for 14 days with continuous natural ventilation schedule.

Getting building parameters

For the above control rules, some building parameters are needed to determine the time constants and convective heat transfer parameter λ, defined in chapter 2. However, it is unlikely that the building's h or thermal mass are predetermined. Assuming that the room's thermal dynamics can be lumped together into one time constant, the room's parameters can be determined based on field experiments and by making use of equation 2.14, which gives the room air temperature solution for continuous natural ventilation at known ACH. The damping factor ζ and phase shift β of the indoor room temperature with respect to the outdoor air temperature are given by $\zeta=\sqrt{\frac{\lambda^2+\omega^2\tau^2}{\lambda^2+\omega^2\tau^2(1+\lambda)^2}}$ and $\beta = \tan^{-1}[\frac{\lambda^2\omega\tau}{\lambda^2+\omega^2\tau^2(1+\lambda)}]$ respectively. From these measurable data points, it is possible to solve for λ and τ numerically. Since $\tau = \frac{(mc)_{thermal\ mass}}{\dot{m}c_p}$, $\lambda = \frac{hA}{\dot{m}c_p}$, and the mass flow rate $\dot{m}$ is known, it is possible to deduce the room's thermal characteristics: $(mc)_{T\ mass}$ and hA.

$$T(t) = T_{mean} + T_E + \Delta T_{out}\sqrt{\frac{\lambda^2+\omega^2\tau^2}{\lambda^2+\omega^2\tau^2(1+\lambda)^2}}\sin(\omega t - \beta) + constant * e^{-\lambda/(1+\lambda)\omega\tau} \qquad (2.14)$$

Where $\beta = \tan^{-1}[\frac{\lambda^2\omega\tau}{\lambda^2+\omega^2\tau^2(1+\lambda)}]$.

6.3 Case studies with sinusoidal outside temperature

The results of all the simulation runs done with both the 1-slice model (with effective h) and the 10-slice model are listed in tables C.1-C.4 in Appendix C. For each parametric run, comparisons in terms of thermal cost and window schedules are done for the different window control strategies: (i) always open, (ii) optimal technique, (iii) heuristic rule, (iv) 1-hour horizon rule. The latter two were applied only during occupational hours. It should be noted that the second-order finite-difference rule gave similar results to the 1-hour horizon rule as expected. It is also reasonable to say that the 1-slice model with effective h and the 10-slice model in general give corresponding results in terms of thermal performance (thermal cost), the exception being when there is no forcing signal, i.e. windows are closed. As illustration, see figure 6-4 below, which shows the resulting temperature profile and optimum window schedules, as well as the used occupational schedule.

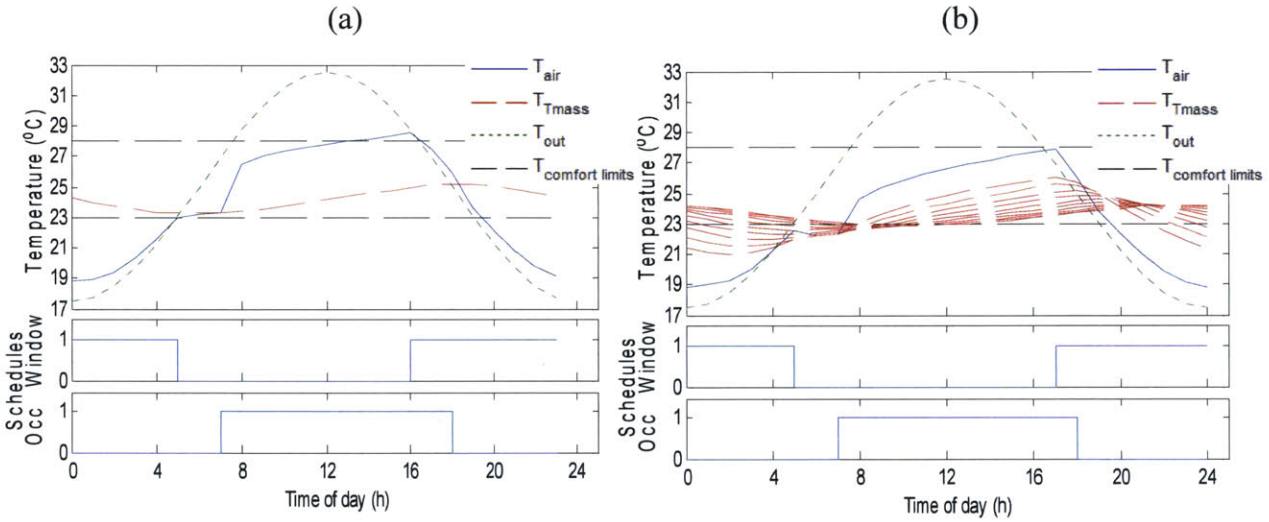

Figure 6-4: Comparison of performance of the 2 optimization techniques: (a) dynamic programming with 1-slice model, (b) global search optimization with 10-slice model. Parameters used: T_{mean}=25°C, T_{amp}=7.5 °C, low q=15W/m^2, normal c=880 J/kgK. Note that the horizontal lines represent the adaptive thermal comfort band.

Two observations can be made from figure 6-4: (i) for warm weather, the optimal schedule is that of night-ventilation; (ii) during occupational schedule and with room air is above minimum thermal comfort, the best closing or opening time is that at the cross-over points, i.e. when the outer temperature is respectively greater or less than indoor room air temperature.

In a few case studies however, it was better to open windows even though the outdoor temperature is greater than the current indoor temperature. This occurred for medium to high

heat gains: it is better to allow natural ventilation to flush out the interior heat gain more beneficial to allow natural ventilation, such that the convective heat transfer and the air mass outflux prevent the interior heat gain from accumulating. However, in these cases, the open or closing times were only within an hour of a more optimal window schedule. As shown in figure 6-5 below, the heuristic rule result (red line) incurs a greater thermal cost penalty because it closed windows from 7-8am.

Figure 6-5 also shows the slight limitation of the 1-hour horizon rule (black dotted line). In all case-studies, the 1-hour horizon rule is only activated during occupational hours to prevent overcooling beforehand. In this case, it is actually beneficial to have pre-emptive overcooling to be able to sustain the subsequent high heat gains. Hence, a better rule is to activate the 1-hour horizon rule when the minimum thermal comfort limit is surpassed.

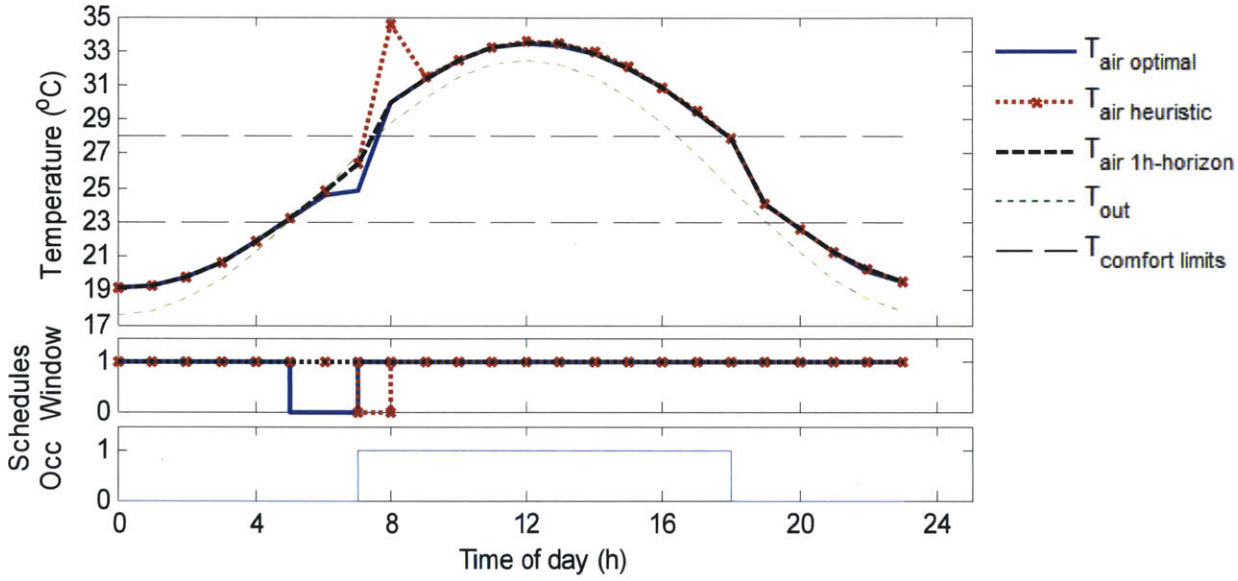

Figure 6-5: Comparison of optimal and rule-based control performances for sinusoidal input outdoor temperature with 1-slice model. Parameters used: T_{mean}=25°C, T_{amp}=7.5 °C, medium q=45W/m^2 during occupancy (7-18pm), normal c=880 J/kgK. Thermal cost for optimal policy (blue), heuristic rule (red) and the 1-hour horizon rule (black) are 15.8, 17.2 and 15.9 respectively.

Varying thermal mass parameters

Figure 6-6 shows that increasing thermal mass results in decreasing thermal cost. As explained in chapter 2, greater thermal mass means greater damping factor and phase lag in the room air's thermal response. With no ventilation, the temperature rise with occupational heat gain is also

inversely proportional to the amount of thermal mass. It should be noted that the optimal window schedule follows the heuristic rule, i.e. close/open at cross-over points.

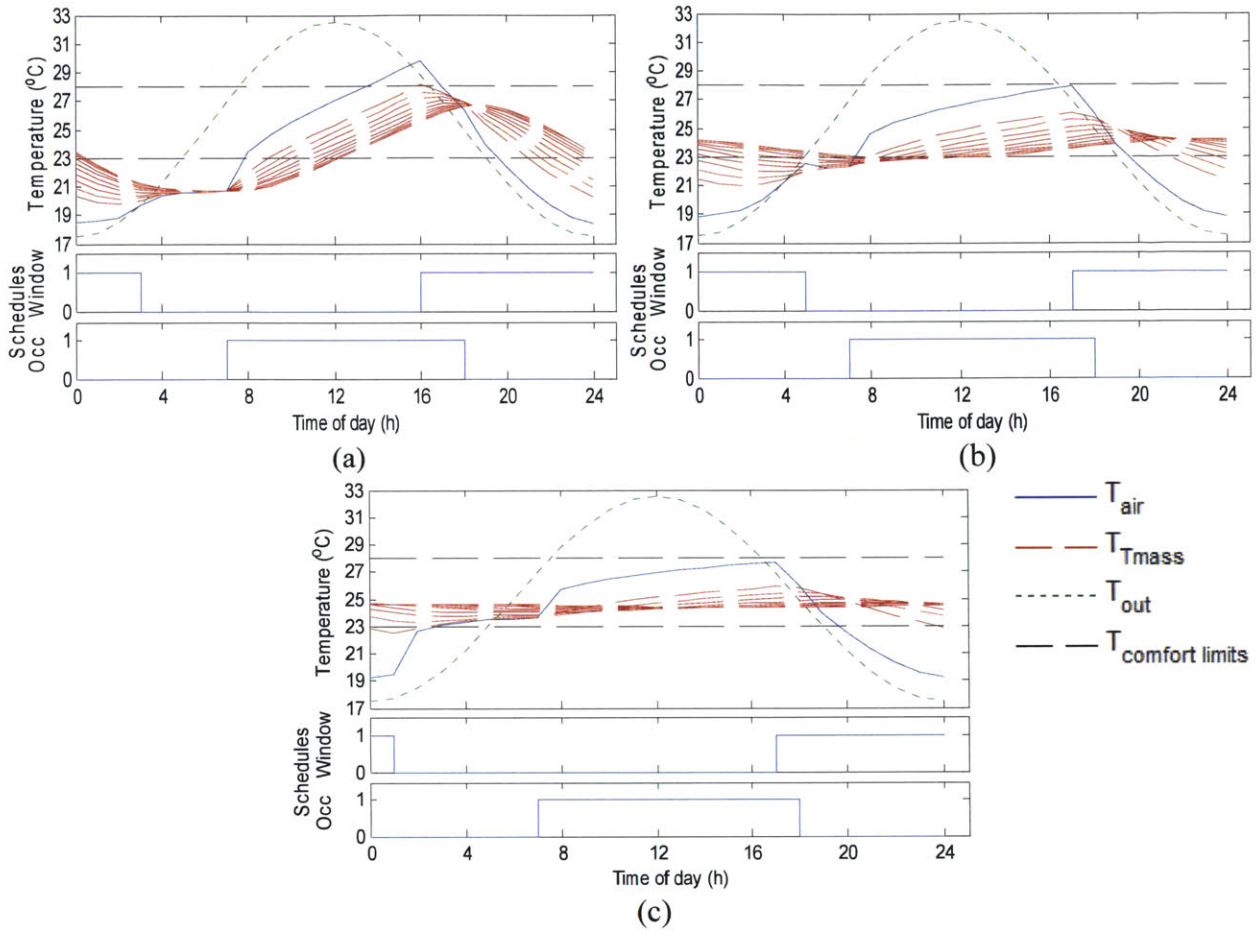

Figure 6-6: 1-day temperature profiles with optimal ventilation schedule for case studies with parameters: T_{mean}=25°C, T_{amp}=7.5 °C, low q=15W/m^2 and (a)low thermal mass, (b) normal thermal mass, (c) high thermal mass

Medium to high heat gains

Figure 6-7(a) shows the resulting optimal temperature profile for the case-study with baseline parameters and T_{mean}=20°C, normal c=880 J/kgK and medium q=30W/m^2. The optimal window strategy gives the best thermal cost of 1.02 as expected, as the earlier closing time gives a thermal cost of 1.46 and the later closing time gives a thermal cost of 1.34. With an earlier closing time, at the start of occupancy (7am), the initial room temperature has not cooled down enough (18.93°C compared to 18.43°C) and thus heats up to a higher maximum room temperature (28.01 °C compared to 27.67 °C). On the other hand, with a later closing time,

occupancy starts with a higher temperature closer to minimum thermal comfort threshold, but ends up with a higher maximum temperature. The thermal mass, whose minimum has a time-lag over the outdoor temperature, does not cool down enough at the earlier closing time. On the other hand, with a later closing time, the thermal mass is on the "heating up" slope as the outdoor and room air temperatures are then higher than that of the thermal mass.

This case-study shows that with medium or high heat gains, the thermal cost which occurs during occupancy is more consequential than having the room slightly overcooled at the start of occupancy as the thermal mass is cooled to its maximum potential. Heat gain quickly brings back the temperature to thermal comfort range within the first hour of occupancy.

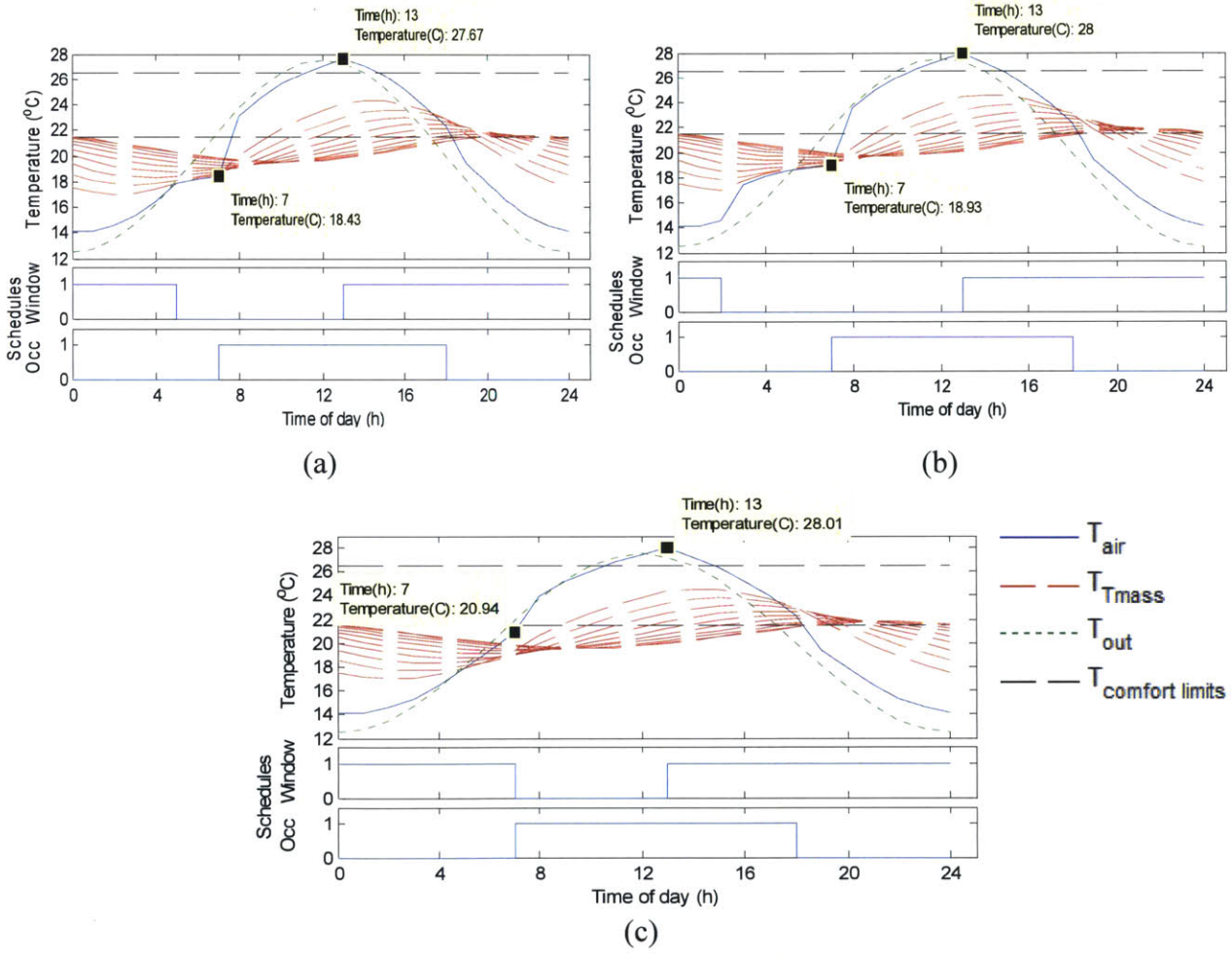

Figure 6-7: 2-day temperature profiles for case (c=880 J/kgK, q=30W/m^2) with (a) optimal strategy's closing and opening times (6am and 14pm), thermal cost=1.02; (b) with an earlier closing time of 3am, thermal cost=1.46; (c) with a later closing time of 8am, thermal cost=1.34

Low mean outdoor temperature and overcooling risks

For low mean outdoor temperatures, which lie outside of the corresponding thermal comfort band, there is the risk of overcooling if the night-cooling is too extensive. Both optimization techniques come up with 2 modes of night-cooling schedules for such cases (figure 6-8): (i) an early mode ventilation whereby the windows are closed much earlier than occupancy start; (ii) an late mode ventilation whereby night-ventilation does not start as early but continues up to occupancy start.

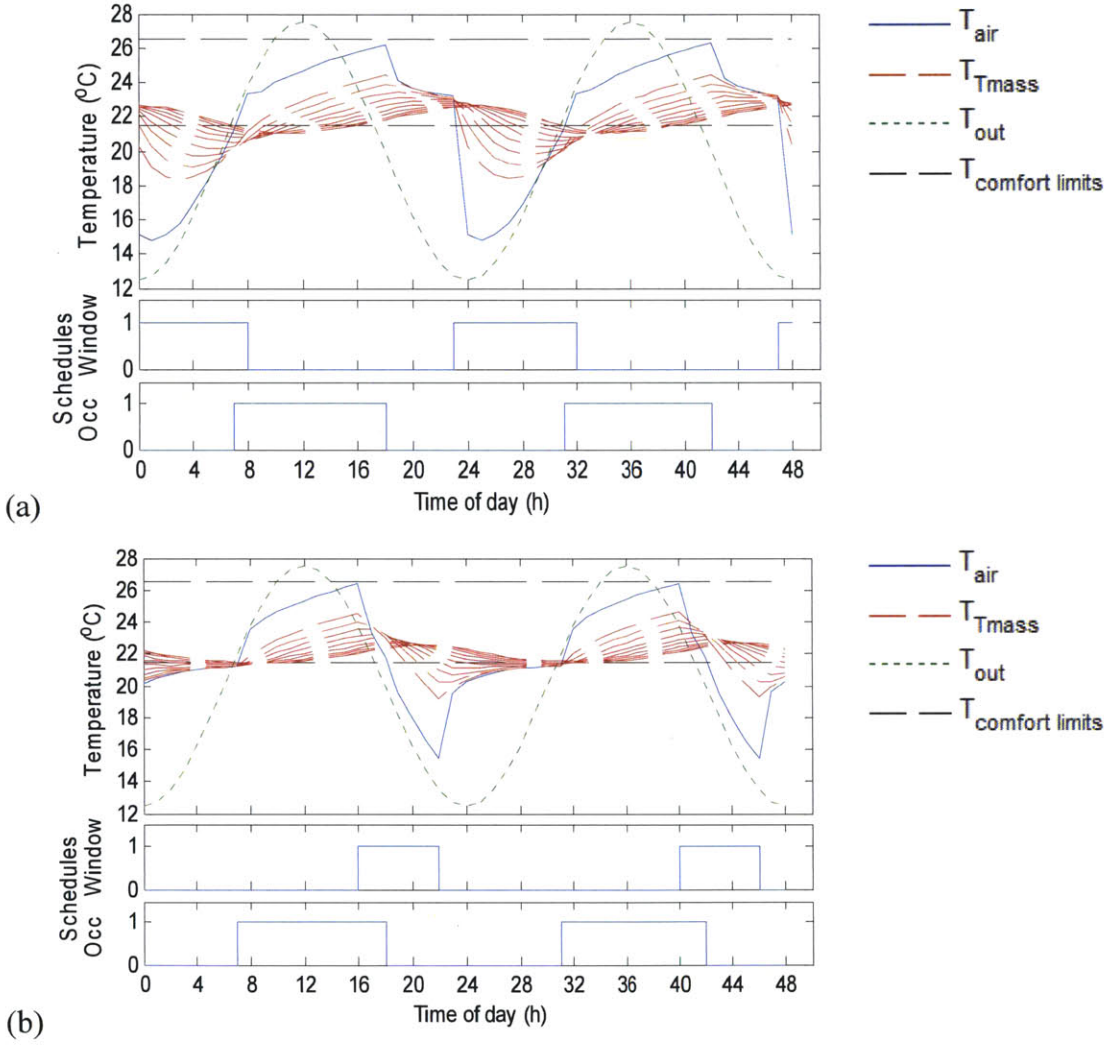

Figure 6-8: Comparison of 2 optimal night-cooling schedules: ventilation (a) just before occupation (b) early in the night. Parameters used: T_{mean}=20°C, T_{amp}=7.5 °C, low q=15W/m^2, normal c=880 J/kgK.

The overcooling-prevention strategies developed make use of the early night-ventilation mode because it is easier to predict the thermal behavior of the model once the windows are closed: the outdoor weather disturbance, not as neat as the used sinusoidal outdoor temperature used above, till occupancy needs not be forecasted and accounted for. Figure 6-9 shows that overcooling strategy 1 does a good job of estimating the thermal mass temperature (magenta squares) using equation 6.4 and based on current variable values ($T_{air}(t)$, $T_{out}(t)$, $q(t)$) and assumed parameters (ACH, h). Ventilation control based on this estimate enables the thermal mass temperature, and hence the room air temperature to equilibrate to the minimum thermal comfort limit at occupation onset. Note that in figure 6-9, the rule-based ventilation control consists of the heuristic rule during occupation period and overcooling-prevention strategy during non-occupation period.

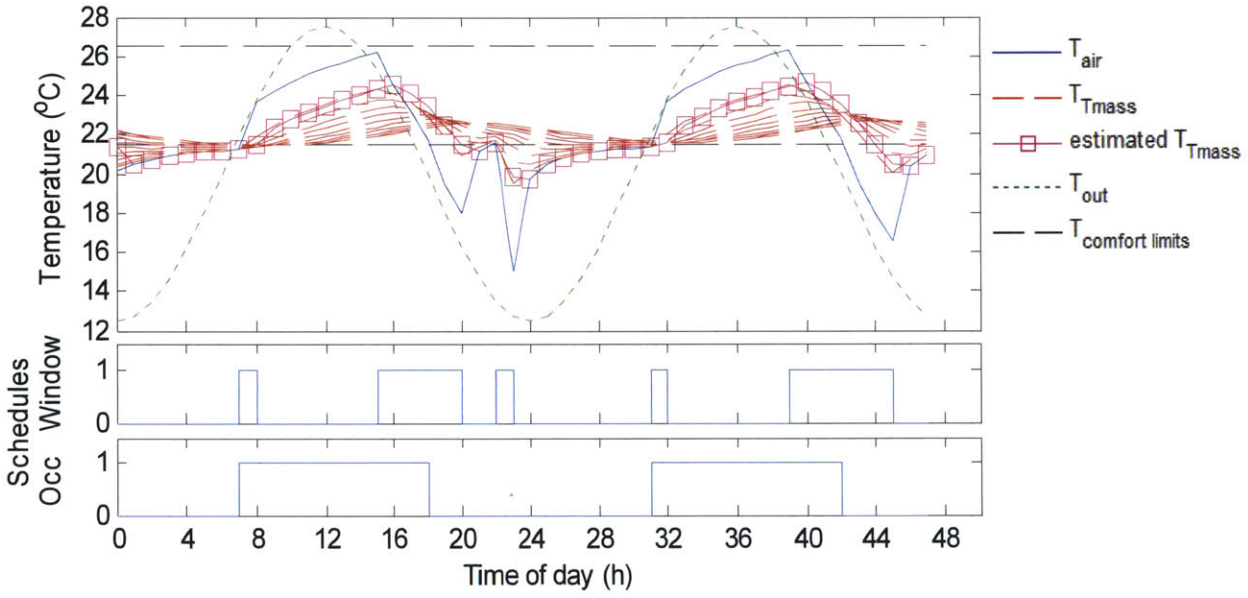

Figure 6-9: Resulting temperature profiles for ventilation controls with overcooling strategy 1. Parameters used: T_{mean}=20°C, T_{amp}=7.5 °C, low q=15W/m^2, normal c=880 J/kgK.

Comparatively, the second overcooling strategy (defined by the algorithm on page 110) needs several days to train and stabilize towards having minimum comfort temperature limit at occupation schedule onset. There are many ways to define the ratio increment in the self-learning algorithm. The first way explored is as follows: with the ratio levels chosen from a user-defined lookup table (e.g. table 6-2 below), the ratio change is a unit ratio level increase, decrease or no-change relative to the previous day's ratio level.

Ratio level	-4	-3	-2	-1	0	1	2	3	4
Ratio of heating degree hours to cooling degree hours	1:10	5:10	7:10	9:10	1:1	10:9	10:7	10:5	10:1

Table 6-2: Degree-hour ratio used for arbitrary increment in self-learning algorithm to prevent over-cooling

A sample resulting temperature profile with overcooling strategy 2 is shown in figure 6-10. The parameters used by the self-learning algorithm (page 110) are plotted by day in figure 6-11: the direction of ratio increment, the resulting ratio, the resulting $\Delta T=(T_{air}-T_{min\ comfort})_{t=occupation\ start}$, and the degree hours plot. The latter includes the heating degree hours, calculated maximum degree hours and the possible cooling degree hours. Note that the possible cooling degree hours is greater than the maximum cooling degree hours defined by the ratio, because the former additionally records the integral of $T_{air}-T_{min\ comfort}$ after closing while the latter only integrates till closing. For day 1, the ratio is arbitrarily set to $ratio_{day\ 1}$= 10:9 because $\Delta T_{day\ 1}<0$, i.e. more on the heating side because there is overcooling. When $\Delta T_{day\ 1}<0$ still, the ratio level is incremented to $ratio_{day\ 2}$= 10:7 so that the maximum cooling degree hours for day 2 could decrease, recalling that ratio here is defined as heating degree hour: cooling degree hour. This goes on till $\Delta T_{day\ 4}\sim=0$. The algorithm therefore sticks to the previous day's ratio, i.e. $ratio_{day\ 5}$= $ratio_{day\ 4}$. However, this leads to a slight undercooling as $\Delta T_{day\ 5}>0$. Consequently, the algorithm chooses a ratio decrement (level 4 to 3 in table 6-2 above) such that $ratio_{day\ 6}$=10:5. For the subsequent days, the self-learning algorithm maintains ΔT close to 0 by increasing and decreasing the ratio.
This example shows that the self-learning algorithm requires several training days before it becomes effective in maintaining ΔT close to 0 at occupation start, and that care should be taken in choosing the ratio level.

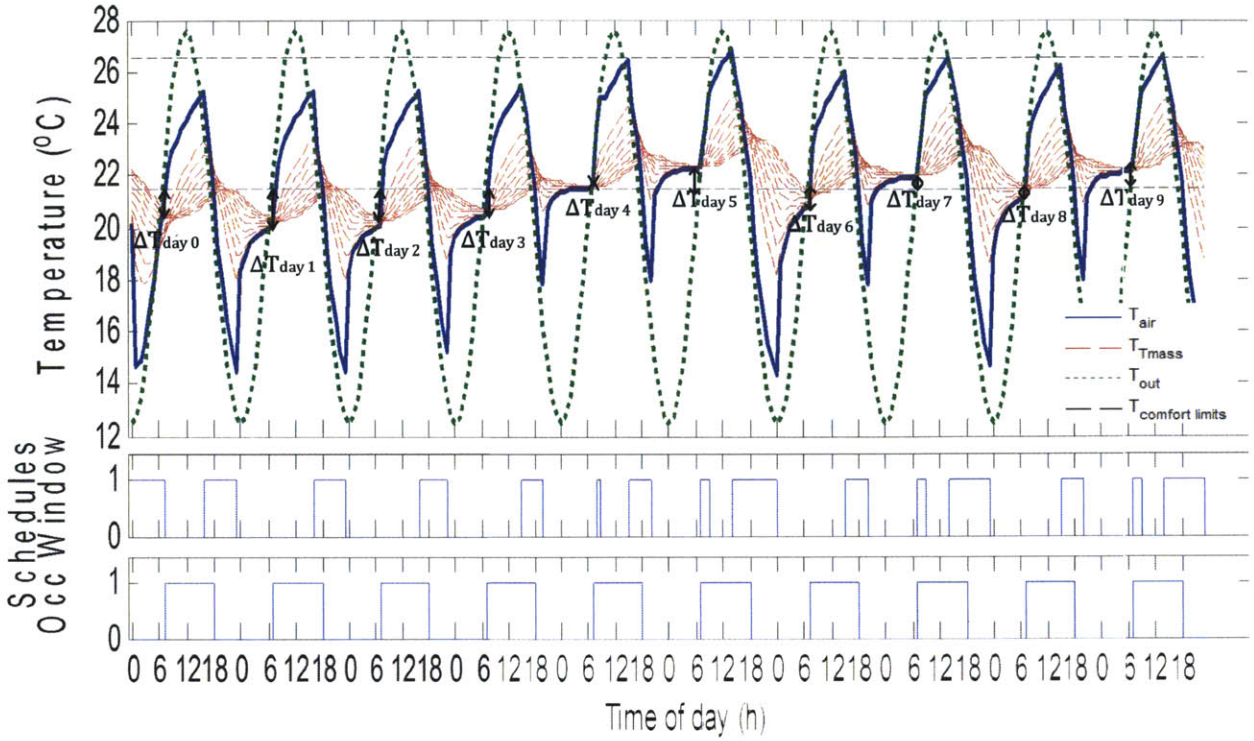

Figure 6-10: Resulting temperature profiles over 5 days for ventilation controls with overcooling strategy 2. Parameters used: T_{mean}=20°C, T_{amp}=7.5 °C, low q=15W/m^2, normal c=880 J/kgK.

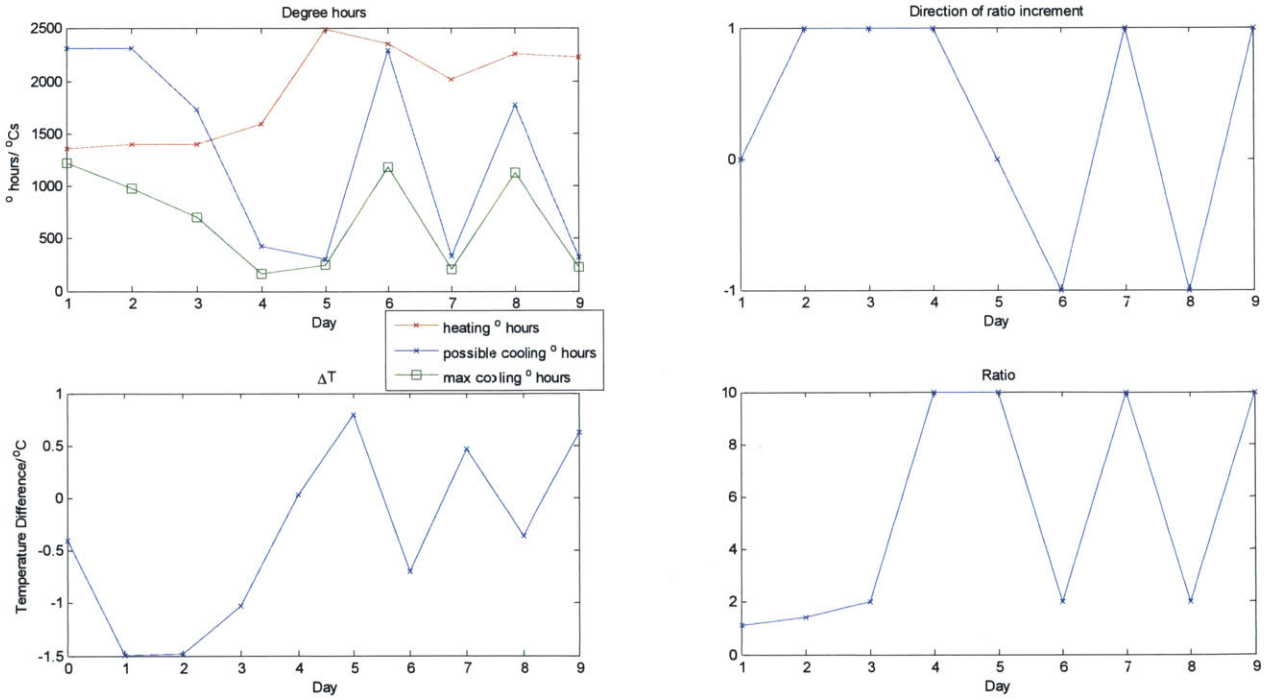

Figure 6-11: Plots of parameters used by the overcooling-prevention self-learning algorithm corresponding to temperature profile of figure 6-10. Clockwise from top left: plots of degree

hours, direction of ratio increment, ratio of degree hours defined for that day, and resulting $\Delta T=(T_{air}-T_{min\ comfort})_{t=occupation\ start}$. Note that day is defined 7am-6am, i.e. on occupation onset.

6.4 Results with weather data

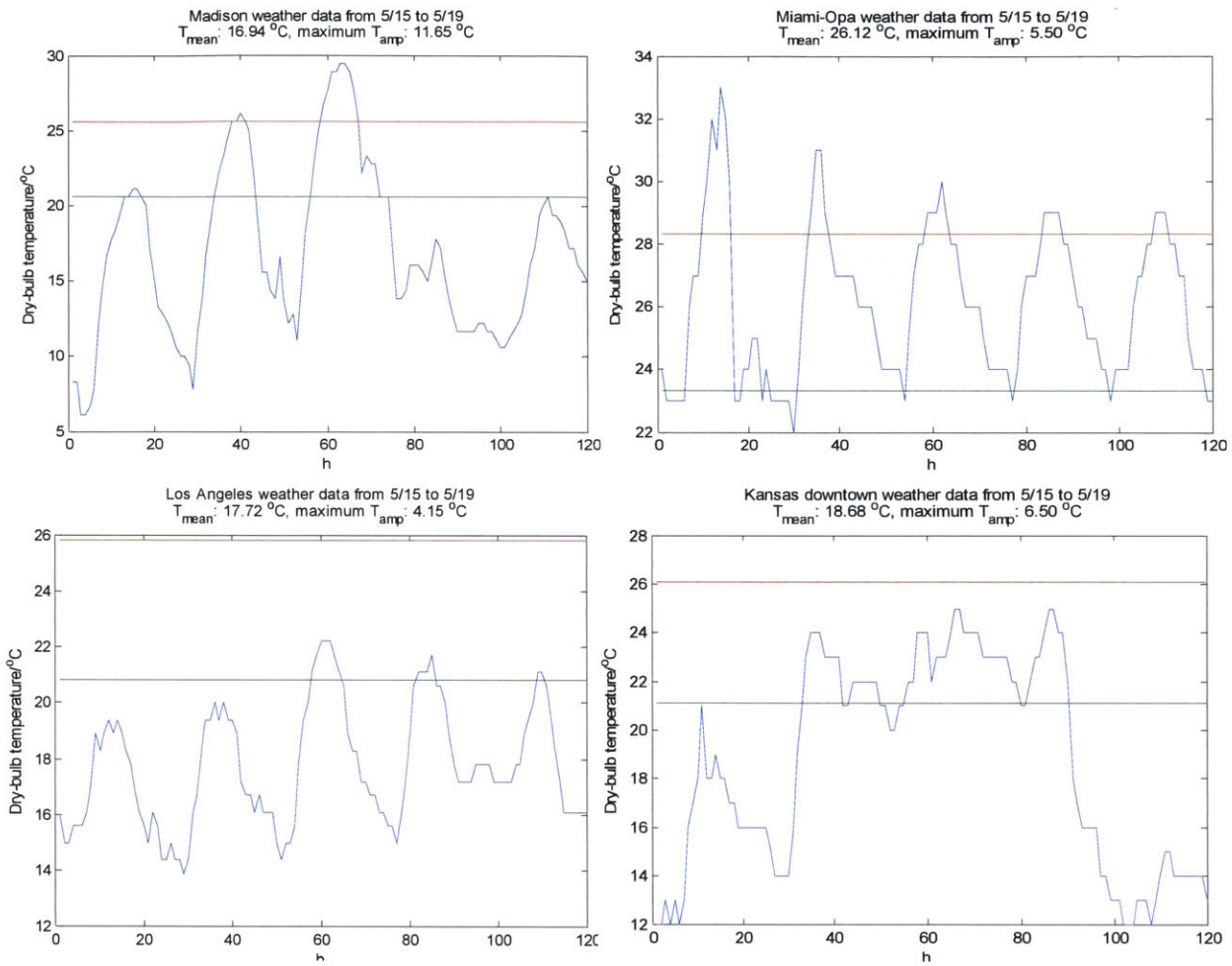

Figure 6-12: Week weather data and the respective thermal comfort range for four cities (Madison, Miami, Kansas, Los Angeles going clockwise from the top left)

Our assumptions up till now with our simulation runs were that the outdoor temperature profiles were (i) sinusoidal; (ii) did not vary from day to day. However, with real weather data, the dry-bulb outdoor temperature does not follow such a nice pattern. Simulations similar to those run in section 6.3 are carried out using weather data from the four cities identified by Axley et al [32] in table 4-1: (i) Miami-FL, (ii) Los Angeles-CA, (iii) Kansas City-MO, (iv) Madison-WI. The weather data was obtained from NREL's website [57] and is in TYM3 format, i.e. hourly-value data sets derived from 1991-2005 National Solar Radiation Data Base archive. The week-long

(May 15 to May 19) weather data used for each city are shown in the figure above., and were chosen to represent different weather patterns: Madison weather fairly steady day-to-day temperatures with high amplitudes; Miami weather represents hot and fairly steady day-to-day temperatures with low amplitudes; Kansas weather represents moderate but highly variable day-to-day temperatures; Los-Angeles weather represents moderate but fairly steady day-to-day temperatures.

Simulation results with optimization techniques

Simulations were run to find the optimal ventilation schedule as per the schematic in figure 6-1, with the baseline parameters and with parametric variations in thermal mass and heat gain as listed in table 6-1. Similar to section 6.3, the optimization was carried out using the 2 methods, i.e. brute-force global optimization and dynamic programming. The energy room model was first trained over 14 days, with the weather data prior to the optimization start date. The optimization was carried out over a 5-day period using a rolling 1-day horizon, in the same line as an off-line model predictive control algorithm, i.e. the optimal ventilation day-schedule at the start of each day was determined using the day weather forecast data and the initial starting conditions (room air and thermal mass temperatures). It should be noted that the domain space of the temperature states needed to be re-defined from each day optimization as the daily weather is not steady. The domain space is defined according to equations 2.16-2.19. If the calculated maximum air temperature is lower than the maximum thermal comfort temperature (as set by ASHRAE's adaptive comfort standard, figure 5-3(b)), the room air and thermal mass temperatures' domain spaces' upper bounds are expanded to include it. Similarly, if the calculated minimum air temperature is higher than the minimum thermal comfort temperature, the domain spaces' lower bounds are also expanded. These two cases occur when a particular day's temperature profile is drastically far from the week's mean temperature.

Both optimization techniques effectively pick out the day's optimal ventilation schedule which minimizes the thermal cost during occupancy based, using as input the day's weather forecast and initial temperature conditions. Sample results for Miami and Madison weather data and are shown below for illustration. Results for other parameter runs and cities can be found in Appendix C. Similar observations to those drawn in section 6.3 can be made: if the outdoor temperature is greater than the indoor room temperature, the windows are in general

preferentially shut, and vice-versa, as seen in figure 6-13. The exception arises when the outdoor temperature is below the minimum thermal comfort temperature limit, or when the maximum subsequent outdoor temperature does not exceed the maximum thermal comfort temperature limit by much, as can be seen in figure 6-14. The highly variable weather of Madison below the minimum thermal comfort temperature limit also shows the need for an overcooling-prevention strategy.

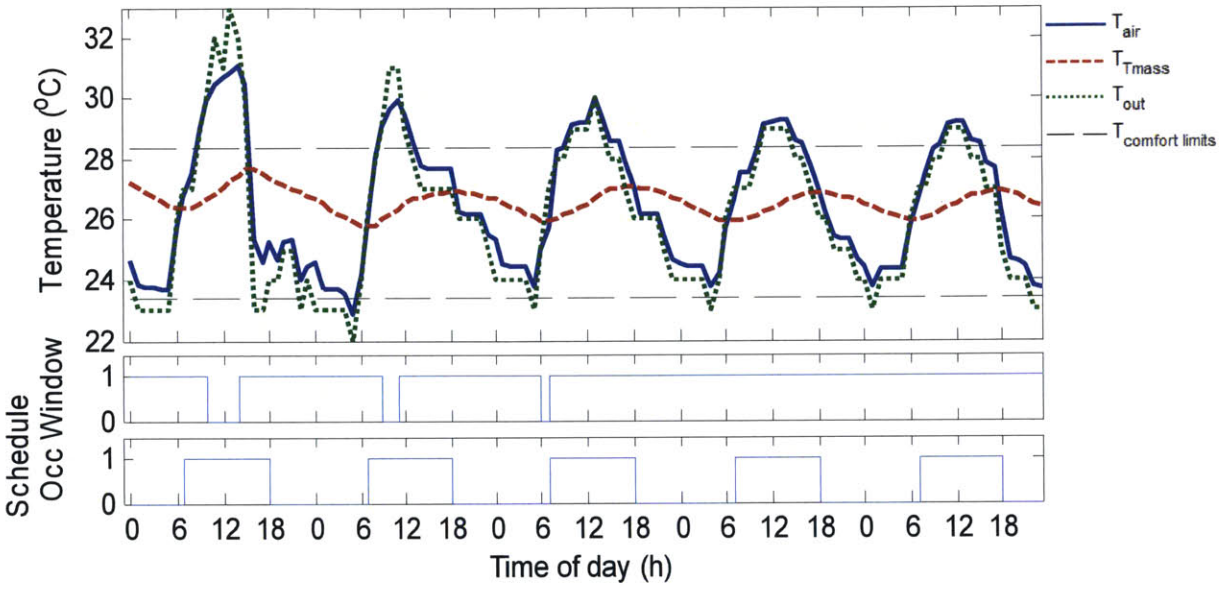

(a)

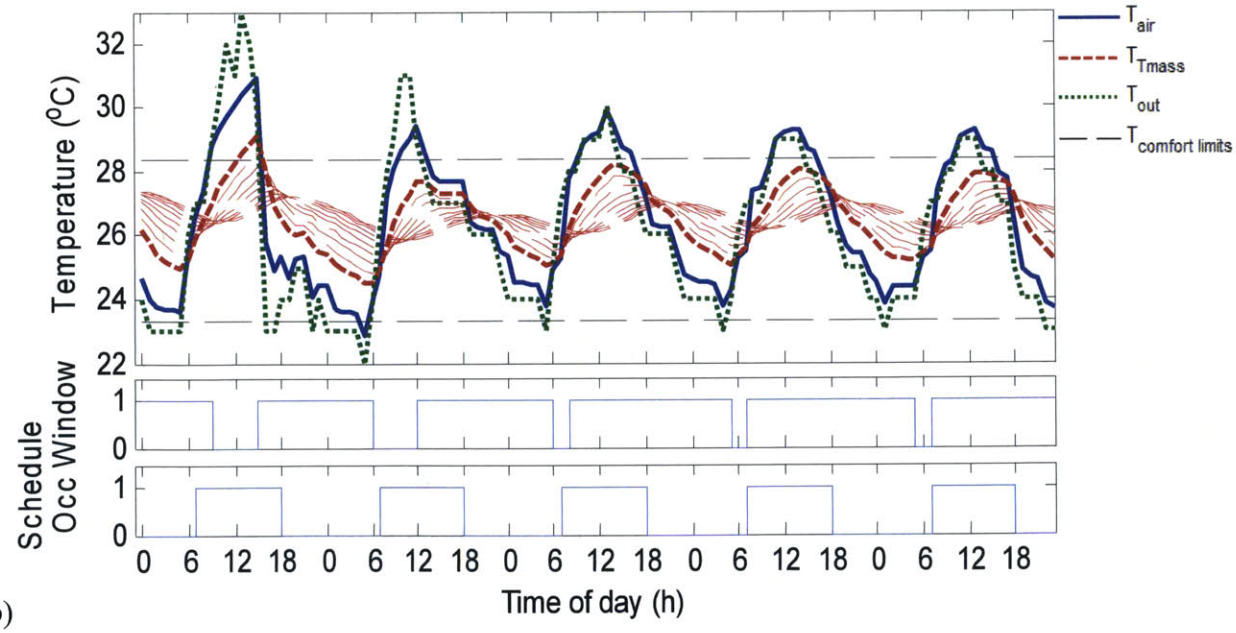

(b)

Figure 6-13: Optimization results for Miami weather, May 15-19 using (a) dynamic programming and 1-slice model, (b) global search optimization and 10-slice model. Parameters used: low heat gain, q=15W/m^2; normal thermal mass heat capacity c=880 J/kgK.

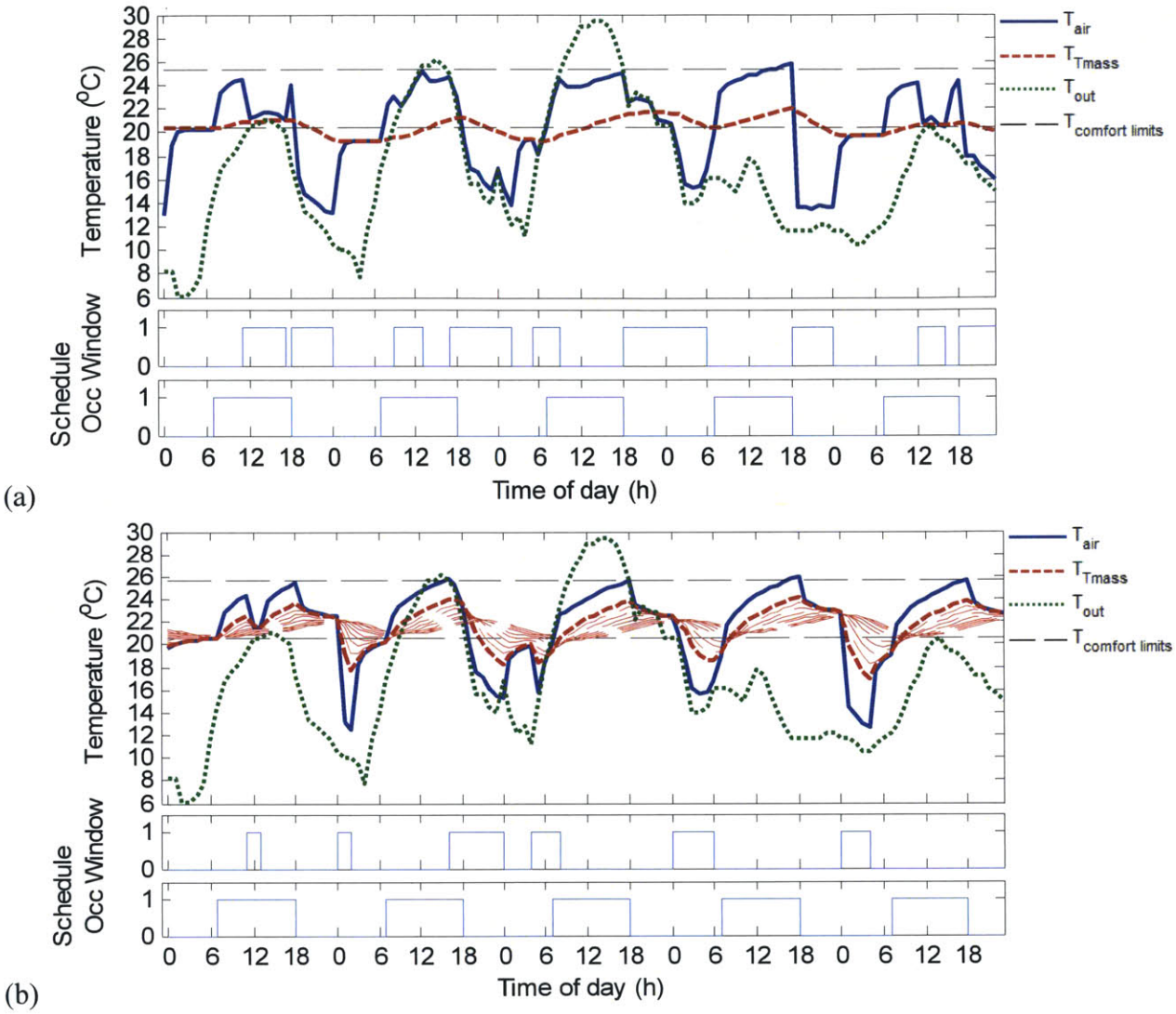

Figure 6-14: Optimization results for Madison weather, May 15-19 using (a) dynamic programming and 1-slice model, (b) global search optimization and 10-slice model. Parameters used: low heat gain, q=15W/m^2; normal thermal mass heat capacity c=880 J/kgK.

With irregular weather data as the input signal to the thermal system, it is necessary to verify whether the 1-slice model with effective h can substitute for a 10-slice model. Although an irregular weather can be thought of as the sum of several sinusoidal signals of differing frequencies, the strongest frequency remains a sinusoidal signal of a day frequency. Hence, the effective h remains valid. However, when there is no ventilation, the 1-slice effective model slightly overestimates the resulting room air temperature: this is to be expected as when the thermal mass discharges, the 1-slice model assumes a higher stored amount of heat than if there were temperature gradation as in the 10-slice model. While figures 6-13 and 6-14 show the 1-

slice and 10-slice models give slightly different optimal ventilation schedules, it could be that there are several optimal ones with minimal thermal cost. Hence, additional simulations were run using the optimal schedules obtained using dynamic programming but where the 10-slice energy model (temperature profiles in solid lines) was substituted for the original 1-slice model (temperature profiles in diamond markers), as shown in figures 6-15 to 6-16. This comparison testing for the validity of the effective h for other weather data and parametric runs can be found in appendix C. In general, it was found that when ventilation was on, the effective model was valid. When it was not, the above-mentioned overestimation occurred.

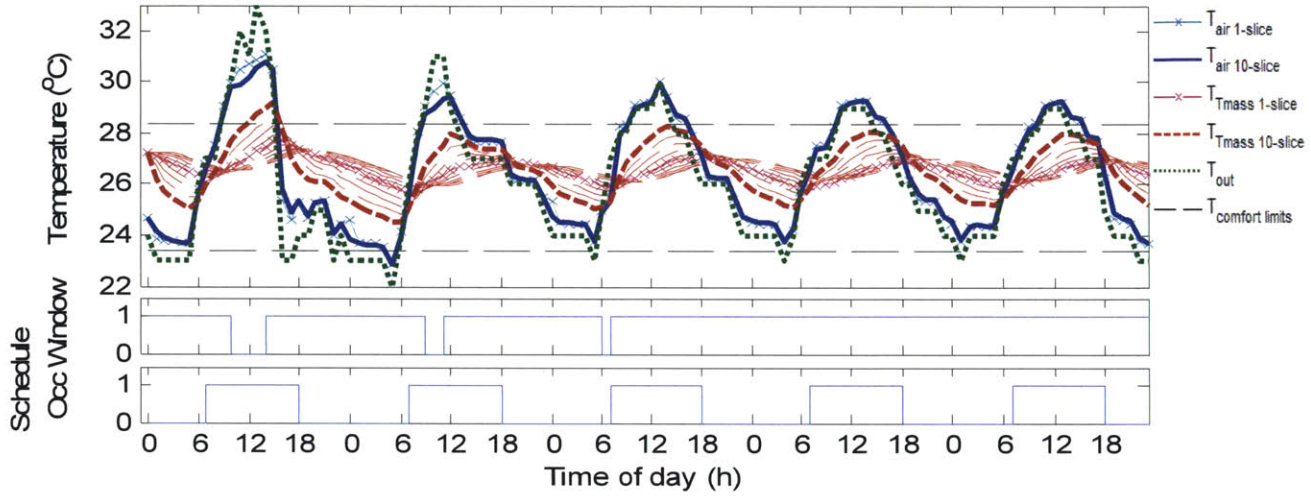

Figure 6-15: Testing the effectiveness of effective h with 1-slice model for Miami weather, May 15-19. Parameters used: low heat gain, q=15W/m^2; normal thermal mass heat capacity c=880 J/kgK.

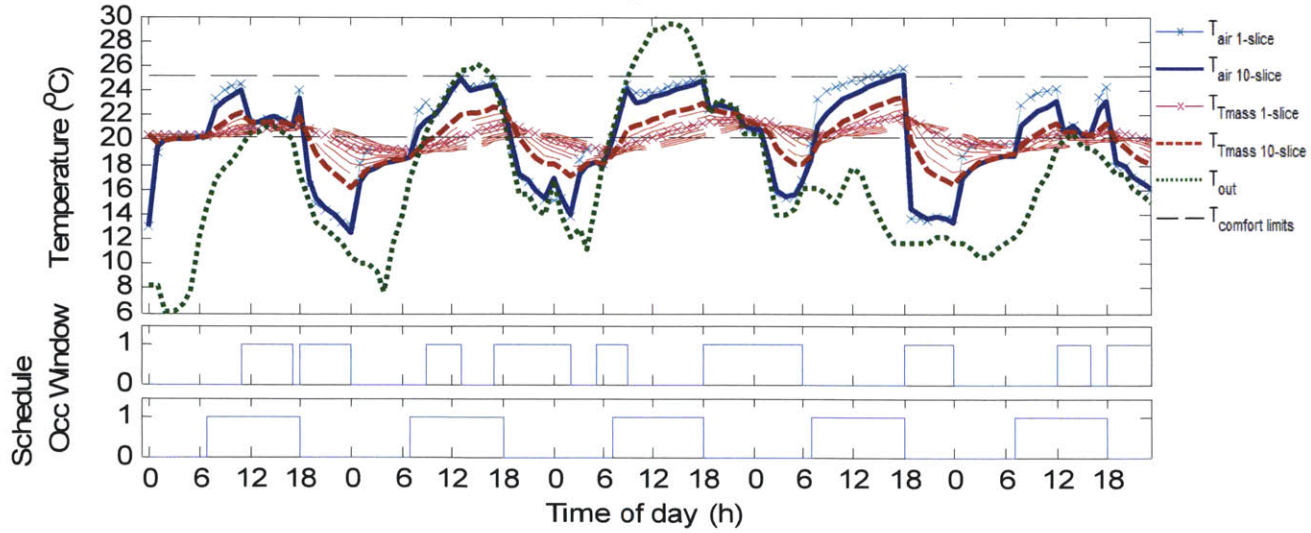

Figure 6-16: Testing the effectiveness of effective 1-slice model for Madison weather, May 15-19. Parameters used: low heat gain, q=15W/m^2; normal thermal mass heat capacity c=880 J/kgK.

Simulation results with rule-based controls

As was found in section 6.3, a holistic rule-based control needs to be applied, even more so with irregular daily outdoor temperatures. A holistic rule-base control should include heuristic rules to prevent overheating and overcooling during occupational hours, as well as an overcooling-prevention strategy during non-occupational hours. During occupational hours, windows are closed only if that action allows the room air temperature to be maintained within thermal comfort limit, according to the control logic defined in table 6-3 below. Table 6-3 shows that the control can be broken down into different modes: when the measured variables exceed the corresponding control threshold parameters, a particular window action is required. In effect, when the During non-occupational hours, the 2 overcooling strategies discussed in section 6.3 are implemented according to the control logic defined in table 6-4 below. Each strategy has its own advantage and shortcoming. Overcooling strategy 1 (RBC-1), unlike overcooling strategy 2 (RBC-2), does not require training. However, the self-learning algorithm in overcooling strategy 2, whilst not needing building parameters, only approximates the limit to night-cooling as it learns from the previous day's performance. Because it was found out in section 6.3 that it was tricky to use of a user-defined ratio look-up table such as table 6-2 (RBC-2a), a new version of overcooling strategy 2 is also explored, whereby the ratio increment is defined by the algorithm on page 132 (RBC-2b). Table C-5 in the Appendix C compares the thermal costs of these rule-based controls to those of the optimized controls for simulation runs using Madison and Los Angeles, with the 1-slice and 10-slice energy models. The corresponding temperature profiles can be found in figures C-62 to C-84. The optimization was carried out daily over 10 days, so their mean outdoor temperature defined the thermal comfort limit.

Mode	Comparison of measured variables ($T_{room\ air}$, T_{out}) and control threshold parameters ($T_{max\ comfort}$, $T_{min\ comfort}$)			Resulting Window action
	$T_{room\ air} > T_{max\ comfort}$	$T_{out} > T_{room\ air}$	$T_{out} > T_{min\ comfort}$	
1	Yes	Yes	No (by default)	Close
2	Yes	No	No (by default)	Open
3	No	Yes	Yes	Open
4	No	Yes	No	Close
5	No	No	Yes	Close
6	No	No	No	Open

Table 6-3: Control logic for heuristic rules implemented during occupational hours for RBC-1 and RBC-2

Algorithm	mode	Calculated variable	Control	Resulting window action
RBC-1	7	Estimated thermal mass temperature, T_{Tmass}	$T_{Tmass} < T_{min\ comfort}$	Close
	8	Estimated thermal mass temperature, T_{Tmass}	$T_{Tmass} > T_{min\ comfort}$	Leave open
RBC-2	7	Cumulative cooling degree hours for day D, $CDH_{day\ D}$	$CDH_{day\ D}$ > calculated maximum cooling degree hours for day D	Close
	8	Cumulative cooling degree hours for day D, $CDH_{day\ D}$	$CDH_{day\ D}$ < calculated maximum cooling degree hours for day D	Leave open
	9	If training for learning algorithm has started		Leave open

Table 6-4: Over-cooling strategies implemented during non-occupational hours in RBC-1 and RBC-2, giving resulting window mode action when calculated variable exceeds the threshold parameter

Figure 6-17 below shows the resulting room temperature profile with RBC-1 (blue line) compared to the optimal one calculated through dynamic programming (cyan dash lines). The second subplot shows the ventilation mode schedule dictated by the algorithm, with the modes defined in tables 6-3 and 6-4. Similar to figure 6-9, the magenta line shows the estimated $T_{Tmass\ est}$ closely matching the actual T_{Tmass} (red line). The ventilation control which prevents overcooling during non-occupancy hours can be seen from the shift from mode 8 to 7. This occurs at the cross-over point of the $T_{Tmass\ est}$ with $T_{min\ thermal}$ comfort (dashed horizontal line). This control does a good job of keeping $T_{room\ air}$ at that minimum limit as it eventually equilibrates to T_{Tmass} upon window-closing. The optimal ventilation performs slightly better in days 3 and 4, as seen by the difference between the blue solid line and diamond series. By simulating the results over the following hours, the optimization technique picks out that it is better to prolong the night-cooling such that T_{Tmass} is below T_{Tmass} at occupation start, as seen in figure B-61.This results in a lower T_{Tmass} at 7am on day 3 when window is closed in the optimization simulation, and lower T_{air}. The optimization technique's predictive capability again leads to a lower thermal cost on day 4: at noon, it determines that the T_{out} is so low that it would lower $T_{room\ air}$ to below $T_{min\ thermal\ comfort}$ if the window were opened, showing the limitations of day controls modes 1-6.

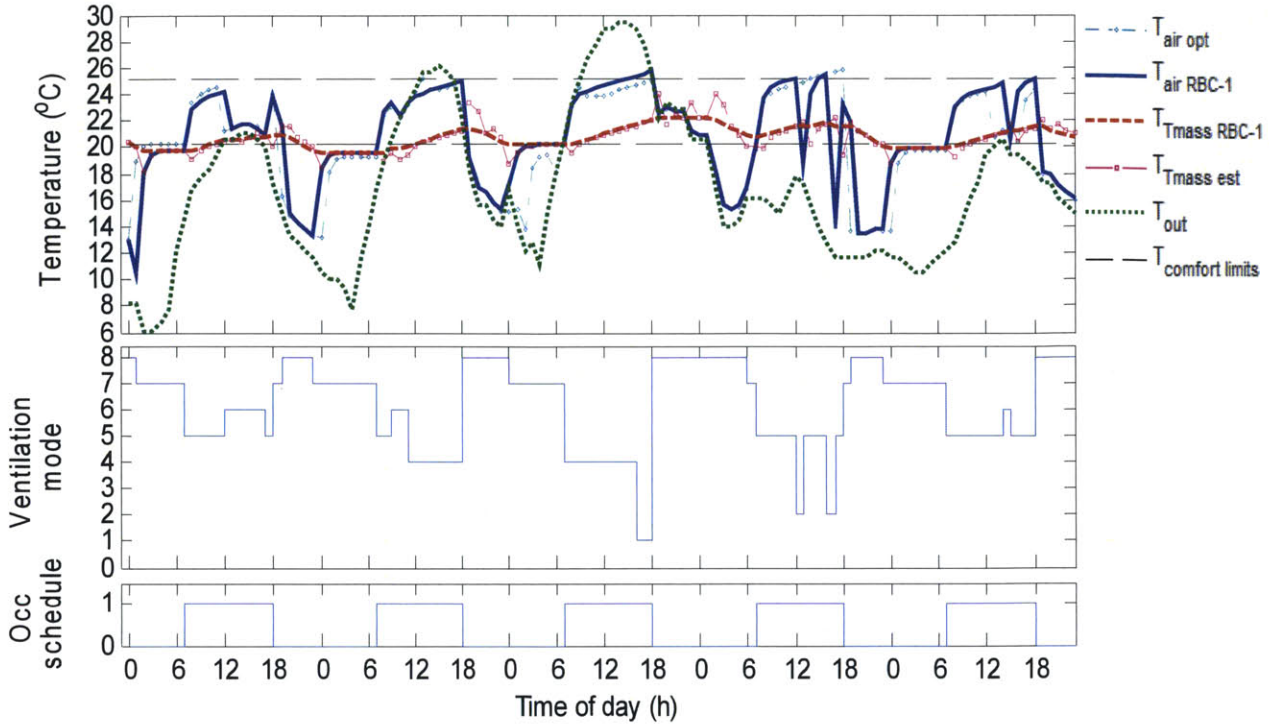

Figure 6-17: 5-day temperature profile for ventilation control with overcooling strategy 1 (RBC-1).Parameters used: city: Madison, low heat gain, q=15W/m^2; normal thermal mass heat capacity c=880 J/kgK. Thermal cost for each day=[0, 0, 0.2, 1.3, 0]

Figure 6-18 shows the resulting room temperature profile with RBC-2a (blue line), i.e. self-learning algorithm with arbitrary ratio level (defined in table 6-2) to prevent overcooling. The thermal cost of 0.4 on the first day is due to overcooling, since the algorithm leaves the window open all night prior to the self-learning. Because (degree hour) day one starts in the overcooled state $\Delta T_{Day\ 0}$=-5.4, $ratio_{Day\ 1}$ is set to 10/9, leading to ΔT_1 =-1.5 in 'delta T' plot (figure 6-19) and the degree hours defined for day 1 in 'degree hours' plot. Note that the possible cooling degree hours is greater than the maximum cooling degree hours defined by the ratio, because the former additionally records the integral of $T_{air} - T_{min\ comfort}$ after closing (mode 7 to 8). Afterwards, the day ratio is adjusted: if there is overcooling, ratio is incremented by 1 level (day 2 value in 'direction' plot) leading to $ratio_{day\ 2}$=10/7 and ΔT_3 =-1; if there is not enough cooling, ratio is decreased by 1 level, leading to a drop in ratio, for example $ratio_{Day\ 4}$=10/1 to $ratio_{Day\ 5}$=10/5; if -0.2<ΔT<0.2, the ratio does not change as for days 6 & 7. The dips of $\Delta T_{Day\ 3}$ =-3.2 and $\Delta T_{Day\ 7}$ =-7 occurred because the windows were kept open as the day's ratio has not been met yet, and $T_{room\ air}$ did not equilibrate to $T_{Tmass\ strat}$, unlike previous days. However, these were not significant in terms of thermal cost, because $T_{Tmass\ strat}$ was above $T_{min\ thermal\ comfort}$ due to the

previous day's high T_{out}. In fact, thermal cost during days 2-3 is negligible, even though $T_{room\ air}$ is slightly below $T_{min\ thermal\ comfort}$ at occupation start (7am), $T_{room\ air}$ quickly ramps up with occupational gain. In reality, the ramping will be slower as a stair function has been assumed for the occupational gain. The thermal cost mostly stems from the ventilation controls during occupational hours (modes 1-6) as seen previously for RBC-1, as during days 9 & 10: figure 6-18 shows that opening windows when $T_{room\ air} << T_{min\ thermlal\ comfort}$ results in day-overcooling.

However, the above shortcomings of RBC-2a mostly occur for Madison, which has a varying daily outdoor temperature profile. With a more stable weather like Los Angeles', RBC-2a gives better results as shown in figure 6-20 to 6-21. As seen in the 'Delta T' plot, the algorithm learns from previous days' performance (ΔT) and eventually gets the right ratio of heating degree hours to cooling degree hours, achieving the aim of $\Delta T=0$, i.e. occupation starting with no overcooling. With Los Angeles having outdoor mean temperature below thermal comfort limit like Madison, the thermal cost also resulted from ventilation controls during occupational period, i.e. overcooling due to closing of windows.

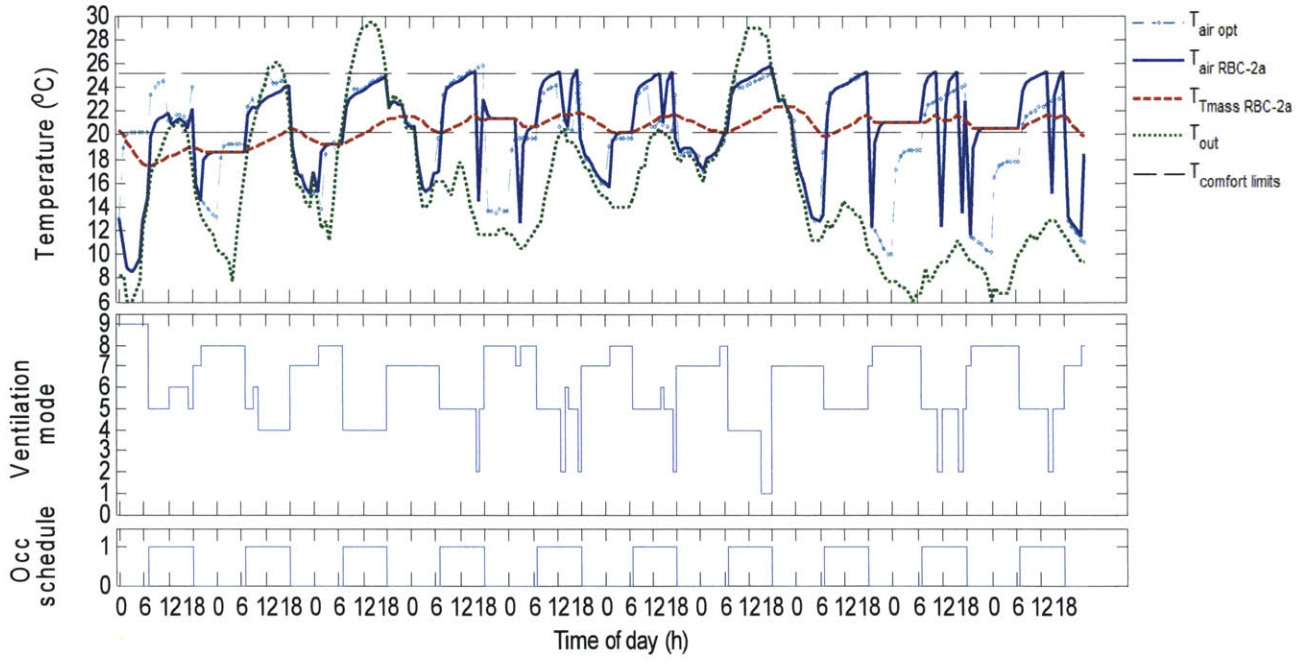

Figure 6-18: 10-day temperature profile for ventilation control with overcooling strategy 2 having arbitrary ratio levels. Parameters used: city: Madison; low heat gain, $q=15W/m^2$; normal thermal mass heat capacity c=880 J/kgK. Thermal cost for each day= [0.4, 0, 0, 1.2, 0, 0, 0.2, 0.4, 3, 1]

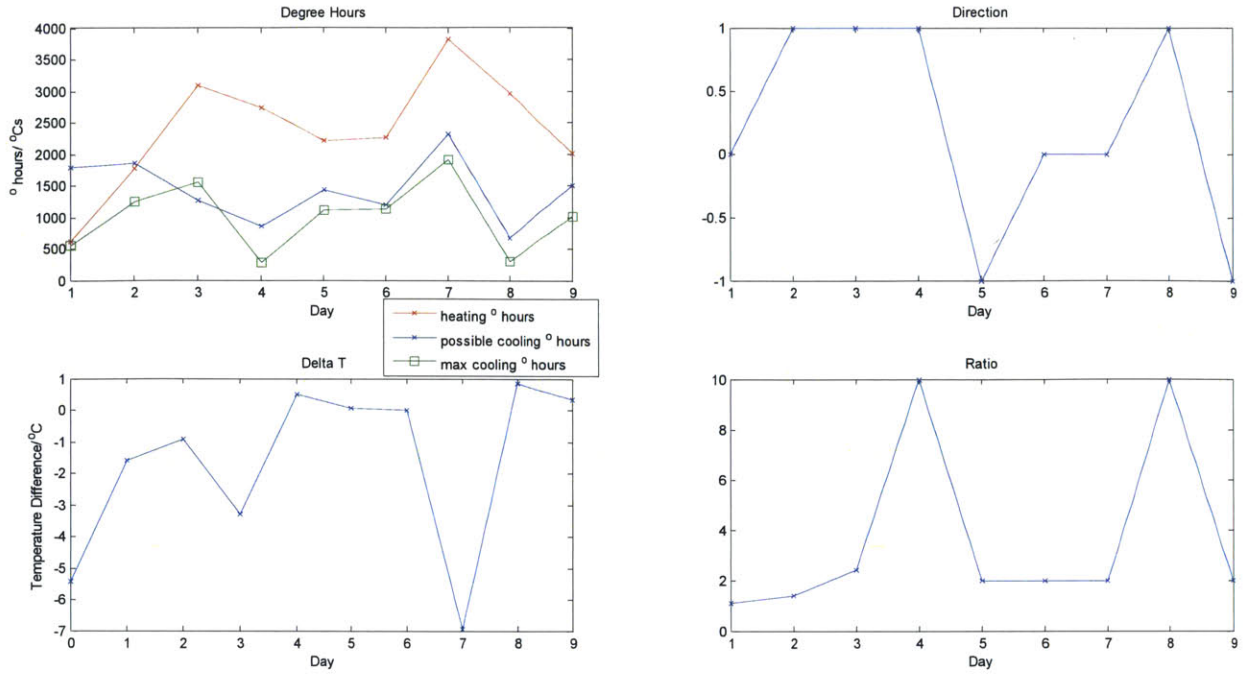

Figure 6-19: Plots of each degree day's parameters used by the overcooling-prevention self-learning algorithm corresponding to temperature profile of figure 6-18: ΔT at the end of the day defined 7am-7am, i.e. occupation onset, degree hours, direction of ratio increment, ratio of degree hours defined for that day.

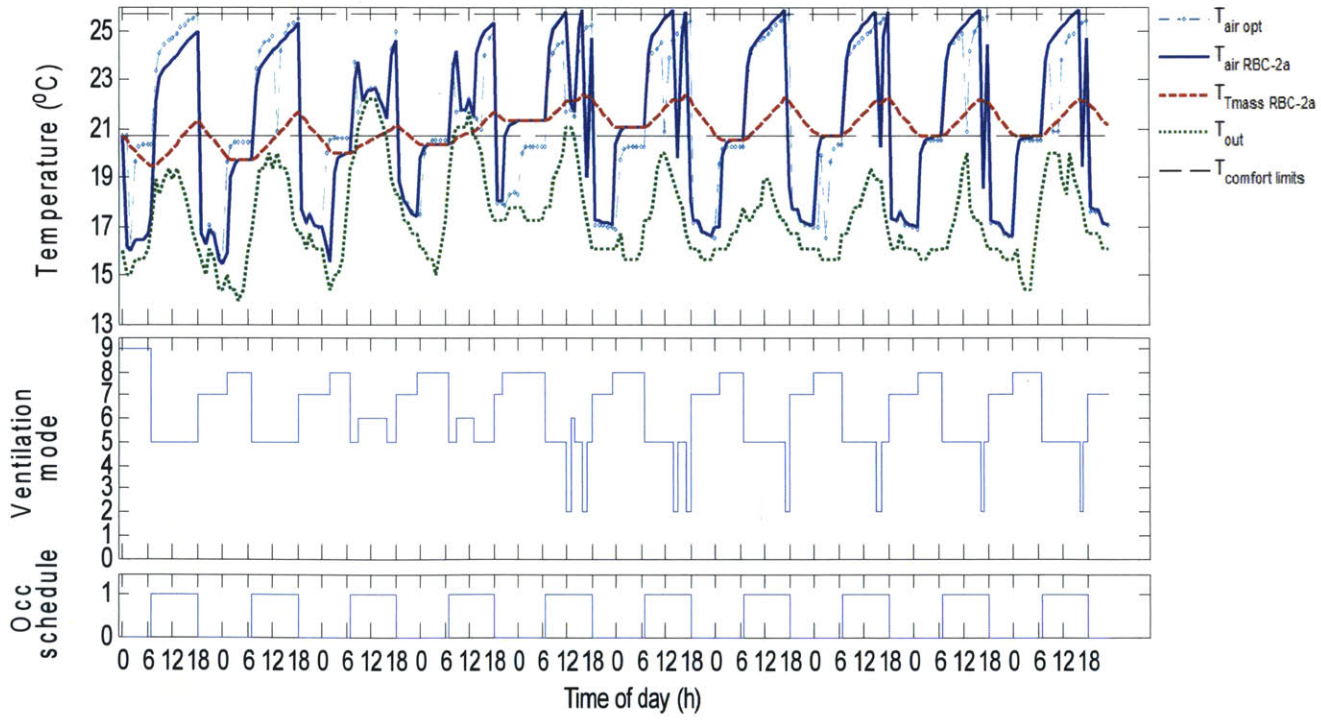

Figure 6-20: 10-day temperature profile for ventilation control with overcooling strategy 2 having arbitrary ratio levels. Parameters used: city: Los Angeles; low heat gain, q=15W/m^2;

normal thermal mass heat capacity c=880 J/kgK. Thermal cost for each day=[0.2, 0, 0, 0, 0.2, 0.5, 0.3, 0, 0.4, 0.2]

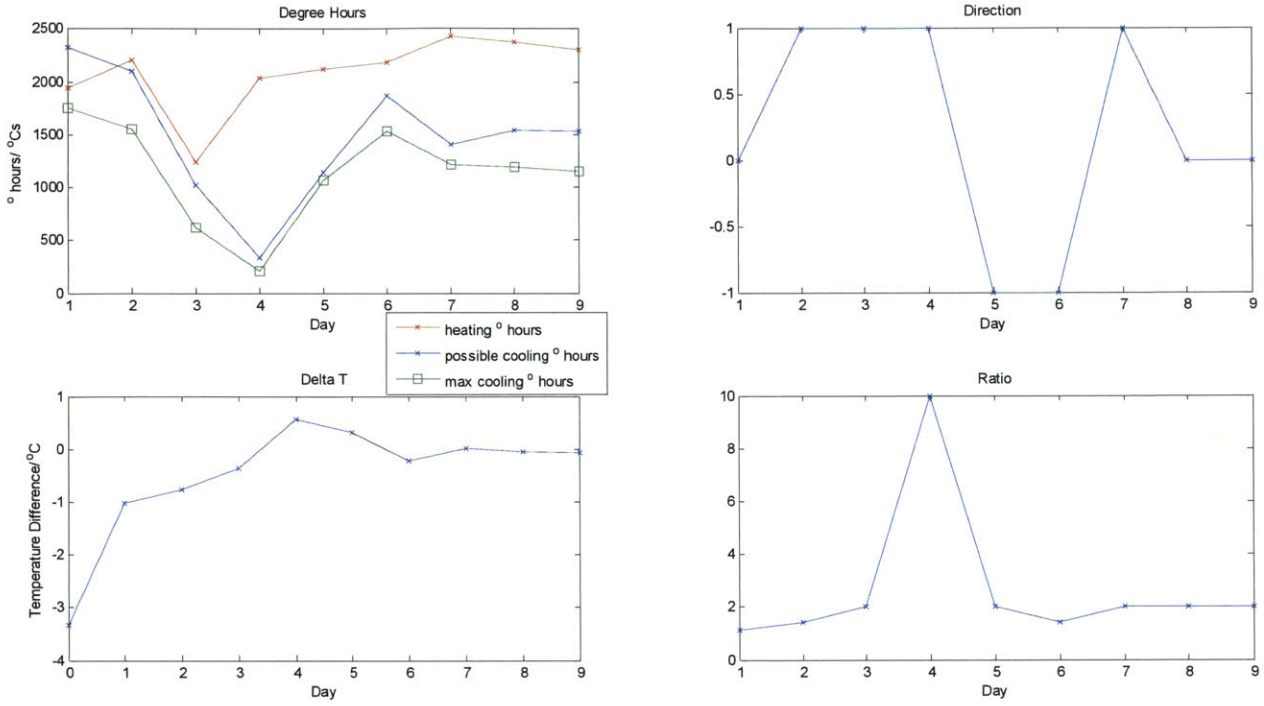

Figure 6-21: Plots of the parameters of the overcooling-prevention self-learning algorithm corresponding to temperature profile of figure 6.20

To verify if the ventilation controls for the occupational hours (modes 1-6) all work, RBC-2a is tested on Miami weather. In figure 6-22, we can see that RBC-2a gives close to the optimal performance. The exception lies when mode 4 is applied: it is the same limitation of heuristic rule highlighted by figure 6-5, i.e. although $T_{out}>T_{room\ air}$, it is beneficial to keep the windows open because the heat gain otherwise accumulated, can be convected away. A solution to this would be to use the 1-hour horizon rule developed in 6.1.1, which however requires building parameters. Note that mode 8 does not kick in here as there is no risk of overcooling, such that windows are always kept open overnight.

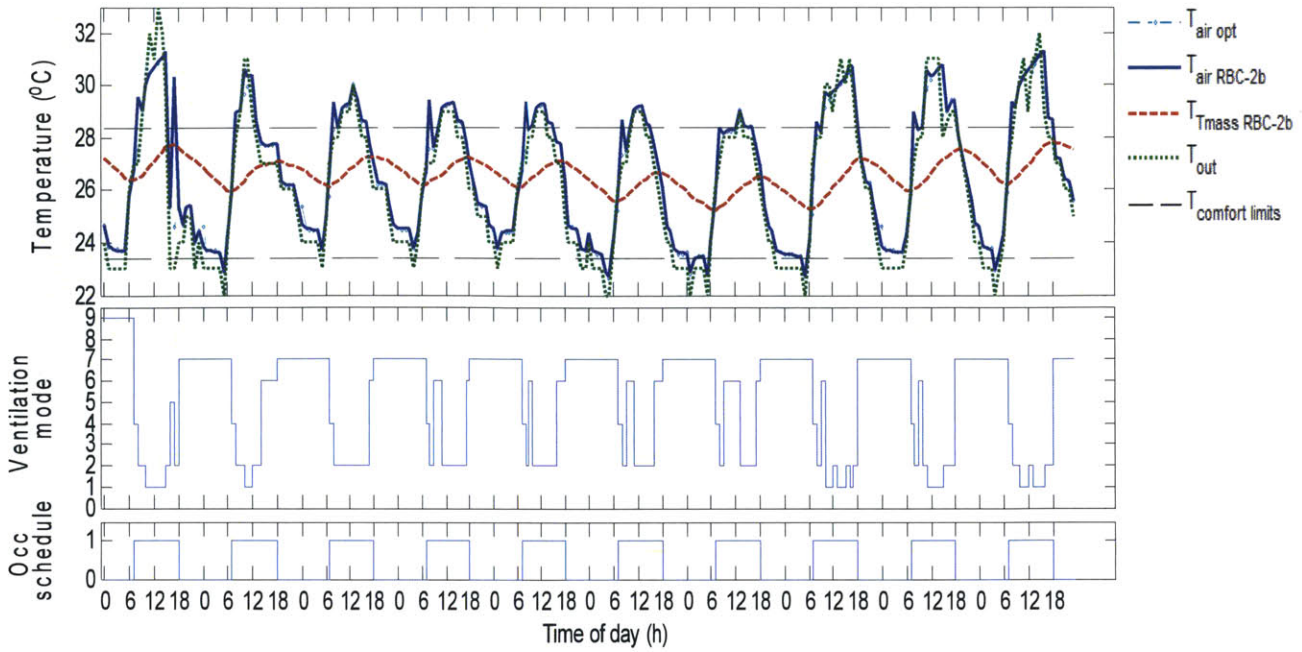

Figure 6-22: 10-day temperature profile for ventilation control with overcooling strategy 2. Parameters used: city: Miami; low heat gain, q=15W/m^2; normal thermal mass heat capacity c=880 J/kgK. Thermal cost for each day=[3, 1.5, 1.3, 0.9, 0.7, 0.5, 0.2, 2.7, 2.4, 3.4]

The ratio levels used in RBC-2a were arbitrarily defined as per table 6-2. To see if the ratio level increment could be defined by the performance of previous days' ratio increments, an algorithm for self-adjusting the ratio level was developed (RBC-2b):

$$\textit{Proportion constant} = \textit{ratio increment}_{\textit{day D-1}} / (\Delta T_{\textit{day D-1}} - \Delta T_{\textit{day D-2}}) ;$$
$$\textit{Ratio increment}_{\textit{day D}} = -\textit{acceptable proportion constant} * \Delta T_{\textit{day D}} ;$$
$$\textit{New ratio}_{\textit{day D}} = \textit{ratio}_{\textit{day D-1}} + \textit{ratio increment}_{\textit{day D}} ;$$

Note that for the first 2 days, the ratio increments' magnitudes were arbitrarily defined by table 6-2, but not their directions.

Figures 6-23 to 6-26 show the results with this RBC-2b for Madison and Los Angeles weather data. The shortcoming of this self-adjusting algorithm is seen with variable Madison weather. From figure 6-24, it can be seen that the algorithm has trouble decreasing ΔT from day 4 onwards, which starts occupation above thermal comfort, because the ratio decrease prescribed by the above algorithm to increase the cooling degree hours is not enough. While the ratio$_{\text{Day 5}}$ used by RBC-2a is 2 (figure 6-19), that prescribed by RBC-2b is decreased to 6 only (figure 6-24).This may be because the proportion constant needed to decrease ΔT is not the same as the proportion constant to increase ΔT, such that $T_{\text{room air}} = T_{\text{min comfort}}$. The above algorithm should

also be improved to catch instances where the ratio level becomes negative, as is the case in day 8. With negative ratio level, negative cooling degree hours result, such that no cooling is actually done overnight.

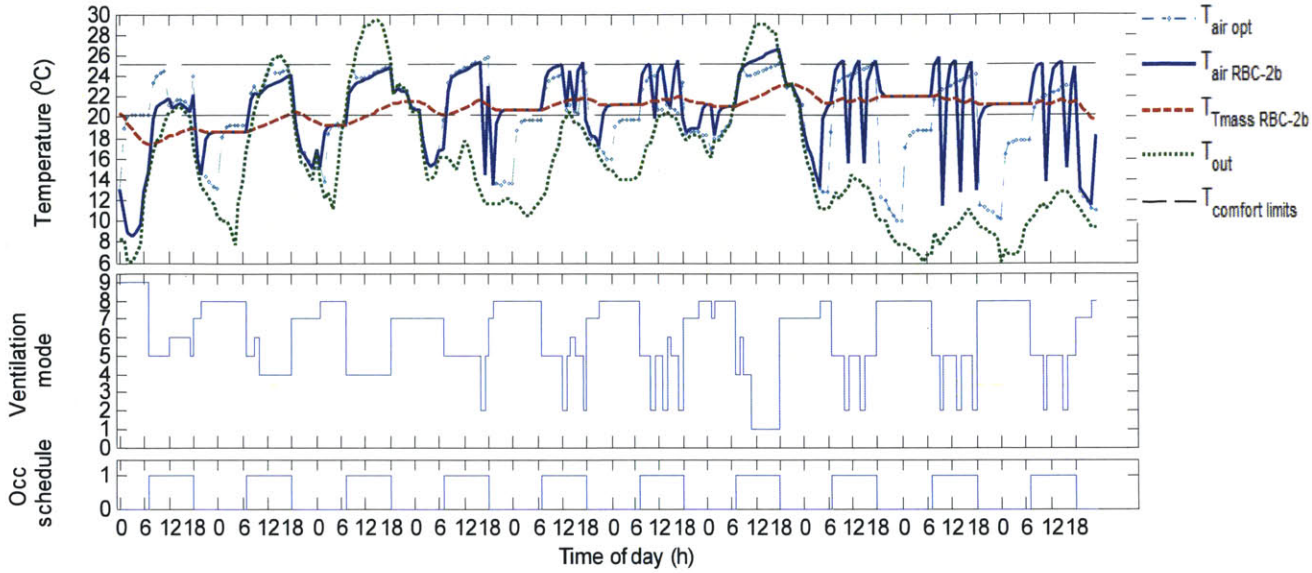

Figure 6-23: 10-day temperature profile for ventilation control with overcooling strategy 2 having self-adjusting ratio levels. Parameters used: city: Madison; low heat gain, q=15W/m^2; normal thermal mass heat capacity c=880 J/kgK. Thermal cost for each day=[0.4, 0, 0, 1.2, 0, 0, 1.1, 1.8, 4.7, 2.3]

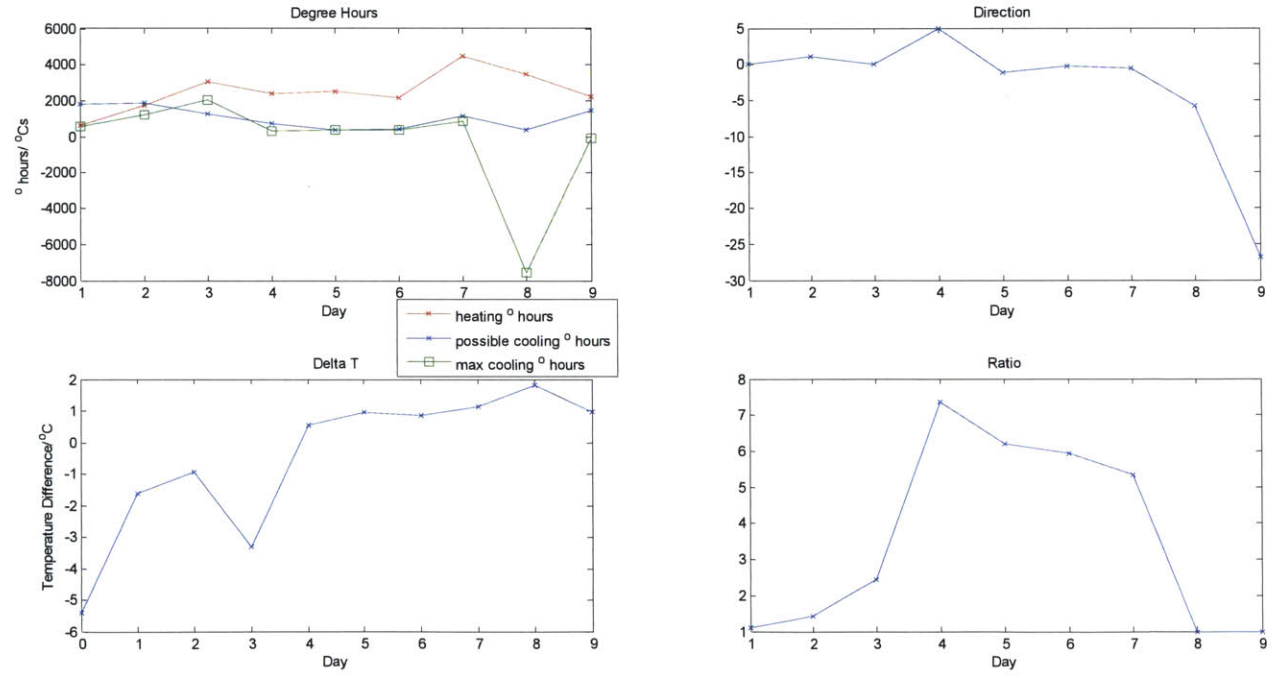

Figure 6-24: Plots of the parameters of the overcooling-prevention self-learning algorithm corresponding to temperature profile of figure 6-23

With Los Angeles' steadier weather, as with RBC-2a, the self-adjusting algorithm is able to find the ratio level, and hence tells when night-cooling should stop to just bring $T_{room\ air}$ to $T_{min\ comfort}$. RBC-2b does so faster, i.e. $\Delta T_{day\ 4} \sim = 0$ is reached on day 4 as seen in figures 6-25 to 6-26. The amount by which the ratio on day 3 should be increased for the ratio on day 4 is dictated by how much improvement previous ratio changes have resulted into, as per the proportion constant defined in the above algorithm, reducing the gap of $\Delta T_{day\ 3} = -0.6$ to $\Delta T_{day\ 4} \sim = 0$.

RBC-2b is better than RBC-2a in that it does not rely on tabulated ratio levels, which have to be defined properly. However, improvements need to be made to it so that the errors highlighted by the simulations of figures 6-23 to 6-24 are corrected; e.g., having 2 proportion constants for ratio increment and ratio decrement separately. It may also happen that the ratio prescribed by the self-learning algorithm, cannot be met, i.e. the night does not get cold enough to provide the required cooling degree hours. In that case, the day ratio is readjusted to reflect what was actually achieved, and the self-learning continues for the subsequent days. Overall, RBC-2 is as good as RBC-1, without the need to pre-determine building parameters such as ACH and h to estimate T_{Tmass}. RBC could be improved if the one-hour horizon rule is integrated in the control, which again requires that the building parameters be known or calculated.

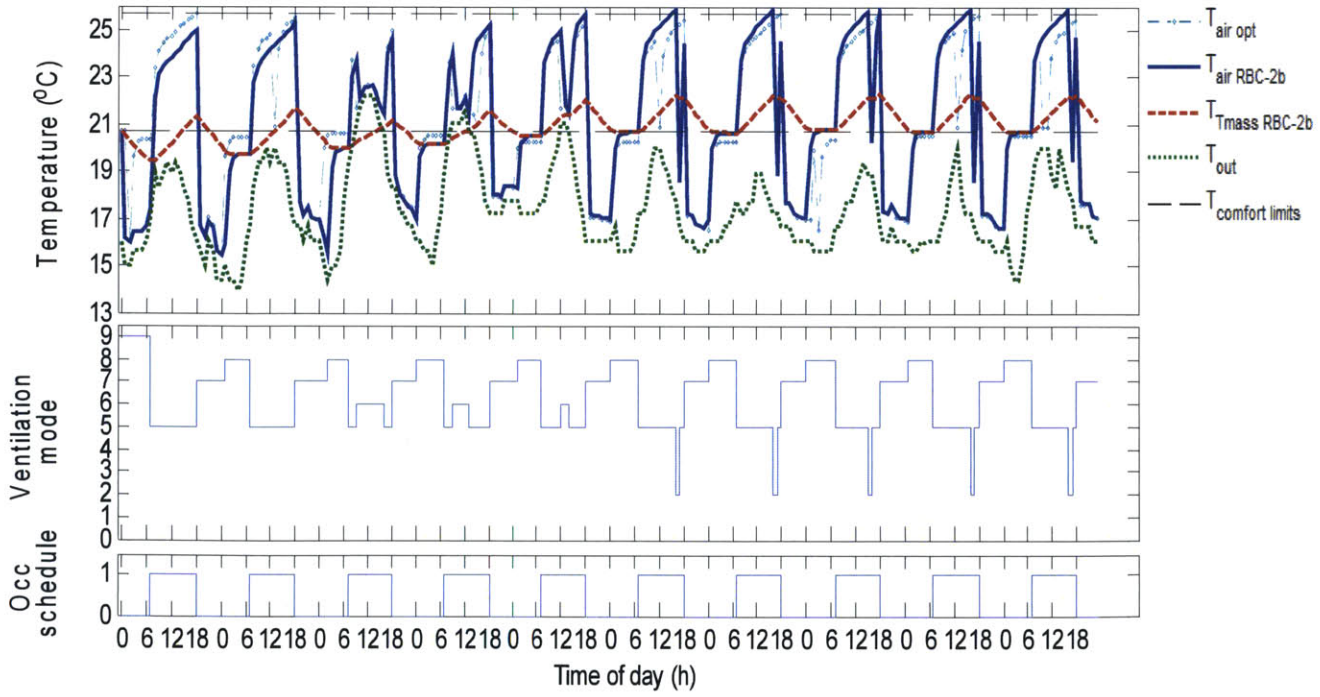

Figure 6-25: 10-day temperature profile for ventilation control with overcooling strategy 2 having self-adjusting ratio levels. Parameters used: city: Los Angeles; low heat gain, $q=15 W/m^2$;

normal thermal mass heat capacity c=880 J/kgK. Thermal cost for each day=[0.2, 0, 0, 0,0,0.3,0.3,0, 0.4, 0.2]

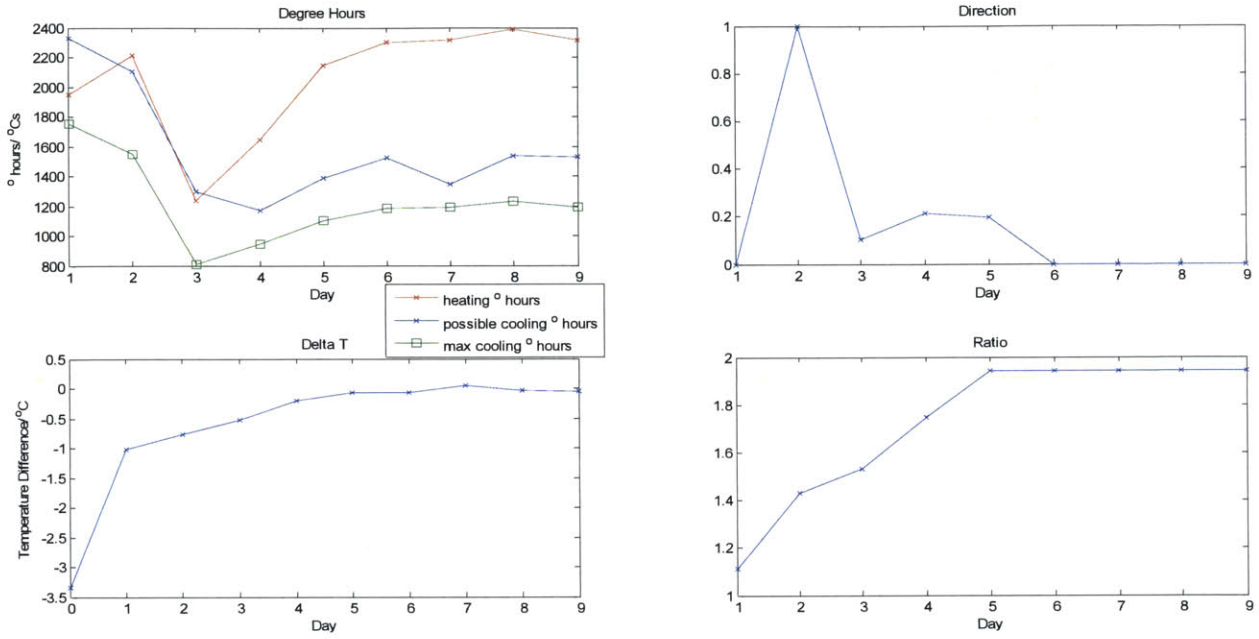

Figure 6-26: Plots of the parameters of the overcooling-prevention self-learning algorithm corresponding to temperature profile of figure 6-25

Chapter 7

Conclusion

The overarching purpose of this research was to investigate how the ventilation schedule can be optimized to make the best use of the direct and night cooling provided by natural ventilation in buildings. To do so, a simple energy model of a room was built to determine the parameters affecting its thermal response to incoming outdoor air, and to serve as the simulation engine for the optimization framework. In the process, an effective heat transfer coefficient was devised to approximate the energy model's thermal response based on a single-slice lumped thermal mass model instead of a multi-slice one. Using the energy model, two channels of ventilation controls were explored: optimization techniques and rule-based controls.

In the above case-studies, it was found that the strength of the optimization techniques lies in being able to forecast the thermal response of the energy model, given known design constraints (thermal comfort limit, occupational gain and schedule), building parameters and model disturbances (outdoor temperatures). For instance, it was able to weigh out the compromise between having the room temperature below minimum thermal comfort limit at occupation start, to having it above maximum thermal comfort limit during occupational hours. However, it requires a proper energy modeling of the building to get the predicted optimal outcome on the building itself. On the other hand, rule-based controls are easy to implement in existing Building Automation Software: it does not require building parameters but measureable inputs of current temperatures. During the day, the heuristic rules work well. Overnight, there is the risk of overcooling. To cater to that, the threshold at which night-cooling should stop needs to be determined. Two criteria were explored: (i) the thermal mass temperature estimate (RBC-1); (ii) the ratio of the day's heating degree hours to cooling degree hours (RBC-2), which does not require building parameters. The importance of the thermal mass in damping the response of the room air temperature to the outdoor incoming air temperature was established in chapter 2. As

the degree hours depend on the resulting room air temperature profile which is itself a function of the thermal mass temperature, the behavior of the thermal mass is encompassed by both criteria. While optimization techniques truly give the optimal ventilation schedule, a holistic rule-based control comprised of day and overcooling rules, does not give a thermal performance that far off for steady weather, provided that it allows for different rules for different scenarios, such as occupational time overheating or night-time overcooling. However, for temperature variations which swing wildly from day-to-day, identifying set-points for the overcooling rules is tricky. To this end, the self-learning algorithm catering to the overcooling rules shows promise but needs to be improved.

A proof-of-concept of a dynamic programming optimization framework was achieved, as well as a comparison of the thermal comfort performance of the optimization techniques to that of rule-based controls for ventilation. The developed framework has potential for further development. Up to now, only one objective was considered, i.e. maximizing thermal comfort. Other objectives are to be considered for future works, with the current energy model expanded to include hybrid/mixed mode ventilation and the associated cost of using fans, and mechanical cooling.

Appendix A

Calculations for effective heat transfer coefficient for lumped thermal mass model

The following is a sample Maple code used to simplify symbolically the effective impedance of the thermal circuit in figure 2-11 so as to reach equation 2.32. Note that for a thermal mass representation of more than 3 slices, the loop is increased to N-1 times if N slices are used.

```
> parallelZ := (x,y) -> x·y/(x+y);
```

$$(x, y) \rightarrow \frac{x\,y}{x + y}$$

```
seriesZ := (x,y) -> x+y;
```

$$(x, y) \rightarrow x + y$$

```
Zr := R; Zc := 1/(w·C·I); p1 := Zr;
```

$$R$$

$$-\frac{\mathrm{I}}{w\,C}$$

$$R$$

```
z := Zc;
```

$$-\frac{\mathrm{I}}{w\,C}$$

```
for i from 1 to 2 do p2 := seriesZ(Zr,z); z := parallelZ(Zc,p2); simplify(evalc(Re(z)));
    simplify(evalc(Im(z))); end do
```

$$R - \frac{\mathrm{I}}{w\,C}$$

$$-\frac{\mathrm{I}\left(R - \frac{\mathrm{I}}{w\,C}\right)}{w\,C\left(-\frac{2\,\mathrm{I}}{w\,C} + R\right)}$$

$$\frac{R}{C^2 R^2 w^2 + 4}$$

$$-\frac{C^2 R^2 w^2 + 2}{w C \left(C^2 R^2 w^2 + 4\right)}$$

$$R - \frac{\mathrm{I}\left(R - \frac{\mathrm{I}}{w C}\right)}{w C \left(-\frac{2\,\mathrm{I}}{w C} + R\right)}$$

$$-\frac{\mathrm{I}\left(R - \frac{\mathrm{I}\left(R - \frac{\mathrm{I}}{w C}\right)}{w C \left(-\frac{2\,\mathrm{I}}{w C} + R\right)}\right)}{w C \left(-\frac{\mathrm{I}}{w C} + R - \frac{\mathrm{I}\left(R - \frac{\mathrm{I}}{w C}\right)}{w C \left(-\frac{2\,\mathrm{I}}{w C} + R\right)}\right)}$$

$$\frac{\left(C^2 R^2 w^2 + 5\right) R}{C^4 R^4 w^4 + 10 C^2 R^2 w^2 + 9}$$

$$-\frac{C^4 R^4 w^4 + 8 C^2 R^2 w^2 + 3}{w C \left(C^4 R^4 w^4 + 10 C^2 R^2 w^2 + 9\right)}$$

>

Appendix B

Input parameter for simulation run of the combined Design Advisor-CoolVent program

Building Properties	Parameter	Value
Climate and location	City	Boston
	Terrain type	Flat terrain
	Height of surrounding buildings	5 m
Occupancy	Occupancy heat loads	30 W/m^2
	Schedule	9am-19pm
	Lighting requirements (office) Lighting control	400 lux efficient
Ventilation control	Night-cooling and window operation	None
Normal thermal mass (floor and ceiling)	Thickness conductivity Density Specific heat capacity Heat transfer coefficient (to room air)	0.10 m 1.0 W/mK 2500 kg/m^3 880 J/kgK 8 W/m^2K
Building geometry (cross-ventilated building)	Window façade width	20 m
	Zone Depth	10 m
	Number of sections	3
	Window façade orientation	North-South
Roof (if present)	Slab conductivity Slab density Slab specific heat capacity Slab thickness	1.4 W/mK 2300 kg/m^3 880 J/kgK 0.15 m
	Insulation (cool or bitumen roof only): R-value Cover-board thickness Cover-board conductivity Cover-board density Cover-board specific heat capacity	 5 m^2K/W 0.0127 m 0.133 W/m^2K 746 kg/m^3 1090 J/kgK
	Soil properties(Green roof only): Conductivity Conductivity x specific heat capacity Soil thickness	 0.8 W/mK 1.4 x 10^6 J/m^3K 0.15 m

Window	% of exterior window façade	20 %
	Window type	Triple glazed
	Blinds (if present): Schedule Closed angle Width Emissivity Absorptivity	 Responds to solar intensity 90° 15mm 0.2 0.9
	Coating	Clear
	Overhang	none
Internal openings	Area	20 m^2
	Discharge coefficient	0.7
Wall	Insulation R-value	3.0 m^2K/W

Table B-1: Input parameters used for simulation run of combined Design Advisor-CoolVent program

Appendix C

Results for case studies for optimized and rule-based control of ventilation

C.1 Comparison of window ventilation strategies in terms of thermal cost and opening hours with sinusoidal outdoor temperatures

This section gives a tabulated summary of the results for the parametric simulation runs with sinusoidal outdoor temperatures and other input parameters defined in table 6-1. The comparison, done in terms of thermal comfort and resulting window schedule, weighs the results of optimized control (dynamic programming (DP) or global search optimization (GSO)) against that of rule-based controls defined in section 6.1, i.e. heuristic and 1h-horizon rule. The scenario where the natural ventilation is continuous, i.e. windows are "always open", is added to gauge when natural ventilation control is actually needed. Tables C-1 and C-2 list the thermal comfort and window schedule comparison respectively for the energy model with a 1-slice uniform thermal mass element (effective heat transfer coefficient=4 W/m^2K), while tables C-3 and C-4 list those for the energy model with a 10-slice discretized thermal mass element (heat transfer coefficient=8 W/m^2K). The thermal cost is computed for each strategy according to equation 5.4, with closing and opening times extracted for each strategy applied over the time period of 2 days.

Parameter Set	**Thermal cost for different window strategies**			
	Always open	**DP**	**Heuristic**	**1h-horizon**
Tmean=20°C; Tamp=7.5°C, c=0.25*880J/kgK, h= 8W/m2K, q=15 W/m2 **(low Tmass, low heat gain)**	0.87	0.01	0.03	0.01
Tmean=20°C; Tamp=7.5°C, c=880J/kgK, h= 8W/m2K, q=15 W/m2 **(normal Tmass, low heat gain)**	0.38	0	0.02	0.02
Tmean=20°C; Tamp=7.5°C, c=3*880J/kgK,	0.32	0	0.03	0.03

h= 8W/m2K, q=15 W/m2 **(high Tmass, low heat gain)**				
Tmean=20°C; Tamp=7.5°C, c=880J/kgK, h= 8W/m2K, q=30 W/m2 **(normal Tmass, medium heat gain)**	1.61	1.61	1.61	1.61
Tmean=20°C; Tamp=7.5°C, c=880J/kgK, h= 8W/m2K, q=45 W/m2 **(normal Tmass, high heat gain)**	3.43	3.43	3.43	3.43
Tmean=25°C; Tamp=7.5°C, c=0.25*880J/kgK, h= 8W/m2K, q=15 W/m2 **(low Tmass, low heat gain)**	10.50	1.73	4.07	4.11
Tmean=25°C; Tamp=7.5°C, c=880J/kgK, h= 8W/m2K, q=15 W/m2 **(normal Tmass, low heat gain)**	9.04	0.51	0.93	0.93
Tmean=25°C; Tamp=7.5°C, c=3*880J/kgK, h= 8W/m2K, q=15 W/m2 **(high Tmass, low heat gain)**	8.49	0.01	0.05	0.07
Tmean=25°C; Tamp=7.5°C, c=880J/kgK, h= 8W/m2K, q=30 W/m2 **(normal Tmass, medium heat gain)**	12.44	12.38	12.97	12.44
Tmean=25°C; Tamp=7.5°C, c=880J/kgK, h= 8W/m2K, q=45 W/m2 **(normal Tmass, high heat gain)**	15.88	15.82	17.21	15.88

Table C-1: Thermal cost for the different ventilation strategies with 1-slice thermal mass (N.B: DP denotes optimal results using dynamic programming)

Parameter set	**24h-window pattern**		
	DP	**Heuristic**	**1h-horizon**
Tmean=20°C; Tamp=7.5°C, c=0.25*880J/kgK, h= 8W/m2K, q=15 W/m2 **(low Tmass, low heat gain)**	Close 2-4am Close 9-15pm	Close 9-16pm	Close 9-15pm
Tmean=20°C; Tamp=7.5°C, c=880J/kgK, h= 8W/m2K, q=15 W/m2 **(normal Tmass, low heat gain)**	Close 2-6am Close 11-15pm Close 18-19pm	Close 9-17pm	Close 11-15pm
Tmean=20°C; Tamp=7.5°C, c=3*880J/kgK, h= 8W/m2K, q=15 W/m2 **(high Tmass, low heat gain)**	Close 2-6am Close 11-15pm Close 18-19pm	Close 9-17pm	Close 9-16pm
Tmean=20°C; Tamp=7.5°C, c=880J/kgK, h= 8W/m2K, q=30 W/m2 **(normal Tmass, medium heat gain)**	Always open	Always open	Always open

Tmean=20°C; Tamp=7.5°C, c=880J/kgK, h= 8W/m2K, q=45 W/m2 **(normal Tmass, high heat gain)**	Always open	Always open	Always open
Tmean=25°C; Tamp=7.5°C, c=0.25*880J/kgK, h= 8W/m2K, q=15 W/m2 **(low Tmass, low heat gain)**	Close 5-16pm	Close 8-16pm	Close 8-15pm
Tmean=25°C; Tamp=7.5°C, c=880J/kgK, h= 8W/m2K, q=15 W/m2 **(normal Tmass, low heat gain)**	Close 6-17pm	Close 8-17pm	Close 8-17pm
Tmean=25°C; Tamp=7.5°C, c=3*880J/kgK, h= 8W/m2K, q=15 W/m2 **(high Tmass, low heat gain)**	Close 7-18pm	Close 8-18pm	Close 8-17pm
Tmean=25°C; Tamp=7.5°C, c=880J/kgK, h= 8W/m2K, q=30 W/m2 **(normal Tmass, medium heat gain)**	Close 6-8pm	Close 8-9pm	Always open
Tmean=25°C; Tamp=7.5°C, c=880J/kgK, h= 8W/m2K, q=45 W/m2 **(normal Tmass, high heat gain)**	Close 7-8pm	Close 8-9pm	Always open

Table C-2: Opening and closing times for the different ventilation strategies with 1-slice thermal mass (N.B: DP denotes optimal results using dynamic programming)

Parameter set	**Thermal cost for different window strategies**				
	Always open	**"DP"**	**Heuristic**	**1h-horizon**	**GSO**
Tmean=20°C; Tamp=7.5°C, c=0.25*880J/kgK, h= 8W/m2K, q=15 W/m2 **(low Tmass, low heat gain)**	0.92	0.01	2.97	0.01	0.01
Tmean=20°C; Tamp=7.5°C, c=880J/kgK, h= 8W/m2K, q=15 W/m2 **(normal Tmass, low heat gain)**	0.41	0	0.37	0	0
Tmean=20°C; Tamp=7.5°C, c=3*880J/kgK, h= 8W/m2K, q=15 W/m2 **(high Tmass, low heat gain)**	0.05	0	0.21	0.01	0
Tmean=20°C; Tamp=7.5°C, c=880J/kgK, h= 8W/m2K, q=30 W/m2 **(normal Tmass, medium heat gain)**	1.39	1.07	1.02	1.15	1.02
Tmean=20°C; Tamp=7.5°C, c=880J/kgK, h= 8W/m2K, q=45 W/m2 **(normal Tmass, high heat gain)**	3.17	3.14	3.20	3.17	3.13
Tmean=25°C; Tamp=7.5°C,	10.59	1.45	1.54	4.08	1.43

c=0.25*880J/kgK, h= 8W/m2K, q=15 W/m2 **(low Tmass, low heat gain)**					
Tmean=25°C; Tamp=7.5°C, c=880J/kgK, h= 8W/m2K, q=15 W/m2 **(normal Tmass, low heat gain)**	8.60	0.02	0.03	0.10	0.02
Tmean=25°C; Tamp=7.5°C, c=3*880J/kgK, h= 8W/m2K, q=15 W/m2 **(high Tmass, low heat gain)**	7.23	0	0	0	0
Tmean=25°C; Tamp=7.5°C, c=880J/kgK, h= 8W/m2K, q=30 W/m2 **(normal Tmass, medium heat gain)**	12.06	10.80	10.52	11.66	10.52
Tmean=25°C; Tamp=7.5°C, c=880J/kgK, h= 8W/m2K, q=45 W/m2 **(normal Tmass, high heat gain)**	15.44	15.26	15.52	15.44	15.24

Table C-3: Thermal cost for the different ventilation strategies with 1-slice thermal mass (N.B: "DP" denotes results using dynamic programming's window schedules and the 10-slice model, while GSO denotes optimal results using the global search optimization technique)

Parameter Set	**24h-window pattern**			
	"DP"	**Heuristic**	**1h-horizon**	**GSO**
Tmean=20°C; Tamp=7.5°C, c=0.25*880J/kgK, h= 8W/m2K, q=15 W/m2 **(low Tmass, low heat gain)**	Close 2-4 Close 9-15	5-17	9-15	10-15
Tmean=20°C; Tamp=7.5°C, c=880J/kgK, h= 8W/m2K, q=15 W/m2 **(normal Tmass, low heat gain)**	Close 2-6 Close11-15 Close 18-19	Close 7-15	Close 9-15	Close 9-24
Tmean=20°C; Tamp=7.5°C, c=3*880J/kgK, h= 8W/m2K, q=15 W/m2 **(high Tmass, low heat gain)**	Close 2-6 Close 11-15 Close 18-19	Close 7-17	Close 9-16	Close 12-24
Tmean=20°C; Tamp=7.5°C, c=880J/kgK, h= 8W/m2K, q=30 W/m2 **(normal Tmass, medium heat gain)**	Always open	Close 6-14	9-13	Close 6-14
Tmean=20°C; Tamp=7.5°C, c=880J/kgK, h= 8W/m2K, q=45 W/m2 **(normal Tmass, high heat gain)**	Always open	Close6-9am	Always open	Close 6-8am
Tmean=25°C; Tamp=7.5°C,	Close 5-16	Close 5-17	Close 8-15	Close 4-17

c=0.25*880J/kgK, h= 8W/m2K, q=15 W/m2 **(low Tmass, low heat gain)**				
Tmean=25°C; Tamp=7.5°C, c=880J/kgK, h= 8W/m2K, q=15 W/m2 **(normal Tmass, low heat gain)**	Close 6-17	Close 5-18	Close 8-17	Close 6-18
Tmean=25°C; Tamp=7.5°C, c=3*880J/kgK, h= 8W/m2K, q=15 W/m2 **(high Tmass, low heat gain)**	Close 7-18pm	Close 6-18	Close 8-17	Close 2-18
Tmean=25°C; Tamp=7.5°C, c=880J/kgK, h= 8W/m2K, q=30 W/m2 **(normal Tmass, medium heat gain)**	Close 6-8	Close 6-14	9-13	Close 6-14
Tmean=25°C; Tamp=7.5°C, c=880J/kgK, h= 8W/m2K, q=45 W/m2 **(normal Tmass, high heat gain)**	Close 7-8	Close 6-9	Always open	Close 6-8

Table C-4: Opening and closing times for the different ventilation strategies with 1-slice thermal mass (N.B: "DP" denotes results using dynamic programming's window schedules and the 10-slice model, while GSO denotes optimal results using the global search optimization technique)

C.2 Optimized and rule-based ventilation control results with weather data

The following graphs show the optimization results for the four cities (Miami, Madison, Los Angeles, Kansas) with varying temperature profiles, using the two optimization techniques developed in chapter 5: (a) dynamic programming with 1-slice thermal mass energy model, (b) global search optimization with a 10-slice one. A third graph is added in each set to show the validity of the effective single-slice lumped thermal mass model. Parametric runs varying thermal mass and occupational heat gain were carried out.

Parameters: Miami, low heat gain q=15W/m^2; low thermal mass specific heat capacity c=220 J/kgK

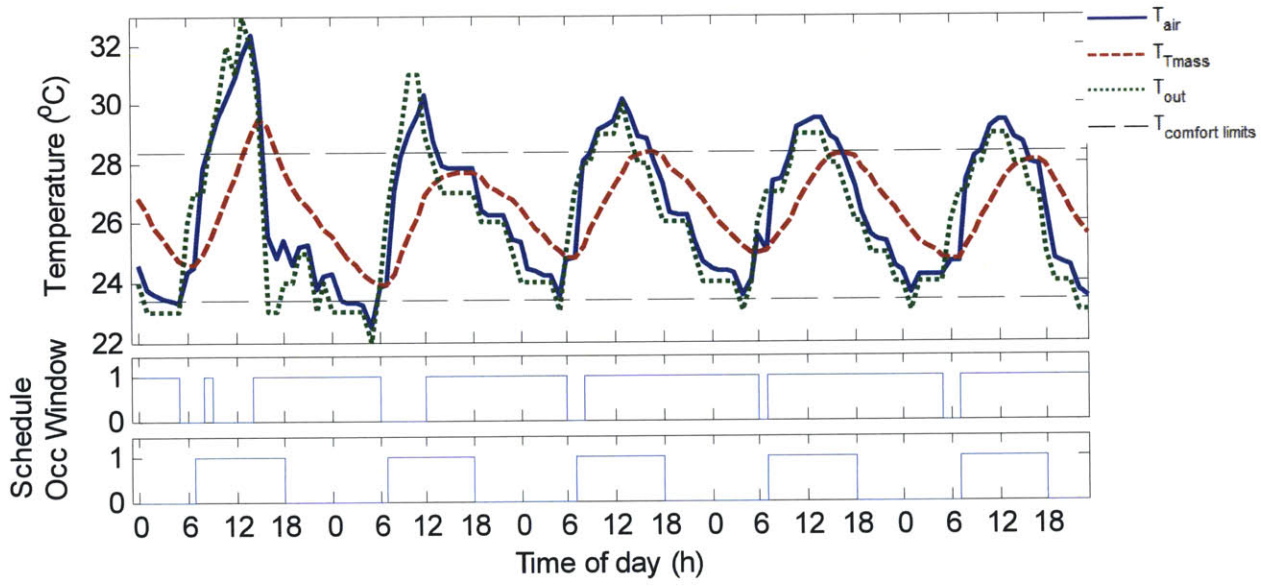

Figure C-1: Optimization results for May 15-19 using dynamic programming and 1-slice model for parameters: Miami, low heat gain q=15W/m^2; low thermal mass specific heat capacity c=220 J/kgK. Resulting day thermal cost = [3.1, 0.8, 1.4, 1.0, 0.8].

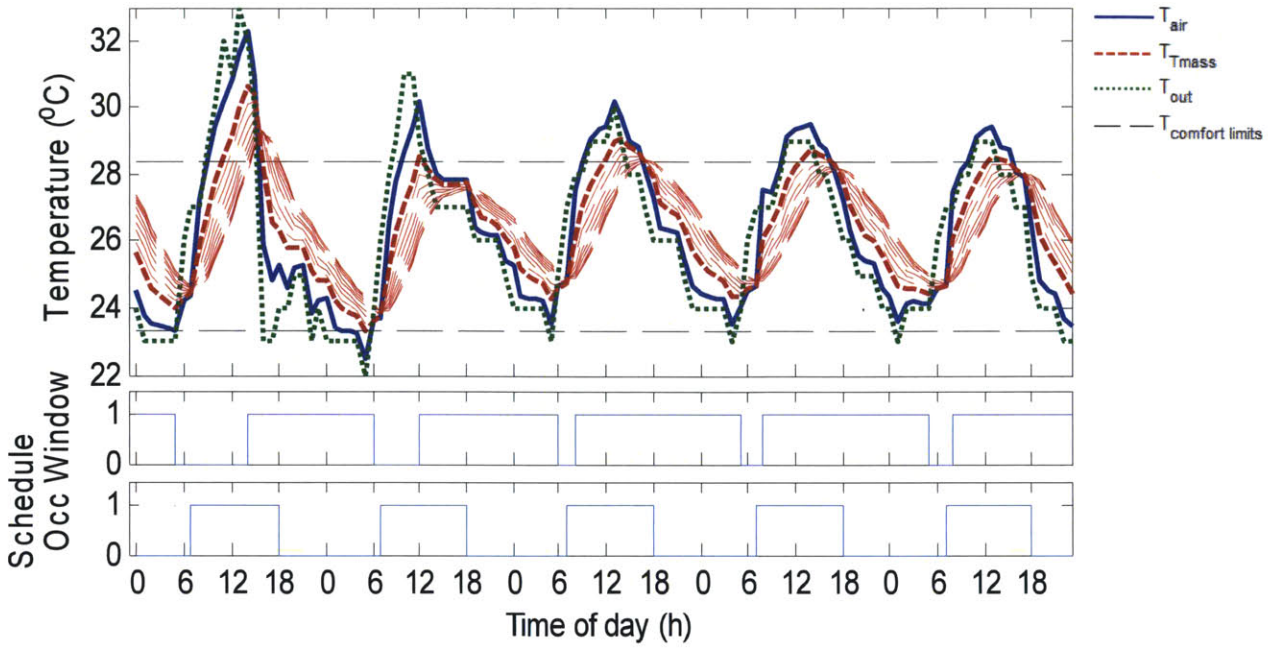

Figure C-2: Optimization results for May 15-19 using global search optimization and 10-slice model for parameters: Miami, low heat gain q=15W/m^2; low thermal mass specific heat capacity c=220 J/kgK. Resulting day thermal cost = [3.0, 0.7, 1.4, 1.0, 0.8]

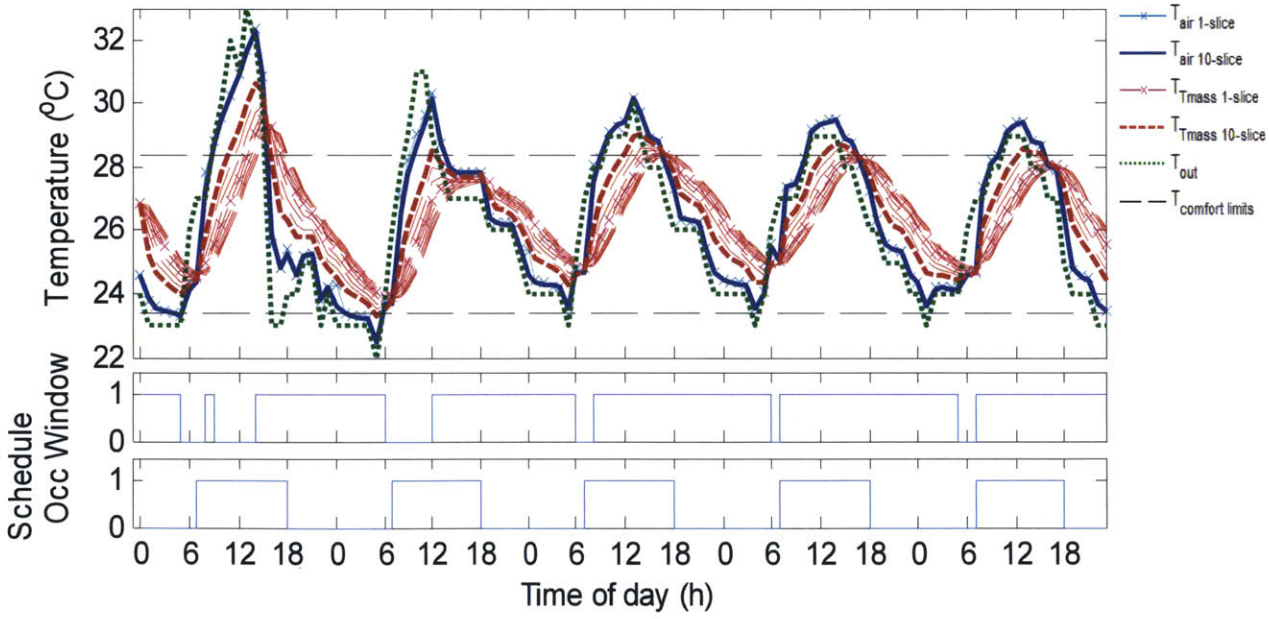

Figure C-3: Testing the effectiveness of effective h with 1-slice model for May 15-19 for parameters: Miami, low heat gain q=15W/m^2; low thermal mass specific heat capacity c=220 J/kgK.

Parameters: Miami, low heat gain q=15W/m^2; normal thermal mass specific heat capacity c=880 J/kgK

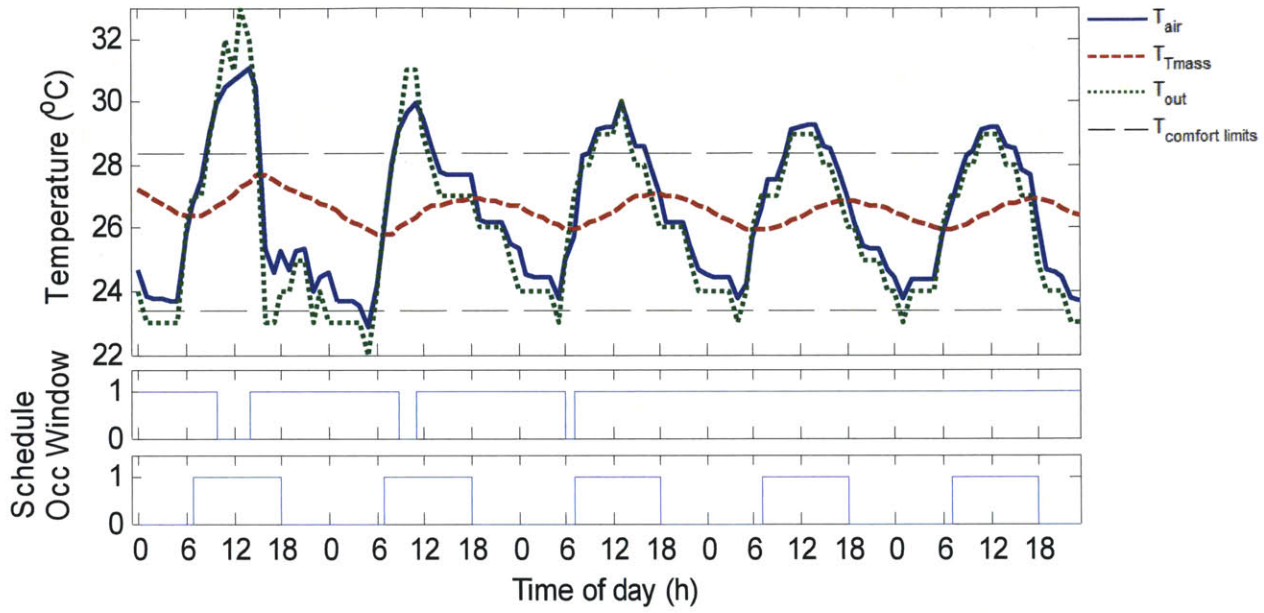

Figure C-4: Optimization results for May 15-19 using dynamic programming and 1-slice model for parameters: Miami, low heat gain q=15W/m^2; normal thermal mass specific heat capacity c=880 J/kgK. Resulting day thermal cost = [2.7, 1.0, 1.1, 0.8, 0.6]

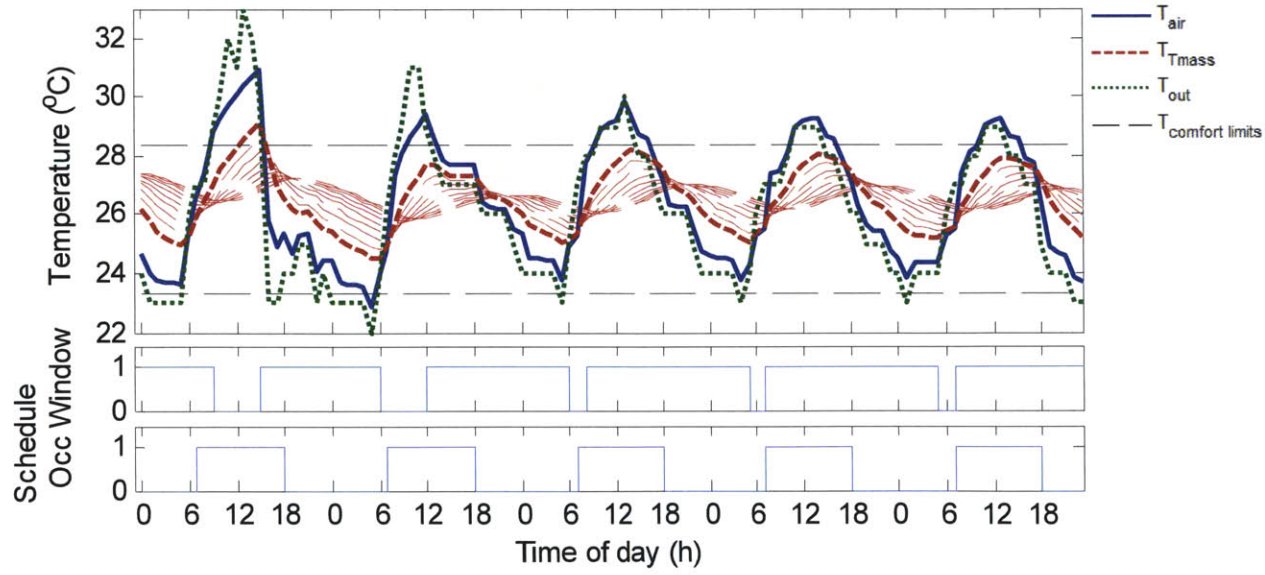

Figure C-5: Optimization results for May 15-19 using global search optimization and 10-slice model for parameters: Miami, low heat gain q=15W/m^2; normal thermal mass specific heat capacity c=880 J/kgK. Resulting day thermal cost = [1.9, 0.4, 1.1, 0.8, 0.6]

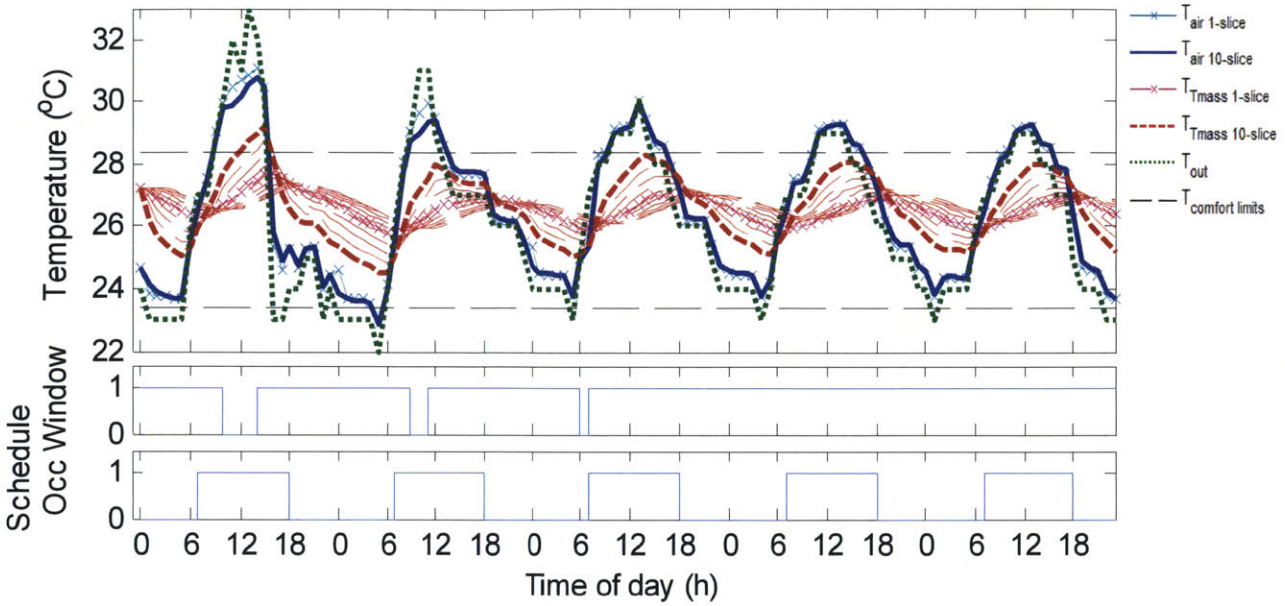

Figure C-6: Testing the effectiveness of effective h with 1-slice model for May 15-19 for parameters: Miami, low heat gain q=15W/m^2; normal thermal mass specific heat capacity c=880 J/kgK.

Parameters: Miami, low heat gain q=15W/m^2; high thermal mass specific heat capacity c=2640 J/kgK

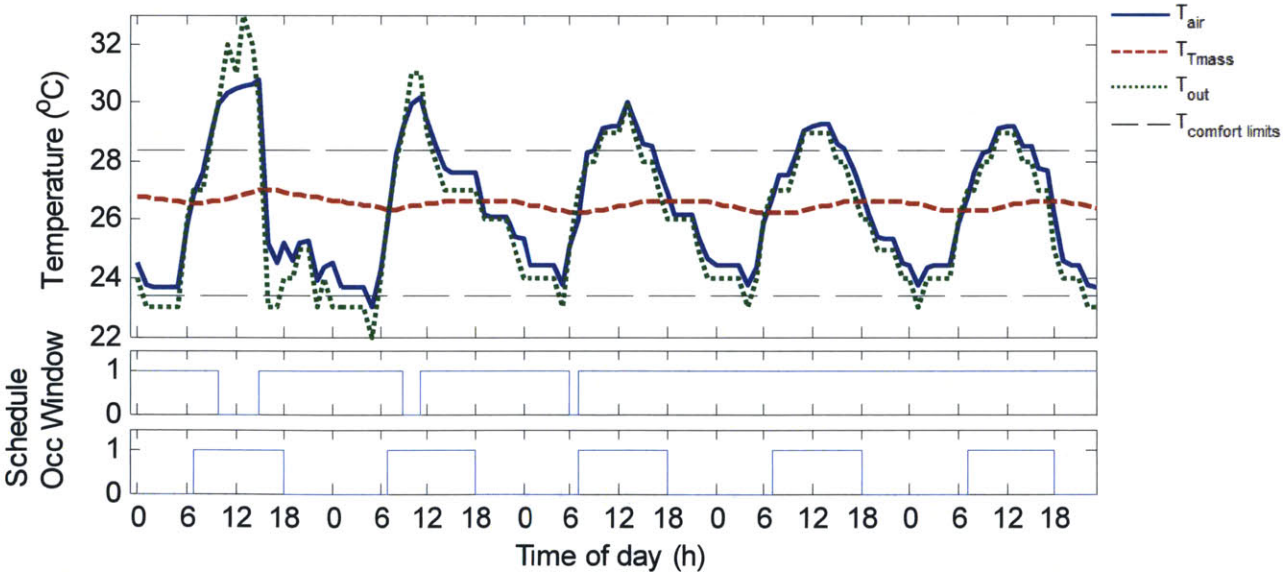

Figure C-7: Optimization results for May 15-19 using dynamic programming and 1-slice model for parameters: Miami, low heat gain q=15W/m^2; high thermal mass specific heat capacity c=2640 J/kgK. Resulting day thermal cost = [1.6, 0.8, 1.0, 0.7, 0.6]

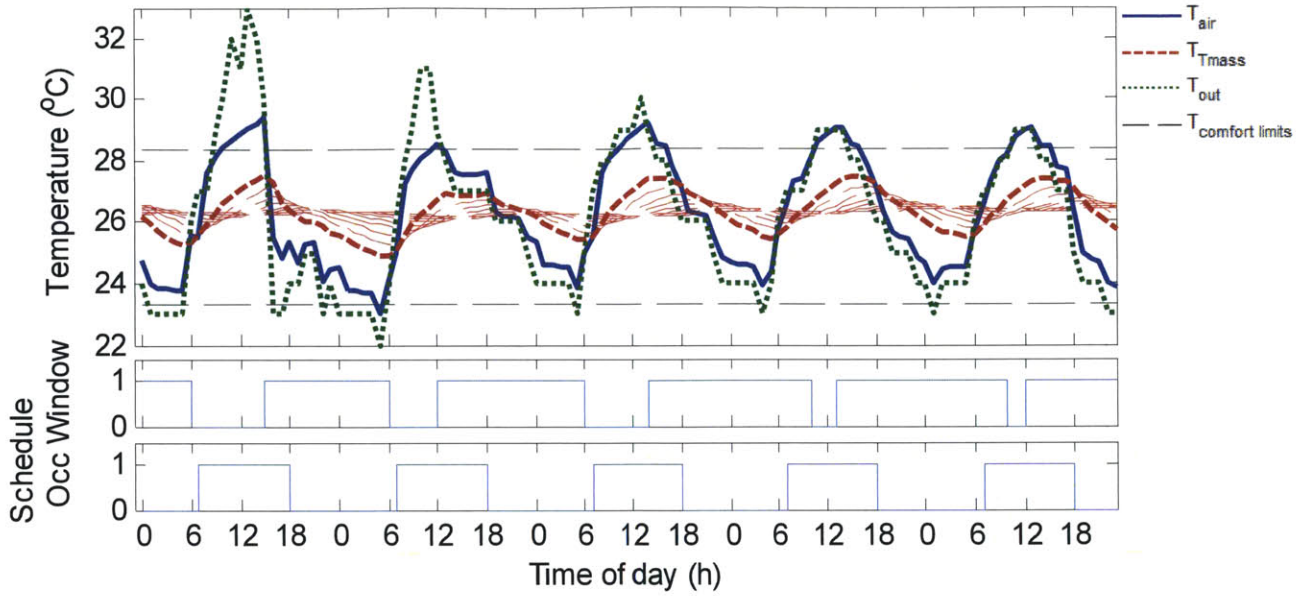

Figure C-8: Optimization results for May 15-19 using global search optimization and 10-slice model for parameters: Miami, low heat gain q=15W/m^2; high thermal mass specific heat capacity c=2640 J/kgK. Resulting day thermal cost = [0.1, 0, 0.2, 0.3, 0.3]

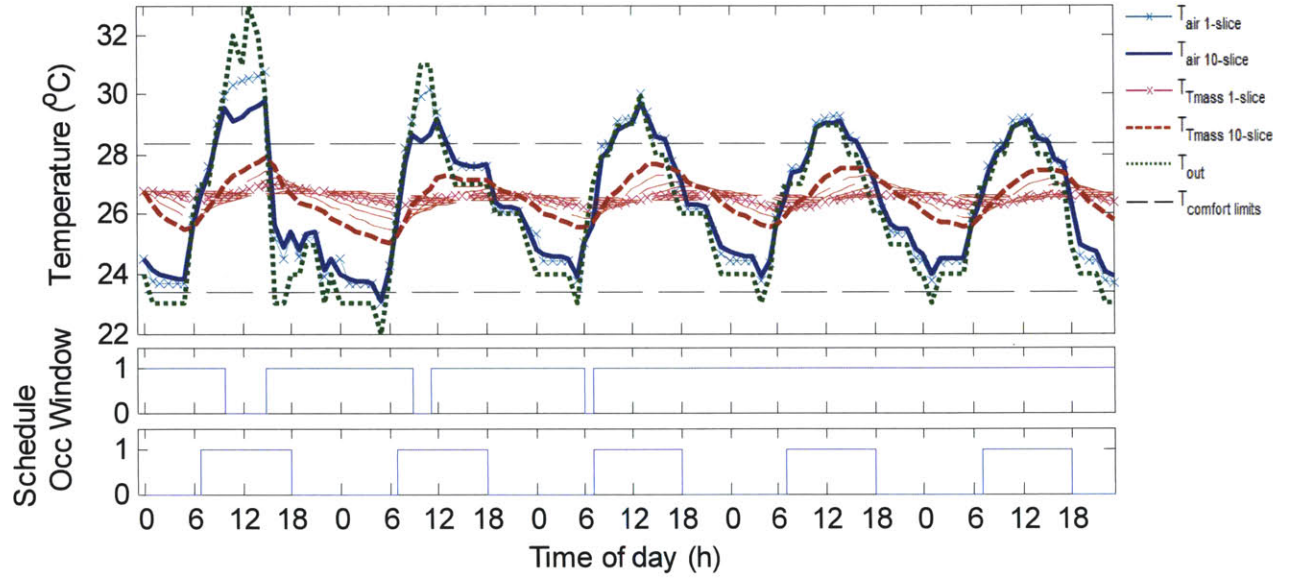

Figure C-9: Testing the effectiveness of effective h with 1-slice model for May 15-19 for parameters: Miami, low heat gain q=15W/m^2; high thermal mass specific heat capacity c=2640 J/kgK.

Parameters: Miami, medium heat gain q=30W/m^2; normal thermal mass specific heat capacity c=880 J/kgK

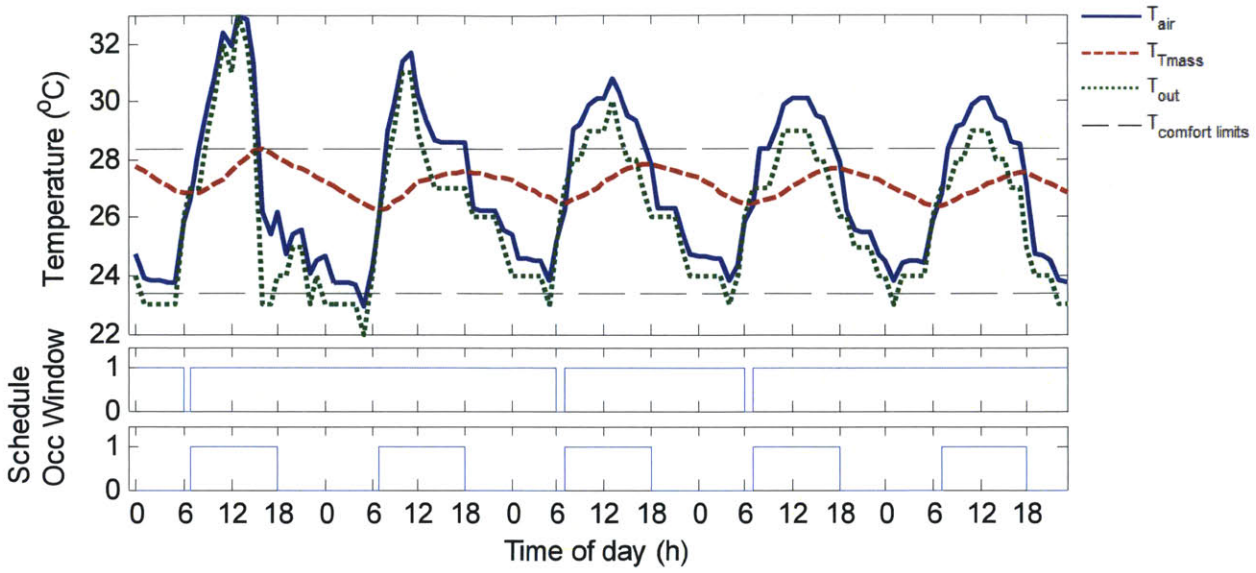

Figure C-10: Optimization results for May 15-19 using dynamic programming and 1-slice model for parameters: Miami, medium heat gain q=30W/m^2; normal thermal mass specific heat capacity c=880 J/kgK. Resulting day thermal cost = [4.7, 2.5, 2.7, 2.0, 1.8]

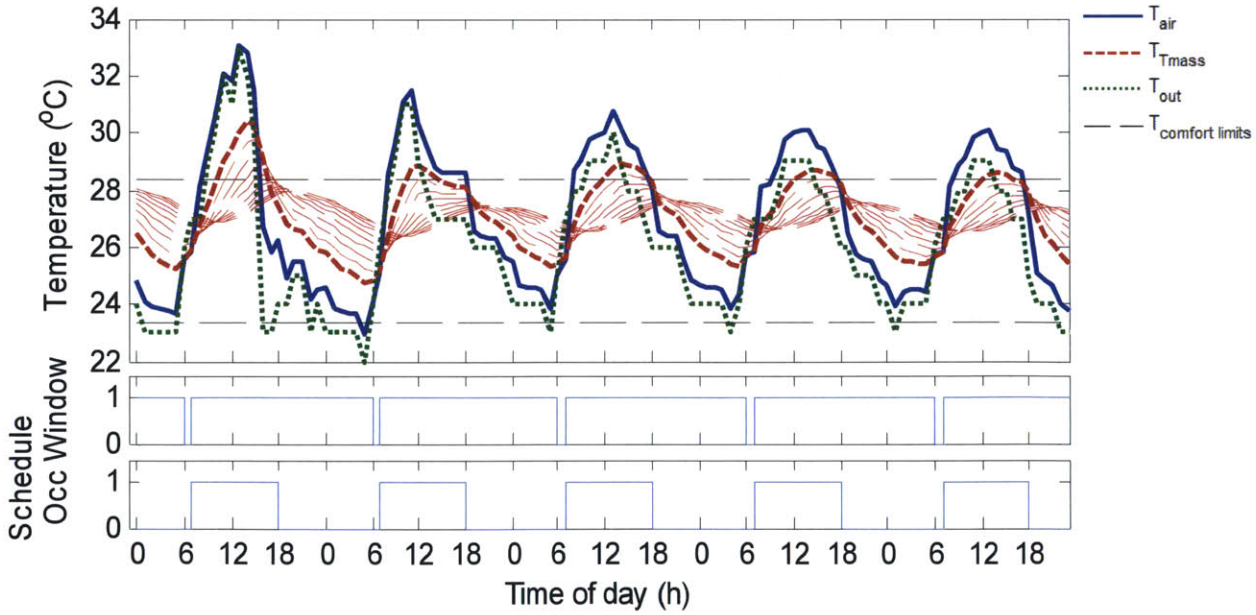

Figure C-11: Optimization results for May 15-19 using global search optimization and 10-slice model for parameters: Miami, medium heat gain q=30W/m^2; normal thermal mass specific heat capacity c=880 J/kgK. Resulting day thermal cost = [4.5, 2.4, 2.6, 2.0, 1.8]

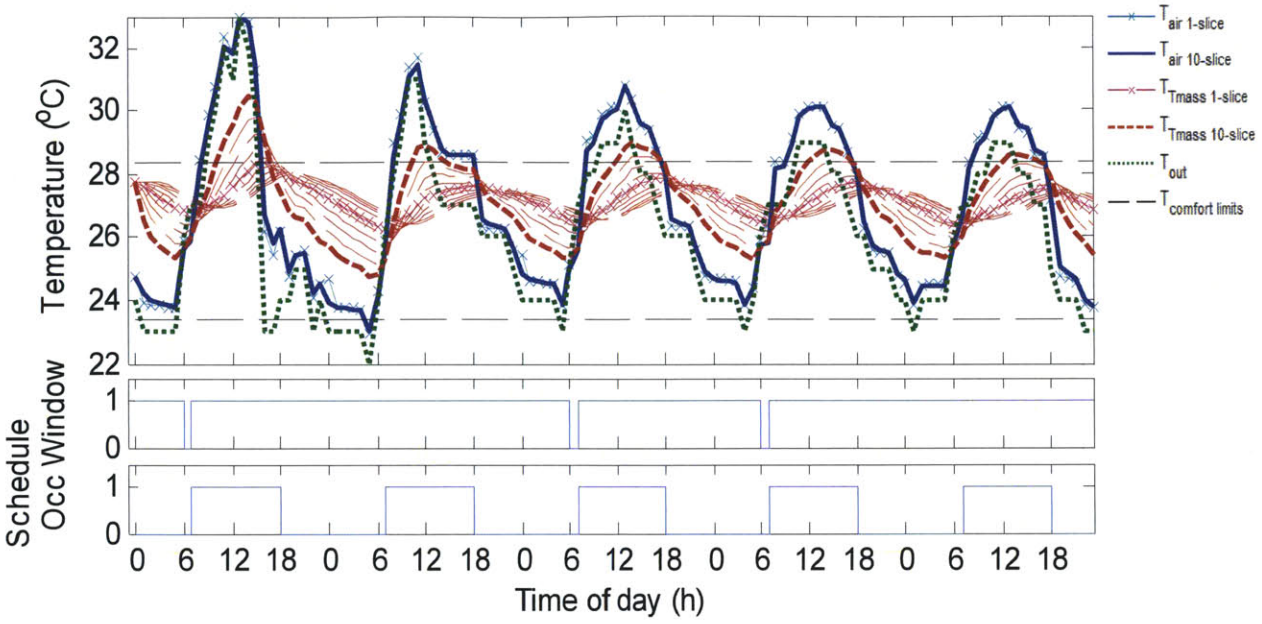

Figure C-12: Testing the effectiveness of effective h with 1-slice model for May 15-19 for parameters: Miami, medium heat gain q=30W/m^2; normal thermal mass specific heat capacity c=880 J/kgK.

Parameters: Miami, high heat gain q=45W/m^2; normal thermal mass specific heat capacity c=880 J/kgK

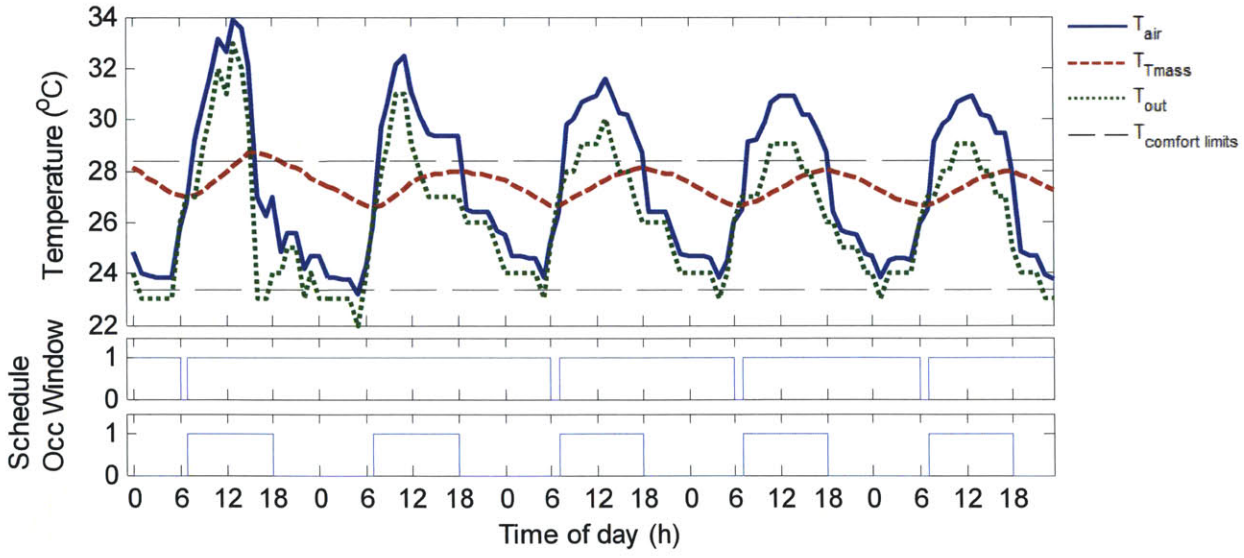

Figure C-13: Optimization results for May 15-19 using dynamic programming and 1-slice model for parameters: Miami, high heat gain q=45W/m^2; normal thermal mass specific heat capacity c=880 J/kgK. Resulting day thermal cost = [5.8, 4.0, 4.3, 3.6, 3.4]

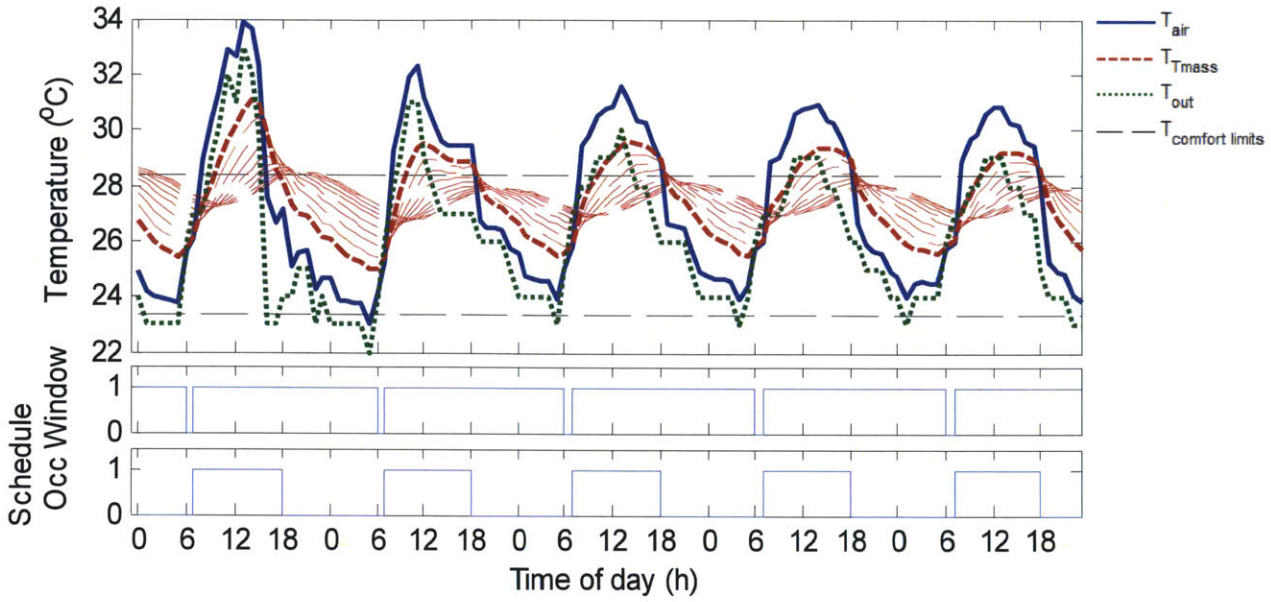

Figure C-14: Optimization results for May 15-19 using global search optimization and 10-slice model for parameters: Miami, high heat gain q=45W/m^2; normal thermal mass specific heat capacity c=880 J/kgK. Resulting day thermal cost = [6.0, 4.2, 4.4, 3.7, 3.5]

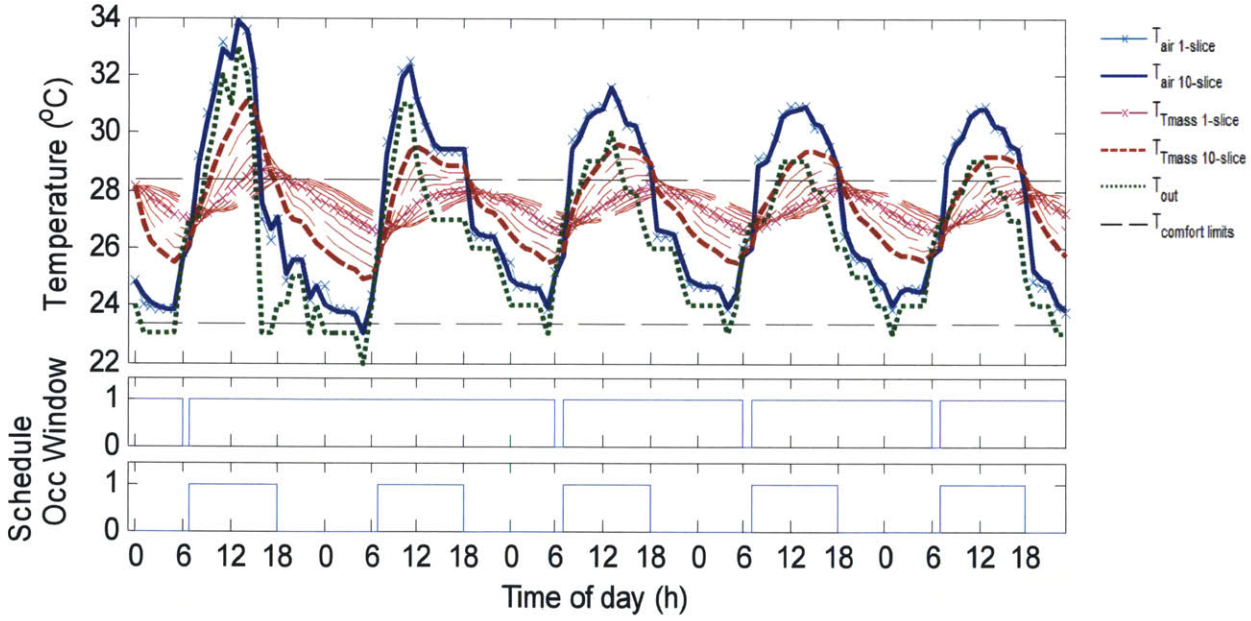

Figure C-15: Testing the effectiveness of effective h with 1-slice model for May 15-19 for parameters: Miami, high heat gain q=45W/m^2; normal thermal mass specific heat capacity c=880 J/kgK.

Parameters: Madison, low heat gain q=15W/m^2; low thermal mass specific heat capacity c=220 J/kgK

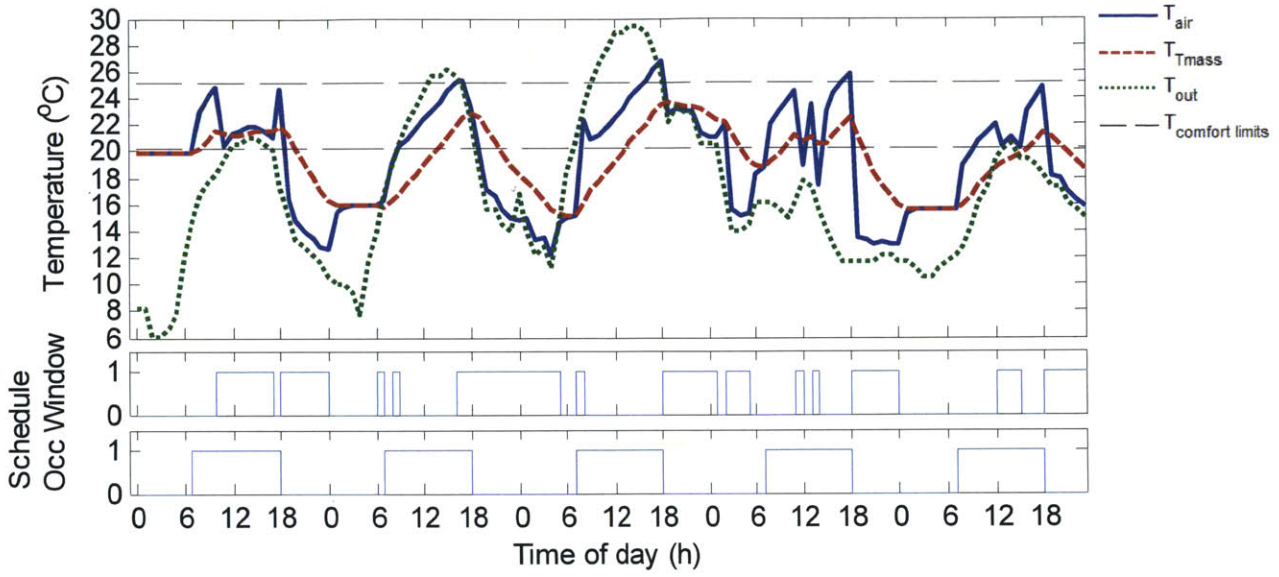

Figure C-16: Optimization results for May 15-19 using dynamic programming and 1-slice model for parameters: Madison, low heat gain q=15W/m^2; low thermal mass specific heat capacity c=220 J/kgK. Resulting day thermal cost = [0, 0.6, 0.7, 0.7, 0.6]

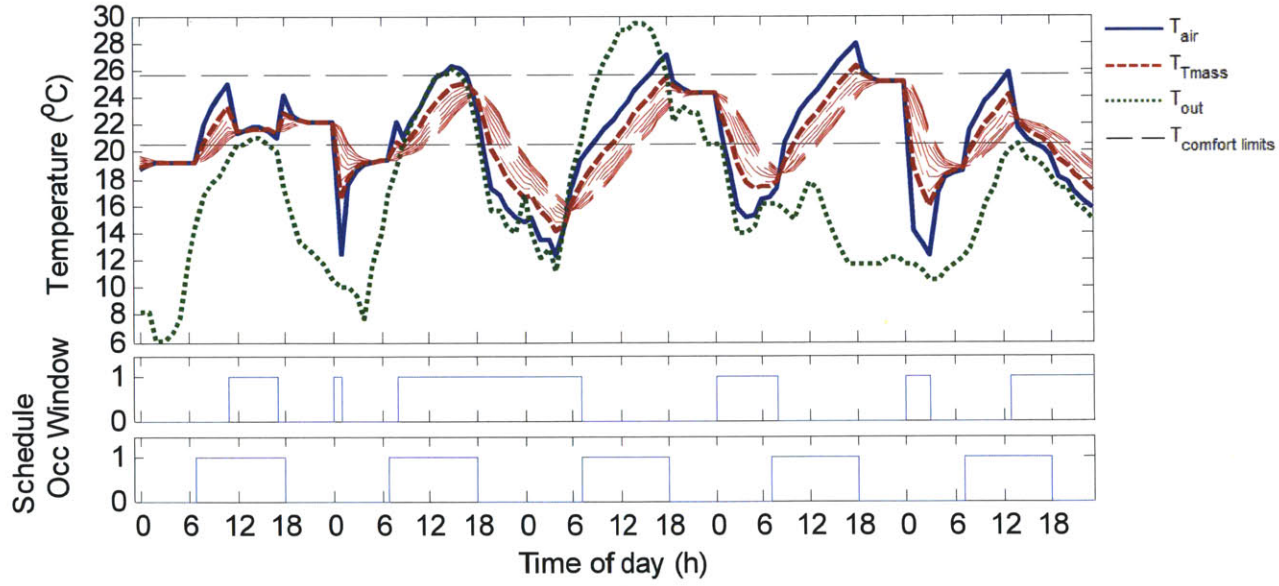

Figure C-17: Optimization results for May 15-19 using global search optimization and 10-slice model for parameters: Madison, low heat gain q=15W/m^2; low thermal mass specific heat capacity c=220 J/kgK. Resulting day thermal cost = [0, 0.3, 0.6, 1.8, 0.3]

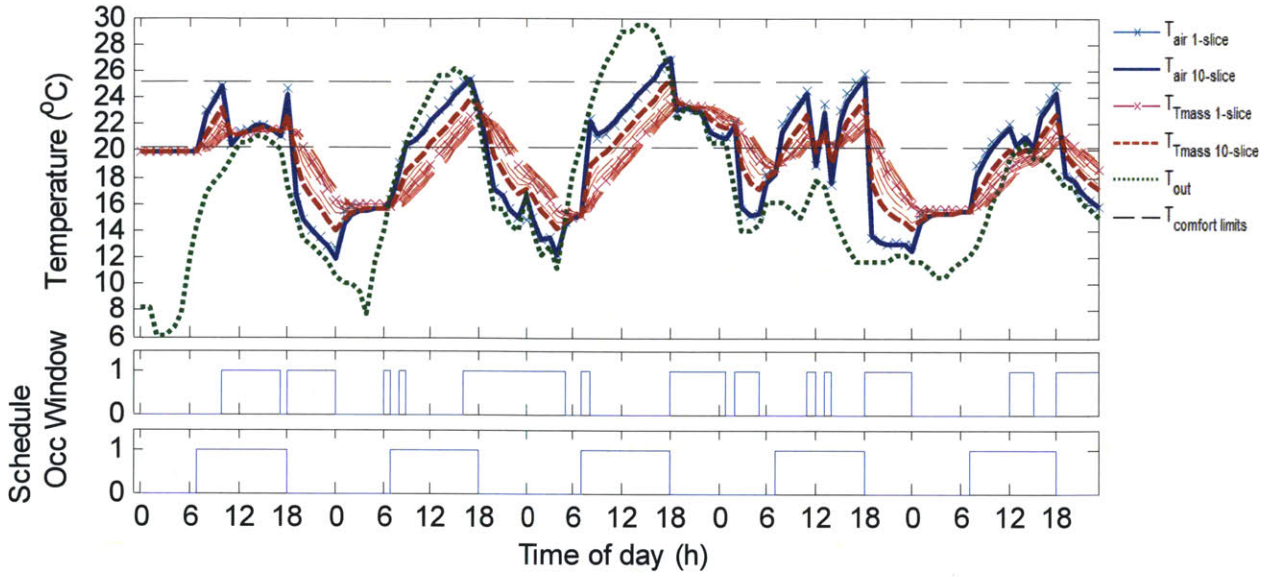

Figure C-18: Testing the effectiveness of effective h with 1-slice model for May 15-19 for parameters: Madison, low heat gain q=15W/m^2; low thermal mass specific heat capacity c=220 J/kgK.

Parameters: Madison, low heat gain q=15W/m^2; normal thermal mass specific heat capacity c=880 J/kgK

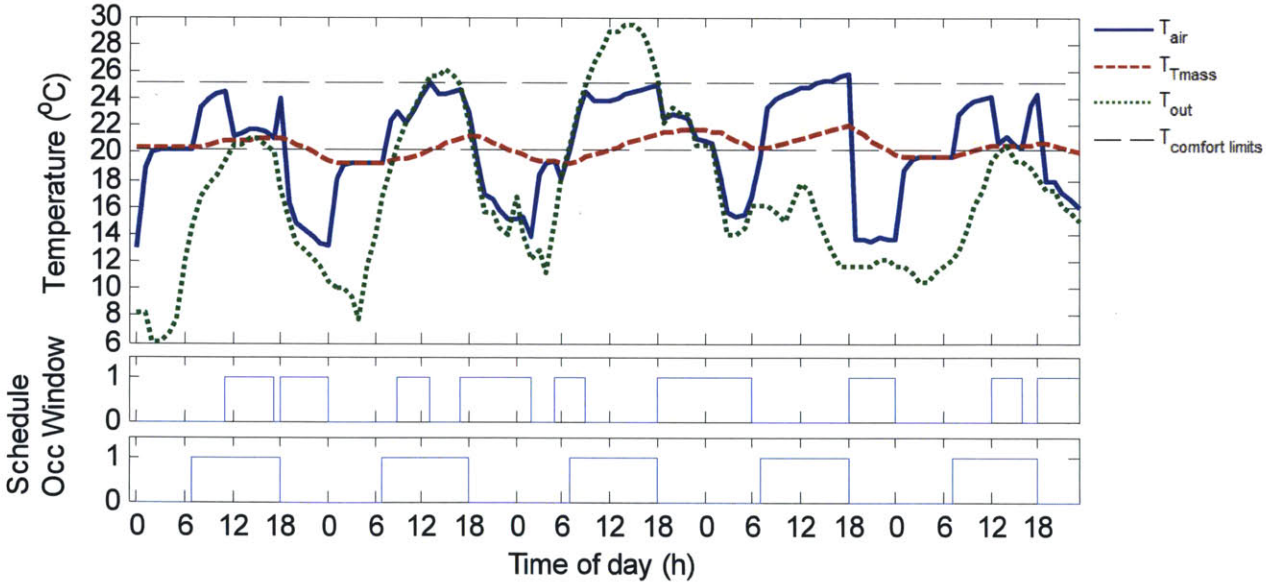

Figure C-19: Optimization results for May 15-19 using dynamic programming and 1-slice model for parameters: Madison, low heat gain q=15W/m^2; normal thermal mass specific heat capacity c=880 J/kgK. Resulting day thermal cost = [0, 0, 0, 0.2, 0]

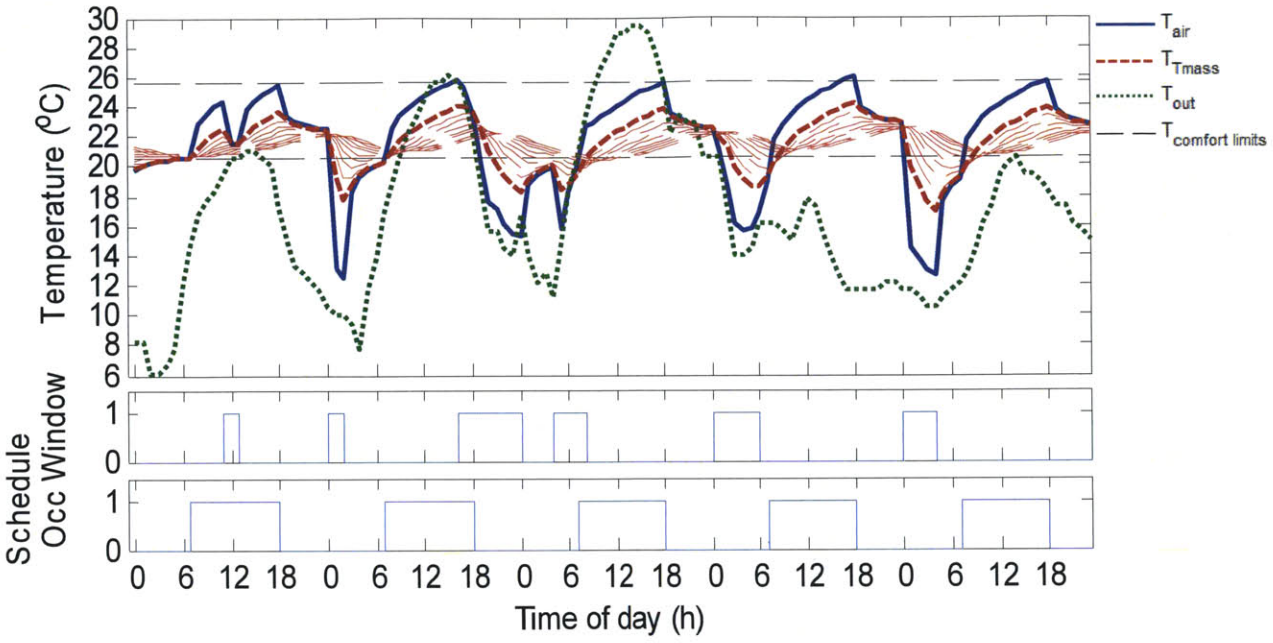

Figure C-20: Optimization results for May 15-19 using global search optimization and 10-slice model for parameters: Madison, low heat gain q=15W/m^2; normal thermal mass specific heat capacity c=880 J/kgK. Resulting day thermal cost = [0, 0, 0, 0.1, 0]

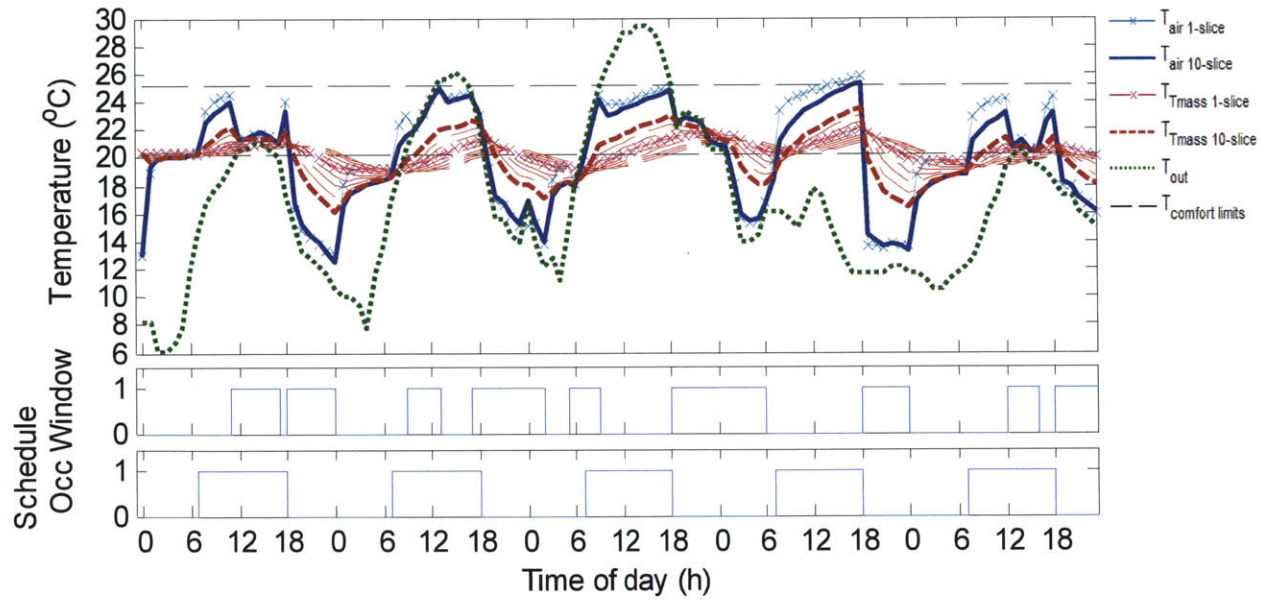

Figure C-21: Testing the effectiveness of effective h with 1-slice model for May 15-19 for parameters: Madison, low heat gain q=15W/m^2; normal thermal mass specific heat capacity c=880 J/kgK.

Parameters: Madison, low heat gain q=15W/m^2; high thermal mass specific heat capacity c=2640 J/kgK

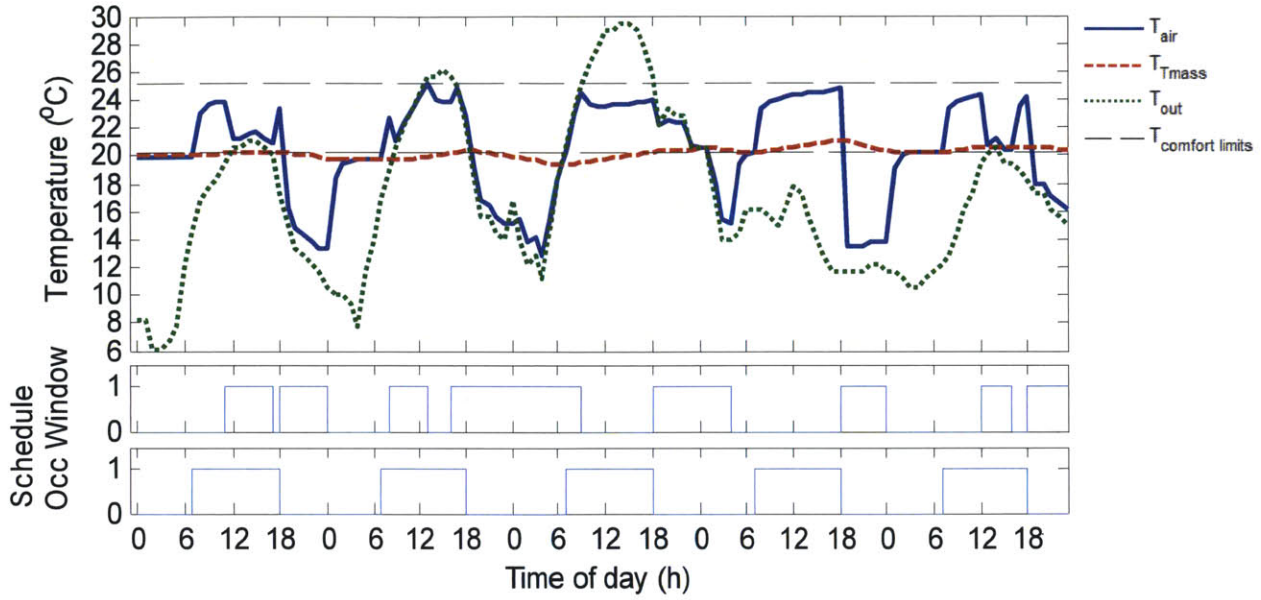

Figure C-22: Optimization results for May 15-19 using dynamic programming and 1-slice model for parameters: Madison, low heat gain q=15W/m^2; high thermal mass specific heat capacity c=2640 J/kgK. Resulting day thermal cost = [0, 0, 0, 0, 0]

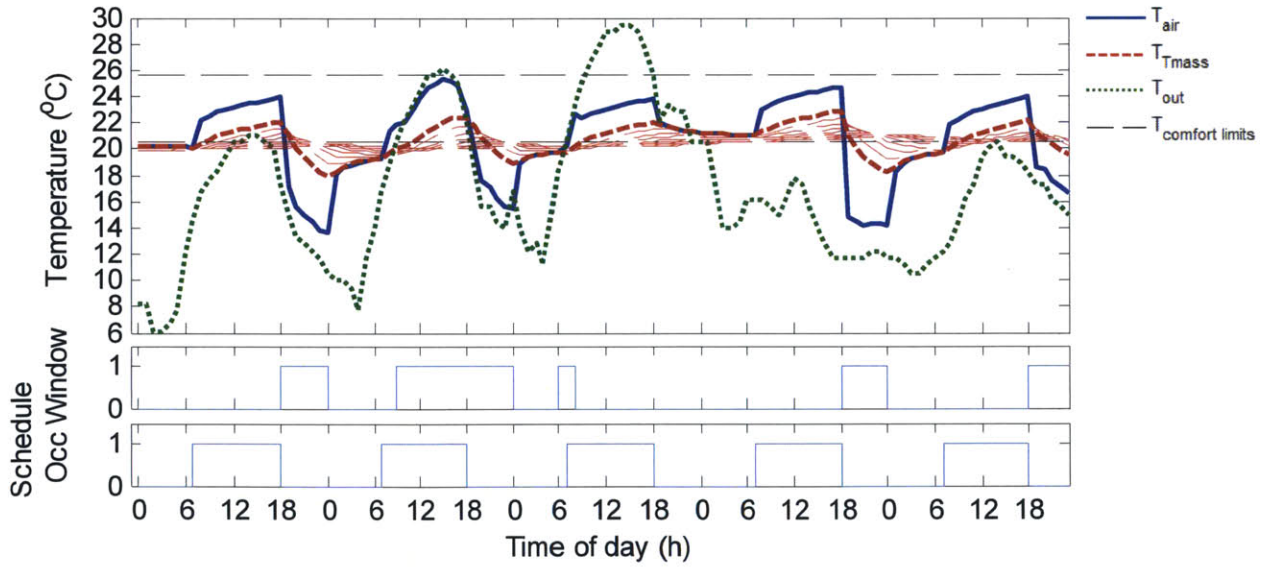

Figure C-23: Optimization results for May 15-19 using global search optimization and 10-slice model for parameters: Madison, low heat gain q=15W/m^2; high thermal mass specific heat capacity c=2640 J/kgK. Resulting day thermal cost = [0, 0, 0, 0, 0]

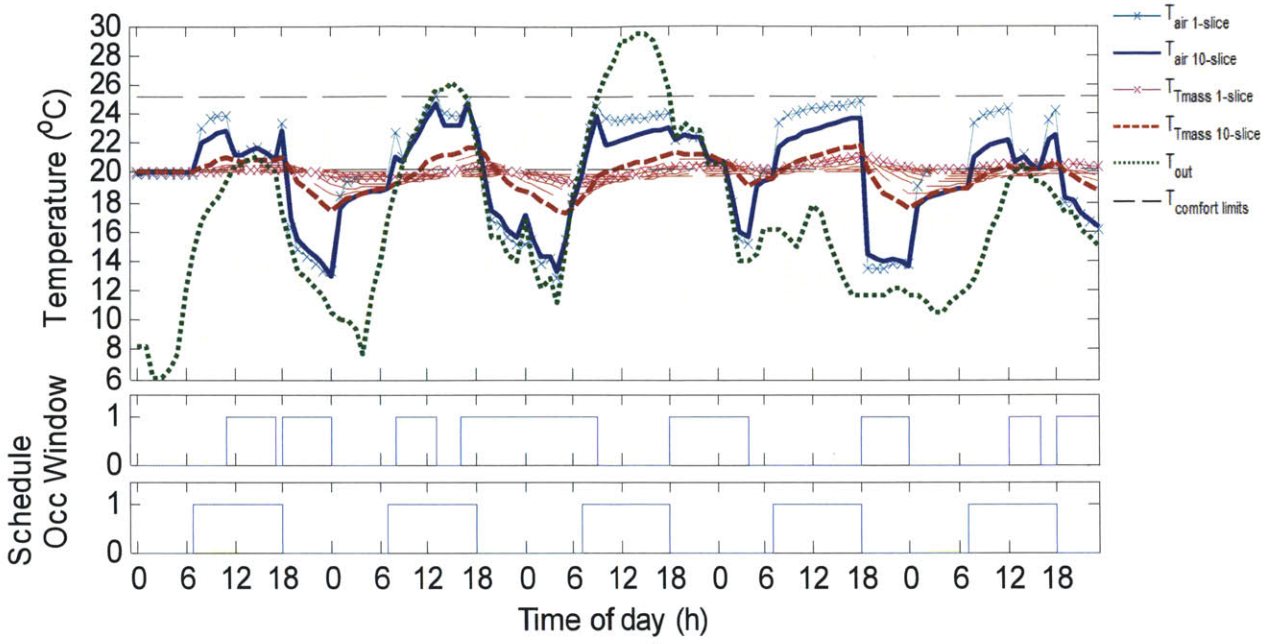

Figure C-24: Testing the effectiveness of effective h with 1-slice model for May 15-19 for parameters: Madison, low heat gain q=15W/m^2; high thermal mass specific heat capacity c=2640 J/kgK.

Parameters: Madison, medium heat gain q=30W/m^2; normal thermal mass specific heat capacity c=880 J/kgK

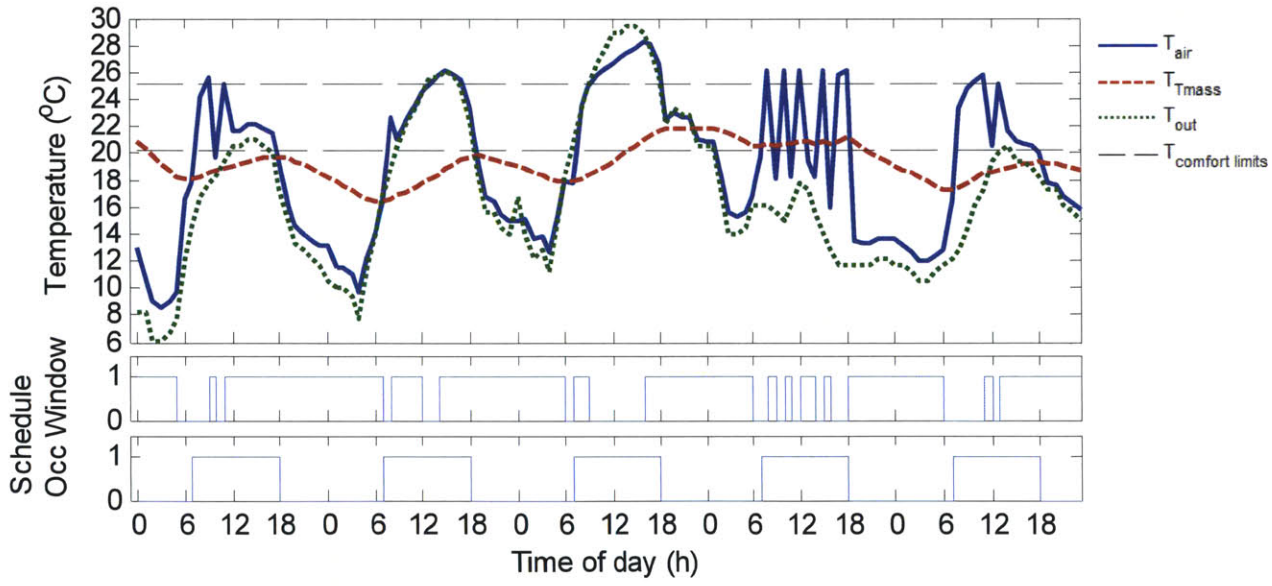

Figure C-25: Optimization results for May 15-19 using dynamic programming and 1-slice model for parameters: Madison, medium heat gain q=30W/m^2; normal thermal mass specific heat capacity c=880 J/kgK. Resulting day thermal cost = [0.2, 0.6, 5.8, 2.8, 0.3]

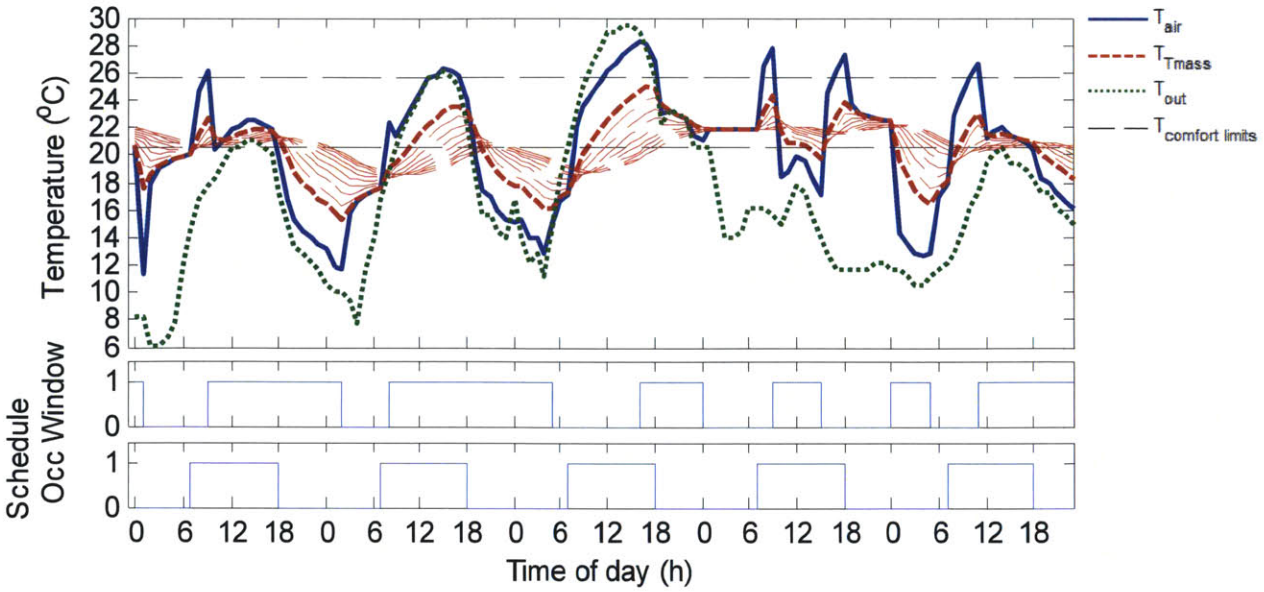

Figure C-26: Optimization results for May 15-19 using global search optimization and 10-slice model for parameters: Madison, medium heat gain q=30W/m^2; normal thermal mass specific heat capacity c=880 J/kgK. Resulting day thermal cost = [0.1, 0.5, 2.5, 2.6, 0.2]

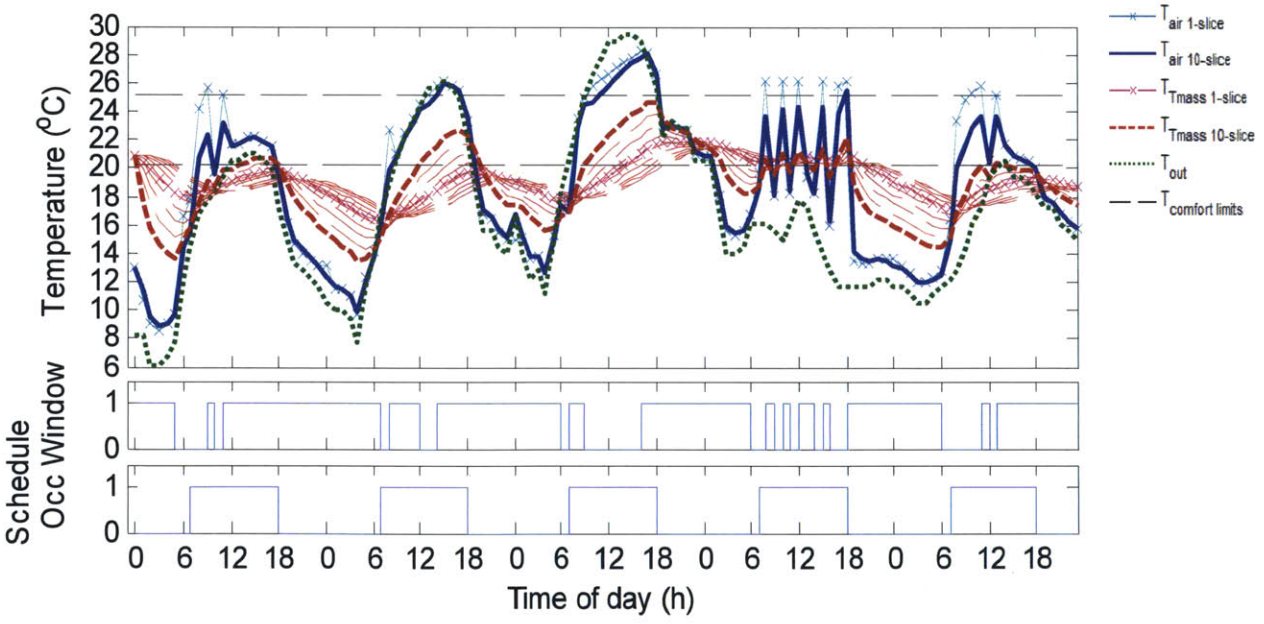

Figure C-27: Testing the effectiveness of effective h with 1-slice model for May 15-19 for parameters: Madison, medium heat gain q=30W/m^2; normal thermal mass specific heat capacity c=880 J/kgK.

Parameters: Madison, high heat gain q=45W/m^2; normal thermal mass specific heat capacity c=880 J/kgK

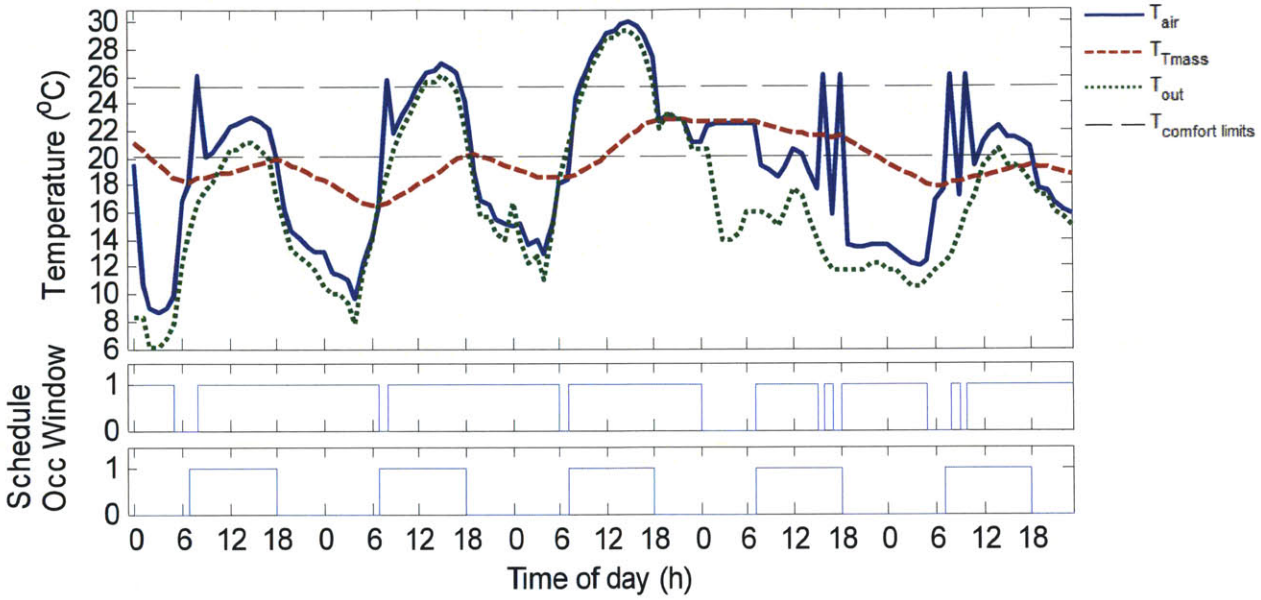

Figure C-28: Optimization results for May 15-19 using dynamic programming and 1-slice model for parameters: Madison, high heat gain q=45W/m^2; normal thermal mass specific heat capacity c=880 J/kgK. Resulting day thermal cost = [0.2, 0.7, 3.4, 2.3, 0.3]

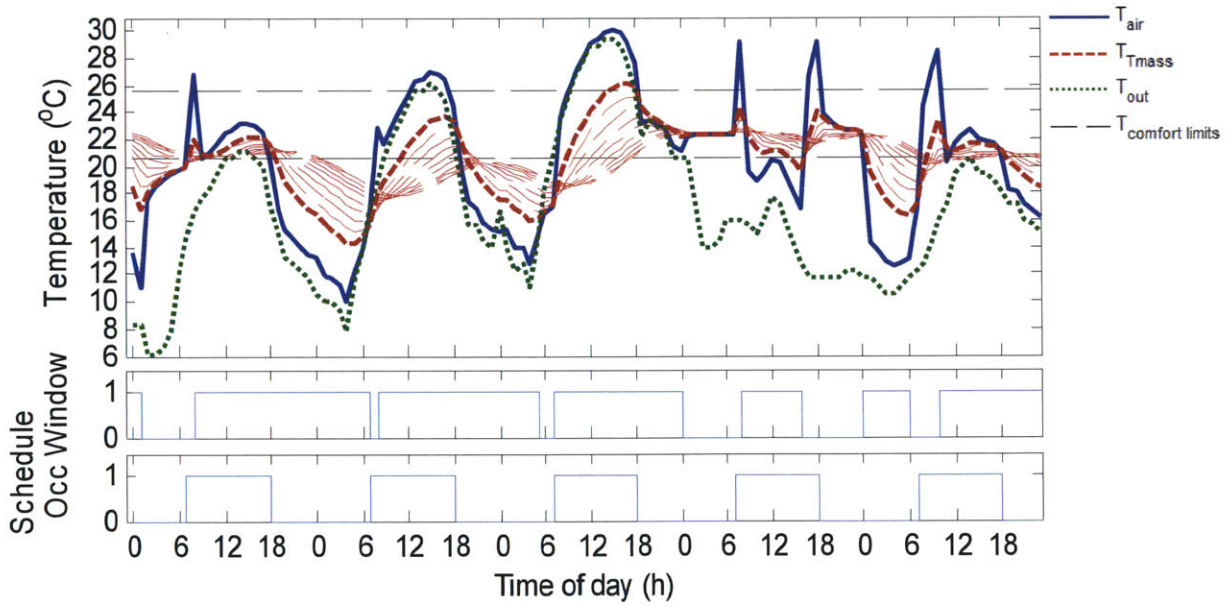

Figure C-29: Optimization results for May 15-19 using global search optimization and 10-slice model for parameters: Madison, high heat gain q=45W/m^2; normal thermal mass specific heat capacity c=880 J/kgK. Resulting day thermal cost = [0.1, 1.1, 5.8, 2.9, 0.7]

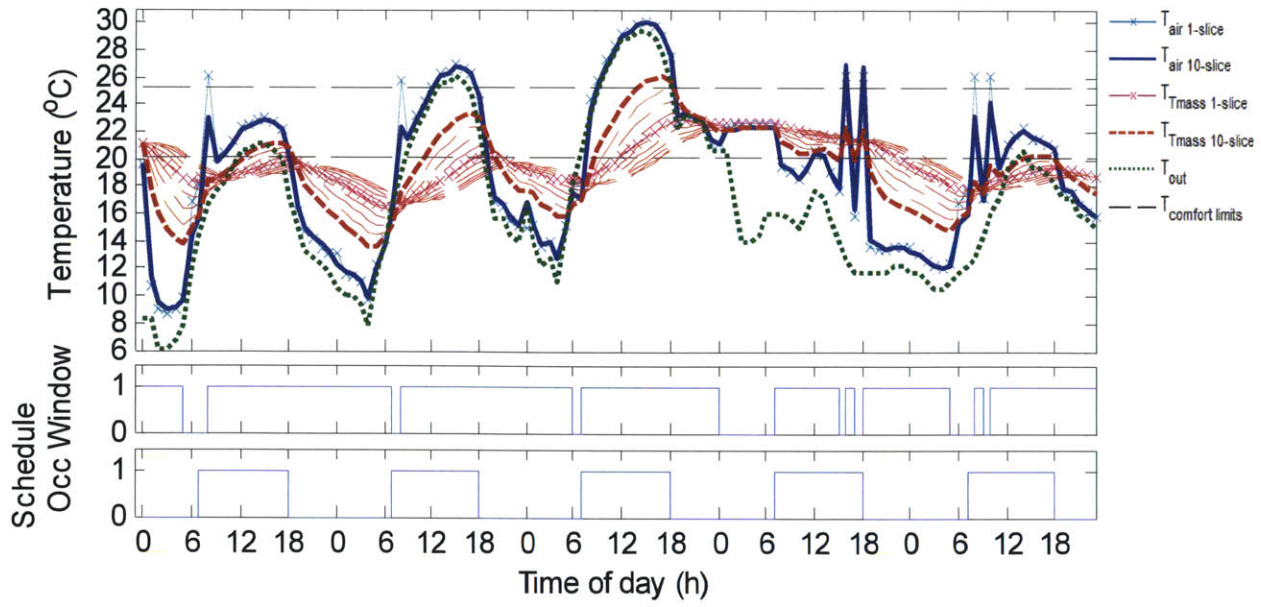

Figure C-30: Testing the effectiveness of effective h with 1-slice model for May 15-19 for parameters: Madison, high heat gain q=45W/m^2; normal thermal mass specific heat capacity c=880 J/kgK.

Parameters: Los Angeles, low heat gain q=15W/m^2; low thermal mass specific heat capacity c=220 J/kgK

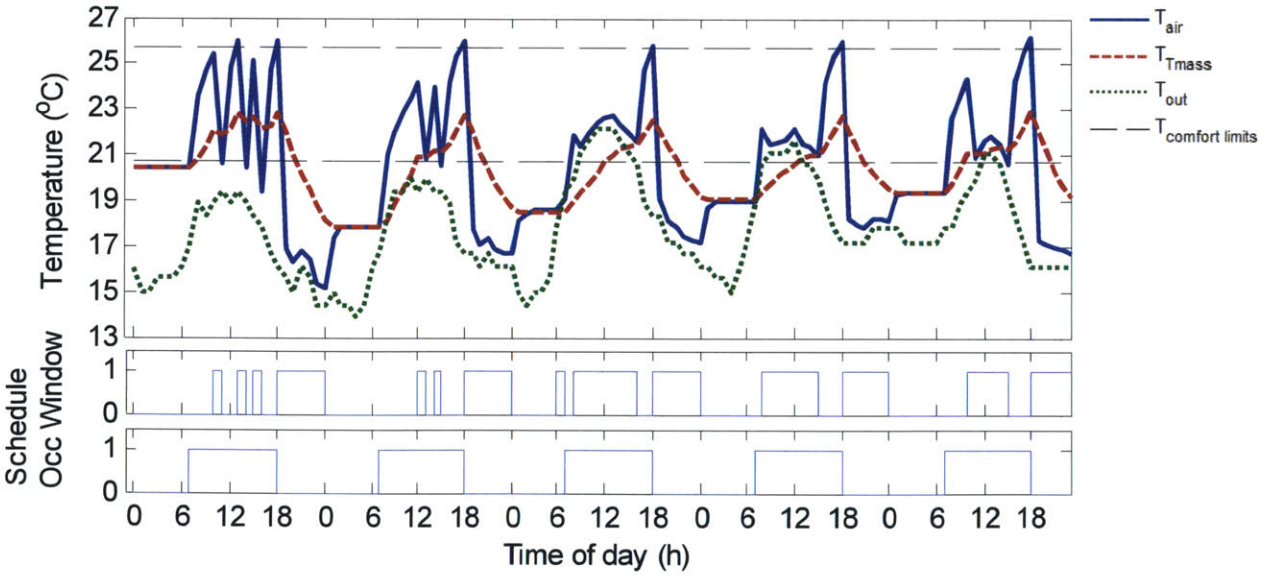

Figure C-31: Optimization results for May 15-19 using dynamic programming and 1-slice model for parameters: Los Angeles, low heat gain q=15W/m^2; low thermal mass specific heat capacity c=220 J/kgK. Resulting day thermal cost = [0.3, 0.3, 0.1, 0.1, 0.1]

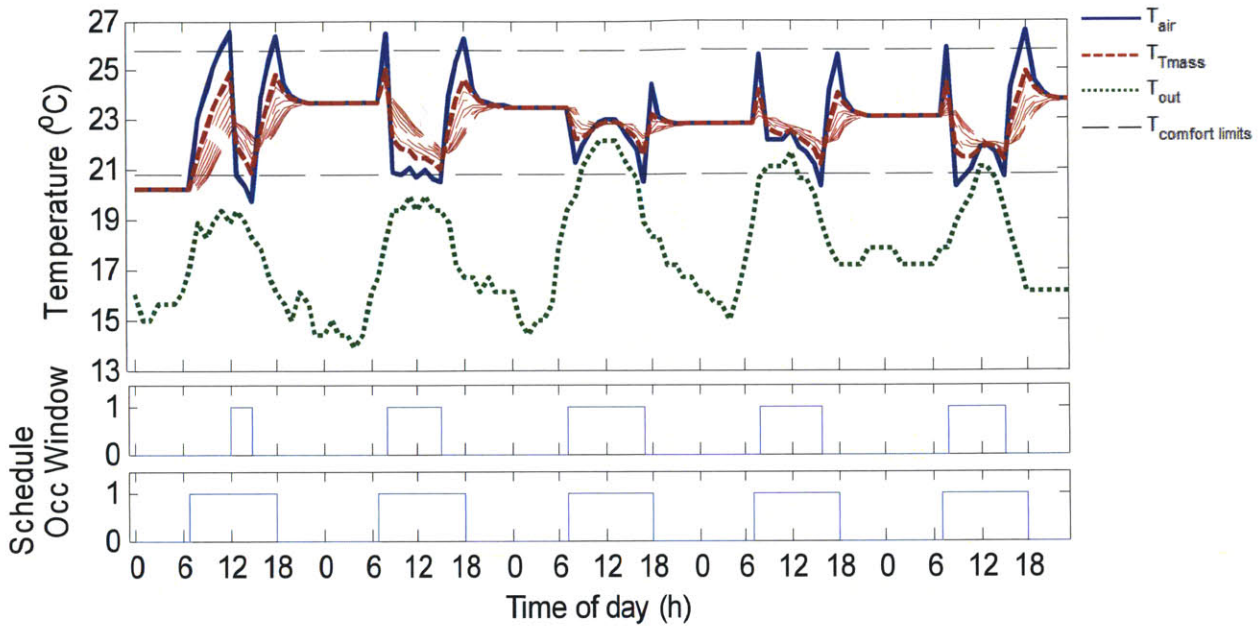

Figure C-32: Optimization results for May 15-19 using global search optimization and 10-slice model for parameters: Los Angeles, low heat gain q=15W/m^2; low thermal mass specific heat capacity c=220 J/kgK. Resulting day thermal cost = [0.3, 0.1, 0, 0, 0.2]

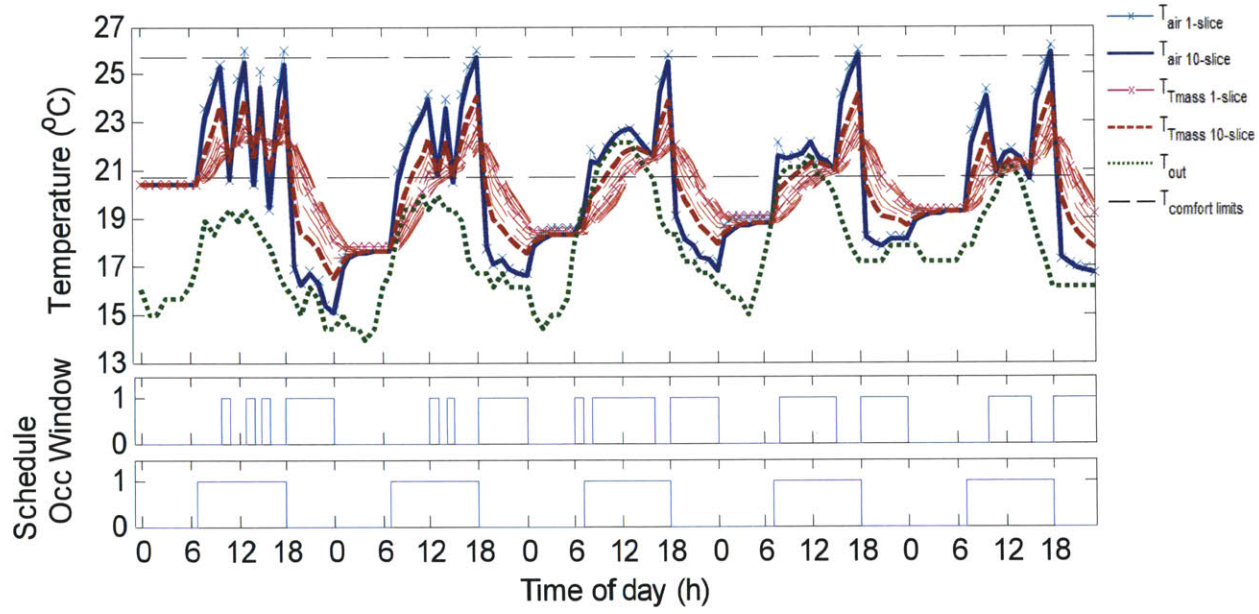

Figure C-33: Testing the effectiveness of effective h with 1-slice model for May 15-19 for parameters: Los Angeles, low heat gain q=15W/m^2; low thermal mass specific heat capacity c=220 J/kgK.

Parameters: Los Angeles, low heat gain q=15W/m^2; normal thermal mass specific heat capacity c=880 J/kgK

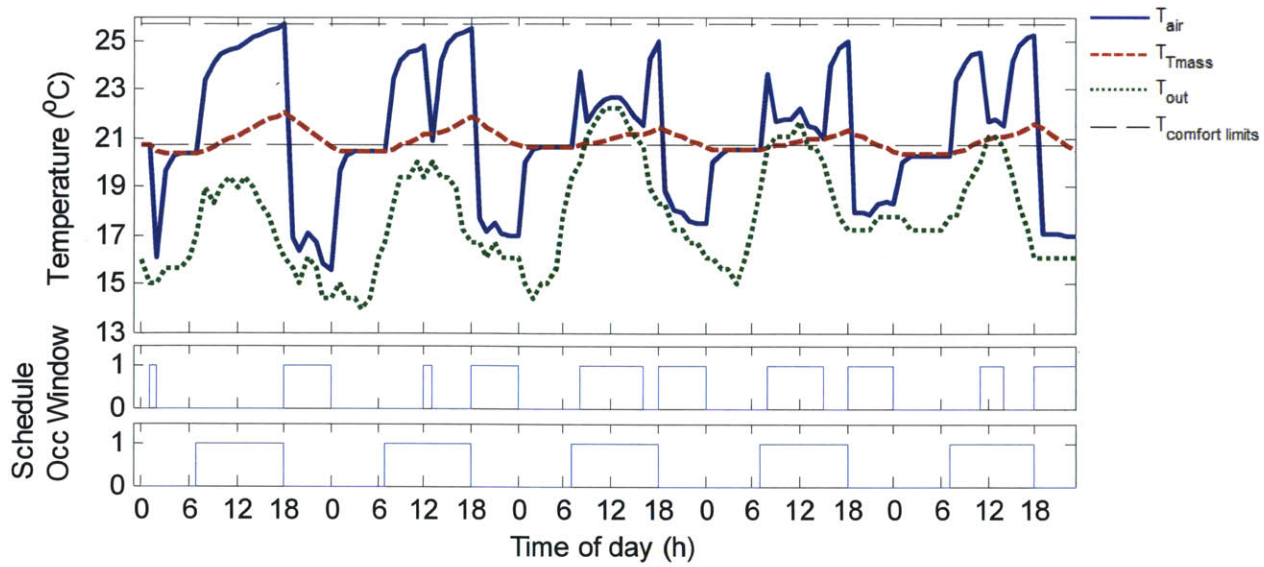

Figure C-34: Optimization results for May 15-19 using dynamic programming and 1-slice model for parameters: Los Angeles, low heat gain q=15W/m^2; normal thermal mass specific heat capacity c=880 J/kgK. Resulting day thermal cost = [0, 0, 0, 0, 0]

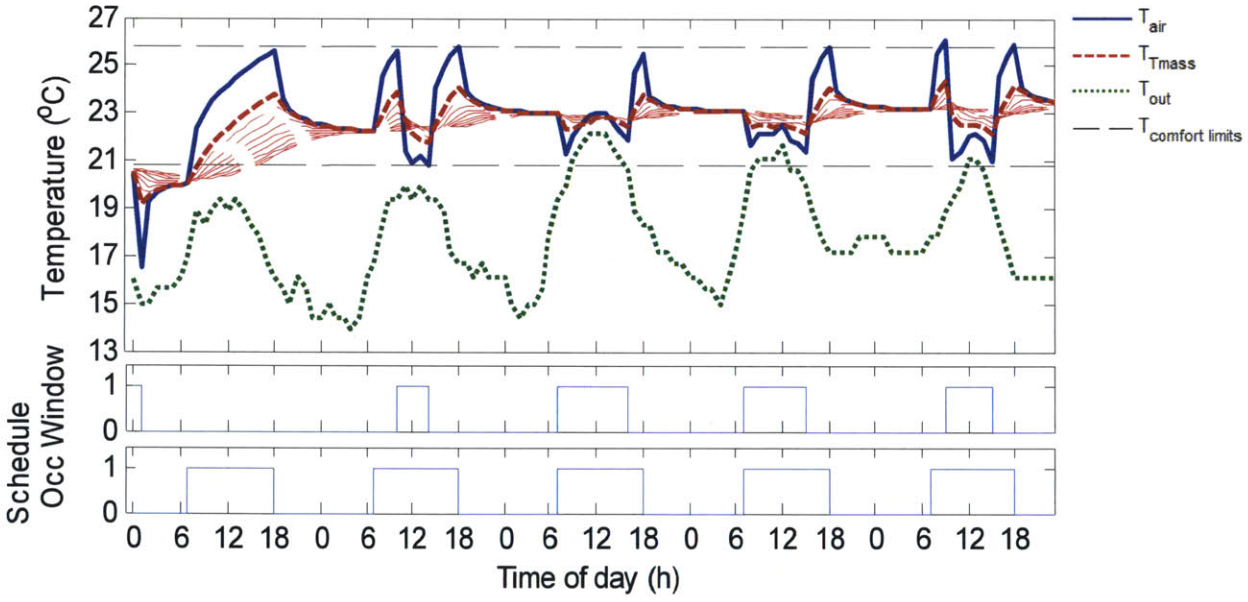

Figure C-35: Optimization results for May 15-19 using global search optimization and 10-slice model for parameters: Los Angeles, low heat gain q=15W/m^2; normal thermal mass specific heat capacity c=880 J/kgK. Resulting day thermal cost = [0, 0, 0, 0, 0]

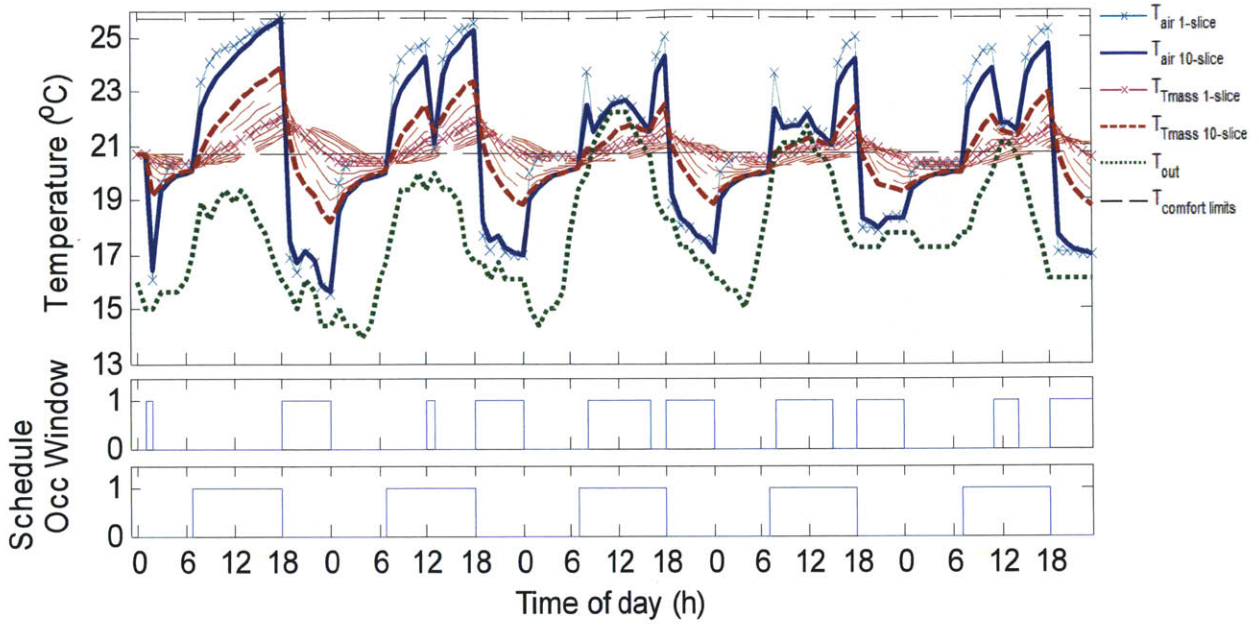

Figure C-36: Testing the effectiveness of effective h with 1-slice model for May 15-19 for parameters: Los Angeles, low heat gain q=15W/m^2; normal thermal mass specific heat capacity c=880 J/kgK.

<u>Parameters: Los Angeles, low heat gain q=15W/m^2;high thermal mass specific heat capacity c=2640 J/kgK</u>

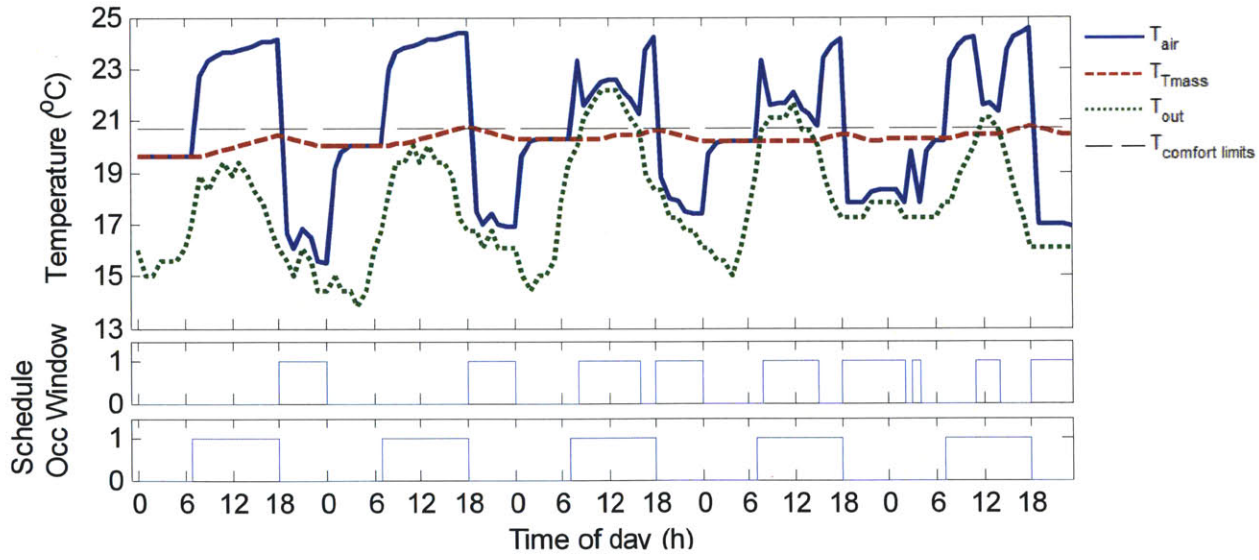

Figure C-37: Optimization results for May 15-19 using dynamic programming and 1-slice model for parameters: Los Angeles, low heat gain q=15W/m^2;high thermal mass specific heat capacity c=2640 J/kgK. Resulting day thermal cost = [0, 0, 0, 0, 0]

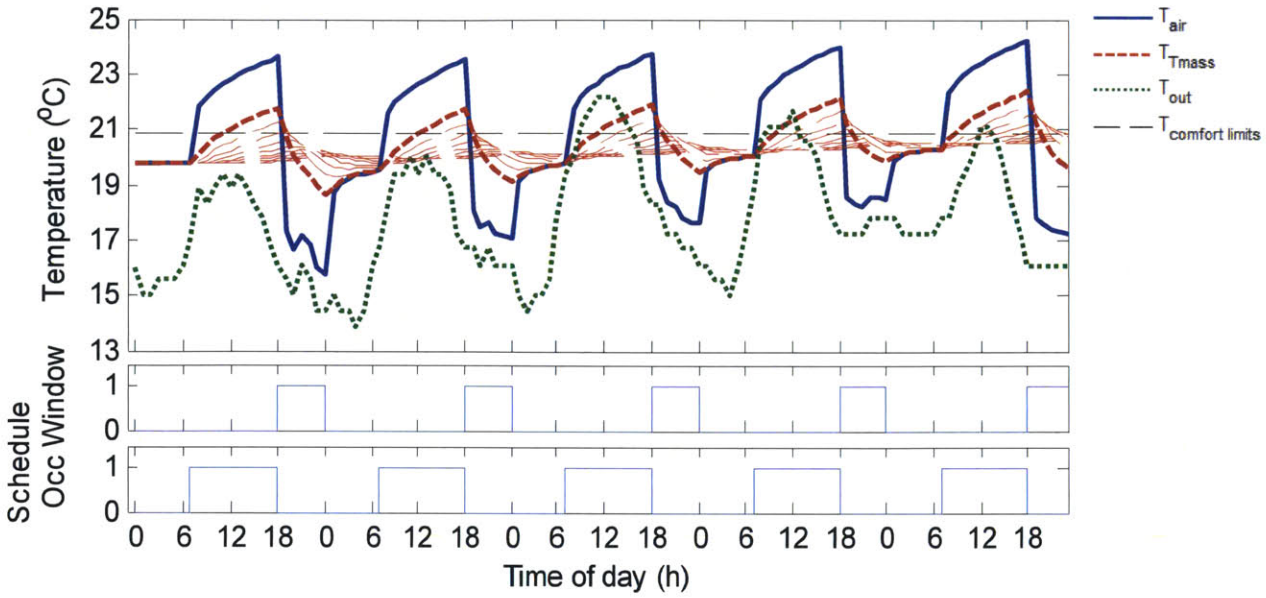

Figure C-38: Optimization results for May 15-19 using global search optimization and 10-slice model for parameters: Los Angeles, low heat gain q=15W/m^2;high thermal mass specific heat capacity c=2640 J/kgK. Resulting day thermal cost = [0, 0, 0, 0, 0]

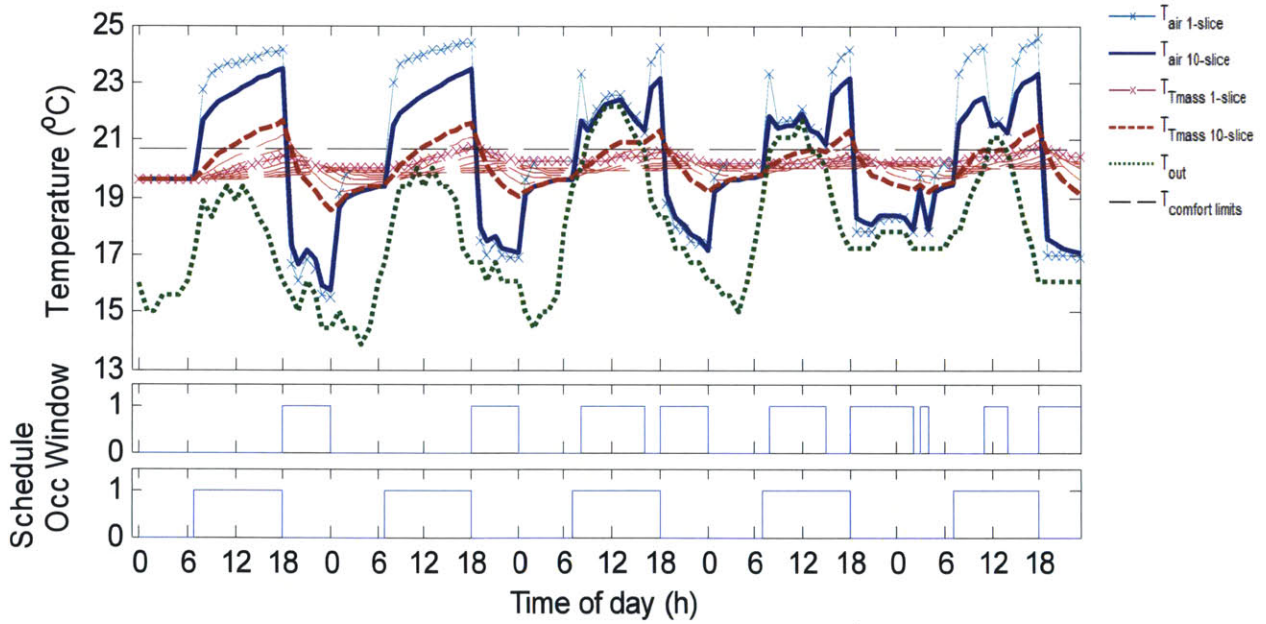

Figure C-39: Testing the effectiveness of effective h with 1-slice model for May 15-19 for parameters: Los Angeles, low heat gain q=15W/m^2;high thermal mass specific heat capacity c=2640 J/kgK.

Parameters: Los Angeles, medium heat gain q=30W/m^2;normal thermal mass specific heat capacity c=880 J/kgK

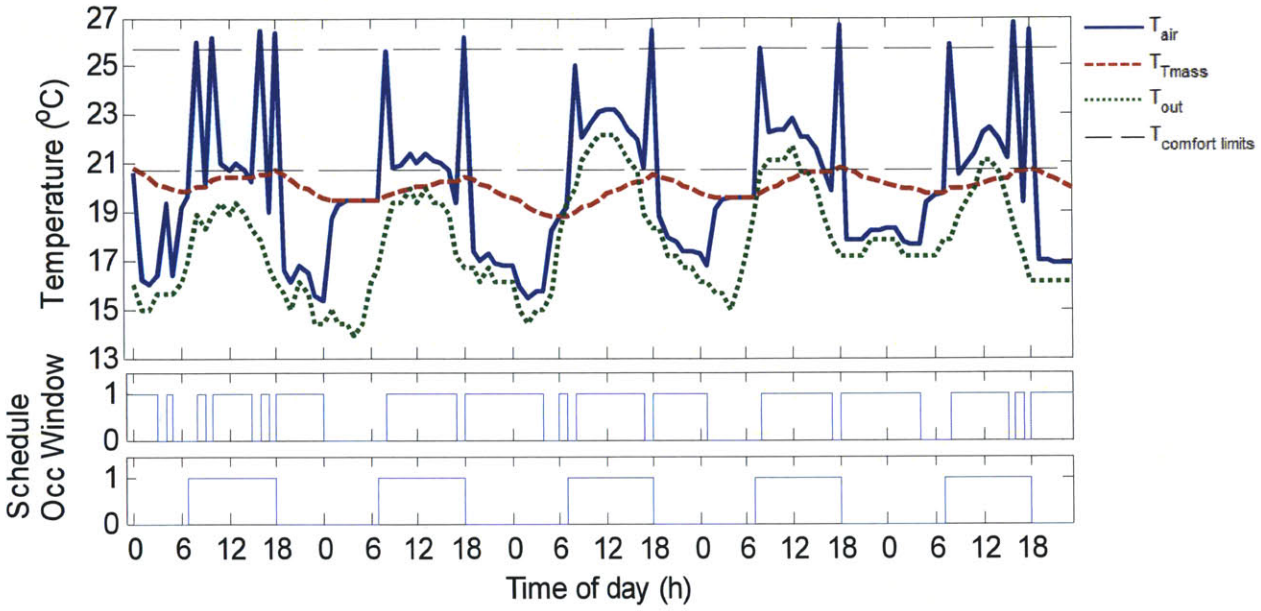

Figure C-40: Optimization results for May 15-19 using dynamic programming and 1-slice model for parameters: Los Angeles, medium heat gain q=30W/m^2;normal thermal mass specific heat capacity c=880 J/kgK. Resulting day thermal cost = [0.4, 0.2, 0, 0.1, 0.3]

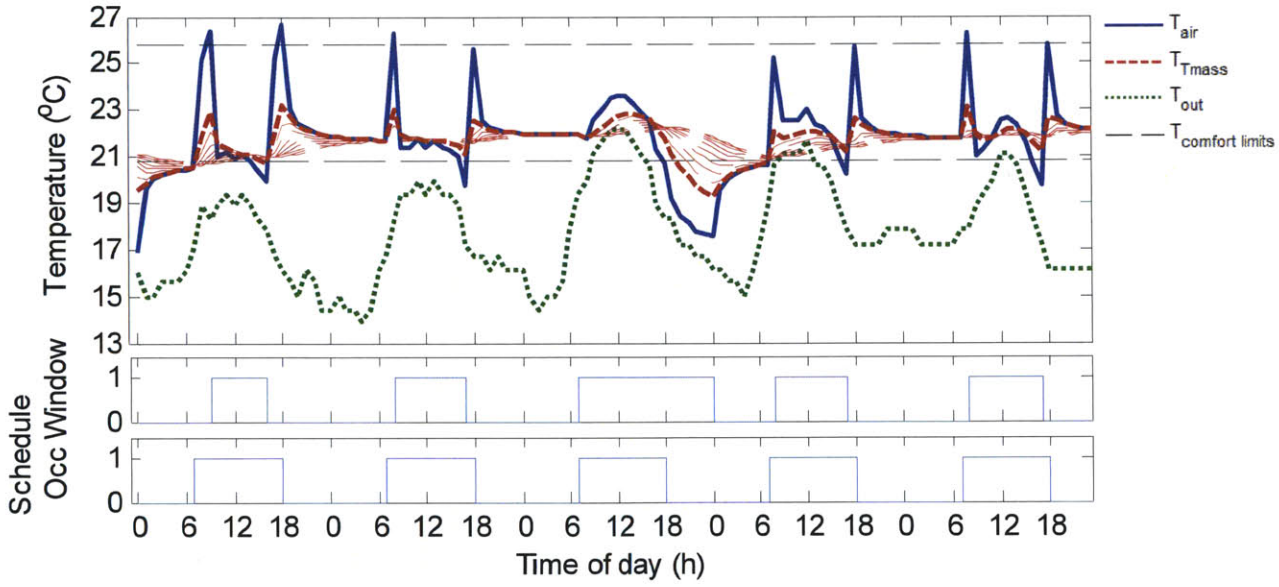

Figure C-41: Optimization results for May 15-19 using global search optimization and 10-slice model for parameters: Los Angeles, medium heat gain q=30W/m^2;normal thermal mass specific heat capacity c=880 J/kgK. Resulting day thermal cost = [0.3, 0.1, 0, 0, 0.1]

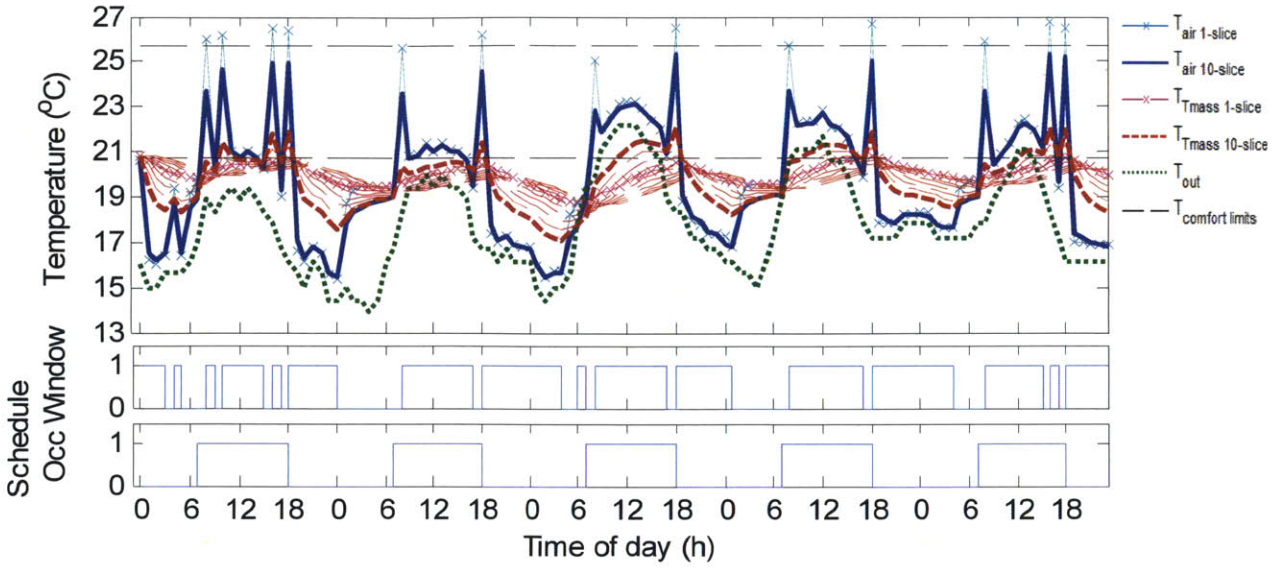

Figure C-42: Testing the effectiveness of effective h with 1-slice model for May 15-19 for parameters: Los Angeles, medium heat gain q=30W/m^2;normal thermal mass specific heat capacity c=880 J/kgK.

Parameters: Los Angeles, high heat gain q=45W/m^2;normal thermal mass specific heat capacity c=880 J/kgK

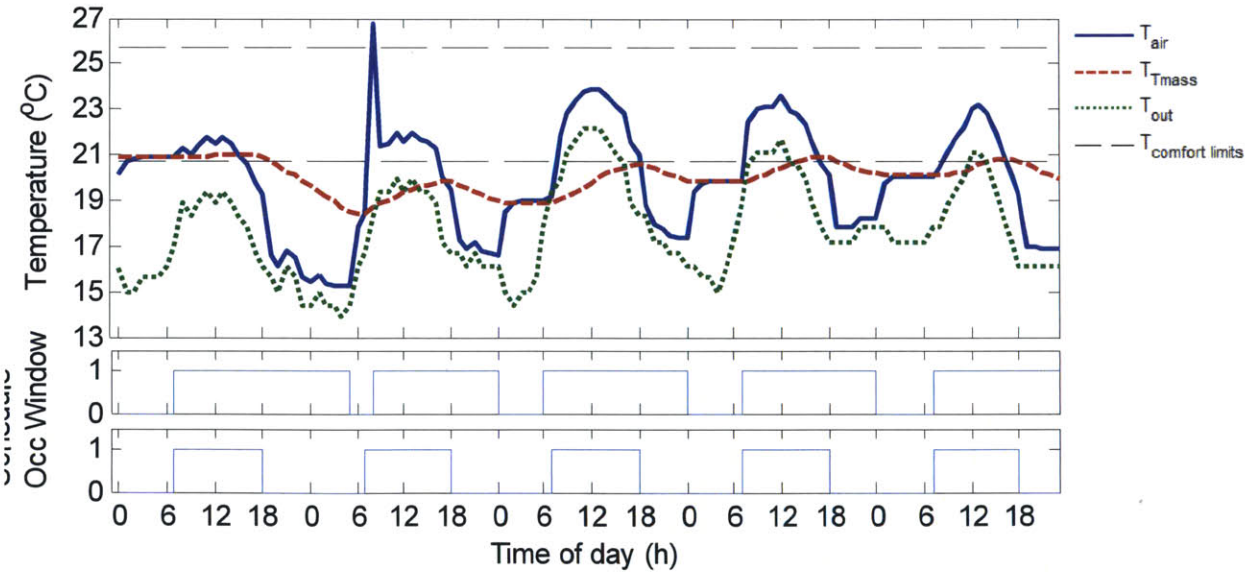

Figure C-43: Optimization results for May 15-19 using dynamic programming and 1-slice model for parameters: Los Angeles, high heat gain q=45W/m^2;normal thermal mass specific heat capacity c=880 J/kgK. Resulting day thermal cost = [0.4, 0.4, 0, 0.1, 0.3]

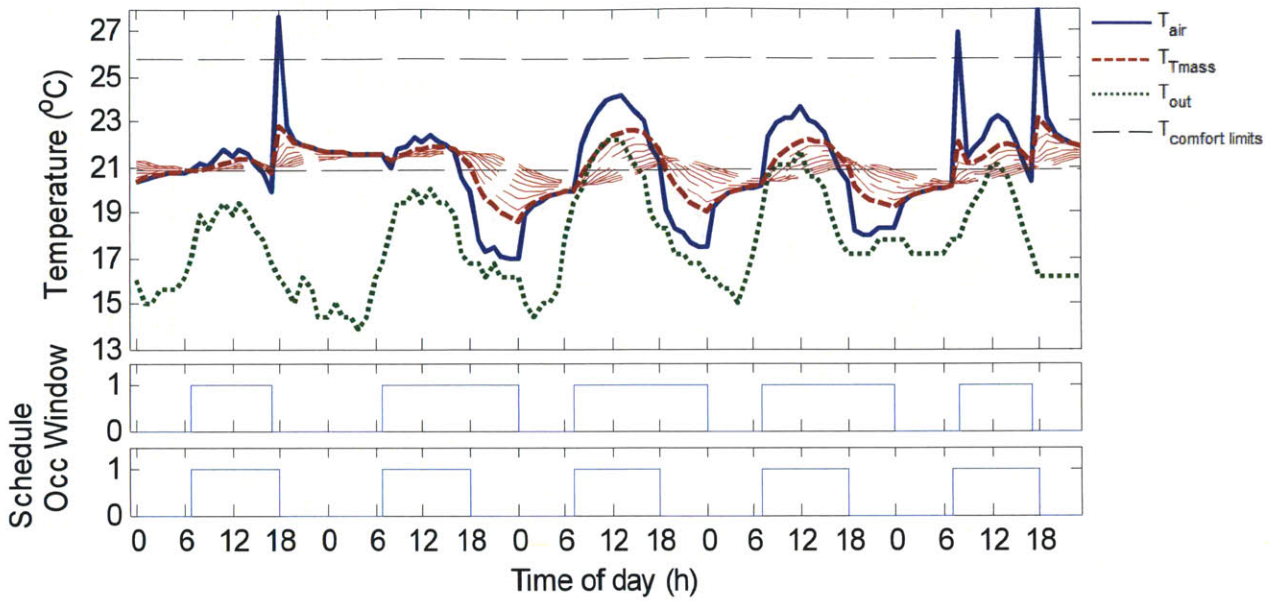

Figure C-44: Optimization results for May 15-19 using global search optimization and 10-slice model for parameters: Los Angeles, high heat gain q=45W/m^2; normal thermal mass specific heat capacity c=880 J/kgK. Resulting day thermal cost = [0.2, 0.2, 0.1, 0, 0.2]

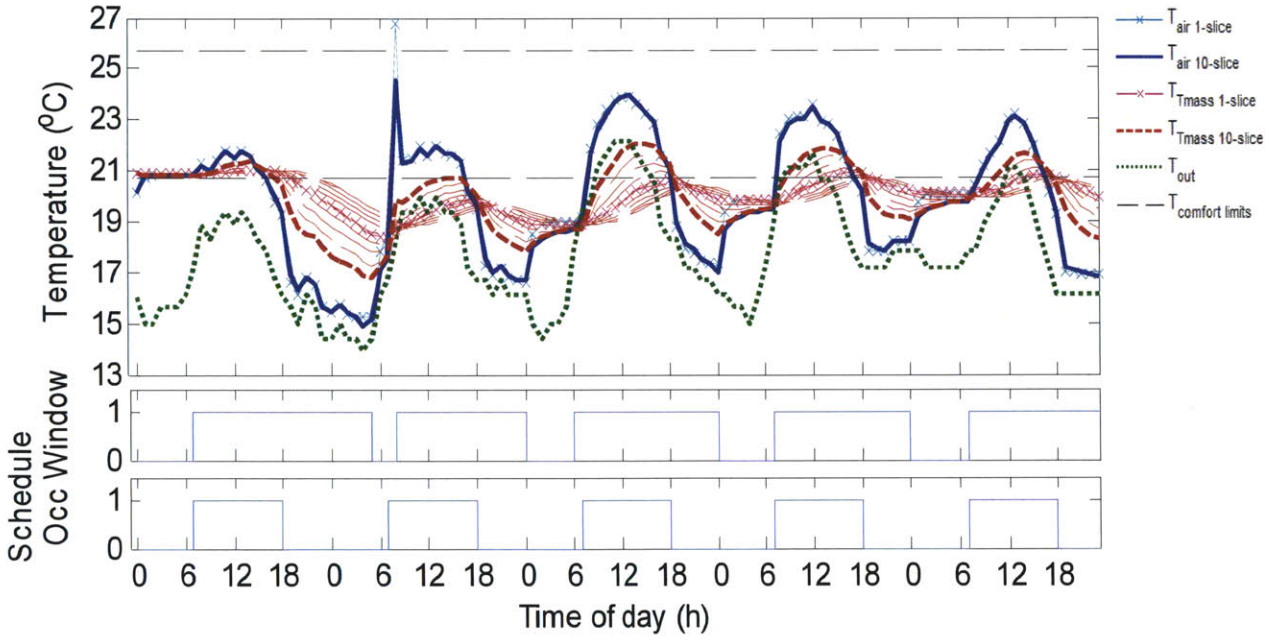

Figure C-45: Testing the effectiveness of effective h with 1-slice model for May 15-19 for parameters: Los Angeles, high heat gain q=45W/m^2; normal thermal mass specific heat capacity c=880 J/kgK.

Parameters: Kansas, low heat gain q=15W/m^2;low thermal mass specific heat capacity c=220 J/kgK

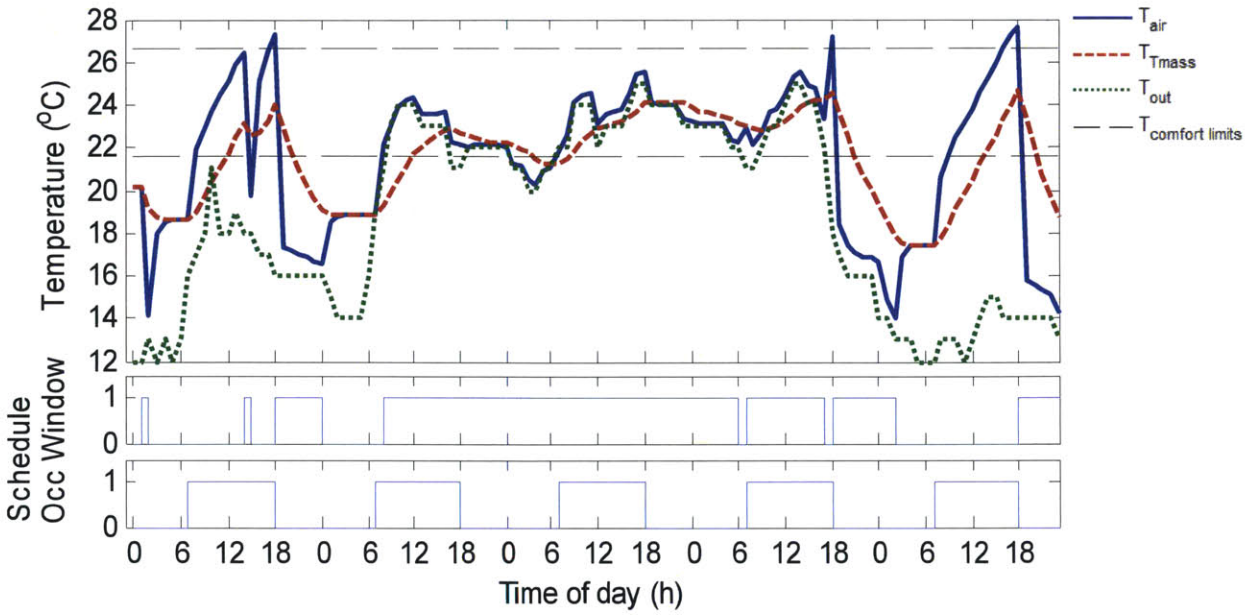

Figure C-46: Optimization results for May 15-19 using dynamic programming and 1-slice model for parameters: Kansas, low heat gain q=15W/m^2; low thermal mass specific heat capacity c=220 J/kgK. Resulting day thermal cost = [0.6, 0.2, 0, 0, 0.8]

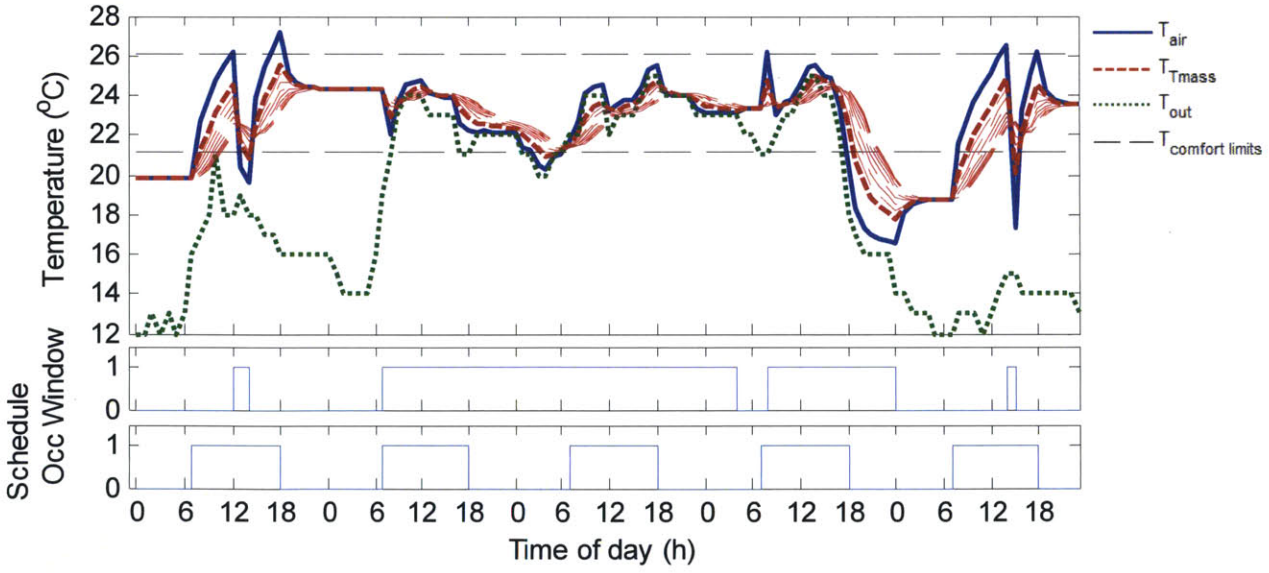

Figure C-47: Optimization results for May 15-19 using global search optimization and 10-slice model for parameters: Kansas, low heat gain q=15W/m^2;low thermal mass specific heat capacity c=220 J/kgK. Resulting day thermal cost = [0.5, 0, 0, 0, 0.8]

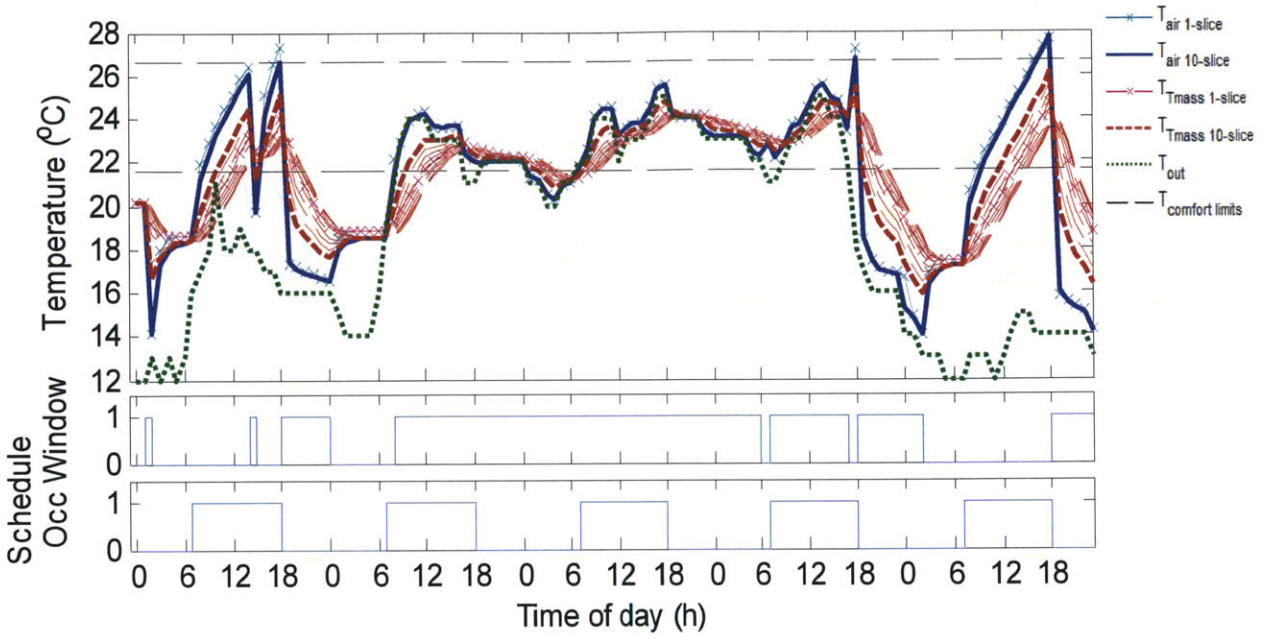

Figure C-48: Testing the effectiveness of effective h with 1-slice model for May 15-19 for parameters: Kansas, low heat gain q=15W/m^2;low thermal mass specific heat capacity c=220 J/kgK.

Parameters: Kansas, low heat gain q=15W/m^2;normal thermal mass specific heat capacity c=880 J/kgK

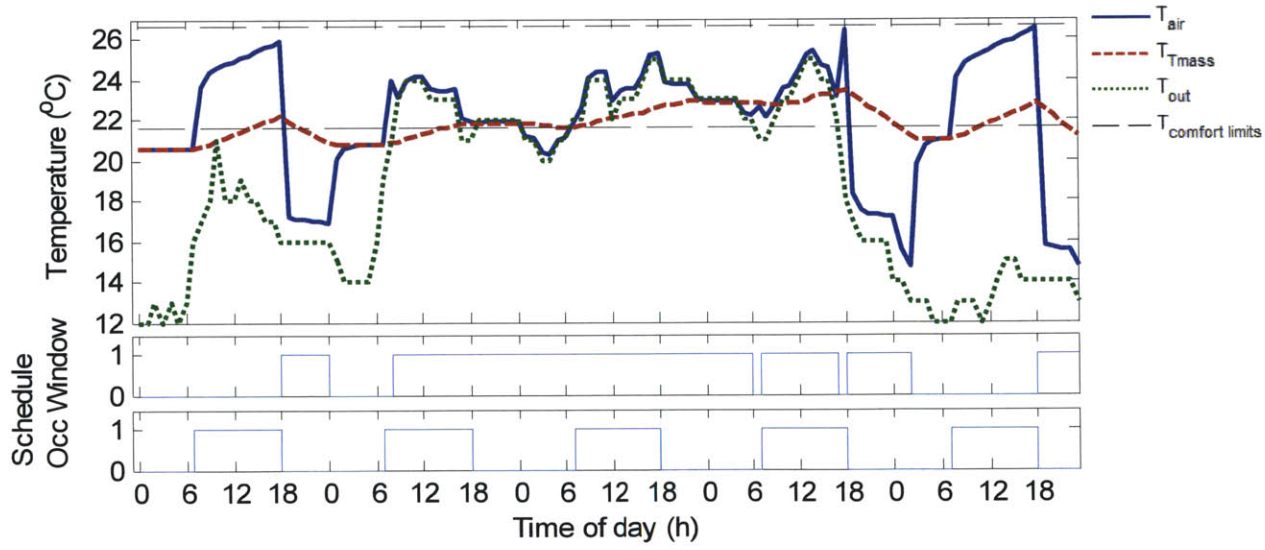

Figure C-49: Optimization results for May 15-19 using dynamic programming and 1-slice model for parameters: Kansas, low heat gain q=15W/m^2; normal thermal mass specific heat capacity c=880 J/kgK. Resulting day thermal cost = [0, 0, 0, 0, 0]

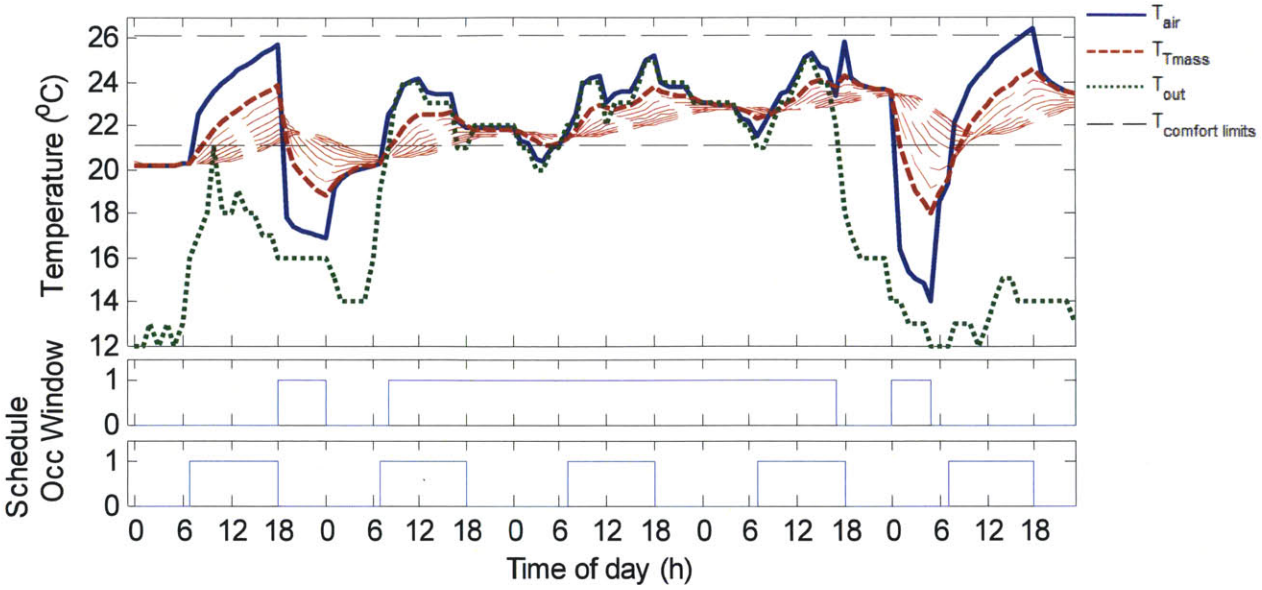

Figure C-50: Optimization results for May 15-19 using global search optimization and 10-slice model for parameters: Kansas, low heat gain q=15W/m^2; normal thermal mass specific heat capacity c=880 J/kgK. Resulting day thermal cost = [0, 0 ,0, 0, 0,1]

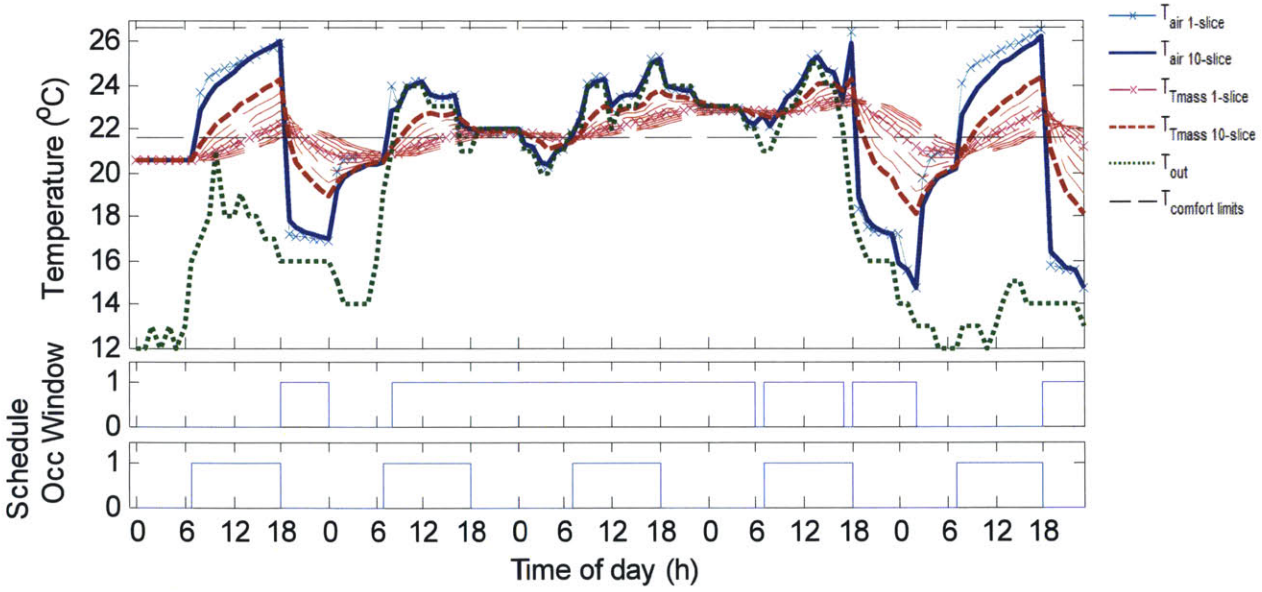

Figure C-51: Testing the effectiveness of effective h with 1-slice model for May 15-19 for Parameters: Kansas, low heat gain q=15W/m^2;normal thermal mass specific heat capacity c=880 J/kgK.

Parameters: Kansas, low heat gain q=15W/m^2;high thermal mass specific heat capacity c=2640 J/kgK

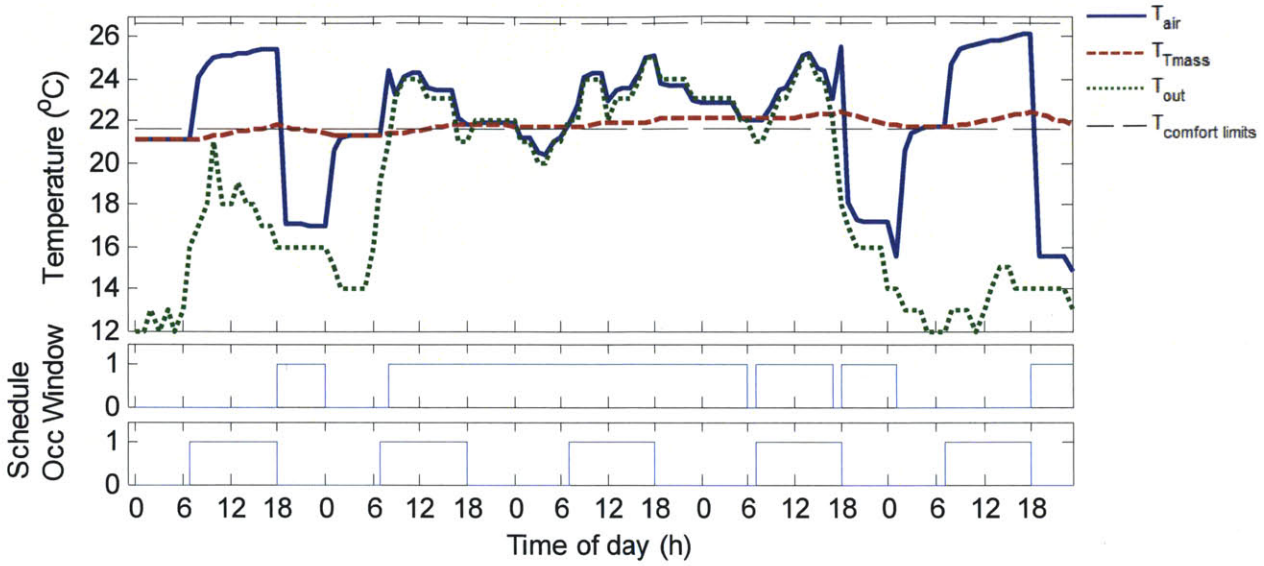

Figure C-52: Optimization results for May 15-19 using dynamic programming and 1-slice model for parameters: Kansas, low heat gain q=15W/m^2; high thermal mass specific heat capacity c=2640 J/kgK. Resulting day thermal cost = [0, 0, 0, 0, 0].

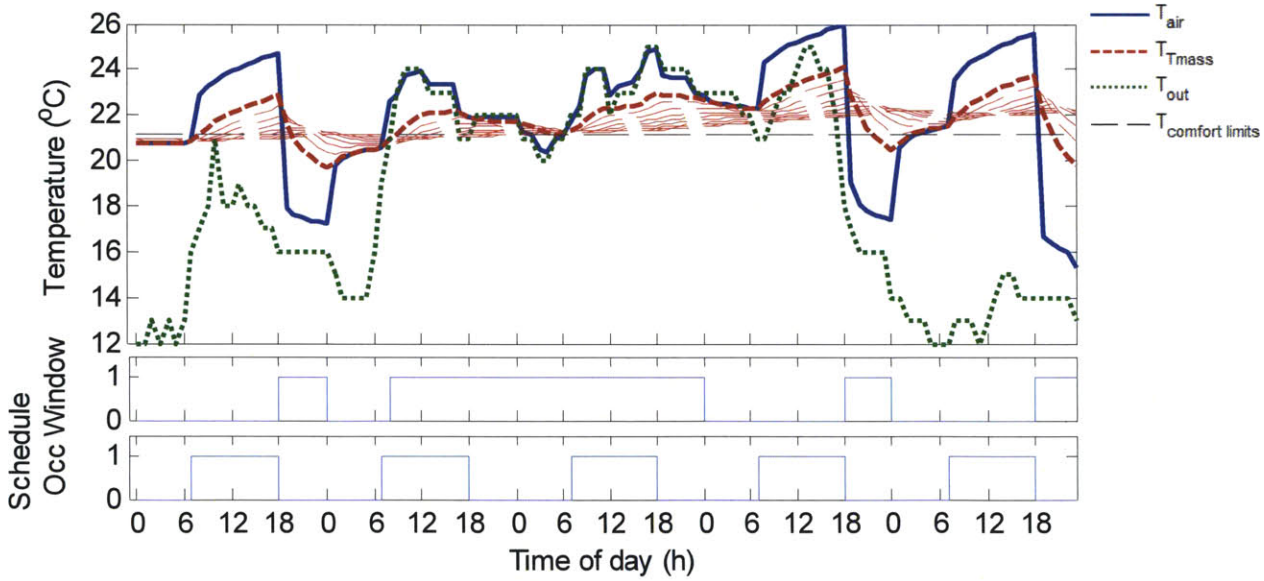

Figure C-53: Optimization results for May 15-19 using global search optimization and 10-slice model for parameters: Kansas, low heat gain q=15W/m^2;high thermal mass specific heat capacity c=2640 J/kgK. Resulting day thermal cost = [0, 0, 0, 0, 0]

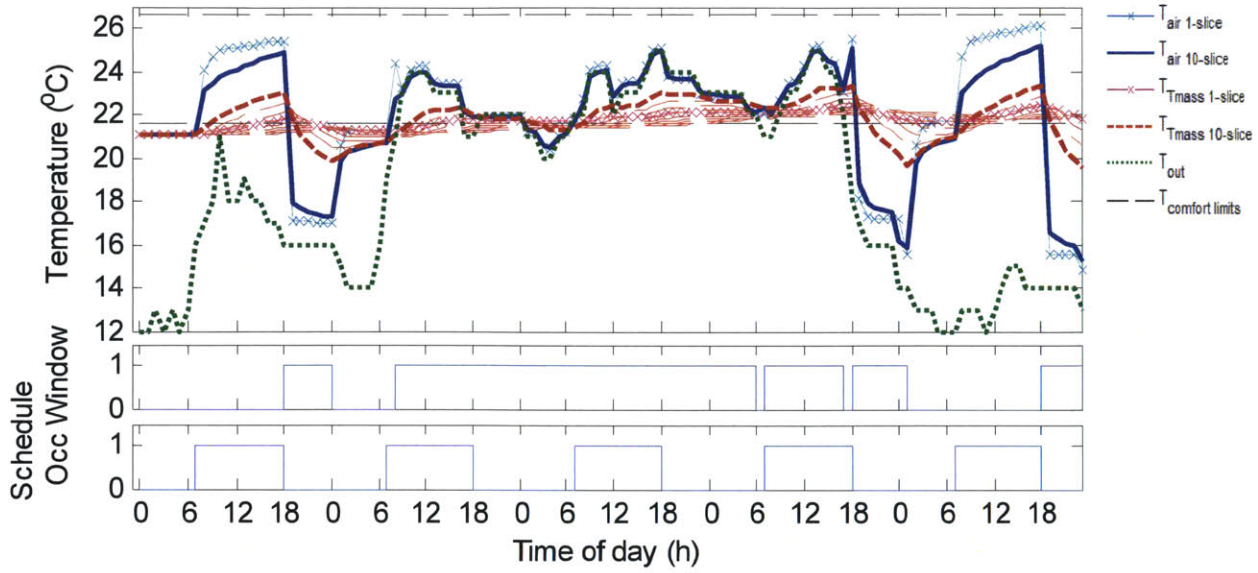

Figure C-54: Testing the effectiveness of effective h with 1-slice model for May 15-19 for Parameters: Kansas, low heat gain q=15W/m^2;high thermal mass specific heat capacity c=2640 J/kgK.

Parameters: Kansas, medium heat gain q=30W/m^2; normal thermal mass specific heat capacity c=880 J/kgK

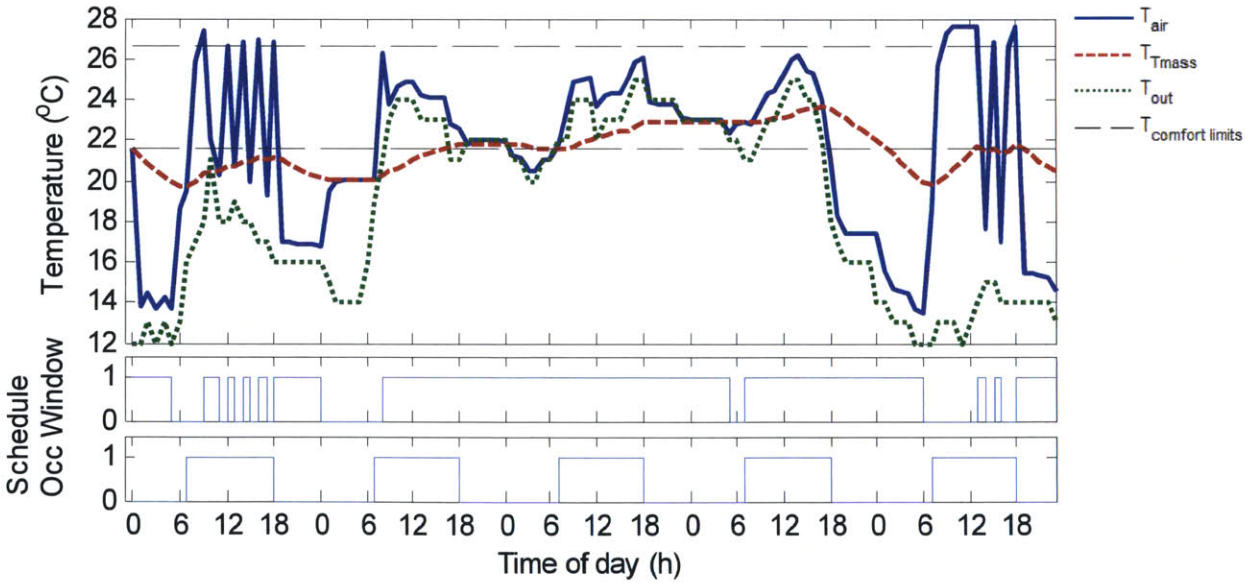

Figure C-55: Optimization results for May 15-19 using dynamic programming and 1-slice model for parameters: Kansas, medium heat gain q=30W/m^2; normal thermal mass specific heat capacity c=880 J/kgK. Resulting day thermal cost = [1.1, 0, 0, 0, 3.1]

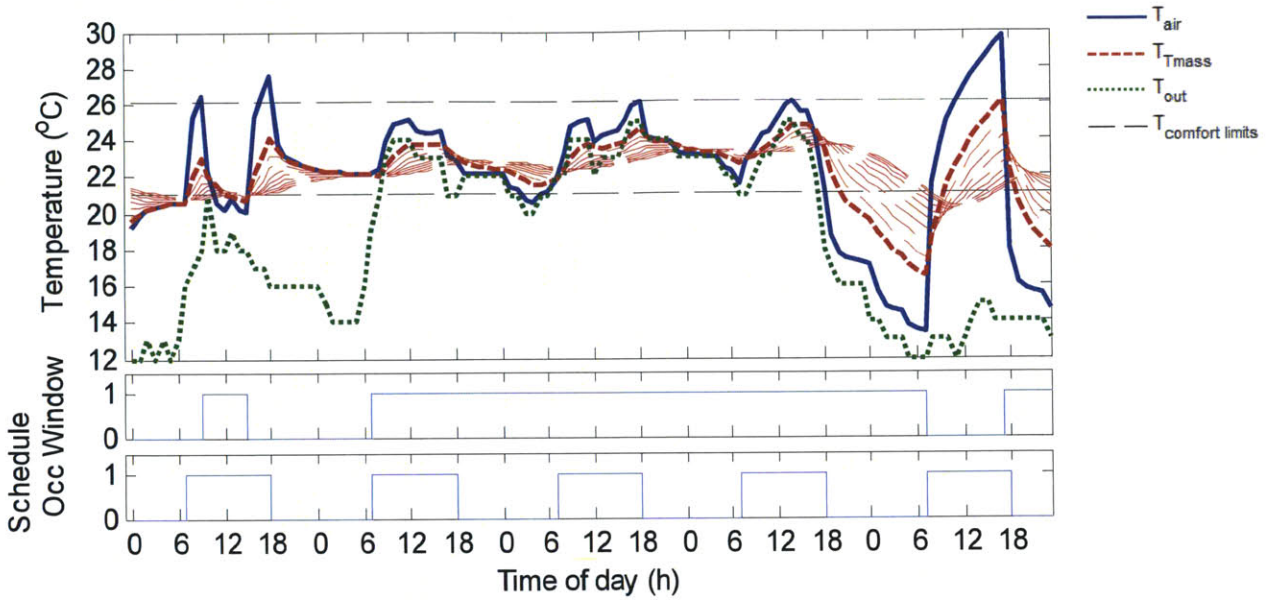

Figure C-56: Optimization results for May 15-19 using global search optimization and 10-slice model for parameters: Kansas, medium heat gain q=30W/m^2; normal thermal mass specific heat capacity c=880 J/kgK. Resulting day thermal cost = [0.9, 0, 0, 0, 3.2]

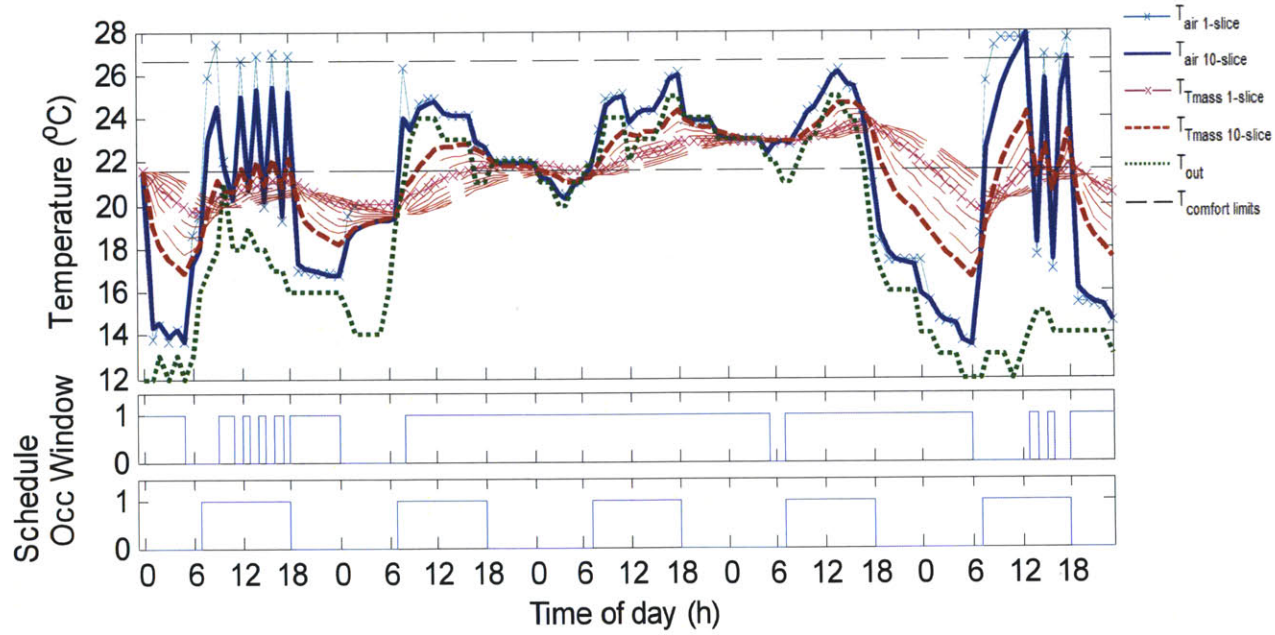

Figure C-57: Testing the effectiveness of effective h with 1-slice model for May 15-19 for parameters: Kansas, medium heat gain q=30W/m^2; normal thermal mass specific heat capacity c=880 J/kgK.

Parameters: Kansas, high heat gain q=45W/m^2; normal thermal mass specific heat capacity c=880 J/kgK

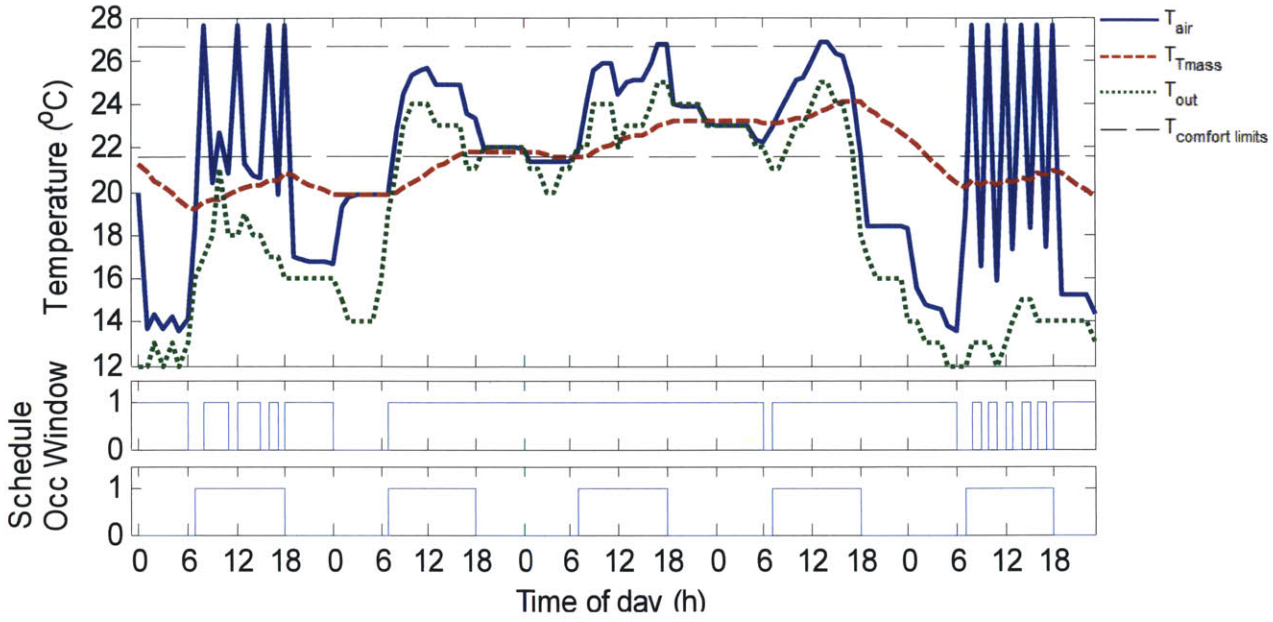

Figure C-58: Optimization results for May 15-19 using dynamic programming and 1-slice model for parameters: Kansas, high heat gain q=45W/m^2; normal thermal mass specific heat capacity c=880 J/kgK. Resulting day thermal cost = [1.0, 0, 0, 0.1, 4.8]

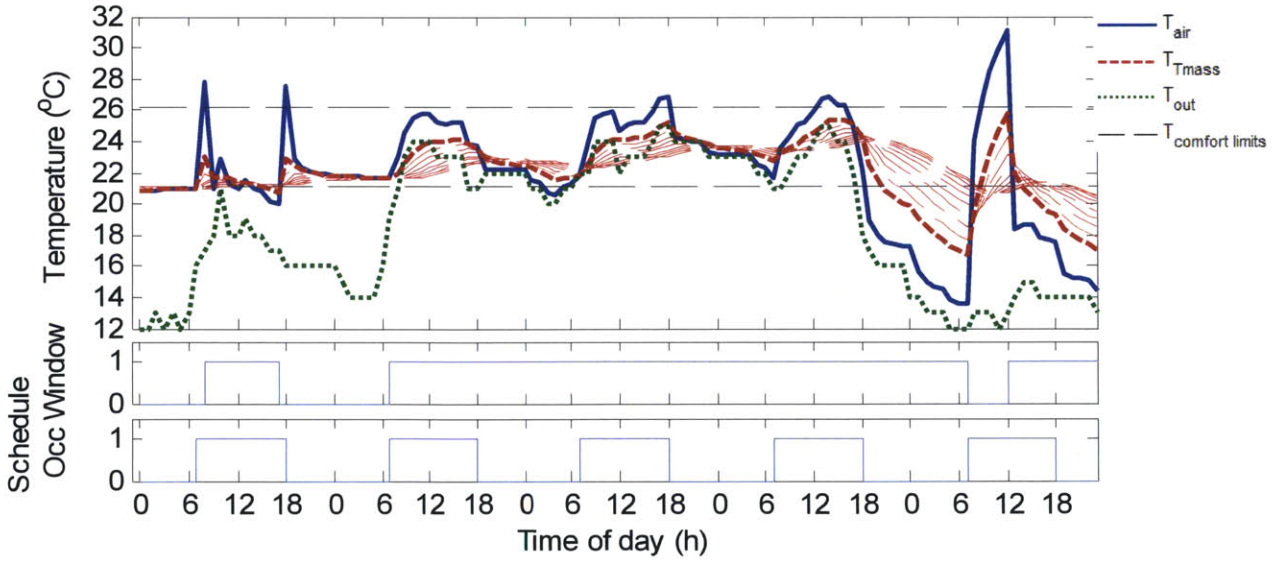

Figure C-59: Optimization results for May 15-19 using global search optimization and 10-slice model for parameters: Kansas, high heat gain q=45W/m^2; normal thermal mass specific heat capacity c=880 J/kgK. Resulting day thermal cost = [0.6, 0, 0.2, 0.3, 5.5]

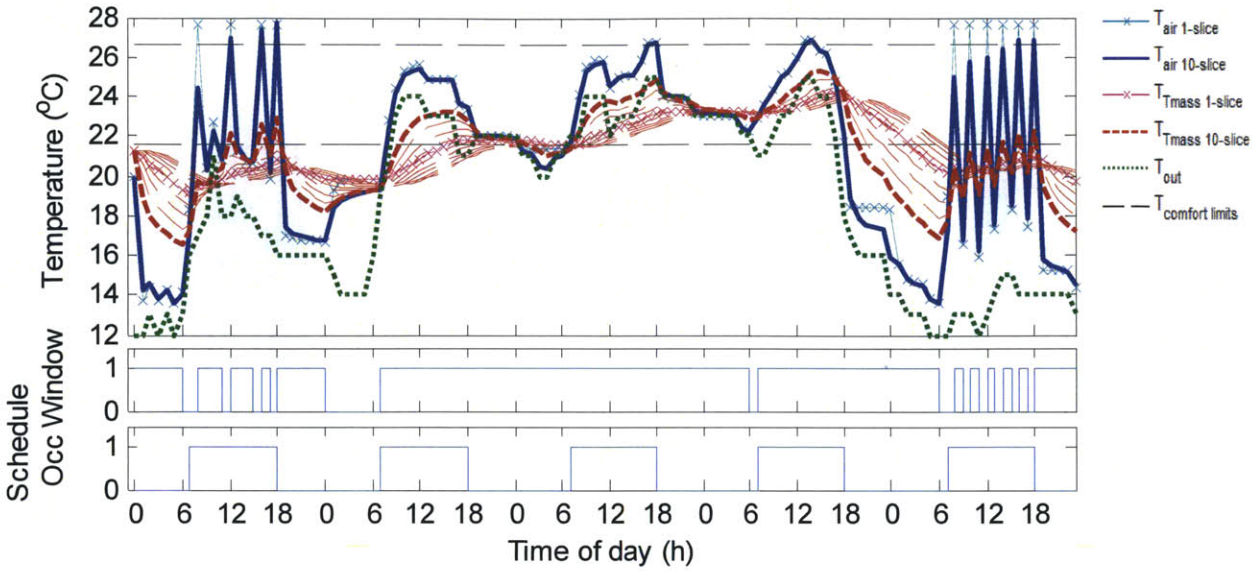

Figure C-60: Testing the effectiveness of effective h with 1-slice model for May 15-19 for Parameters: Kansas, high heat gain q=45W/m^2; normal thermal mass specific heat capacity c=880 J/kgK.

C.3 Comparison of rule-based control to optimized control for ventilation

City	Ventilation control	Thermal cost for each day
Madison	DP(1-slice)	[0,0,0,0.2,0,0,0,0,0,0.1]
	GSO (10-slices)	[0, 0, 0, 0.1,0,0,0.5,0.2, 0, 0.1]
	RBC-1 (1-slice)	[0, 0, 0.2, 1.3, 0]
	RBC-1 (10-slices)	[0, 0, 0, 0.5, 0]
	RBC-2a (1-slice)	[0.4, 0, 0, 1.2, 0, 0, 0.2, 0.4, 3, 1]
	RBC-2a (10-slices)	[1.6, 0, 0, 0.2,0, 0, 0.7, 0.6, 1.2, 0.8]
	RBC-2b (1-slice)	[0.4, 0, 0, 1.2, 0, 0, 1.1, 1.8, 4.7, 2.3]
	RBC-2b (10-slices)	[1.6, 0, 0, 0, 0, 0, 0.5, 0.8, 1.0, 1.7]
Los Angeles	DP(1-slice)	[0,0,0,0,0,0,0,0,0,0]
	GSO (10-slices)	[0, 0, 0, 0,0,0.1,0.6,0, 0.2, 0.2]
	RBC-1 (1-slice)	[0.1, 0, 0, 0, 0]
	RBC-1 (10-slices)	[0, 0.1, 0, 0, 0]
	RBC-2a (1-slice)	[0.2, 0, 0, 0, 0.2, 0.5, 0.3, 0, 0.4, 0.2]
	RBC-2a (10-slices)	[2.7, 0, 0, 0.2, 0, 0,0.6, 0.6, 1.2, 0.8]
	RBC-2b (1-slice)	[0.2, 0, 0, 0,0,0.3,0.3,0, 0.4, 0.2]
	RBC-2b (10-slices)	[2.7, 0, 0, 0.2, 0.2, 0, 1.4, 1.3, 0, 0.8]

Table C-5: Performance of optimized (dynamic programming, DP and global search optimization, GS0) versus rule-based control of ventilation in terms of thermal cost. Note that the rule-based control (RBC) 1 is that with overcooling strategy 1, while RBC-2 is that with overcooling strategy 2, with RBC-2a using arbitrary ratio increment and RBC-2b using self-improving ratio. Parameters used: city: low heat gain, q=15W/m^2; normal thermal mass heat capacity c=880 J/kgK. Thermal comfort limit is based on mean outdoor temperature for the 10 days.

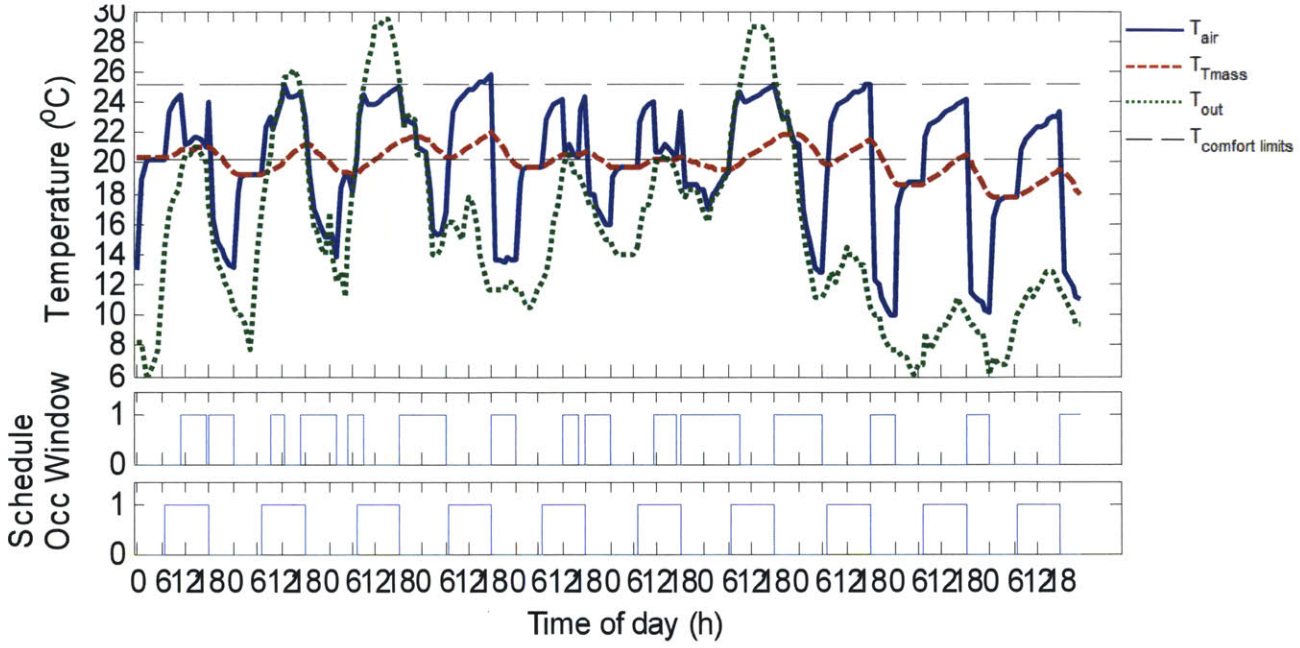

Figure C-61: Madison 10-day temperature profile with 1-slice model and optimal ventilation schedule computed with dynamic programming

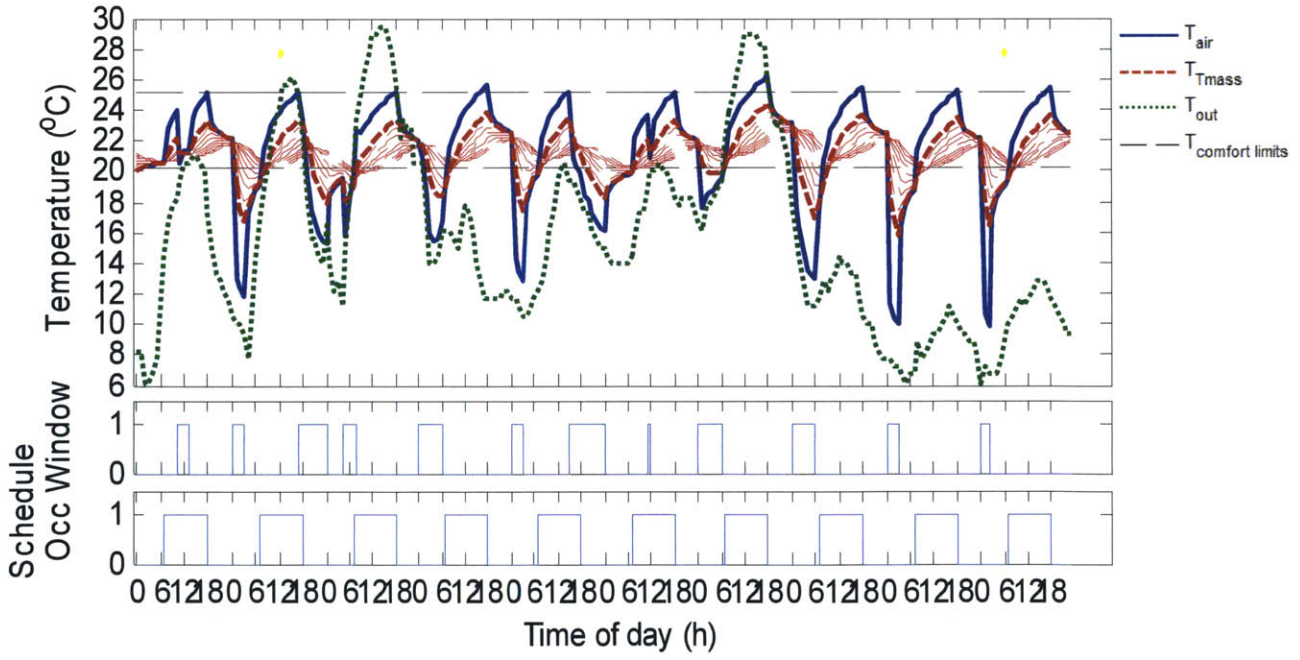

Figure C-62: Madison 10-day temperature profile with 10-slice model and optimal ventilation schedule computed with global search optimization

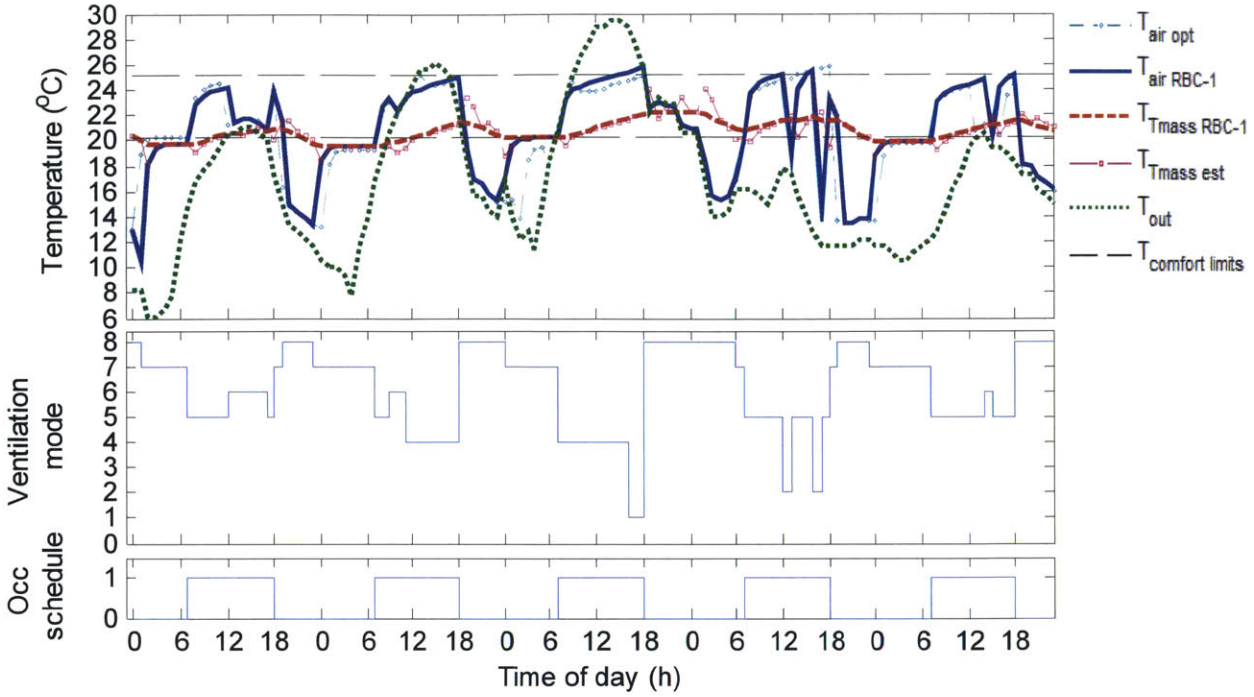

Figure C-63: Madison 5-day temperature profile with 1-slice model and RBC-1 ventilation schedule

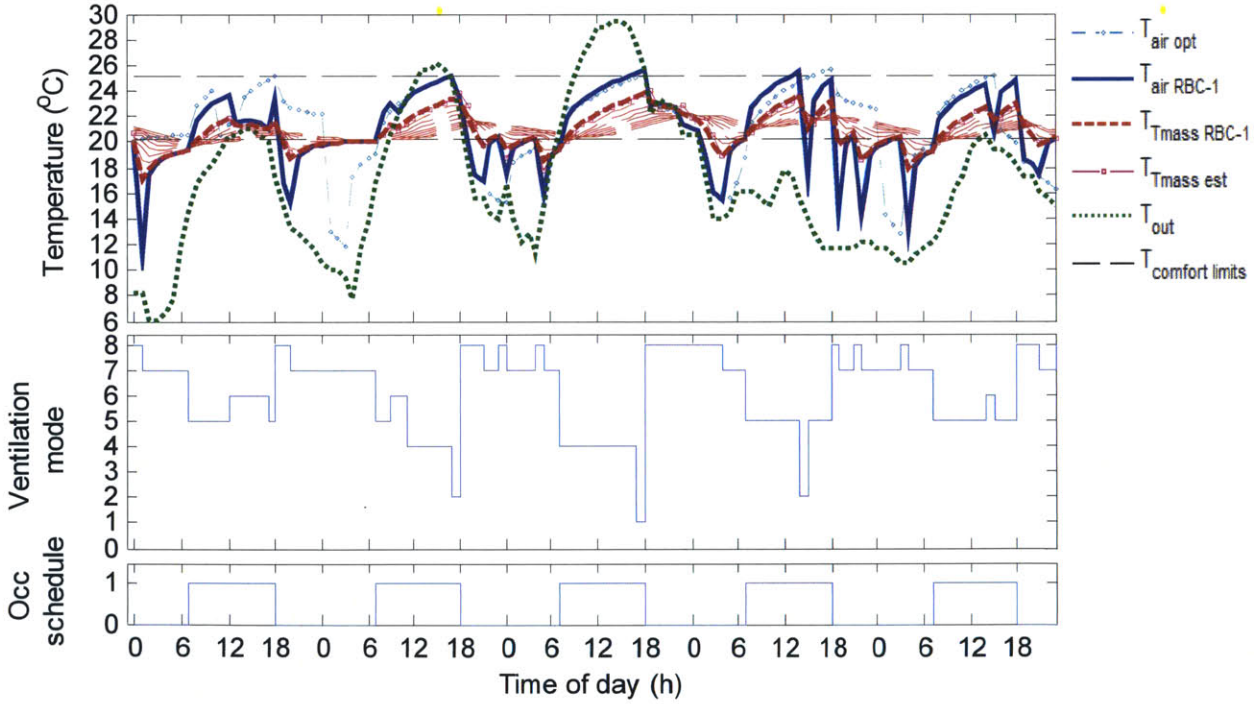

Figure C-64: Madison 5-day temperature profile with 10-slice model and RBC-1 ventilation schedule

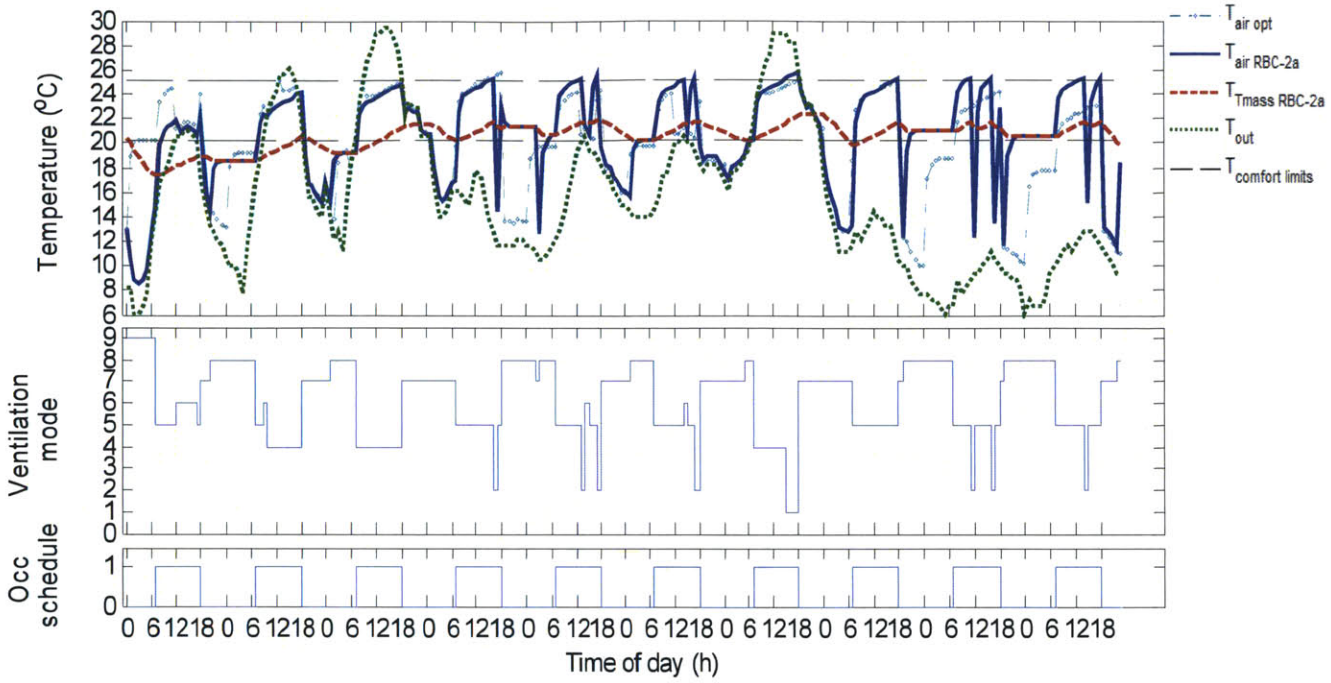

Figure C-65: Madison 10-day temperature profile with 1-slice model and RBC-2a ventilation schedule

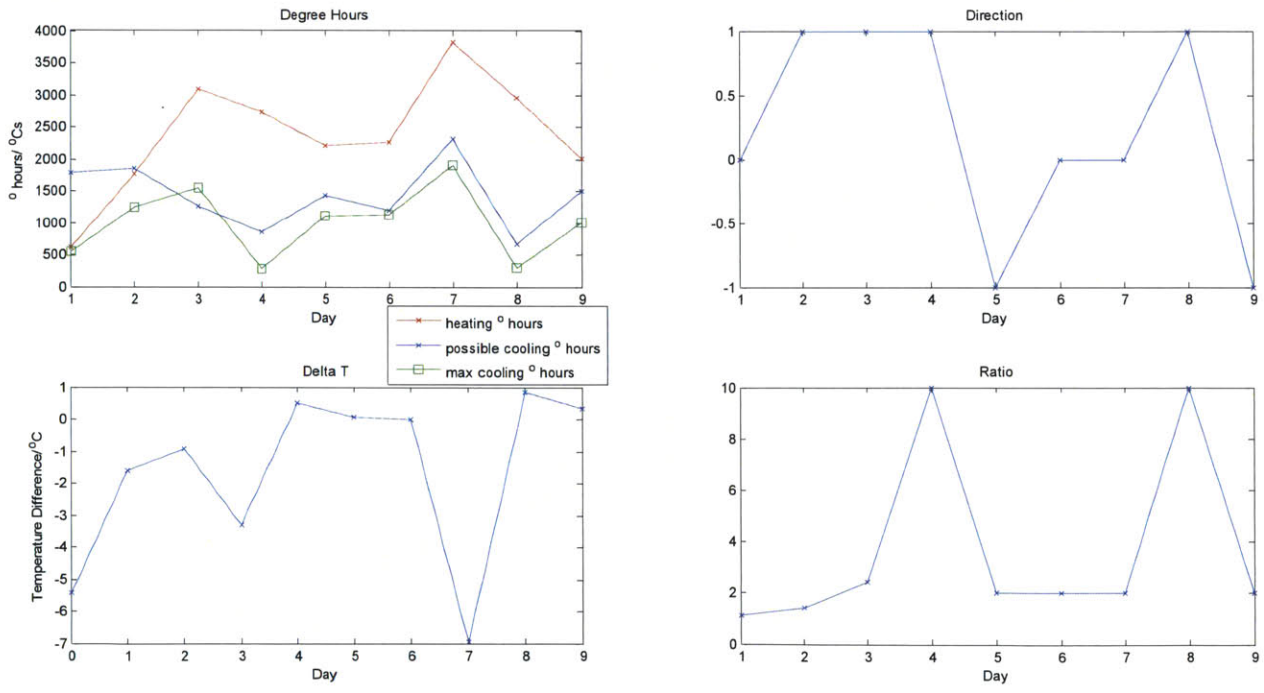

Figure C-66: Plots of the parameters of the overcooling-prevention self-learning algorithm corresponding to temperature profile of figure above

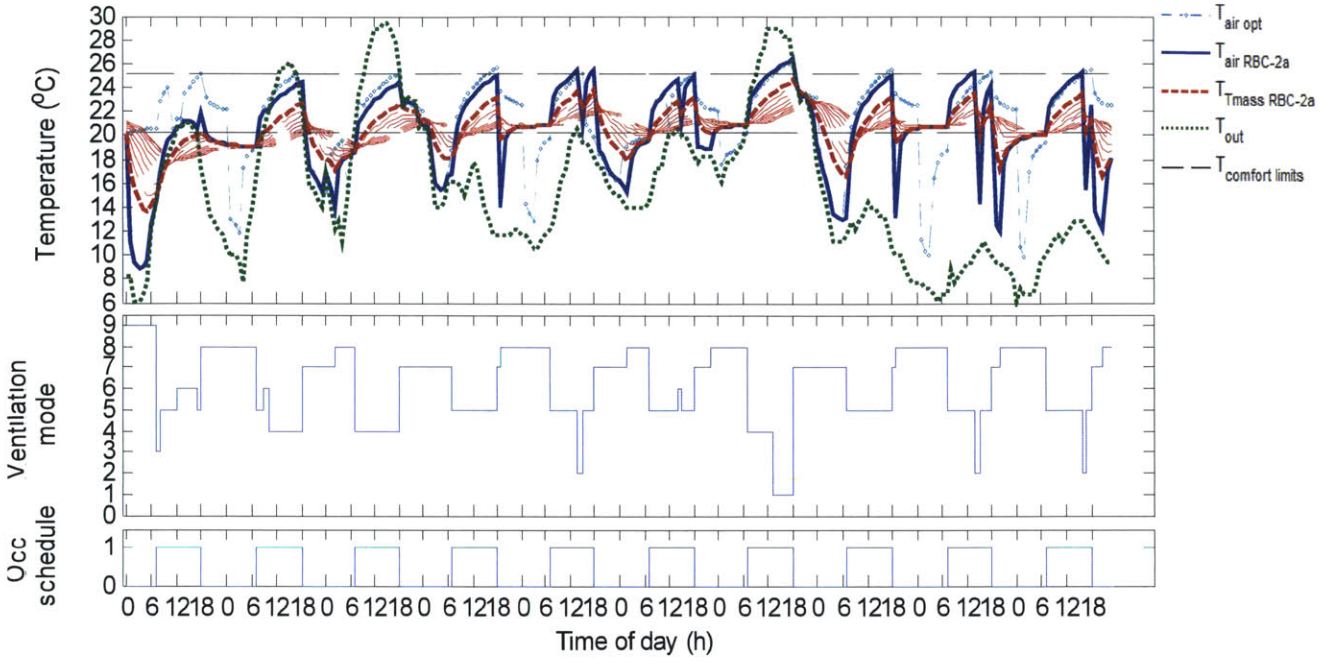

Figure C-67: Madison 10-day temperature profile with 10-slice model and RBC-2a ventilation schedule

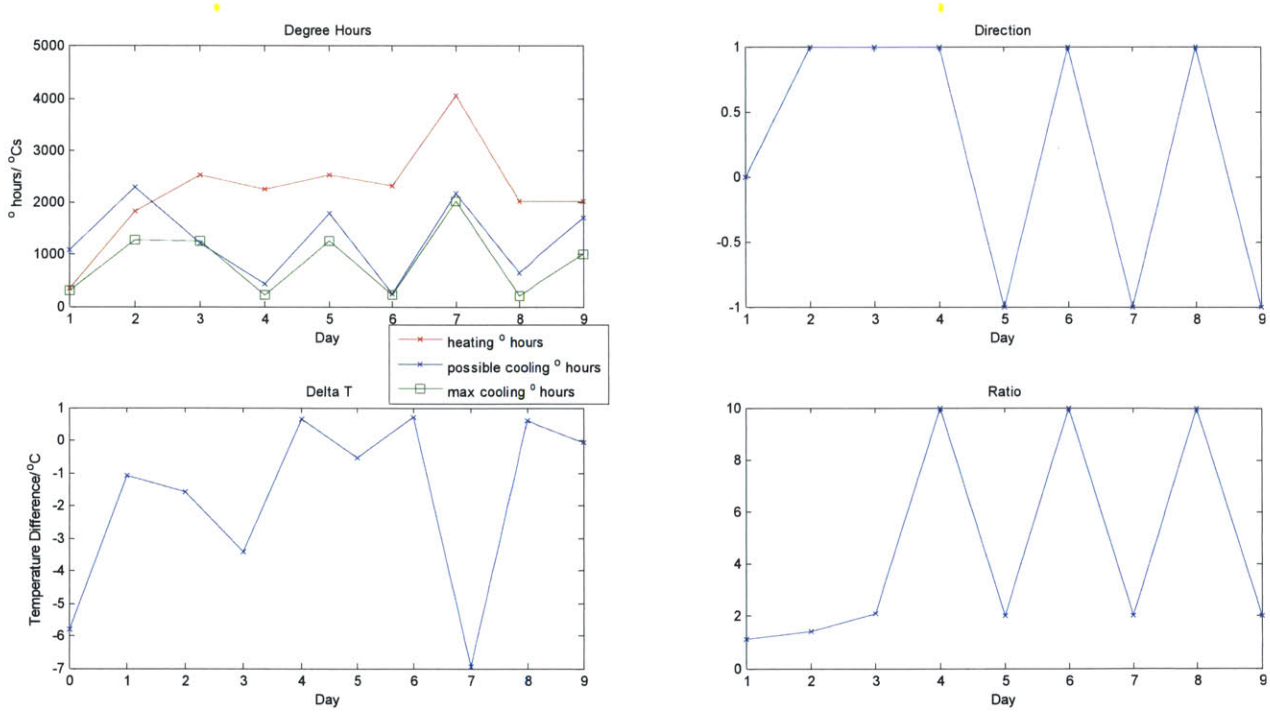

Figure C-68: Plots of the parameters of the overcooling-prevention self-learning algorithm corresponding to temperature profile of figure above

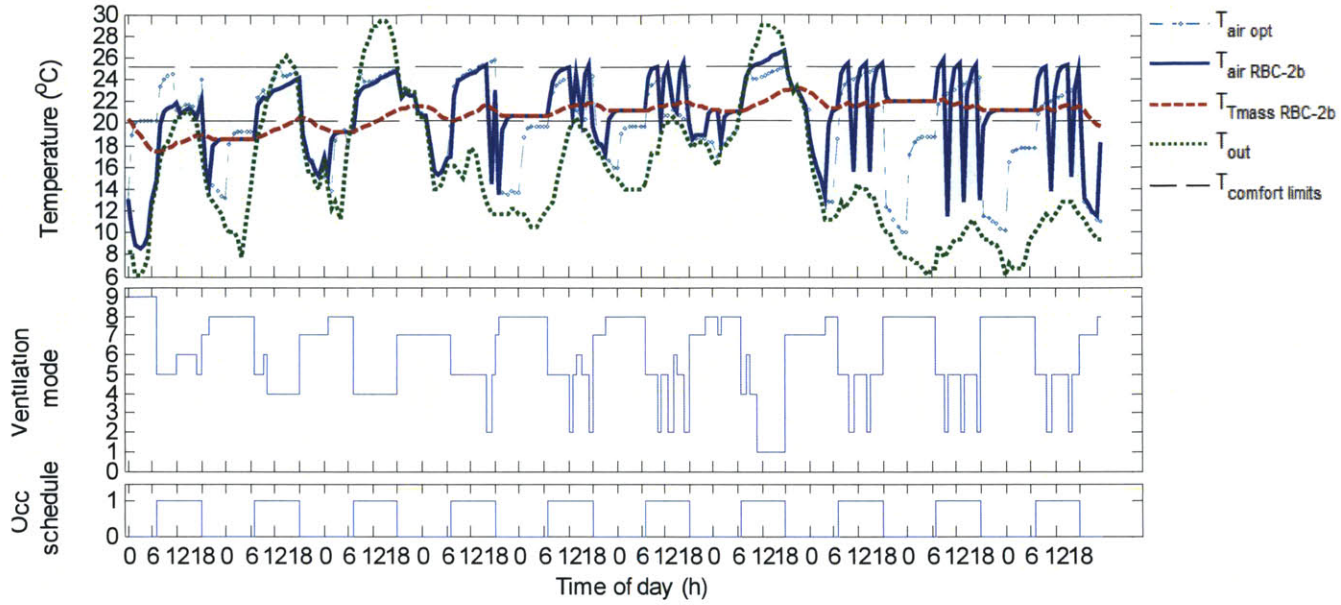

Figure C-69: Madison 10-day temperature profile with 1-slice model and RBC-2b ventilation schedule

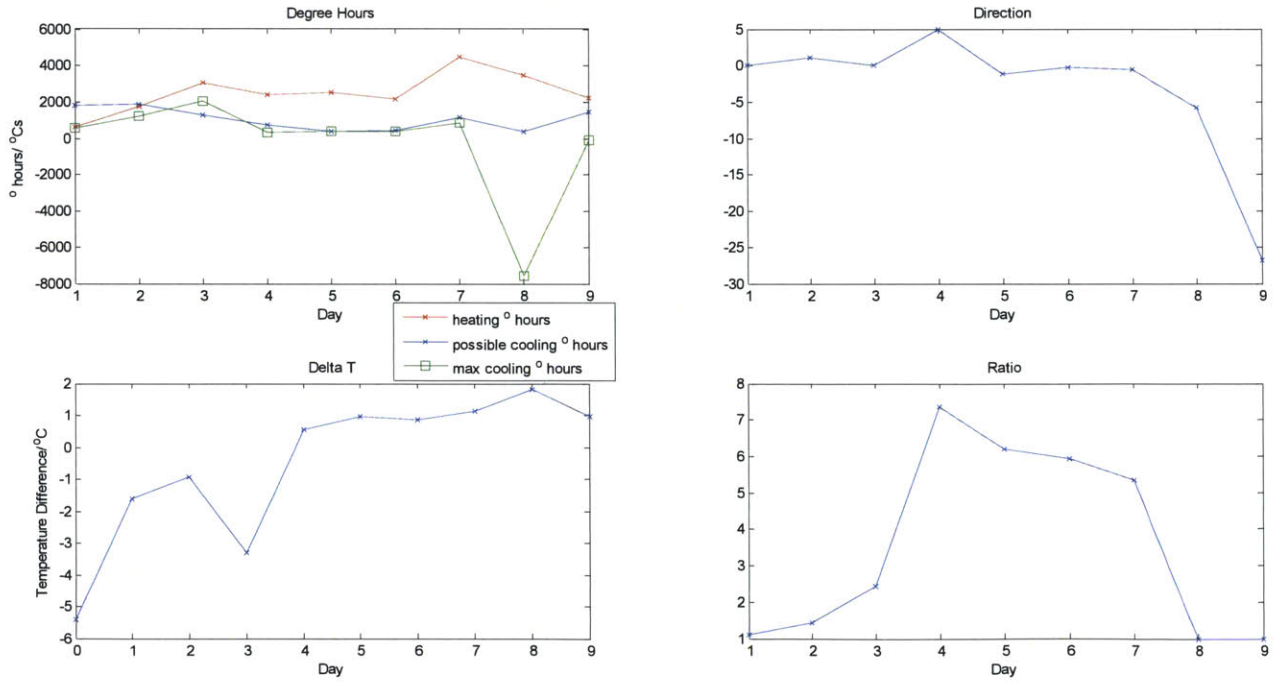

Figure C-70: Plots of the parameters of the overcooling-prevention self-learning algorithm corresponding to temperature profile of figure above

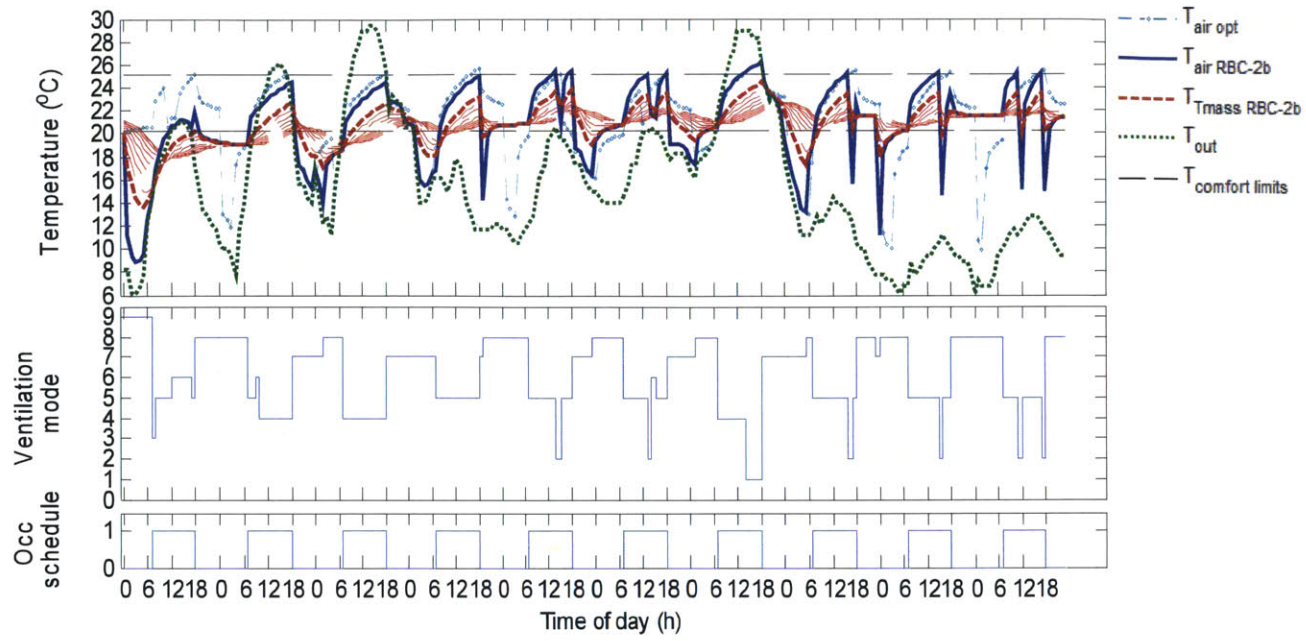

Figure C-71: Madison 10-day temperature profile with 10-slice model and RBC-2b ventilation schedule

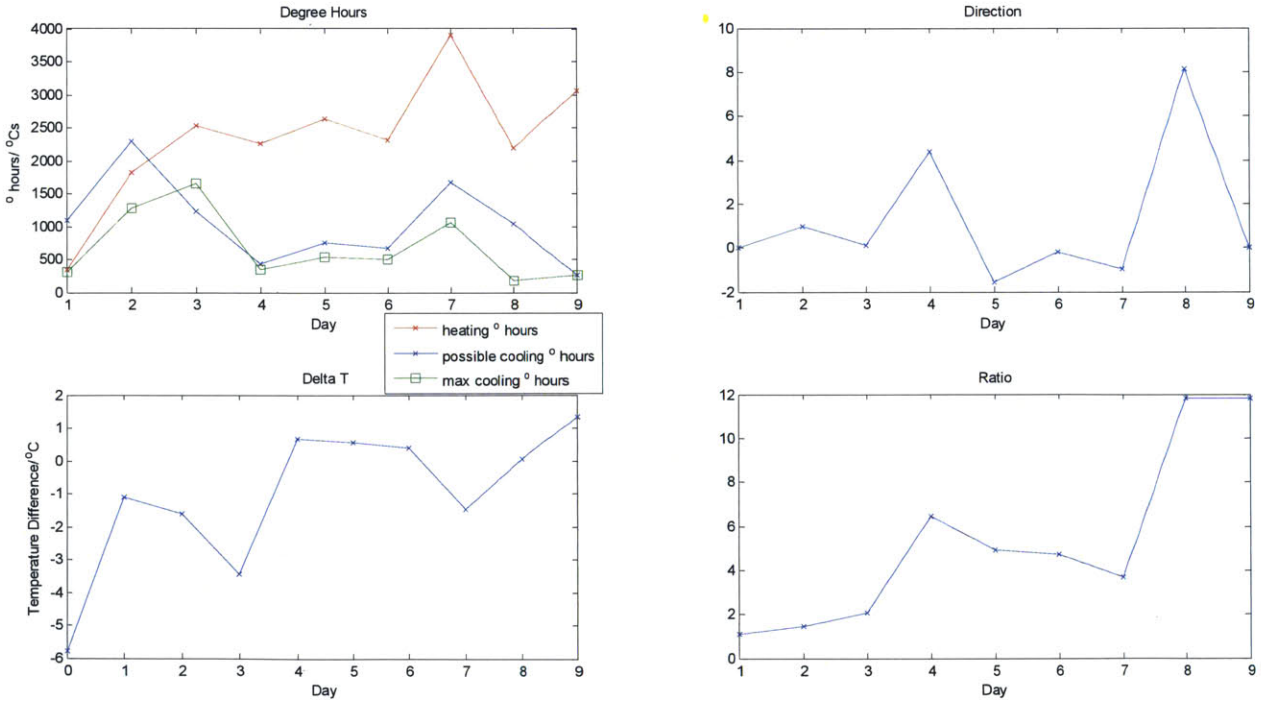

Figure C-72: Plots of the parameters of the overcooling-prevention self-learning algorithm corresponding to temperature profile of figure above

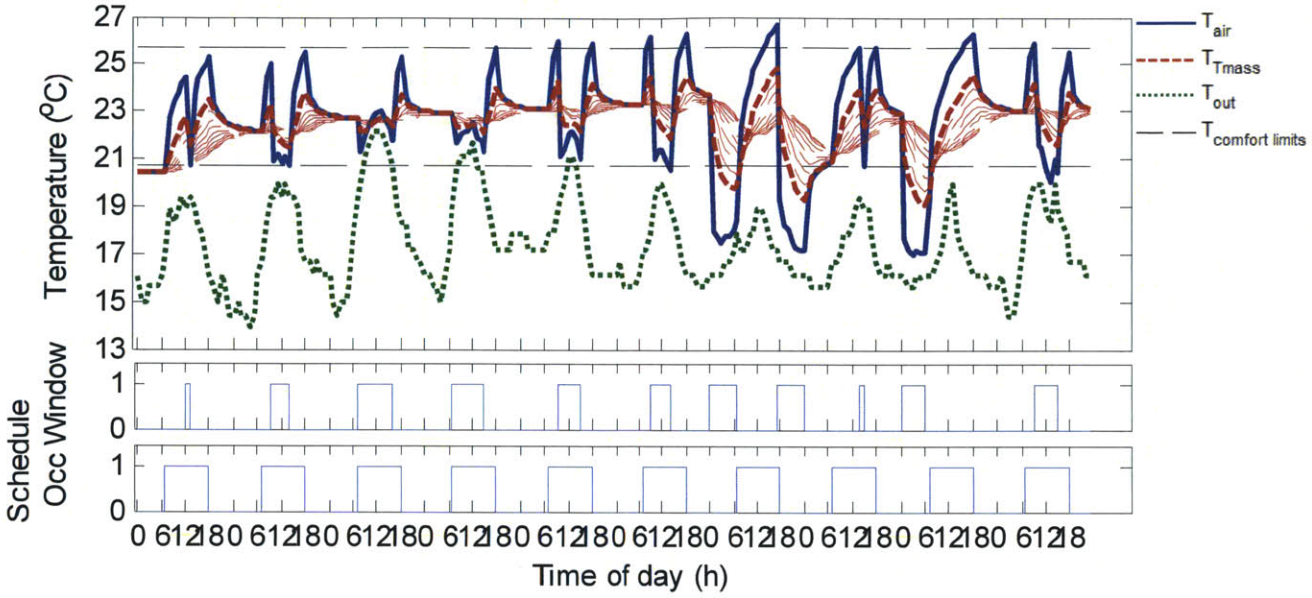

Figure C-73: Los Angeles 10-day temperature profile with 10-slice model and optimal ventilation schedule computed with global search optimization

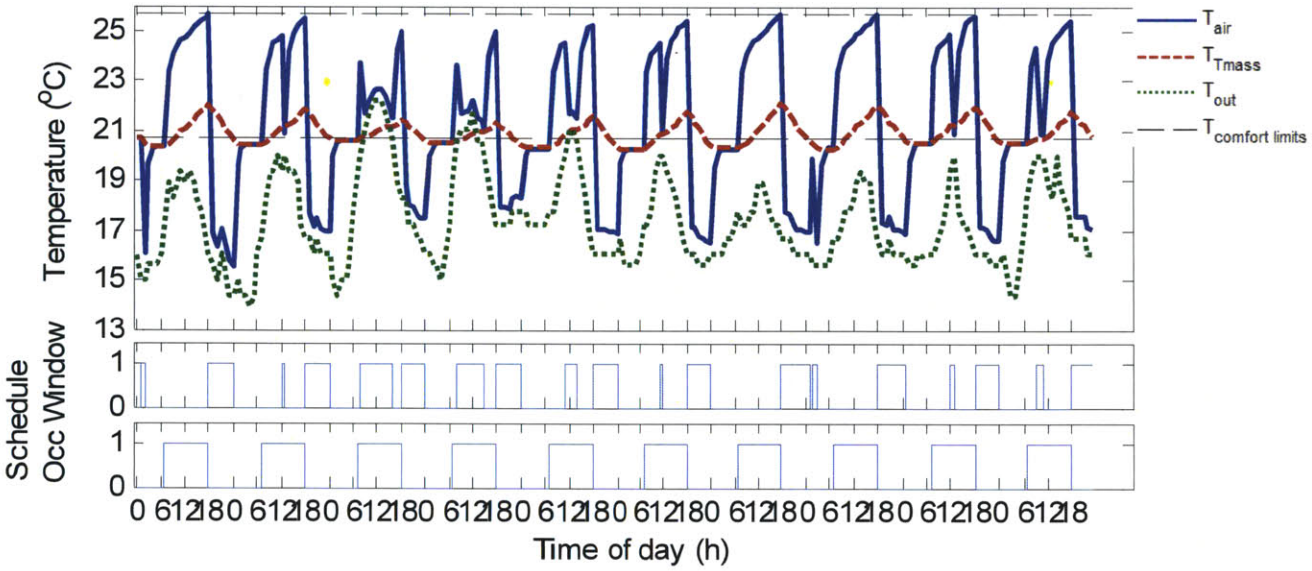

Figure C-74: Los Angeles 10-day temperature profile with 1-slice model and optimal ventilation schedule computed with dynamic programming

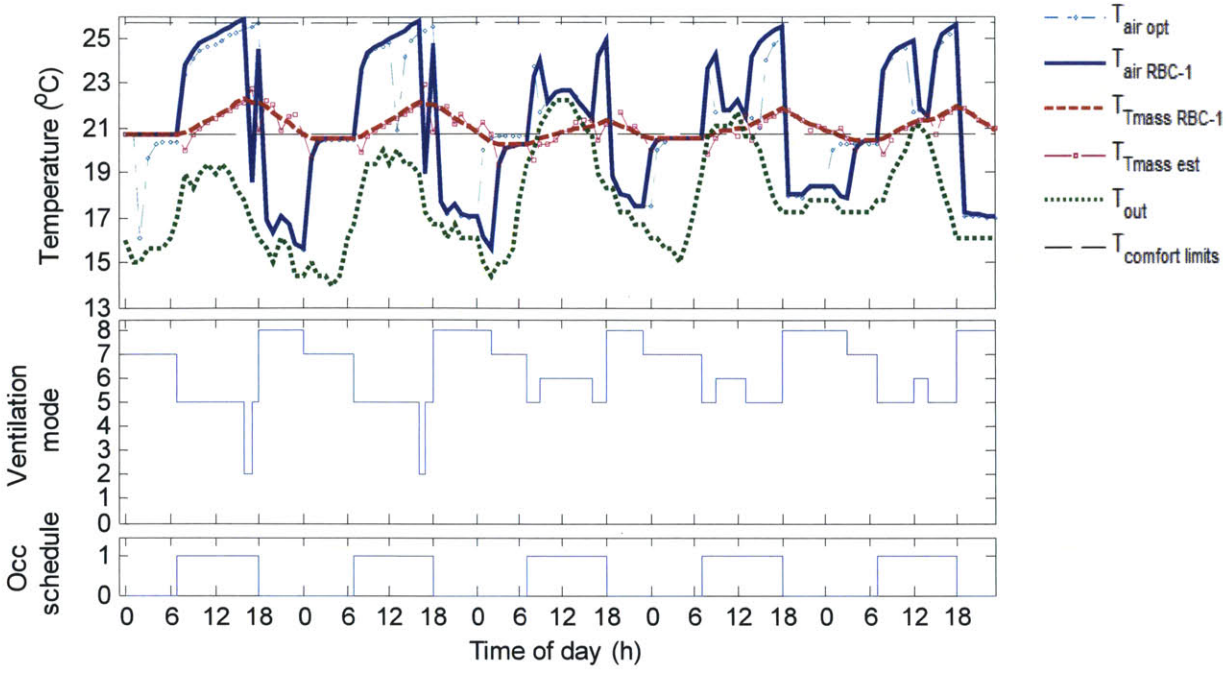

Figure C-75: Los Angeles 5-day temperature profile with 1-slice model and RBC-1 ventilation schedule

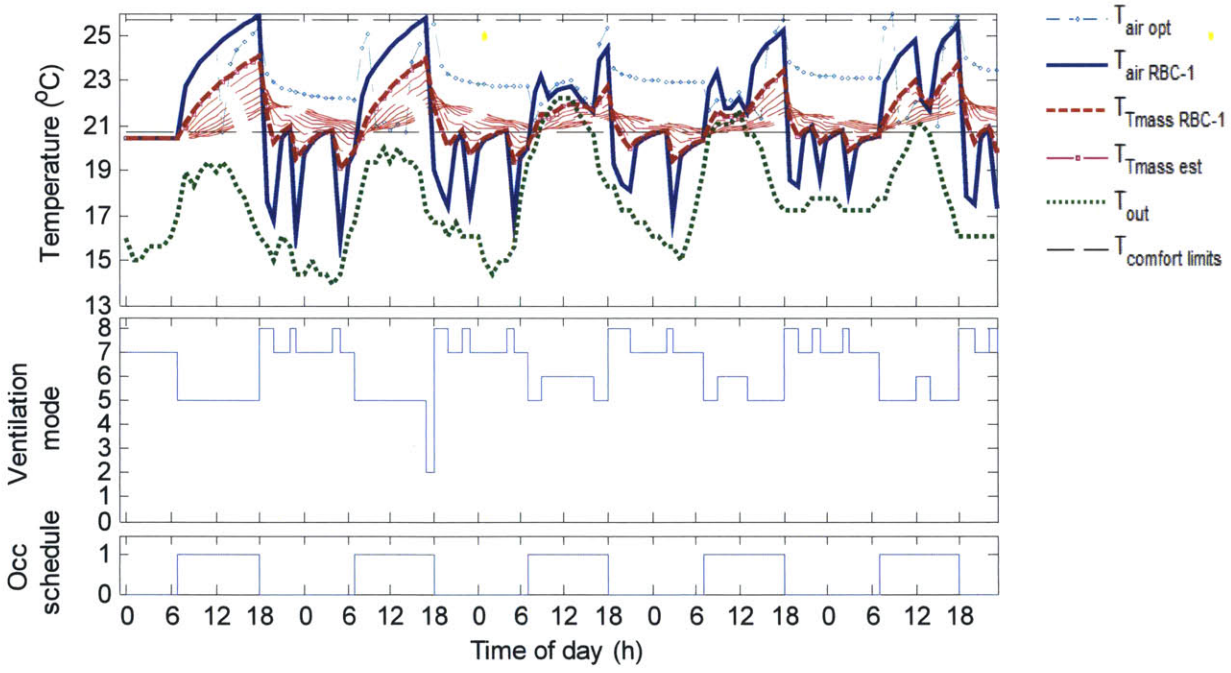

Figure C-76: Los Angeles 5-day temperature profile with 10-slice model and RBC-1 ventilation schedule

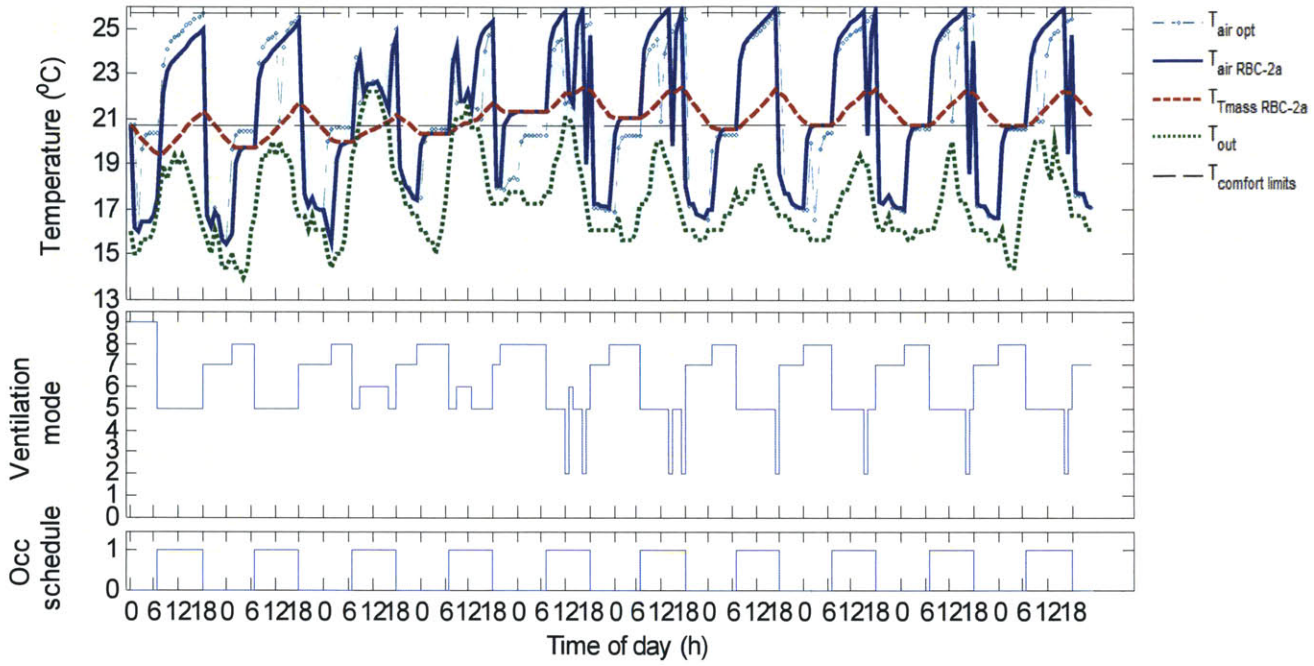

Figure C-77: Los Angeles 10-day temperature profile with 1-slice model and RBC-2a ventilation schedule

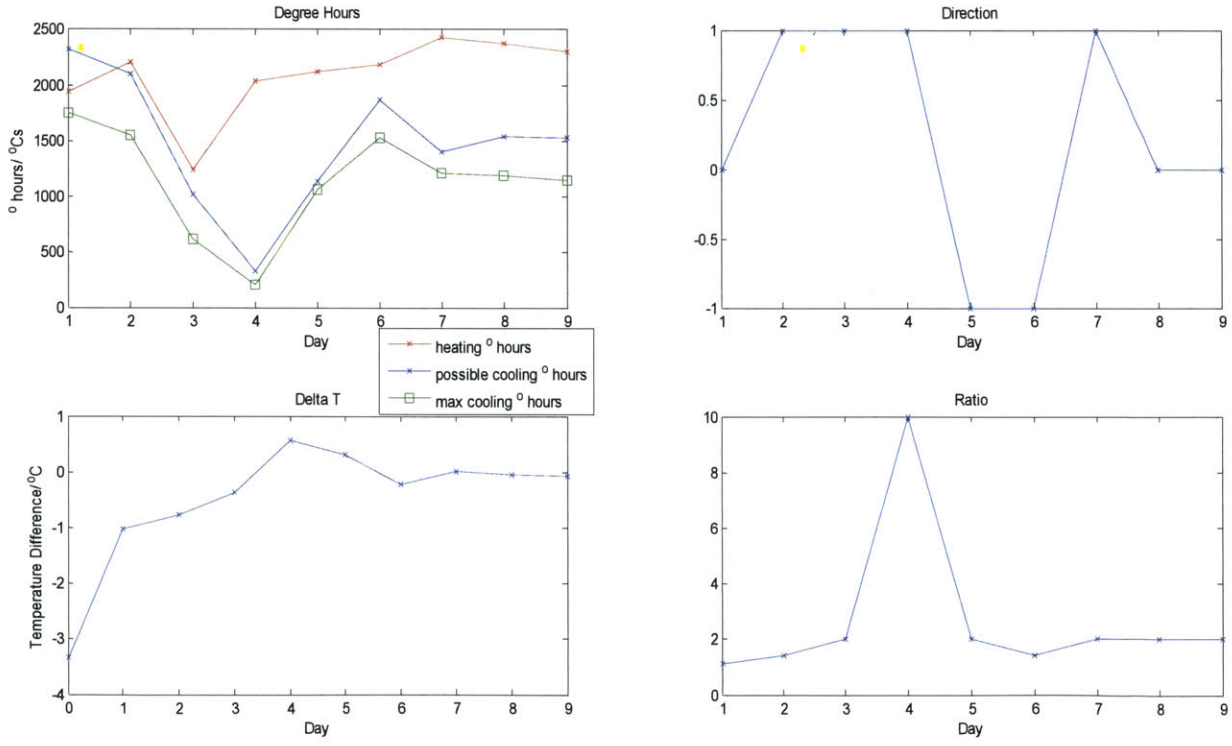

Figure C-78: Plots of the parameters of the overcooling-prevention self-learning algorithm corresponding to temperature profile of figure above

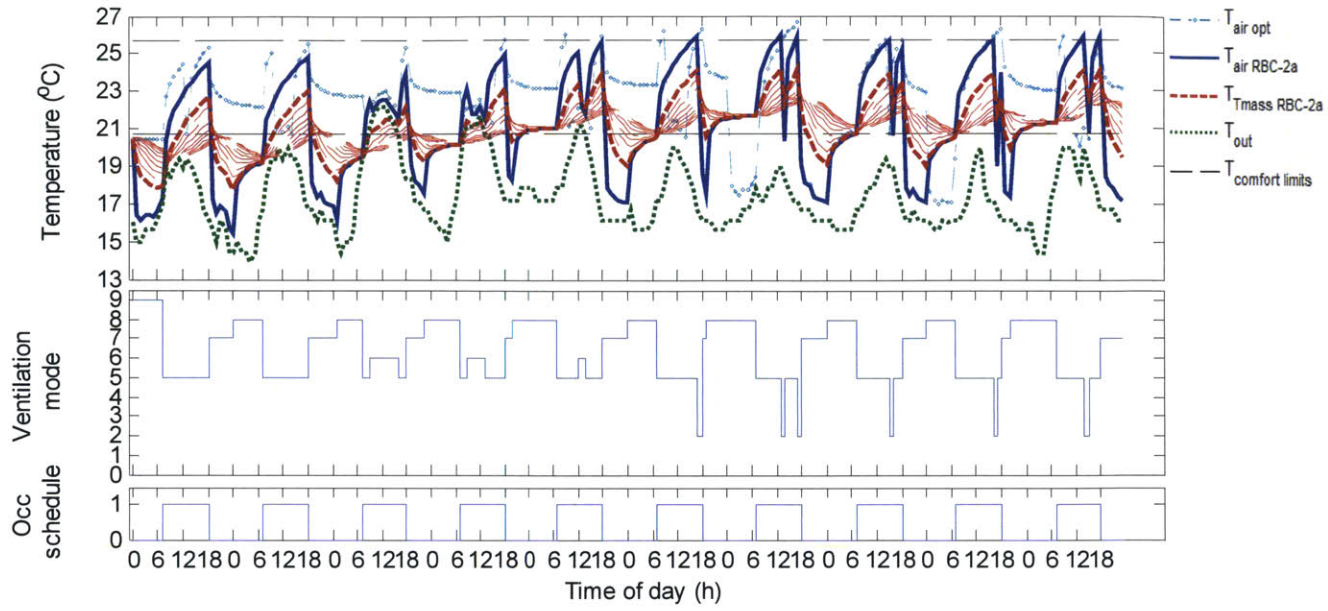

Figure C-79: Los Angeles 10-day temperature profile with 10-slice model and RBC-2a ventilation schedule

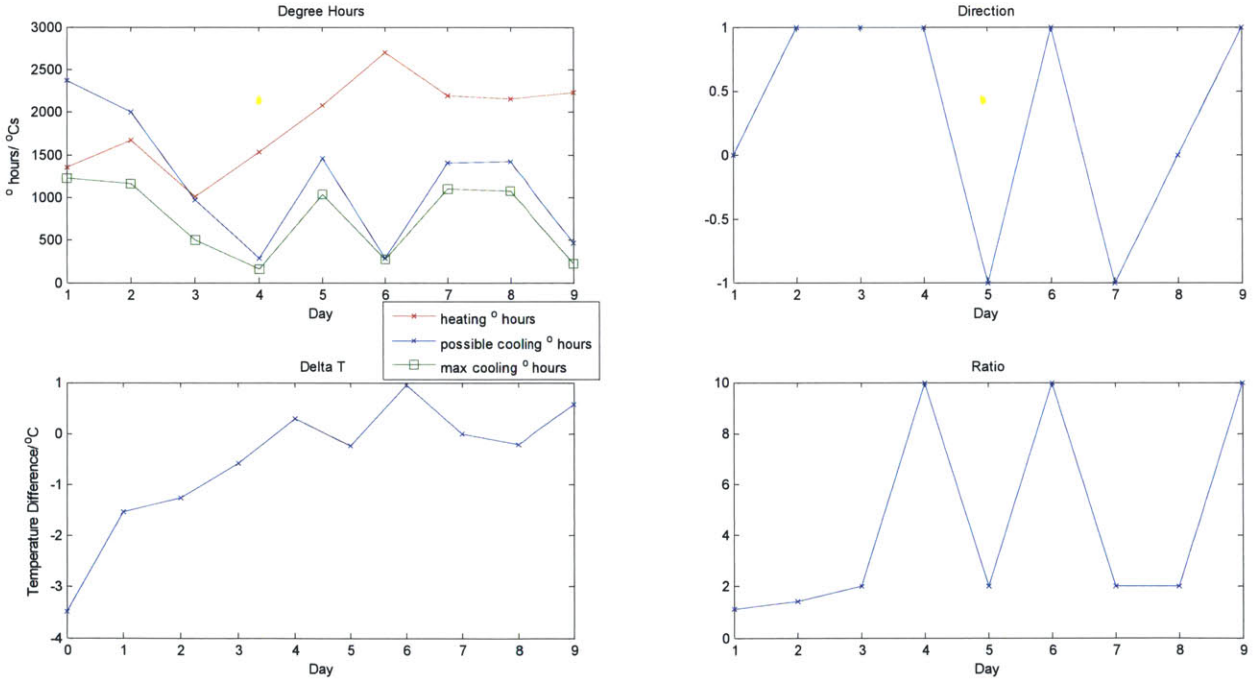

Figure C-80: Plots of the parameters of the overcooling-prevention self-learning algorithm corresponding to temperature profile of figure above

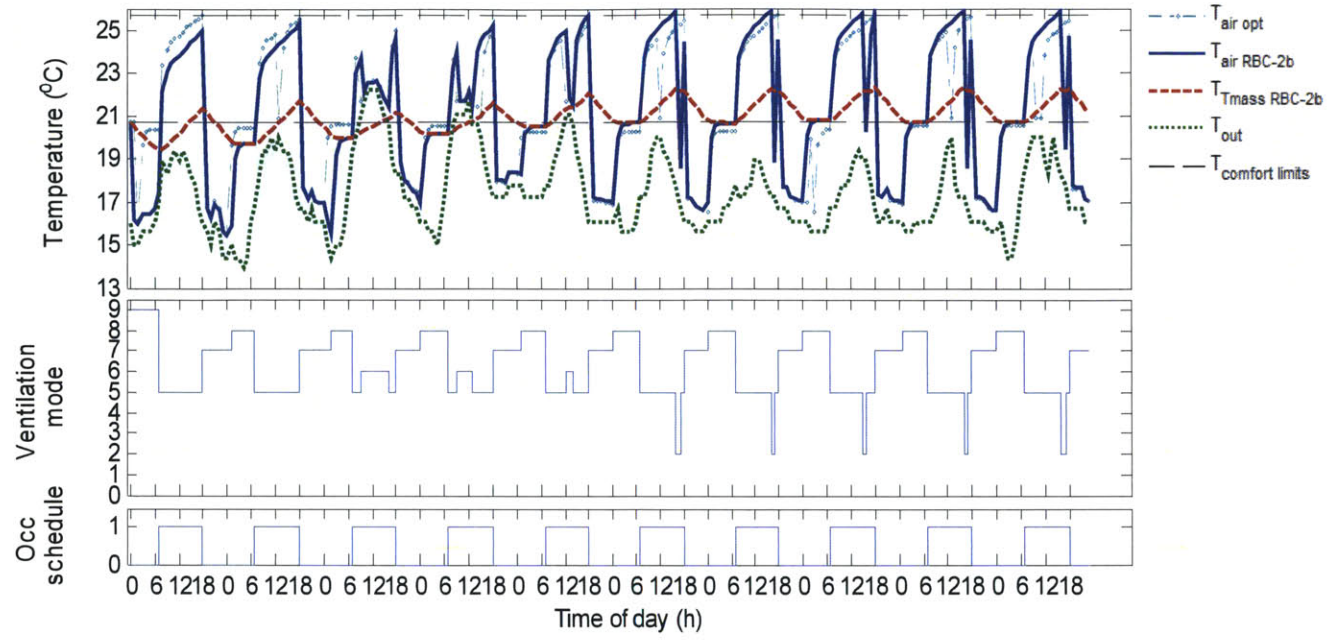

Figure C-81: Los Angeles 10-day temperature profile with 1-slice model and RBC-2b ventilation schedule

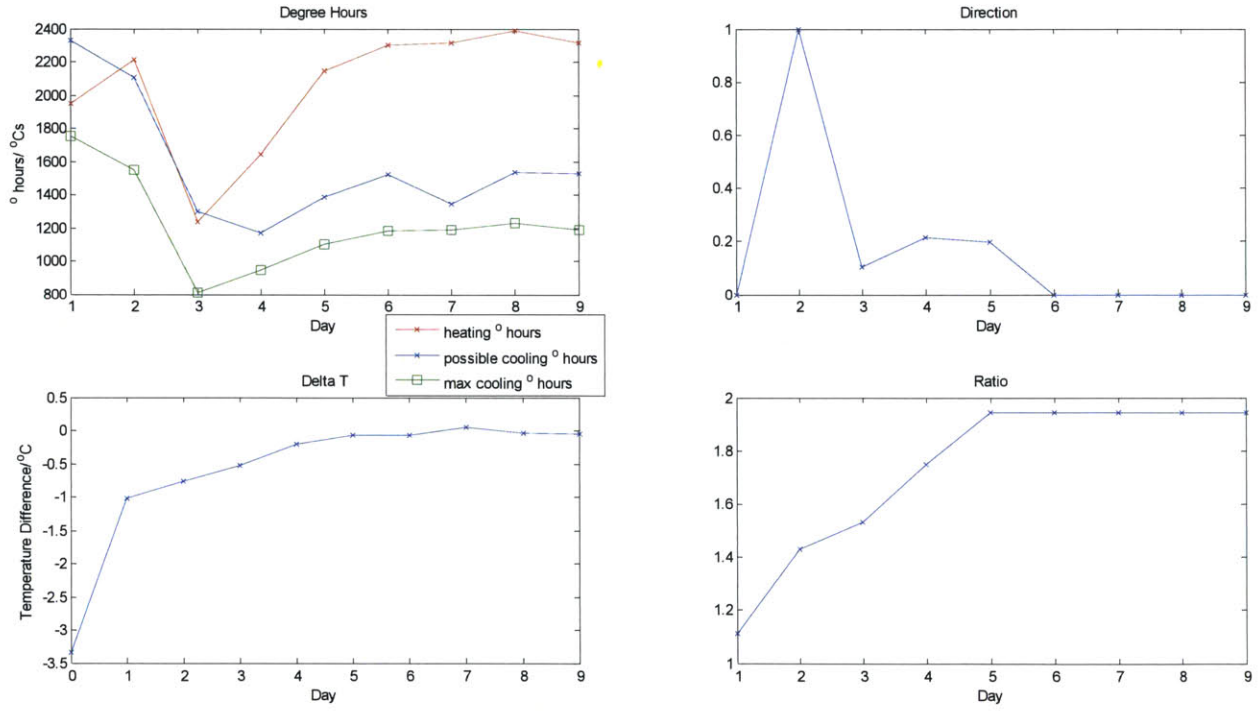

Figure C-82: Plots of the parameters of the overcooling-prevention self-learning algorithm corresponding to temperature profile of figure above

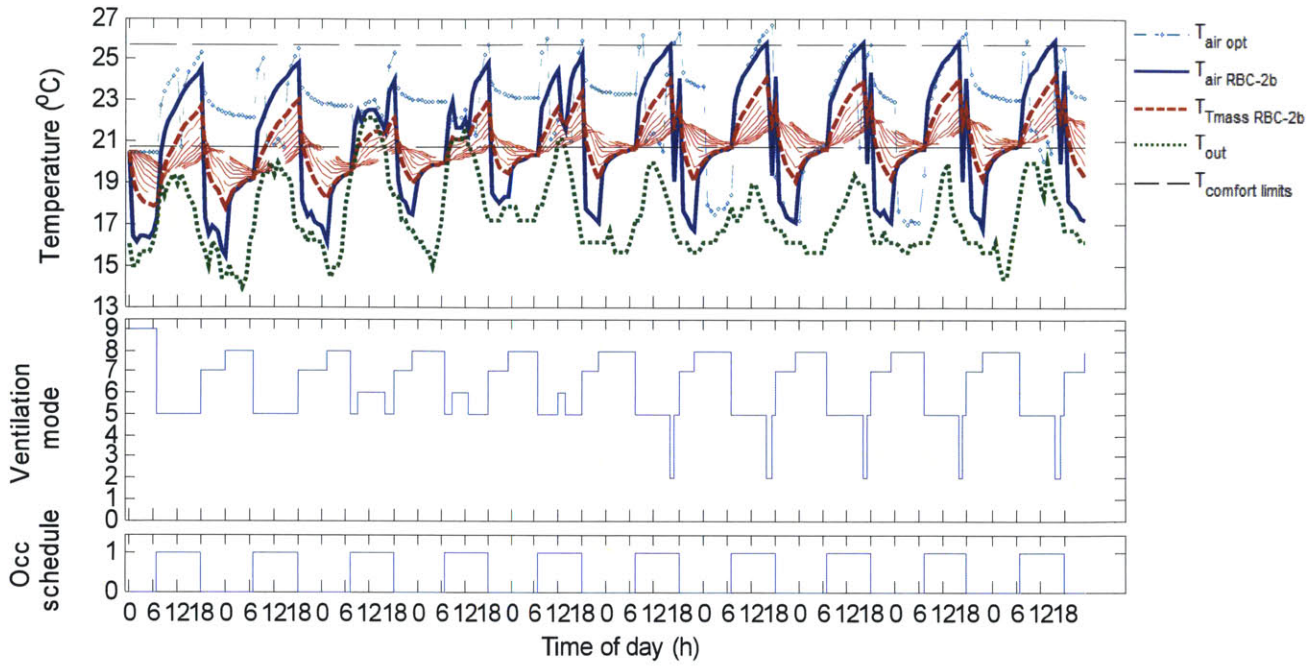

Figure C-83: Los Angeles 10-day temperature profile with 10-slice model and RBC-2b ventilation schedule

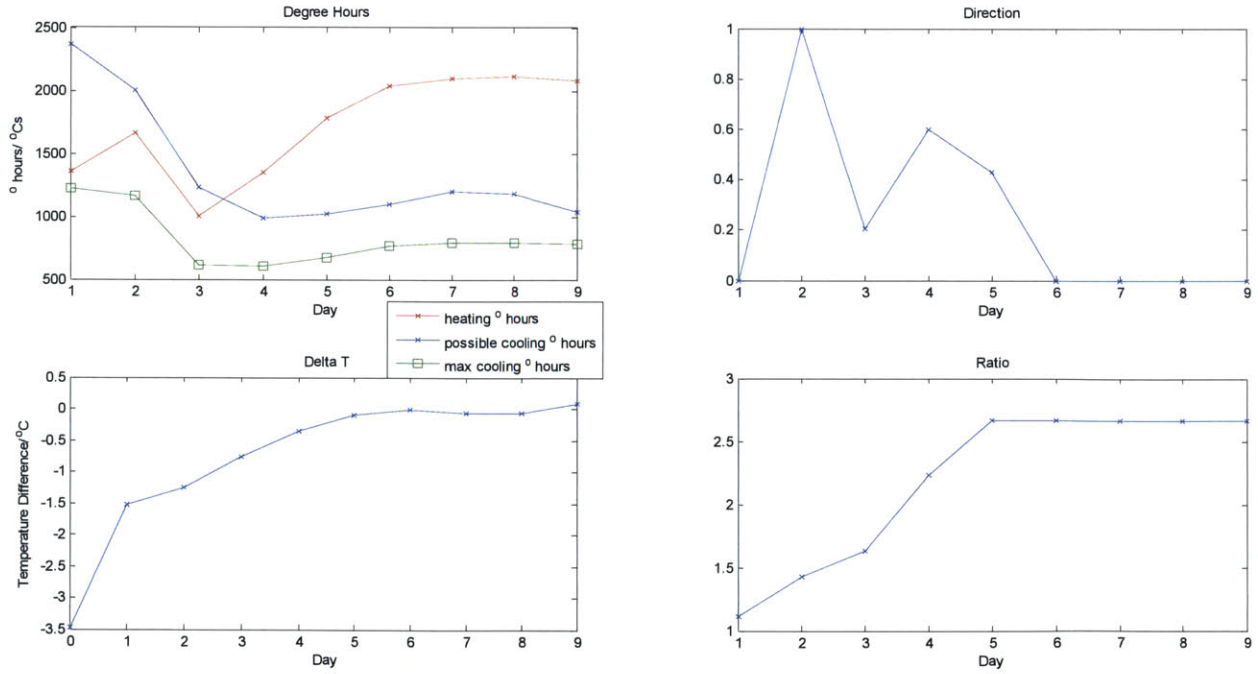

Figure C-84:Plots of the parameters of the overcooling-prevention self-learning algorithm corresponding to temperature profile of figure above

References

[1] L. Pérez-Lombard, J. Ortiz, and C. Pout, "A review on buildings energy consumption information," *Energy Build.*, vol. 40, no. 3, pp. 394–398, Jan. 2008.

[2] U. . DoE, "Buildings energy databook," *Energy Effic. Renew. Energy Dep.*, 2011.

[3] S. J. Emmerich, W. S. Dols, and J. W. Axley, "Natural Ventilation Review and Plan for Design and Analysis Tools," *US Dep. Commer. Technol. Adm. Natl. Inst. Stand. Technol.*, 2001.

[4] W. J. Fisk and A. H. Rosenfeld, "Estimates of Improved Productivity and Health from Better Indoor Environments," *Indoor Air*, vol. 7, no. 3, pp. 158–172, Sep. 1997.

[5] N. Artmann, H. Manz, and P. Heiselberg, "Climatic potential for passive cooling of buildings by night-time ventilation in Europe," *Appl. Energy*, vol. 84, no. 2, pp. 187–201, Feb. 2007.

[6] H. C. Spindler, "System Identification and Optimal Control for Mixed-Mode Cooling," Massachusetts Institute of Technology, 2004.

[7] "Se Controls Partners In Facade Fabrication | Item | News | Smoke Ventilation, Natural Ventilation & Window Automation News | SE Controls." [Online]. Available: http://www.secontrols.com/news/item/se-controls-partners-in-facade-fabrication/. [Accessed: 04-Jul-2014].

[8] G. (Blackpool), "Mistrale 100, Natural Ventilation System, The Complete Solution," 2009. [Online]. Available: http://www.angus-air.co.uk/natural_vent_pdfs/Mistrale_100_July_2009.pdf. [Accessed: 04-Jul-2014].

[9] B. Givoni, *Passive low energy cooling of buildings*. John Wiley & Sons, 1994.

[10] D. Gyalistras and B. T. Division, *Use of Weather and Occupancy Forecasts For Optimal Building Climate Control (OptiControl): Two Years Progress Report*, no. September. 2010.

[11] A.S.H.R.A.E, "Standard 62.1 Ventilation for acceptable indoor air quality," *Refiregeration Air-Conditioning Eng. Atlanta*, 2007.

[12] A.S.H.R.A.E, "Standard 55, Thermal environmental conditions for human occupancy," *Am. Soc. Heating, Refrig. Air Cond. Eng. 145*, 2010.

[13] D. M. M. Arons, "Properties and Applications of Double-Skin Building Facades by," Massachusetts Institute of Technology, 2000.

[14] B. J. Urban, "The MIT Design Advisor : Simple and Rapid Energy Simulation of Early-Stage Building Designs by," Massachusetts Institute of Technology, 2007.

[15] S. D. Ray, "Energy Saving Potential of Various Roof Technologies," Massachusetts Institute of Technology, 2010.

[16] J. Zhou, G. Zhang, Y. Lin, and Y. Li, "Coupling of thermal mass and natural ventilation in buildings," *Energy Build.*, vol. 40, no. 6, pp. 979–986, Jan. 2008.

[17] Weatherbase, "Hayfork, California Travel Weather." [Online]. Available: http://www.weatherbase.com/weather/weather.php3?s=958340. [Accessed: 05-Dec-2014].

[18] A. F. Mills, *Basic heat and mass transfer*. Prentice Hall, 1999.

[19] J. Yam, Y. Li, and Z. Zheng, "Nonlinear coupling between thermal mass and natural ventilation in buildings," *Int. J. Heat Mass Transf.*, vol. 46, no. 7, pp. 1251–1264, Mar. 2003.

[20] W. E. Boyce, R. C. DiPrima, and Haines Charles W., *Elementary differential equations and boundary value problems*. Wiley, 1992.

[21] I. Beausoleil-Morrison, "An algorithm for calculating convection coefficients for internal building surfaces for the case of mixed flow in rooms," *Energy Build.*, vol. 33, no. 4, pp. 351–361, 2001.

[22] L. Glicksman and Lienhard john H.V, *Modelling and Approximation in Heat Transfer, Subject 2.52 notes.* .

[23] G. Tan, "Study of Natural Ventilation Design by Integrating the Multizone Model with CFD Simulation," Massachusetts Institutate of Technology, 2005.

[24] S. C. Chapra and R. P. Canale, *Numerical methods for engineers*. McGraw-Hill Higher Education, 2010.

[25] J. Yuan, "Transition Dynamics Between the Multiple Steady States in Natural Ventilation Systems: From Theories to Applications in Optimal Controls," Massachusetts Institute of Technology, 2007.

[26] M. . Swami and S. Chandra, "Correlations for pressure distribution on buildings and calculation of natural ventilaion airflow," *ASHRAE Trans.*, vol. 94.3112, pp. 243–266, 1988.

[27] M. Lehar, "A simulation tool for the estimation and optimization of electrical lighting energy," Massachusetts Institute of Technology, 2003.

[28] A.S.H.R.A.E, "Solar heat gain and visible transmittance," in *ASHRAE Handbook - Fundamentals*, Atlanta, 2005.

[29] H. Breesch, a. Bossaer, and a. Janssens, "Passive cooling in a low-energy office building," *Sol. Energy*, vol. 79, no. 6, pp. 682–696, Dec. 2005.

[30] P. Blondeau and M. Spe, "NIGHT VENTILATION FOR BUILDING COOLING IN SUMMER," vol. 61, no. 5, pp. 327–335, 1997.

[31] M. Kolokotroni, B. C. Webb, and S. D. Hayes, "Summer cooling with night ventilation for office buildings in moderate climates," *Energy Build.*, vol. 27, no. 3, pp. 231–237, Jun. 1998.

[32] J. Axley and S. Emmerich, "A METHOD TO ASSESS THE SUITABILITY OF A CLIMATE FOR NATURAL VENTILATION OF By," 2002.

[33] M. Kolokotroni and A. Aronis, "Cooling-energy reduction in air-conditioned spaces by using night ventilation," vol. 63, pp. 241–253, 1999.

[34] Swiss Federal Laboratories for Material Testing and Research, "HELIOS software: Building energy simulation code." Switzerland: Duebendorf.

[35] N. Artmann, H. Manz, and P. Heiselberg, "Parameter study on performance of building cooling by night-time ventilation," *Renew. Energy*, vol. 33, no. 12, pp. 2589–2598, Dec. 2008.

[36] M. Zimmermann, "Handbuch der passiven Kühlung," *EMPA ZEN*, 1999.

[37] U. Eicker, *Low energy cooling for sustainable buildings*. John Wiley & Sons, 2009.

[38] G. J. Levermore, *Building energy management systems: applications to low-energy HVAC and natural ventilation control*. Taylor & Francis, 2000.

[39] H. Wang and Q. Chen, "A semi-empirical model for studying the impact of thermal mass and cost-return analysis on mixed-mode ventilation in office buildings," *Energy Build.*, vol. 67, pp. 267–274, Dec. 2013.

[40] H. B. Rijal, "Using results from field surveys to predict the effect of open windows on thermal comfort and energy use in buildings," *Energy Build.*, vol. 39, no. 7, pp. 823–836, 2007.

[41] J. E. Braun and N. Chaturvedi, "An inverse gray-boc model for transient building load prediction," *HVAC&R Res.*, vol. 8.1, pp. 73–99, 2002.

[42] G. P. Henze, C. Felsmann, and G. Knabe, "Evaluation of optimal control for active and passive building thermal storage," *Int. J. Therm. Sci.*, vol. 43, no. 2, pp. 173–183, 2004.

[43] H. C. Spindler and L. K. Norford, "Naturally ventilated and mixed-mode buildings—Part I: Thermal modeling," *Build. Environ.*, vol. 44, no. 4, pp. 736–749, Apr. 2009.

[44] P. May-Ostendorp, "Model-predictive control of mixed-mode buildings with rule extraction," *Build. Environ.*, vol. 46, no. 2, pp. 428–437, 2011.

[45] J. Hu and P. Karava, "Model predictive control strategies for buildings with mixed-mode cooling," *Build. Environ.*, vol. 71, pp. 233–244, Jan. 2014.

[46] D. Gyalistras and B. T. Division, *Use of Weather and Occupancy Forecasts For Optimal Building Climate Control (OptiControl): Two Years Progress Report*, no. September. 2010.

[47] H. C. Spindler and L. K. Norford, "Naturally ventilated and mixed-mode buildings—Part II: Optimal control," *Build. Environ.*, vol. 44, no. 4, pp. 750–761, Apr. 2009.

[48] P. May-Ostendorp, "Extraction of supervisory building control rules from model predictive control of windows in a mixed-mode building," *J. Build. Perform. Simul.*, vol. 6, no. 3, pp. 199–219, 2013.

[49] P. Karava, a. K. Athienitis, T. Stathopoulos, and E. Mouriki, "Experimental study of the thermal performance of a large institutional building with mixed-mode cooling and hybrid ventilation," *Build. Environ.*, vol. 57, pp. 313–326, Nov. 2012.

[50] J. Cigler, "Beyond theory : the challenge of implementing Model Predictive Control in buildings," *Proc. 11th Rehva World Congr. Clima*, 2013.

[51] A. Martin and J. Fletcher, "Night-cooling strategies," *BSRIA Tech. Apprais. 14/96*, 1996.

[52] A. Van Paassen, S. Liem, and B. Groninger, "Control of night cooling with natural ventilation: sensitivity analysis of control strategies and vent openings," in *19th AIVC Conference*, 1998.

[53] M. Gwerder, D. Gyalistras, F. Oldewurtel, B. Lehmann, V. Stauch, and J. Tödtli, "Potential Assessment of Rule-Based Control for Integrated Room Automation," *10th REHVA World Congr. Clima*, no. May, 2010.

[54] C. H. Papadimitriou and K. Steiglitz, *Combinatorial optimization: algorithms and complexity*. Courier Dover Publications, 1998.

[55] M. L. Puterman, *Markov decision processes: discrete stochastic dynamic programming*. John Wiley & Sons, 2009.

[56] A.S.H.R.A.E, *A.S.H.R.A.E. Handbook, HVAC Applications*. Atlanta, GA, 2007.

[57] S. Wilcox and W. Marion, "User's Manual for TMY3 Data Sets, NREL/TP-581-43156," Golden, Colorado, 2008.